EXPERIMENTAL STUDIES OF THE PROCESSES OCCURRING IN ION PLATING DISCHARGES

by

HOSSEIN VALIZADEH

A THESIS SUBMITTED TO THE UNIVERSITY OF SALFORD FOR THE DEGREE OF DOCTOR OF PHILOSOPHY.

APRIL 1982

Department of Electrical Engineering,
University of Salford,
Salford M5 4WT,
ENGLAND.

to my brothers :

Prof. Dr. Yousef Valizadeh

Assoc. Prof. Dr. Mohammad V. Valizadeh

and my sister :

Soraya Valizadeh B.Sc.

EXPERIMENTAL STUDIES OF THE PROCESSES OCCURRING IN ION PLATING DISCHARGES

Abstract

A theoretical study of the processes occurring in ion plating is carried out and the potential of various mechanisms affecting properties of ion-plated films is studied.

Three pieces of apparatus are designed and developed to study the contributions of the mechanisms responsible for the properties of ion-plated films.

A thorough experimental investigation of the processes occurring in ion plating discharges is carried out.

ACKNOWLEDGEMENTS

The Author wishes to thank, most sincerely, all the people who contributed to the work presented in this thesis.

Special thanks are due to Professor George Carter, for providing him with the facilities of the Department of Electrical Engineering to carry out the present research.

It is a pleasure to thank Dr. David George Armour for his very invaluable supervision, guidance, help and encouragement throughout the entire work presented in this thesis.

Thanks are due to Mr. Charles Barber (Technician of Atomic Collision Group of the Department of Electrical Engineering),without whose skill, the excellent performance of the experimental systems would not have been possible.

A special word of thanks is due to the staff of the Mechanical Workshops of the Electrical Engineering Department for their skill and manufacturing various component parts of the apparatus and also for their patience in instructing the author in the use of machines and equipments, which enabled him to build parts of the apparatus.

Thanks are also due to Ms. Eleanor McDonagh for typing the manuscript.

Finally, the contribution of Mr. Joseph Delaney of Sligo Regional Technical College, for his reprographic skill is appreciated.

SUMMARY

The work described in this thesis is concerned with an investigation of the mechanisms of ion plating. The importance of ion plating as the most suitable technique in production of films which are superior in terms of adhesion and hardness is discussed in a critical review of various coating techniques and it is indicated that although these properties (which are well-established facts) have been utilised in a wide range of applications, very little information is available regarding the deposition processes responsible for the observed characteristics. It is also emphasised that in order to optimise deposition parameters, it is necessary to understand the basic plating mechanisms. In order to improve this understanding, comprehensive theoretical and experimental studies of the process occurring in ion plating discharges have been carried out at Salford. The present thesis is concerned primarily with the experimental studies which covered the following aspects of the process:

1. The effect of substrate surface conditions in film-substrate adhesion.
2. A study of the energy and mass distributions of the particles impinging on the cathode of plating discharge both prior to and during evaporation. The work involved was primarily concerned with the energy distributions of the ionic and neutral species of the carrier gas and the film material arriving at the substrate.
3. A study of the mechanisms responsible for the film-substrate interface.
4. An investigation of the concentration of the trapped carrier gas in the deposited film.

Three different experimental systems were designed and developed to facilitate these investigations and the overall project includes a thorough evaluation of the performance of these equipments.

Adhesion properties of the experimental samples were investigated by subjecting them to scratches, created under various mechanical loads and the results indicated that to achieve maximum adhesion for the substrate/film combinations studied,

deposition in a discharge is absolutely essential. The energy measurement experiments revealed that the ion and energetic atom energy range of importance is from thermal energies to the order of 2.5keV for the discharge voltages normally employed in ion plating. Rutherford backscattering was used in the investigation of the film-substrate interface and also in the evaluation of the role of trapped carrier gas. The results indicated that the most important factors contributing to the film-substrate interface are energy deposition and cascade mixing, and that the concentration of the trapped carrier gas in films deposited at practically useful rates is not high enough to lead to the formation of a significant density of gas bubbles.

CONTENTS

PAGE NO

PAGE NO

CHAPTER I

INTRODUCTION

CHAPTER I

INTRODUCTION

1.1 Introduction

1.2 References

1.1 Introduction

The term "Ion Plating" is used to describe a coating technique in which the material to be deposited is evaporated into a gas discharge maintained between the substrate (cathode) and the evaporation source (anode). The substrate, in this process, is bombarded with energetic ions and neutral particles both before and during the deposition of the coating. The technique has been shown [1-9] to have good throwing power (i.e. surfaces out of line of sight of the source, including cavities to a certain extent, are coated with good uniformity) and to produce dense, fine-grained and pore-free films of a wide range of materials with excellent adherance to an equally wide range of substrates. This process, which is one of a number of bombardment assisted coating techniques that have developed in the past decade, offers a number of advantages over alternative coating methods, the main one which is the excellent adhesion between the coating and the substrate, even in cases where the material of the coating and the substrate do not normally alloy. Coatings of virtually any metal (including alloys) can be deposited on any metallic substrate and the technique has been extended to include hard ceramic coatings, carbon coatings, and non-metallic substrates (including plastics).[8-12] The durability of ion-plated films, for instance, is attributed to the good adhesion between the film and the substrate and it is clearly necessary, in order to optimise deposition parameters such as discharge conditions, carrier gas species, evaporation rate substrate surface condition, to understand the basic plating mechanisms.

Despite the fact that the use of ion plating as a technique for surface coating has increased dramatically, in the last few years, little is known about the mechanisms actually responsible for the properties of ion-plated films. The amlost universally observed good adhesion, for example, has been ascribed to processes such as ion implantation, recoil implantation and radiation enhanced diffusion without proper consideration of the characteristics of the bombarding particle fluxes. The need to understand the reasons for the properties of ion-plated films has been emphasised by the lack of consistency frequently observed in film production, e.g. carbon films. In fact, the role played by carrier gas

bombardment, substrate surface conditions, the discharge conditions, the impurities present in the plating environment, and the energy distributions of the particles impinging on the substrate all appear to be of significance in the plating process. The work described in this thesis is concerned with a comprehensive investigation of mechanisms operating during ion plating and with the relationship between these mechanisms and the properties of the films.

Adhesion between the film and substrate in ion plating has been found[3,14-16] to depend on a number of factors such as chemical bonding across the interfacial region, the type of interfacial region and the fracture mechanisms which results in failure. For good adhesion the substrate must be free of contaminants which prevents intimate contact and the nucleation and growth of the film must be such that there is a high interfacial contact area. The interface will have a graded appearance with a gradual change in composition if the film material can penetrate into the substrate material (or vice versa) by diffusion or some other mechanisms. This would lead to an improved adhesion. When a graded interface is formed, the inherent stresses produced during film deposition, which are due to the differences in the lattice parameters and thermal expansion mismatch between the metal film and the substrate, are always minimised.[14]

As already indicated for the adhesion properties, the superior properties of ion-plated films have been explained in terms of the mechanisms that are known to be associated with ion bombardment of surfaces.[13-16] Consequently, ion implantation, recoil implantation, radiation enhanced diffusion, thermal diffusion, cascade mixing, sputtering and sputter-redeposition, and surface damage effects have all been considered to play a role. The extent to which the film properties are, or can be, affected by these processes is, however, unclear and it is this factor which prompted the present investigations.

The programme of research presented in this thesis has been designed to study, in detail, the basic gas discharge and ion-surface interaction processes involved in the production of ion-plated films in order to provide a basis for the derivation of a suitable theoretical model to explain the film properties and to allow the relative importance of the various experimental parameters to be assessed. The programme was essentially devided into the following distinct

sections.

(a) An investigation and comparison of adhesion properties of films deposited by vacuum evaporation under ultra high vacuum (uhv) and conventional base conditions, and uhv ion plating condition.

b) To study the energy distributions of the ionic and neutral species of the carrier gas impinging on the cathode of a typical ion plating discharge.

c) An attempt to measure the energy distributions of the 'film' particles, impinging on the cathode, using either electron gun evaporation in conjunction with appropriate differential pumping or evaporation from a boat mounted inside the discharge chamber.

d) A more detail study of gas trapping and sputter - redeposition effects, and

e) A theoretical treatment of the processes associated with the production of a film-substrate interface of sufficient width to account for the almost universally good adhesion of ion-plated films.

The importance of ion plating as the most suitable technique in production of films with the properties discussed earlier in this Chapter has been emphasised in a critical review of various coating techniques presented in Chapter 2. A comprehensive theoretical study of ion plating is presented in Chapter 3. Three different pieces of apparatus have been designed to fulfill the requirements of the research programme presented in this thesis and Chapter 4 is concerned with the design, constructional details and performances of these apparatus. The results of the investigations are presented and assessed in Chapter 5. Finally, conclusions are presented in Chapter 6.

1.2 References - Chapter 1

1. Mattox D.M. J. Appl. Phys. 34, P.2403, 1963.
2. Teer D.G. Tribology International P.247, 1975.
3. Mattox D.M. J. Electrochem. 2, P.295, 1965
4. Mattox D.M. J. Vac. Sci. and Technol. 10, P.47, 1973.
5. Mattox D.M. Sandia Lab. report No. SLA-73-0619 June 1973.
6. Spalvins T. Pamphlet No. 438, Corp. Develop. Lab., Brit. Steel, Corp., Sheffield Feb. 1975.
7. Mattox D.M. Sandia Corp. Monograph SC-R-65-852.
8. Wolfson Ion Plating Unit report.
9. Walley P.A. Proc. of Conference on Ion Plating and Allied Techniques (IPAT) Edinburgh, June 1977.
10. Burt R.A. Ibid P. 135.
11. Pitt. C.W., Ibid P.149
12. Jones K., Griffiths A.J., Williams E.W., Ibid P. 115
13. Mattox D.M. Sandia Corp. report No. SC-DR-281.63., 1963.
14. Teer D.G. Delcea B.L. Proc. Conf. on IPAT, P.58, Edinburgh, June 1977.
15. Nelson R.S. Ibid. P.32
16. Teer D.G. J. Adhesion, 8, P.289. 1977

CHAPTER II

CRITICAL REVIEW OF FILM DEPOSITION TECHNIQUES

CHAPTER 2

CRITICAL REVIEW OF FILM DEPOSITION TECHNIQUES

2.1 Introduction

The engineer or researcher who is faced with the need to utilise film deposition can choose from a wide range of deposition processes most of which can be carried out in commercially available apparatus . In general it is impossible to design an all-purpose system and in many cases it is necessary to employ only one method (among all the available methods) to accomplish a given task.

In this Chapter, various techniques and the related methods of preparing solid films are described. Each of these techniques has its advantages and disadvantages in a particular application. Hence the method to be used must be selected to the users specific needs. Modifications to standard methods have been used to offset or minimise the disadvantages in particular applications.

2.2 Electrodeposition

Electrodeposition (or electroplating) is the process of depositing a coating on a substrate by means of electrolysis. The birth of electroplating may be considered to have taken place with Volta's discovery of electricity by chemical means in 1799.[1] Electrolysis is carried out in a solution "bath" which may consist of fused salts or of solutions of various kinds. However, in most cases it is a water solution.[2] The discovery of cyanides for plating baths widened the scope of electroplating from deposition of copper in solution of simple copper salts to deposition of a variety of metals in the form of thin/thick, dense coatings for decorative and protective purposes.

2.2.1 Method

A schematic diagram of a typical electroplating setup is given[4] in Figure 2.1. It consists of a d.c. source, a plating tank and bath, and two electrodes. The film material forms the anode while the substrate is connected to the cathode.

When electrodes are dipped into the bath, the coating material produces hydrated mobile ions in it. Under the action of electric field between the electrodes the ions travel towards the cathode and are deposited on it. The distribution of the metal coating depends on[1-4]

(i) shape and dimension of the object

(ii) the geometry of the plating cell arrangement,

(iii) the conductivity of the bath, and

(iv) the variations of cathode current efficiency (defined as the ratio of the weight of metal actually deposited to that which would have resulted if all the current had been used for depositing) with current density.

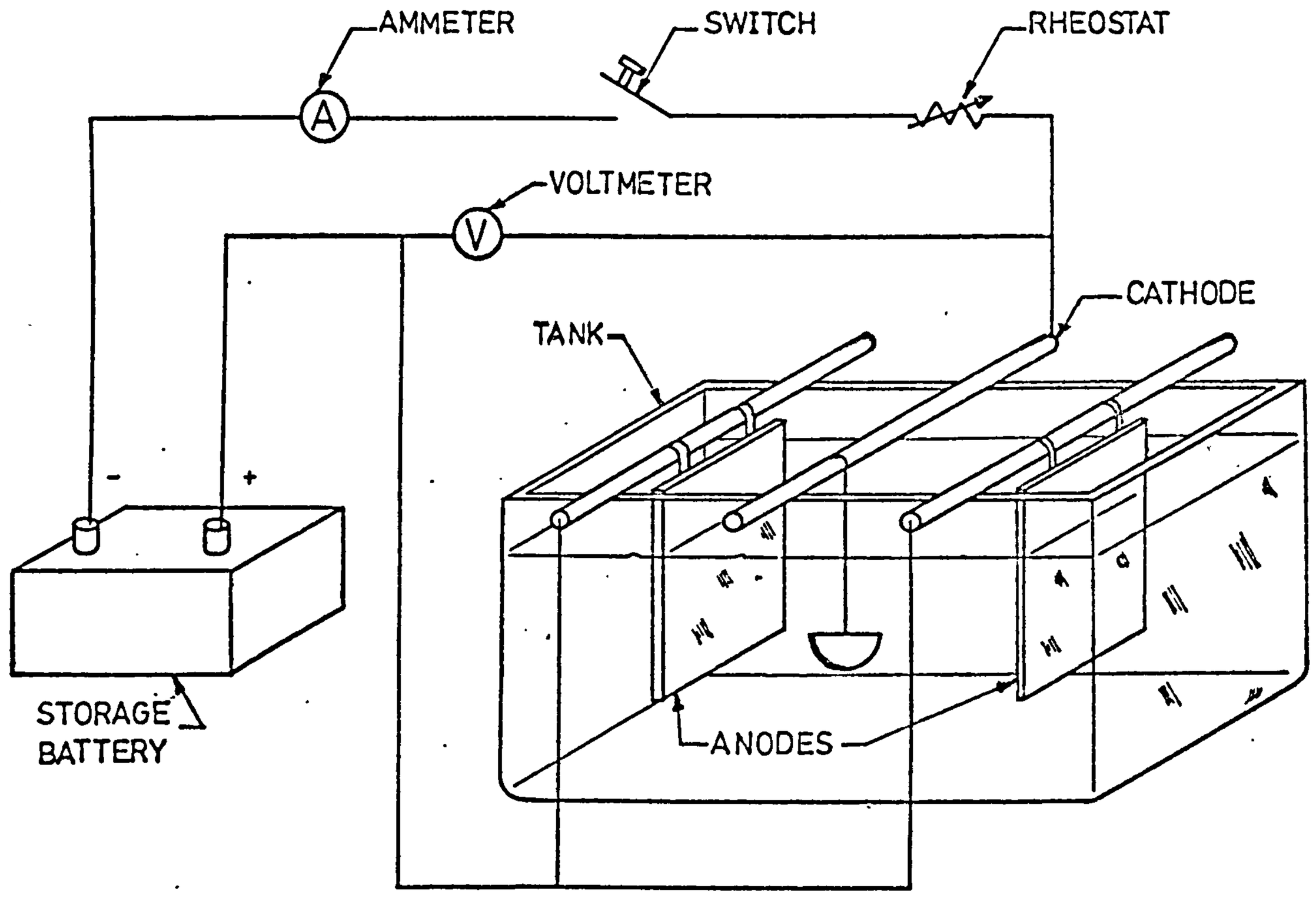

FIGURE 2.1.

SCHEMATIC DIAGRAM OF ELECTRO – DEPOSITION SET UP [3]

The mean free path of the moving ions in the solution is very short[3] and they undergo a large number of collisions during their passage to the cathode. Therefore, the kinetic energy of an ion arriving at the substrate is usually of the order of 0.1eV.

In the deposition process, the hydrated coating material ions, instead of being deposited as a continuous film over the entire surface of the substrate, tend to concentrate on favoured sites where they lose some of the water and other impurities attached to them and form bonds with the cathode surface with partial neutralisation of their charges.[1-4] The first layer of the deposited particles, then, bonds to the substrate lattice and the strength of this bond is similar to that of the basis (substrate) material.[2,3] Hence, films with high orders of adhesion to the substrate can be deposited. The optimum bonding occurs when the substrate is clean and imperceptible residual films or other contaminations are removed in the plating bath, prior to deposition, so that deposit approaches the basic metal within atomic dimensions. The bond ions diffuse over the substrate surface to edges, steps, and other irregularities where they may become incorporated into the metal lattice[4]. Monoatomic growth layers are then produced. The layers are bounded by microsteps and grow until they encounter absorbed impurities and branch up to form multilayer growth stacks.

The degree of adherence of the film to the substrate decreases[3] when there is a pronounced mismatch between the two lattices or faulty practices are employed in preparing the substrate.

2.2.2 Assessment

So far as the purity of the film is concerned it is practically impossible to obtain high purity deposits by this technique.[1-3] This is because it is impractical to either produce a completely clean bath, initially, or to maintain clean conditions due to the introduction of impurities in the form of dissolved components from anode, dust, debries introduced during preliminary surface preparation etc. Impurity particles existing in the bath in suspended form become attached to the cathode during deposition

and growth of the deposit around them can seriously affect not only the purity of the deposited film, but also its adhesion and other mechanical or electrical properties. Despite these problems it is possible, to produce films with high growth rates and a high order of adhesion to the substrate, in the same environment. The method is therefore widely used both for corrosion resistance and decorative purposes in industrial products. However, it suffers from a number of limitations the most important of which are:-

1. Films can only be grown on metallic or conducting substrates.
2. Possible incorporation of water and OH ions into the films. This can have a deletrious effect on their electrical properties, and,
3. Of increasing importance from both economic and environmental points of view, the production of effluents which give rise to disposal problems.

As a result of the latter, water authorities have increased the demand for metal finishers to reduce the concentration of heavy metals and cyanides in industrial effluents. These disadvantages have motivated interests in alternative coating methods.

2.3 Chemical Vapour Deposition

Chemical Vapour Deposition (CVD) has emerged as a very successful technique in semiconductor research and one of its most important applications is in the production of semiconductor films[5] in single crystal form. In the electronics industry, chemical vapour deposition of silicon and related compounds is of major importance for the production of thin film layers on the various types of substrate used in the fabrication of devices such as diodes, transistors and integrated circuits.[5]

2.3.1 Method

In the chemical vapour deposition process, the material to be deposited is vapourised and the vapour is mixed with a reactive vapour, and passed over a heated substrate. A chemical decomposition of the vapour or reaction with other gas vapours takes place at the substrate and results in non volatile products

which deposit atomistically on the substrate.[5,6] Most chemical vapour deposition processes operate in the reactant pressure range from a few torr to above atmospheric pressure.[6,7] The growth rate of substances such as Si, Ge, and GaAs is reported [8] to increase if a transverse electric field is applied to the substrate during deposition.

In preparation of films by chemical vapour deposition there are four basic reaction systems. They are[5,6,8]

(i) pyrolysis

(ii) hydrogen reduction

(iii) disproportionation, and

(iv) transport.

Pyrolysis is the decomposition of a compound to yield a nonvolatile deposit. For organometallic compounds pyrolysis[6] takes place at temperatures below 600°C whereas for metal halides, particularly iodides, the decomposition takes place at about 600°C.

Hydrogen reduction of metal halides is frequently used for deposition of metal films. It is a pyrolysis reaction in which one or more of the gaseous products of decomposition is removed. In this process the reaction temperature is lowered by several hundred degrees below that needed in the absence of hydrogen.

In the disproportionation process the basic idea is to control the equilibrium that exists between Si (or Ge), the tetra-iodide and the di-iodide. At 1100°C, SiI_4 attacks the course, Si, to put SiI_4 into the vapour phase and at 900°C, the reverse reaction takes place resulting in the deposition of Si on the substrate by disproportionation of the SiI_4 vapours.

Finally, in the transport reaction, deposition can be obtained in a heterogeneous chemical reaction system at equilibrium by setting up a temperature differential in the system to disturb the equilibrium condition. A major application of the reaction is in growth of GaAs.

A full characterisation of the chemical vapour deposition process has been

presented by Van den Berkel.[9,10]

2.3.2 Assessment

Chemical vapour deposition is a versatile and flexible technique capable of producing[5 - 10] deposits of pure metals semiconductors and insulators. A major application of the technique is the preparation of single crystal metal oxides notably the ferrites, garnets and sapphires. However, the main disadvantages of the technique are[11] poor adhesion, high cost of the starting materials and very slow deposition rates.

2.4 Thermal Evaporation:

Deposition of thin films by the thermal evaporation of the required material in a vacuum is a widely used method.[12,13] The process involves simply heating the required material (with exception of a few materials which sublime)[12,14] above its vaporisation temperature in vacuum, and allowing the resultant vapour to recondense onto the surfaces of substrate(s) exposed to it. Films so formed are said to be vacuum evaporated.

Holland[15] summarised the reasons for using a vacuum system for thin film deposition as follows:

(i) the material will evaporate significantly at lower temperature under vacuum,

(ii) the effect of oxides formed on the boiling surface of the coating material is reduced.

(iii) there will be a reduction in the number of impurities in the deposit, and

(iv) at low enough pressures (less than 10^{-4} torr) where mean free paths are large compared with the system dimensions it is possible to place a mask between the source and the substrate to obtain a sharp pattern.

2.4.1 Method:

A schematic diagram of the equipment required for the production of thin film by means of the thermal evaporation technique, is shown in Figure 2.2. The range of variables in the evaporation process, e.g. evaporation rates, residual gas pressure, source-substrate geometry etc. is quite wide and it is often necessary to specifically select suitable equipment for a particular application. The apparatus can be described in terms of the following basic systems:-

(i) the vacuum system

(ii) the substrate holder, and

(iii) evaporation source.

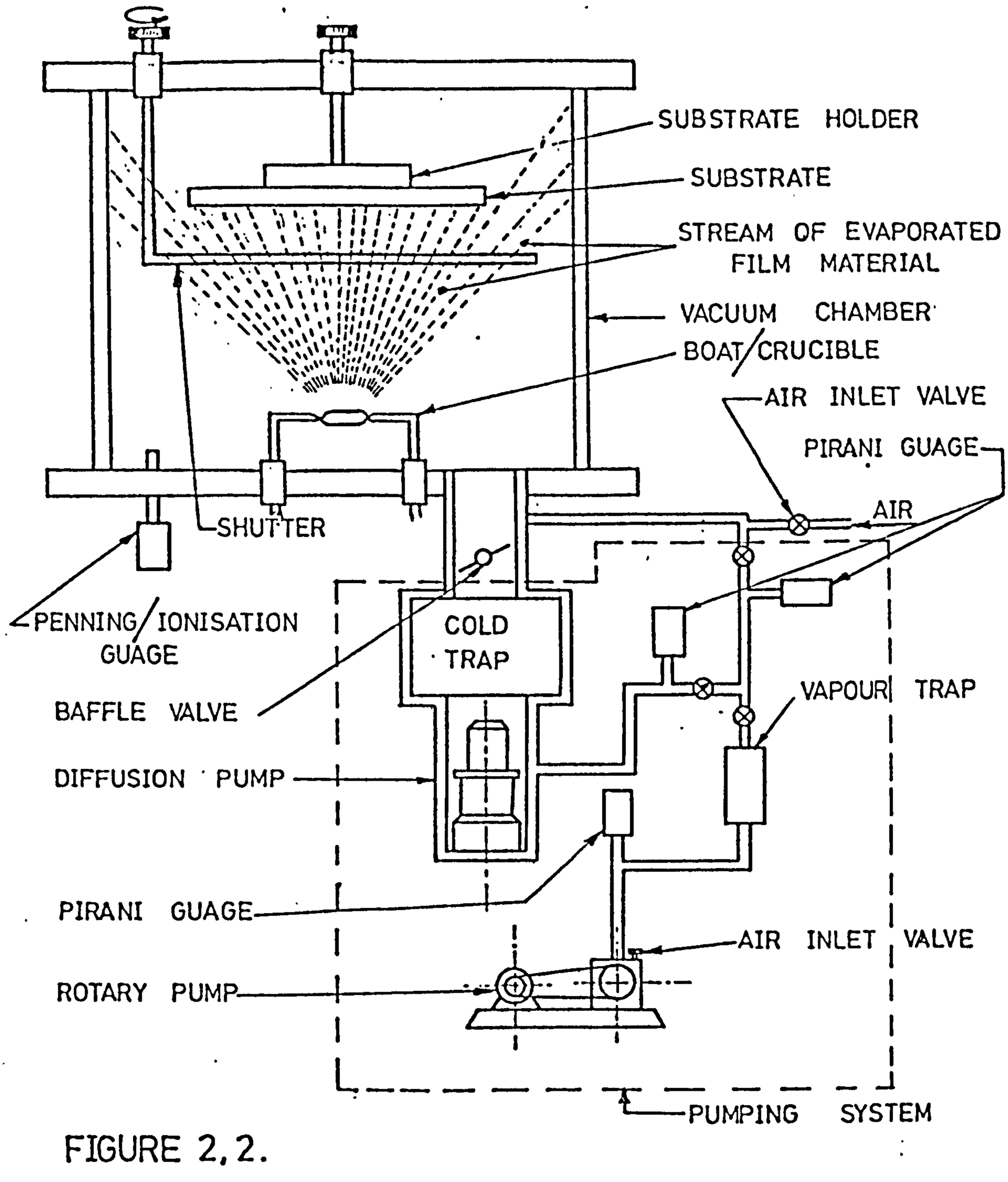

FIGURE 2,2.

SCHEMATIC DIAGRAM OF VACUUM EVAPORATOR SET UP

2.4.1(a) The Vacuum System

The background pressure in the deposition chamber influences the film properties enormously since at any of the pressure levels typically used there is a significant residual gas molecule arrival rate at the substrate surface. For example at 10^{-5} torr, a typical evaporator background pressure, the arrival rate is approximately 2×10^{15} atoms/sec/cm^2. The reactive components of the residual gas mixture which arrive at the substrate stick to it and cause contamination. The growth of the contamination increases rapidly with the background pressure. Thus, on the basis of minimising gas contamination of films one can readily appreciate the idea of having a vacuum system that will maintain the lowest possible pressure during evaporation.

Typically,[6] the pressure range of the deposition chamber is 10^{-5} - 10^{-7} torr. This can be achieved by a series combination of an oil/mercury diffusion pump and a mechanical rotary pump. However, it must be pointed out that as a result of degradation of the lubricating oil of rotary pumps and high local temperature increase due to friction effects, light-weight gas molecules are released and can, when transition or molecular flow condition prevail in the backing line, backstream to the exhaust system of the diffusion pump. This leads eventually to hydrocarbon contamination of the system and increase the ultimate pressure of the chamber. Holland,[16] in a review paper, discussed the backstreaming phenomenon and claimed that the partial pressure of the backstreamed particles can be best reduced by introducing an alumina trap in the backing line. For further reduction of the migration of the oil molecules into the vacuum chamber a cold trap is generally employed above the diffusion pump.[17,18]

2.4.1(b) Substrate Holder:

The substrate holder can be a flat plate or a dome depending on the geometry, size and film uniformity requirements. Both structures of the substrate holder can be either stationary or rotating. The advantage of having a movable substrate holder is to average out non-uniformities in the evaporant distribution and/or allow all surfaces of three dimentional substrates to be

exposed to the evaporant system.

For some particular purposes such as improving film adhesion, increasing the crystalline size in the film, and control of film stress substrates must be heated before and/or during deposition.[19] There are two types of heaters[9] in common use. One type is the resistance heated oven located behind the substrate(s) and the other type is a focused quartz lamp located between the source and the substrate(s), and out of the way of the evaporant stream. Quartz lamps permit faster heating and cooling of the substrate(s) than the oven type heating assemblies.

Sometimes it is necessary to mask certain areas of the substrate from the evaporant. The simple shutter, shown in Figure 2.2,can fulfill this requirement in some cases while in others e.g. integrated circuit fabrication, highly sophisticated and precise masking techniques are necessary.

2.4.1(c) Evaporation Sources

The evaporation source is the part of the thin film deposition apparatus in which vapourised coating material is produced by heating the coating material above its vapourisation temperature.

Methods of Evaporation of Source Material

To evaporate the source material its atoms, and/or molecules must attain a thermal energy which surpasses the level of surface tension energy. The temperature at which this process occurs is known as the vapourisation temperature. The recondensation of the source material, consisting of nucleation and film formation, is strongly dependent upon the thermal energy, the rate of arrival of the vapour particles, as well as the physical, chemical, and thermal condition of the receiving surface. Since the vapourisation temperature of different materials varies over a wide range it is necessary to select the most suitable method of evaporating the particular material of interest.

Thermal evaporation may be achieved directly or indirectly by a variety of physical methods.[6,12,13] The most widely used methods are described below.

(a) Resistive Heating Method

The simplest way of raising the temperature of materials is by resistance heating.[13,15] The source material is placed in or on a filament or boat. Filaments and boats are typically fabricated of refractory materials such as tungsten, molybdenum , tantalum, and composites of boron nitride and other materials. The simplicity and utility of resistance heated evaporation sources have led to their widespread use in vacuum coating applications. However, resistive heating methods do have their limitations.[20] They are:-

1. Wear out of the filament or boat
2. The method is only applicable to materials having a relatively low vapourisation temperature ($< 1500^{o}C$),
3. Evaporants often melt and dissolve the filament and boat, or crucible which might result in contamination of the film.
4. The method is not useful for depositing refractory material or high temperature (i.e. low vapour pressure) alloys.

(b) Electron Bombardment Heating Method

As explained above, some of the major disadvantages of the simple resistive heating method are contamination of the film from the support material and the limitation of the input power. These make it difficult to evaporate high-melting point materials. An alternative, highly efficient source of heating, electron bombardment, overcomes these drawbacks. This type of source, in principle, is capable of evaporating any material at rates ranging from fractions of Angstrom to microns per second. The film material is placed in a crucible which is maintained relatively cool,

(usually water cooled) throughout the deposition, hence contamination of the film from support material can be avoided.

The principle of operation of an electron bombardment heating method is as follows: the electrons which are produced from a resistively heated filament are directed and focused, by applying an appropriate magnetic field, onto the evaporant. The kinetic energy of the focused electrons, impinging on the surface of the evaporant, is transformed into thermal energy upon impact and the temperature of the atoms or molecules are raised above their vapourisation point.

Also the intense heat of the electron bombardment causes decomposition and structural changes of some chemical components. This effect is used in production of films of decomposed products.

(c) Flash Evaporation

The vapour pressure of the evaporants, the background pressure in the vacuum system, and the evaporation temperature are the most important factors affecting the evaporation rates obtained using the two heating methods discussed above. In the deposition of films of binary compounds for example it is not necessarily sufficient to simply use the solid (often powdered) form of the compound in the boat. Because of the different evaporation rates films with incorrect stoichiometry are often obtained.

To obviate this problem a technique known as flash evaporation[6,13] can be used. In this technique a fine-sized powder of the compound is dropped at a controlled rate on to a hot boat whose temperature is held well above the minimum vapourisation temperature of the individual elements of the compound.

2.4.2 Assessment

Using the thermal evaporation technique it is possible to deposit high purity films by reducing the deposition chamber pressure, choosing highly pure source material and employing electron bombardment for evaporation of the source material. Although the radiation pattern of evaporation sources, in this tech-

nique, mainly follow a cosine distribution[20] it is possible to deposit films with good uniformity by increasing the distance between the source and the substrate. . This, however, decreases film deposition rate. In addition to the above-mentioned properties the relatively high deposition rates obtainable and the simplicity of the deposition procedure are also attractive features of this technique.

However, the adhesion of vacuum - deposited films to their substrate is generally poor. This is mainly due to the presence of absorbed gases of oxide layers on the surface of the substrate and the low ($<$ 1eV)[20] arrival energies of evaporated particles at the substrate. In addition, since the evaporated particles follow straight line trajectories, holes, indentation, and all parts of the substrate which are shadowed from the straight line trajectories will not be coated. This problem can, to a certain extent, be overcome if the substrate can be made to rotate around different axes. Also the low energy of the evaporated particles causes the density of films prepared by this technique to be lower than that obtained using the following two technqiues.

2.5 Sputter Deposition

The ejection of atoms and molecules from a surface subjected to energetic ion bombardment is known as sputtering.[21-23] The bombarding ions are generated in a rarefied gas (usually argon) either by dc or rf excitation, forming a plasma in which newly arriving gas molecules are continuously ionised.[6] The ejected or sputtered particles can be condensed on a substrate to form a thin film.[6,13,15,21-23] Thus the film material is an ion bombardment target whose atoms/molecules acquire enough energy to escape from the surface and deposit on the substrate.

Sputtering of target material is due to mechanisms such as[24]

(i) direct momentum transfer from the impacting ion to the surface atoms,

(ii) collision cascade, and

(iii) energy released in the impact zone producing a condition resembling the random state of thermal evaporation. (Thermal Spikes).

Most of the sputtered material is ejected from the target as neutral[25] particles, a fraction of which are then ionised during their passage through the plasma.[25,26]

2.5.1 Methods of Sputter Deposition

Several methods have been employed for deposition of thin film by sputtering. Some of the most popular methods are briefly discussed here. Since the vacuum requirements are similar to those specified for vacuum deposition, the pumping system, discussed in Section 2.4, can be used for achieving the desired operating environment for deposition of thin films by these methods.

2.5.1(a) D.C.Glow - Discharge

A schematic diagram of a d.c. glow-discharge method is shown in Figure 2.3. This widely used arrangement[12, 24] is known as a 'diode sputtering' system. The substrate, in this method, is normally placed on the anode and kept at anode potential and a glow-discharge is formed in a gas(normally a rare gas) at pressure between 10^{-1} - 10^{-2} torr with a corresponding applied voltage of 1-5 kV. Under these conditions a cathode current density of 0.5 to 0.1 mA cm^{-2} can be obtained.[24,27,28] A typical voltage current characteristic of such a diode structure and its visual appearance are shown in Figure 2.4.[27,28] The operating point in the voltage-current characteristic is chosen to be somewhere in the region where the current density is a function of the applied voltage at constant pressure. A discharge with this particular biasing condition is known as an abnormal glow-discharge. The gas breaks down to conduct electricity when a certain minimum voltage is reached. The cathode dark space (shown in Figure 2.4(b)) is the most important region

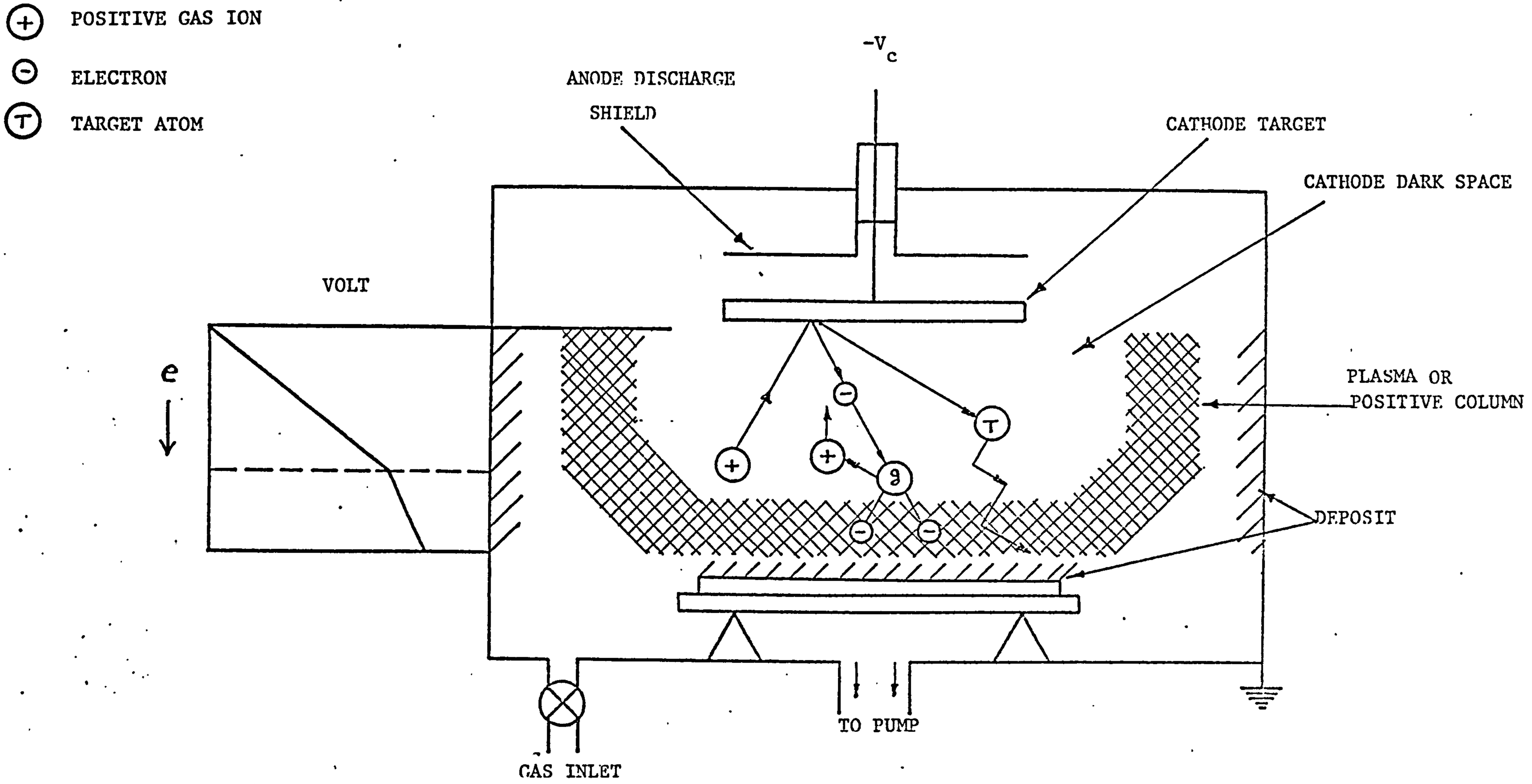

FIGURE 2.3 SCHEMATIC DIAGRAM OF D.C. GLOW DISCHARGE METHOD[24]

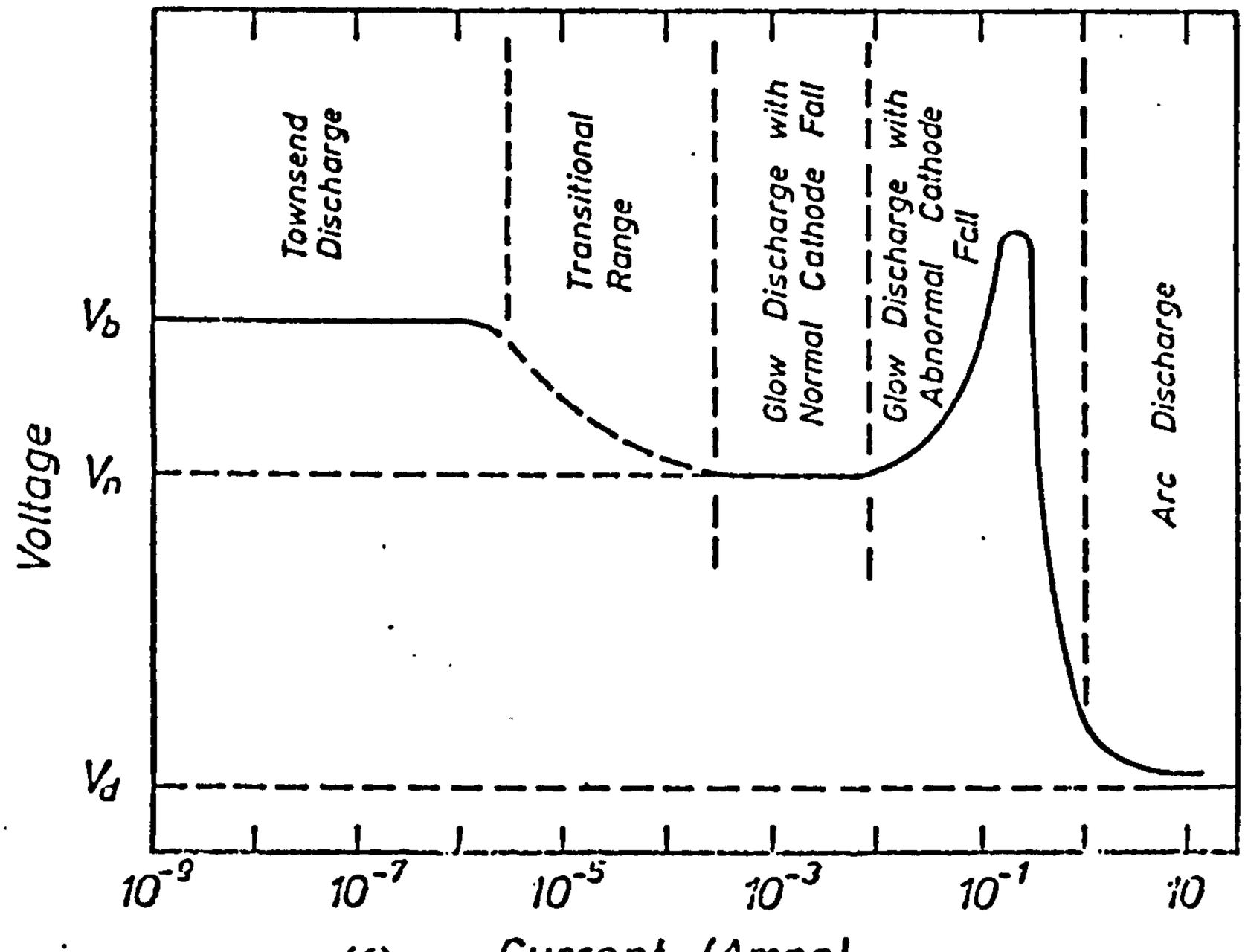

Figure 2.4(a) Typical current voltage characteristic of an electrical discharge through gas at low pressure

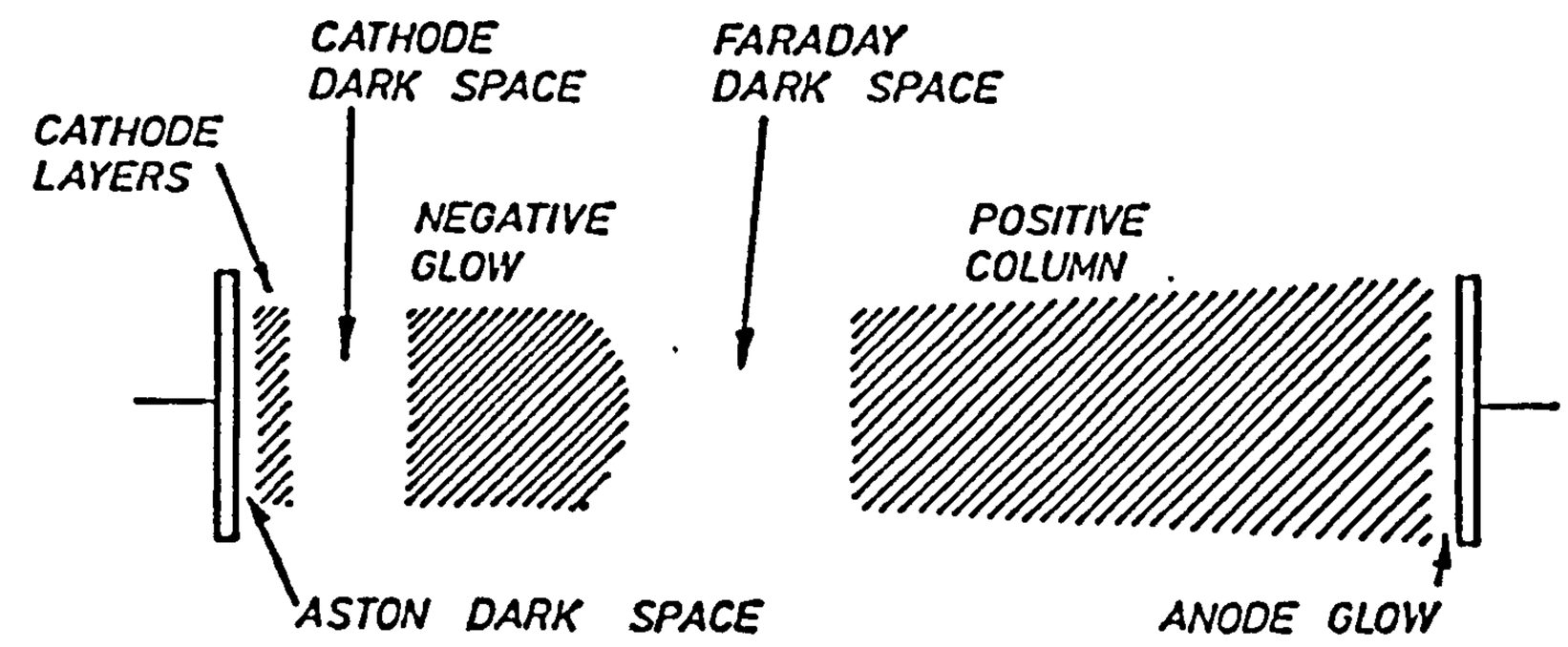

Figure 2.4(b) (6) A visual representation of the principal regions in a low pressure d. c. discharge

because most of the applied voltage is dropped across it.[27,28] Ions and electrons created at the breakdown are accelerated across this region. The energetic electrons produce more ions by collision with the gas atoms in the negative glow (shown in Figure 2.4(b)). The energetic ions strike the cathode to produce sputtering and emit secondary electrons which are essential for sustaining the glow. Effective sputtering is possible only when both the number of ions and their energy are large and controllable.[6] This is conveniently affected in the abnormal glow - discharge region (shown in Figure 2.4(a))

When particles are sputtered from the target, initially, they maintain their paths until they are thermalised[24,27,28] i.e. their energies are reduced by collision and reach gas temperature. The distance a sputtered particle travels before it is thermalised depends on the relative mass of the particle and the discharge gas atoms used. It increases with initial ejection energy and with decreasing pressure of the sputtering gas.[27,28] For a cathode substrate spacing of less than 5cm the sputtered particles reach the substrate by a process of direct impact and gaseous diffusion,[24] in the pressure range of 10^{-1} to 10^{-2} torr.[29] However, in this pressure range, Westwood claimed that apart from very heavy (Ms > 200), energetic (1000 eV or so) particles, essentially all sputtered particles are thermalised before they travel a distance of 1cm, normal to the target. In this case, for a cathode substrate spacing of 1cm and more, the sputtered particles reach the substrate mainly by thermal diffusion.

Extreme simplicity, production of deposits uniform both in thickness and physical properties over very large substrate areas are the main advantages of the dc glow-discharge method. However, the method suffers from the disadvantage of low deposition rate, and hence the films produced can contain a high concentration of adsorbed gases.[21-23,30] Although an increase in the gas pressure increases the number of sputtered particles the increase in pressure reduces the mean free path in the plasma. This in turn reduces the deposition efficiency of the system due to backscattering of particles ejected at the cathode and hence increases the amount of adsorbed gases.[24,31]

2.5.1(b) Triode

In view of the main disadvantages of the d.c. glow-discharge method (discussed above)[6] a system with higher sputtering yield, defined as the number of the sputtered atoms per incident ion, and lower (compared to dc glow-discharge system) operating pressure would appear to be an ideal one. Actually, a reduction in the operating pressure of the discharge does not necessarily mean a reduction in the number of sputtering ions.[30,31] This is because at low pressure reasonably good sputtering yield may be obtained if the ionisation of the sputtering gas is increased. The required condition may be defined by:-[12,31]

(i) increasing the ionisation efficiency of the available ionising electrons by increasing their path length.

(ii) increasing the supply of the ionising electrons

A schematic diagram of a system which fulfills the above requirements is shown in Figure 2.5. It is known as a triode sputtering system in which the supply of ionising electron is increased by thermoionic emmision (the filament) and the magnetic field leads to an increase in the electron path lengths. Hence the ionisation efficiency is enhanced. The use of an auxiliary anode makes the target ion current less dependent on the ionisation conditions. The operating pressure range of a typical triode system is 5×10^{-4} to 10^{-2} torr.

High deposition rates hence purer films (compared to dc glow-discharge system)[6,12,24,31] is one of the major advantages of triode system.[6,31] Another major advantage is that fine control of current density and hence the sputtering yield can be obtained simply by varying the magnetic field. However, the additional fixturing[32] (compared with the diode configuration) of a triode system can act as a source of contamination of the deposited film.

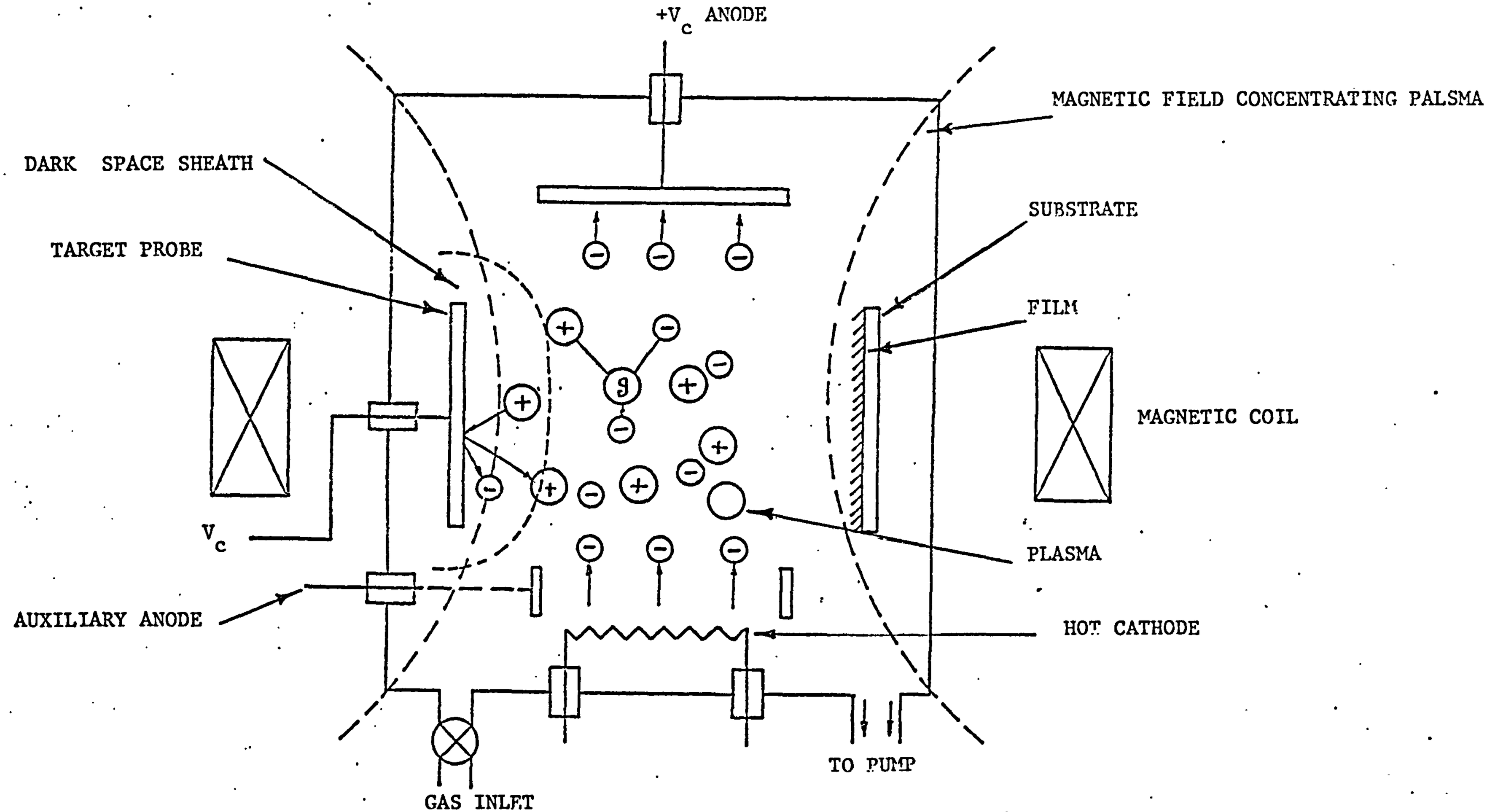

FIGURE 2.5 SCHEMATIC DIAGRAM OF A TYPICAL TRIODE SPUTTERING SYSTEM[24]

This is because the energetic ions causing the sputtering cannot be completely restricted to the target material, thus the additional fixturing and confinement can act as a source of contamination. Ryden[33] et al, succeeded in reducing (by more than an order of magnitude) the Ti contamination of a Pt deposit, with a Ti tube, by splitting the confinement tube into four electrically isolated segments.

2.5.1(c) Radio - Frequency

An alternative method of overcoming the problem associated with the 'diode' sputtering system is[34] to extract positive ions from a plasma excited by a radio-frequency potential. This method is known as'radio-frequency'or 'rf' sputtering.

With a radio-frequency excited plasma it is possible[34] to sputter at pressures (at least an order of magnitude) lower than those typically required using the d.c. glow - discharge method. A significant advantage of the rf excited system is that insulators can also be effectively sputtered since the build up of positive surface charge on the insulator targets which occur in d.c. system is inherently eliminated. Thus the radio- frequency sputtering system is extremely versatile.

A schematic diagram of an rf sputter deposition system is shown in Figure 2.6. The matching network, shown in the diagram is used to match the output impedance of the rf power supply to the impedance of the discharge.[35] When the rf potential is applied to the cathode and the plasma discharge is ignited the electrons and positive ions move towards the cathode as its potential goes positive and negative, respectively, during each half cycle. Since the mobility of electrons is much higher than that of the positive ions a net negative charge, (hence a net negative potential) results at the cathode. This negative charge is capacitively isolated from ground by the capacitor, C, and there is no path for the negative charge to leak off. The cathode voltage comes to an equilibrium[19] determined by the rf power and the net number of ions and electrons arriving at the cathode. The negative dc

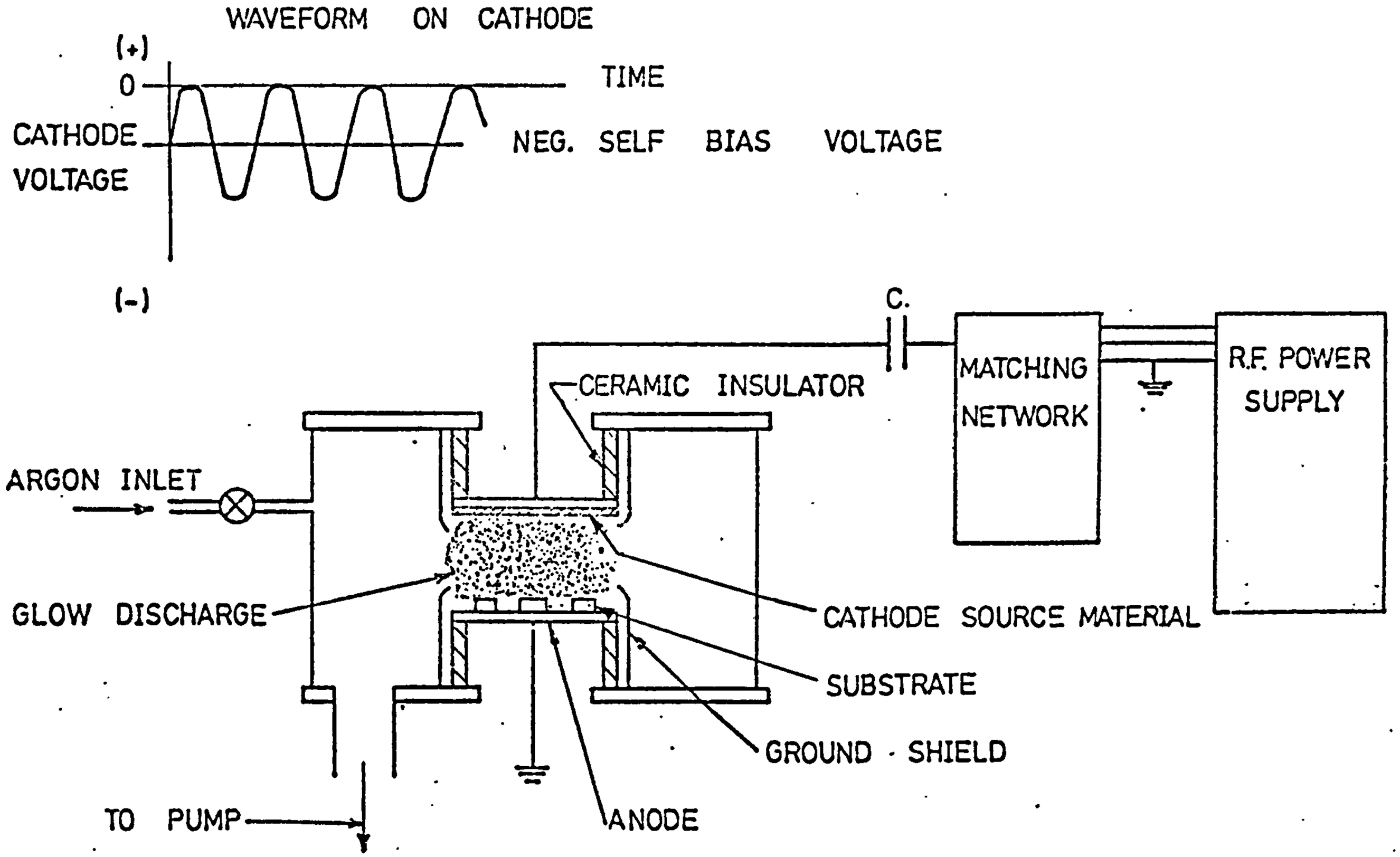

FIGURE 2. 6.

SCHEMATIC DIAGRAM OF R.F. DIODE SPUTTERING SET UP[19]

voltage becomes approximately equal to half of the peak-to-peak rf voltage.[19] To sputter insulating targets they are placed behind a cathode made of very thin wire mesh.

2.5.1(d) Asymmetrical

The substrate in a diode sputter deposition system is exposed to bombardment of positive ions and electrons.[36] In general, sputter - deposited films are prone to impurities such as adsorbed and trapped gases. The adsorbed gas molecules such as hydrocarbons can cross link[36] to each other and form films of polymer contaminants on the deposited film as a result of bombardment by high energy electrons. Bombardment by heavy particles e.g. energetic neutrals, and positive ions (which is very slight compared to the electrons bombardment) is thought to cause[37] the impurities to be preferentially removed out of the growing film. Thus if the substrate is held at a negative H.T. voltage[36] the growing film will be subjected to ion bombardment and gas molecules combining with sputtered atoms would tend to be removed from the growing film.[37,38] This results in a purer film. The amount of sputtering at the substrate must be less than that of the cathode to achieve growth of deposited film. Thus the magnitude of the negative H.T. voltage at the substrate must be less than that of the cathode. Hence it is known as asymmetrical sputtering system.

Frericks[38] suggested the asymmetrical sputter deposition technique, the basic arrangement of which is shown schematically in Figure 2.7(a). In this system the extent to which the impurities are removed depends upon the ratio of sputtering current at the substrate to that of the cathode. This is done by the variable resistor of the rectifier of the a.c. H.T. supply circuit.

Maissel and Schaible[37] suggested the alternative asymmetrical sputter deposition arrangement shown in Figure 2.7(b). This is known as the bias sputtering method in which a negative d.c. bias voltage is applied to the growing film throughout the entire deposition period. Maissel and Schaible claimed that, with this method, a more effective (compared to a.c. asymm-

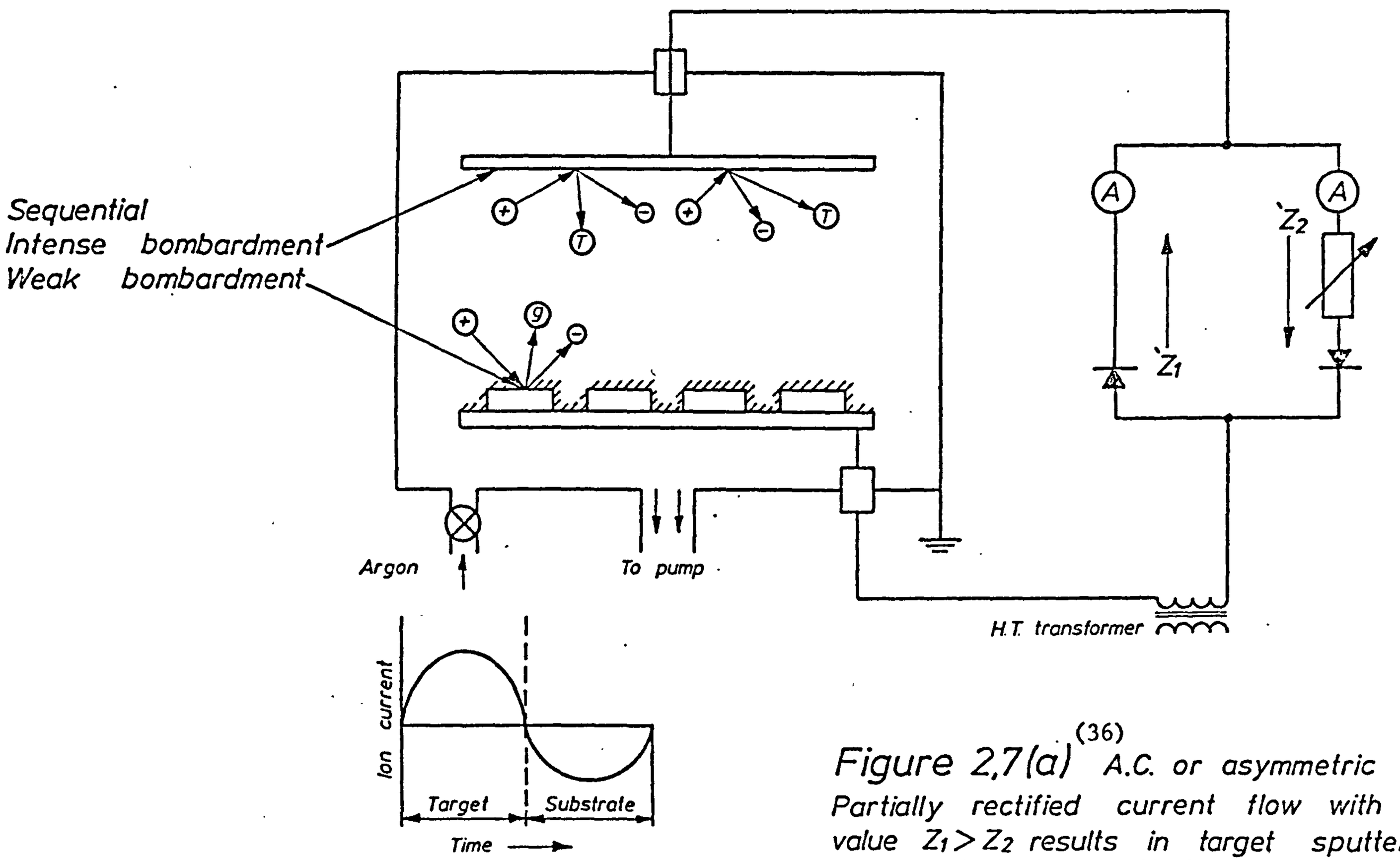

Figure 2,7(a) [36] A.C. or asymmetric system. Partially rectified current flow with average value $Z_1 > Z_2$ results in target sputtering and weak substrate sputtering sequentially

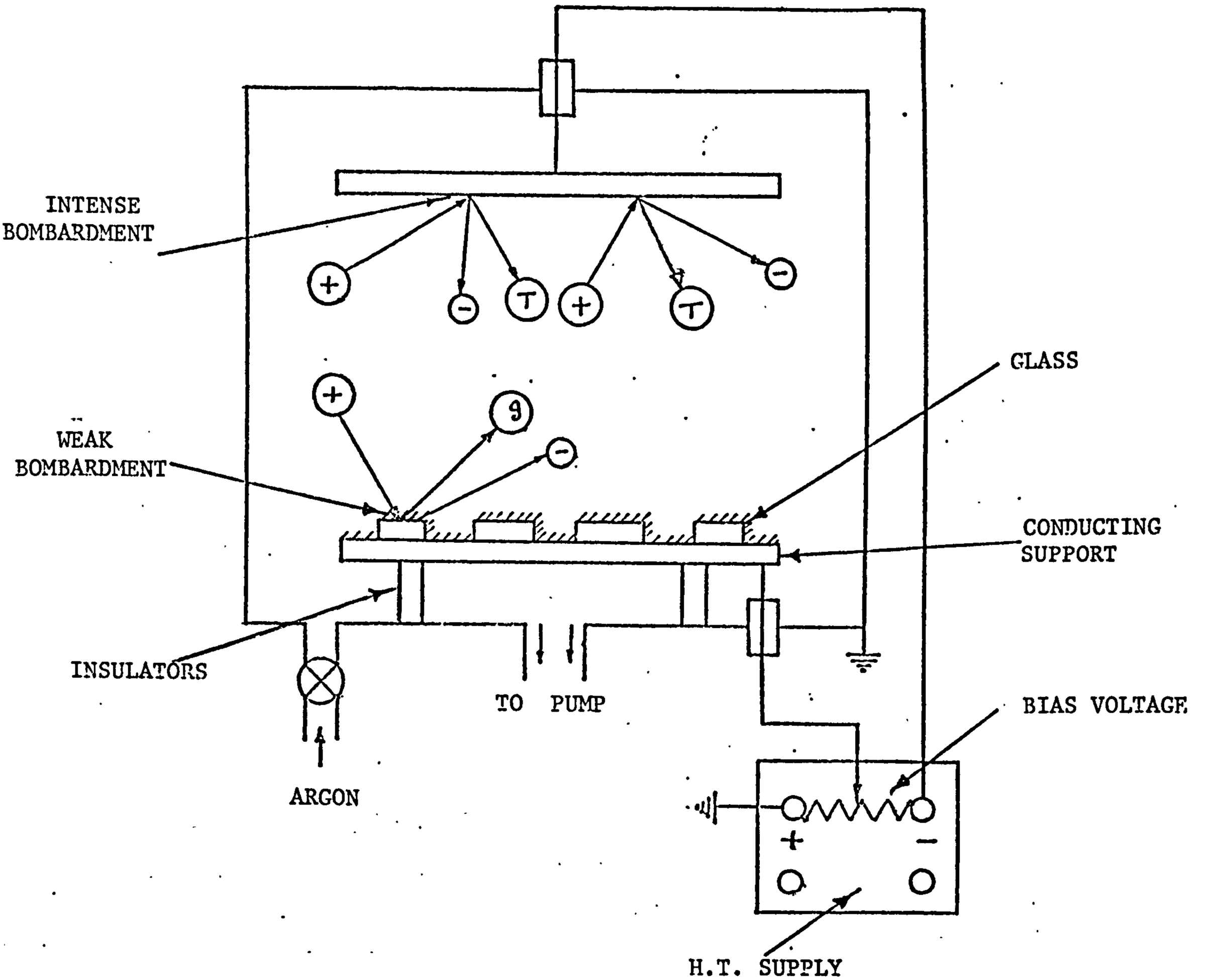

FIGURE 2.7(b) SCHEMATIC DIAGRAM OF BIAS SPUTTERING SYSTEM[36]

etrical method) removal of impurities from a tantalum film has been obtained.

2.5.1(e) Reactive Sputtering

Chemical reaction may take place between active gas(es) in the sputtering atmosphere and particles at the cathode, or sputtered deposits. This is the principle of operation of reactive sputtering method in which active gases are introduced into the discharge to prepare films of metal compounds.[39-41] The sputtering rate and the active gas concentration will affect the film, and it is therefore, necessary to control both these factors to prepare films with desired specifications. At high reactant pressures, according to Schwartz[39] and Krikorion and Sneed,[40] the reaction may take place at the cathode, the product being removed during subsequent sputtering, whereas at low partial pressures of the reactant a reaction at the film surface during growth is expected. At intermediate reactant pressures a combination of both of these possibilities is expected. Sputtering is usually done in argon because of its high sputtering rate. Both the composition and deposition rate of the film is affected by the partial pressure of the active gas, according to Holland,[41] who listed the mechanisms that can occur during reactive sputtering as:-

1. Formation of insulating film, such as Ta_2O_5, on the target can result in accommulation of positive charges on its surface which in turn reduces the energy of the impinging ion.
2. A rise in secondary electron emmision can cause a reduction in the fraction of the total measured current due to ion flow for an oxidised target.
3. Presence of active gases such as O_2 and N_2 reduces the overall sputtering yield since the molecular weights of these gases are lower than that of argon.
4. If the target is covered with gaseous reaction products (e.g. MeO), energy is dissipated in sputtering the gas component (e.g. O_2) which return to the cathode to recombine.
5. It may be possible to form a compound film by either sputtering the

metal compound or the pure target metal with subsequent gas reaction at the receiver.

6. Ion migration of oxide films (known as anodic oxidation) can be caused if there are negative ions such as $\bar{O}$ and $\bar{O}_2$ in the discharge which bombard a receiver at anode potential.

7. If gas is added to the condensing metal (e.g., $Me + O_2 \longrightarrow MeO_2$) and compound formation takes place at the receiver there will be an enhancement in the mass growth rate of the film. There will also be an enhancement in the thickness growth rate if the compound formed at the receiver occupies a greater volume than the metal it contains.

All the above effects tend to be operative in reactive sputtering.(41) In any particular case some of the effect(s) are more dominant depending on the target/gas combination, deposition conditions and apparatus design. The composition and structure of deposited film in reactive sputtering, vary with partial pressure of active gas and other deposition conditions.

2.5.2 Assessment

The density of sputter deposited films is high, sometimes approaching the bulk density of the film material.(20) This is due to two main factors; The first is related to the energy with which the film atoms and molecules (which is one or two order of magnitude higher than that of the evaporated particles)(6,12-14) arrive at the substrate and the second, which is primarily responsible for high density of sputter deposited films, is associated with the reactive or preferential re-sputtering of losely bound atoms in the film lattice.(20,23)

The adherence of sputter-deposited films to their substrate is quite high.(12-14,21-26) This is mainly due to the thorough surface cleaning prior to and during film deposition and also to the heat produced at the substrate surface as a result of conversion of kinetic energy of the arriving film atoms and molecules to thermal energy, upon impact.

With the sputter deposition technique it is possible to achieve film

uniformities of between ±2% to ±5%.[14,20] This is done by placing the substrate at a distance of 1 - 3cm to the Crookes dark space on the anode side and in the flat zone of the cathode radiation pattern.

Three dimensional surface coating is also possible using the sputter deposition technique.[6,12-14,21-26] This is because the throwing power of the ionised film particles is much greater than that of the evaporated particles in thermal evaporation technique.

The largest contamination source of sputter-deposited films is argon inclusion but is has never been shown to be detrimental to the electronic characteristic of the films.[20-24] Other important advantages of sputter deposition technique are low material cost, in the long run, and the short change-over time to another substrate of usual shape and geometry. However, sputter deposition technique suffers from a number of limitations. The most important of which are long cycle time, long change-over time to another film material and finally the most important of all low deposition rate.

2.6 Ion Plating

In recent years ion plating has been developed as a very important method of depositing films. The technique of ion plating was first reported by Mattox,[42] and since that time it has been developed to a great extent. Using the ion plating technique it is now possible to produce not only thin films but also relatively thick films with excellent adherence and other desirable dominant mechanical chemical and electrical characteristics such as high corrosion and wear resistance, and excellent electrical contact properties.

2.6.1 Method

Ion plating is, in some ways, a cross between the thermal evaporation and sputter deposition techniques.[42-46] A schematic diagram of a typical ion

plating apparatus is shown in Figure 2.8. It comprises a vacuum chamber with specimen and vapour source , a pumping system similar to those associated with the thermal evaporation and sputter deposition techniques plus an inert gas inlet into the chamber. The component to be coated is made the negative electrode of a d.c.glow-discharge, usually run in argon, and the evaporation source,which can be either a resistance heated filament or boat or an electron gun,is made the anode. A typical ion plating procedure is as follows: (42-49)

(i) the specimen is degreased and mounted on the cathode electrode of the discharge in such a way as to ensure good electrical and thermal contact(the reason for the latter is to facilitate specimen cooling should the need arise),

(ii) the vapour source is loaded with coating material.

(iii) the chamber is pumped down to a pressure of 10^{-5} torr or less to ensure further cleanliness of the specimen by outgassing.

(iv) the chamber is then backfilled with inert gas (usually argon) to a pressure in the range between 5×10^{-2} torr and 1×10^{-2} torr. The gas flow rate is controlled by means of the inert gas inlet valve and partial closure of the baffle valve on top of the diffusion pump.

(v) a negative H.T. of between 1kV and 5kV is applied to the specimen and an abnormal cold cathode glow discharge is struck between the earthed part (vapour source) of the apparatus and the specimen. (27,28)

(vi) after attaining a steady value of the discharge current the vapour source is energised and the coating material is vapourised into the discharge and deposited on the substrate surface.

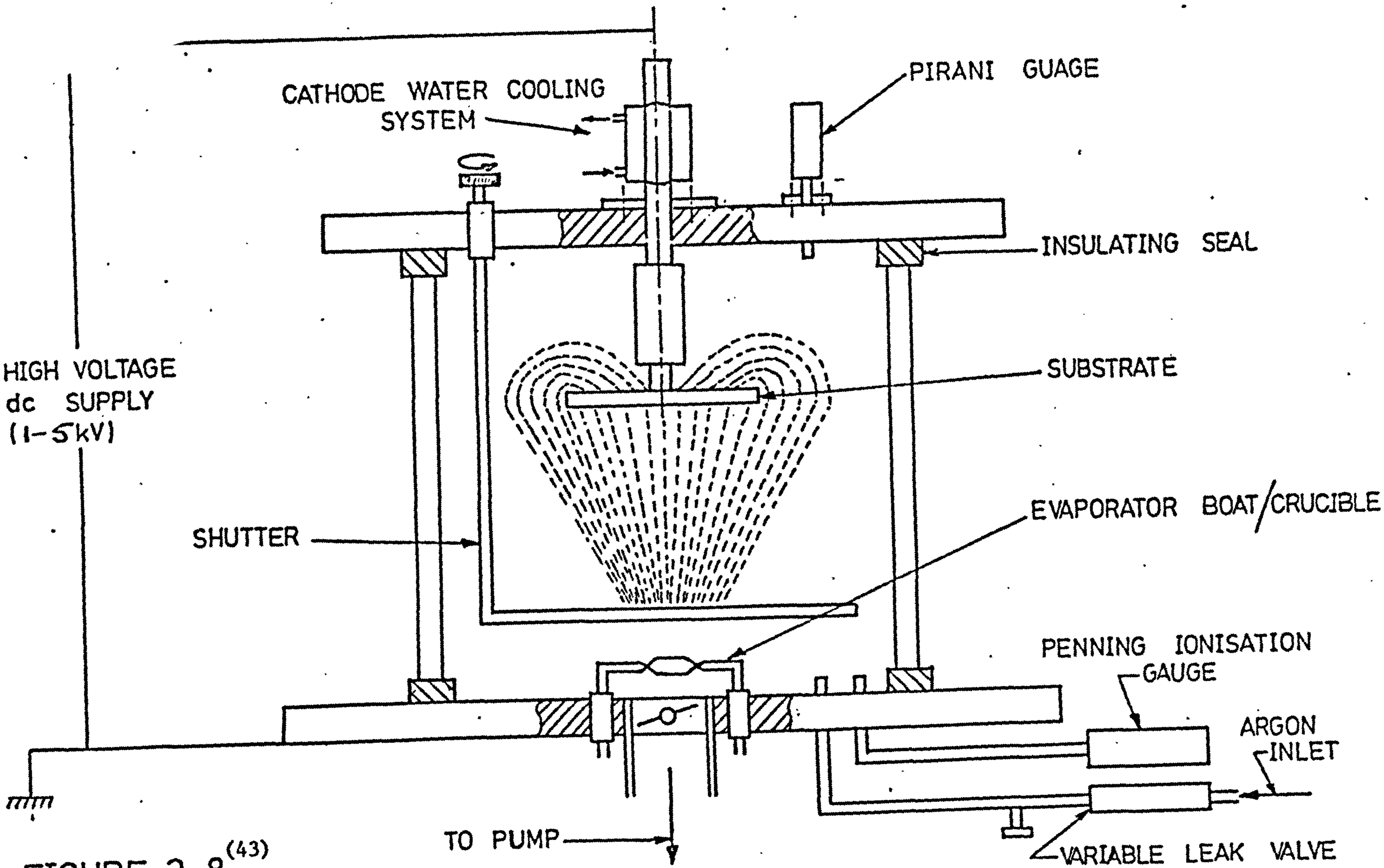

FIGURE 2.8.[43]

SCHEMATIC DIAGRAM OF ION PLATING SET-UP

In the ion plating process, as soon as the discharge is formed, gas atoms/molecules in the discharge are ionised primarily as a result of electron gas atom/molecule collision[45]

$$\bar{e} + G^{o} \rightarrow G^{+} + 2\bar{e}$$

where G^{o} is a neutral gas atom/molecule and G^{+} is a singly charged gas ion. The ions formed are accelerated across the cathode dark space and follow the electric lines of force (see Figure 2.8) to all points on the specimen surface. In this process many of the ions are neutralised by charge exchange collisions with gas atoms [50]

$$\underset{\text{fast}}{G_1^{+}} + \underset{\text{slow}}{G^{o}} \longrightarrow \underset{\text{fast}}{G_1^{o}} + \underset{\text{slow}}{G_2^{+}}$$

Since the electric field is at its maximum in the Cathode dark space, most of the discharge voltage is dropped across it; ions leaving the negative glow are accelerated towards the cathode. In the absence of collisions in the dark space they would reach the cathode with an energy corresponding to the full discharge voltage. However, the short mean free path for charge exchange leads to a significant broadening in the ion energy distribution and the production of energetic neutral particles. These particles also reach the substrate with a broad energy distribution. On impact of these ions and neutrals with the substrate surface sputtering takes place resulting in the removal of contaminating films. It is important to note that this cleaning process takes place during the discharge period prior to evaporation of the coating material i.e. before film deposition, and continues during the deposition process. In fact, the initial instabilities [42-49] in the discharge are related to the changes in the cathode (substrate) surface during this sputter cleaning process and a stable discharge current is often taken as an indication that the bulk of contaminant material has been

removed from the substrate surface. Also the introduction of the coating material vapour into the discharge causes ionisation (less than 0.1%)[51] of the vapour atoms. The film material particles undergo the same ionisation and collision process as the carrier gas particles before reaching the substrate and contributing to formation of the film. It is also important to note, however, that in most cases a major portion of the coating material vapour atoms/molecules reach the substrate surface(s), facing the vapour source, with their thermal energy.[52]

Thus, summing up the works of Mattox,[42,44-46,49] Spalvins[47] and Davis and Vanderslice[50] one can conclude that there are two competing phenomena occurring simultaneously at the surfaces of the substrate in ion plating. They are:-

1. The deposition of the coating material ions and neutrals, and
2. The sputtering of the deposit by the carrier gas and coating material ions and neutrals.

The effective rate of deposition is determined by the relative rates of these two phenomena and to form a film it is obviously necessary for the deposition rate to exceed the sputtering rate.

2.6.2 Assessment

It has already been pointed out that ion plating can be described as a combination of both the thermal evaporation and sputter deposition methods of coating and in this context it effectively combines the advantages of the two contributing techniques. The main advantages of ion plating compared to non-vacuum and alternative vacuum methods of coating are:

1. Fully dense fine-grained and pore free coatings can be produced which have excellent adhesion. In fact it is this combination of properties that has generated great interest in ion plating, particularly for application of corrosion resistant layers. Excellent adhesion can be achieved even if the coating and substrate material combinations are normally incompatible.

2. Metallic, ceramic and plastic substrates can be coated.
3. Complex alloy coatings can be deposited with good control of structure and composition.
4. High deposition rates (up to 0.025 mm/min) can be achieved.
5. Substrates are sputter cleaned prior to deposition thus eliminating the necessity for extensive pre-cleaning.
6. The process has good throwing power and complex geometries can be coated without resorting to substrate rotation.
7. Large numbers of components can be barrel ion plated, obviating the need for individual component jigging.
8. Ion plating is a dry process, therefore no effluents containing heavy metals and cyanides are produced to give rise to disposal problems. This feature has motivated the interest in vacuum coatings methods among which ion plating enjoys the maximum number of advantages.

At this stage it should be pointed out that these advantages do not necessarily rule out the usefulness of any of the methods discussed earlier in this chapter, in particular applications. And again, as has been discussed above, the most important feature of ion plating is production of thick and highly adherent films which fulfills a number of important engineering requirements such as increasing wear and corrosion resistance of materials plus the provision of low friction. It can also be used for decorative purposes. Regarding the operational consideration of ion plating it is a technique with the shortest cycle time but the change over to another substrate can be quite time consuming.

2.7 Discussion

Various methods of coating are reviewed and assessed in this Chapter. Ion plating which is of primary interest in the present work is now an established vapour deposition technique with a wide range of applications in those situations where excellent adhesion, high deposition rate, good throwing power and improved density and uniformity together with improved grain structure of pore free deposited films are of prime importance. Ion plating is now considered as an effective, yet economical,means of depositing a wide variety of materials. In a broader sense, it offers a realistic method by which a given part can have a surface characteristic of a broad range of materials from which a designer may choose. Ion plating offers the possibility of deposition at significantly lower substrate temperature than are necessary in chemical vapour deposition. It has recently been[53] used in coating of tools with refractory metal carbides and nitrides. Also the fact that ion plating produces no effluent to the environment is of immense significance in the view of present and future ecological considerations.

However, it must be pointed out that although ion plating enjoys all the above-mentioned advantages very little is known about its actual mechanisms, particularly with reference to the excellent adhesion. In fact the progress of the theory of ion plating lags, dramatically, behind its progress in practical applications, and very little work has, so far, gone into the physics of the technique . Although some workers have shown interest in understanding the problem, very few substantial conclusions have emerged so far. One of the earliest positive steps taken,in the investigation of the mechanism of ion plating, was at the Department of Electrical Engineering of the University of Salford in 1974. The work described in this thesis is concerned with this investigation.

2.8 References - Chapter 2

1. Bremer A. "Electrodeposition of Alloys" vol.1. Chapter 2. Academic Press New York, London 1963.
2. Graham A.K. "Electrodeposition Engineering Handbook" Part 1, Van Nostrand Reinhold Co. New York, Cincinnati, Toronto, London, Melbourne, 1962.
3. Lowenheim F.A. "Modern Electroplating" Third Ed. John Willey and Sons inc. New York, London, Sydney, Toronto, 1974.
4. Soohoo R.F., "Magnetic Thin Film" Chapter 2, Harper & Row New York, Evanston, London 1965.
5. Anderson J.C. The Use of Thin Films in Physical Investigations"Chapter 5 Academic Press, London New York 1966.
6. Chopra K.L. "Thin Film Phenomena" Chapter 2, Mc Graw Hill book Co., New York, St. Louis, San Francisco London 1969.
7. Sims R.I. Proc. Int. Conf. on Ion Plating and Allied Techniques. Edinburgh 1977.
8. Tauri Y., Teshima H., Okara K & Minamiya A. J. Electrochem. Soc. 114, P. 145, 1967.
9. Van den Berkel C.H.J. Philips Research Report, 32 P. 118, 1977.
10. Van den Berkel C.H.J. Ibid, 32 P.134, 1977.
11. Salem F. Ph. D. Thesis, Department of Mechanical Engineering, University of Salford 1977.
12. Holland L. "Vac. Dep. of Thin Films" John Willey & Sons Inc. New York 1956.
13. Holland L. "Thin Film Microelectronics" Chapter 1 John Willey & Sons Inc. New York 1956.
14. Maissel L.I. & Glang R. "Handbook of Thin Film Technology" Chapter 1, New York 1970.
15. Anderson J.C. "The Use of Thin Films in Physical Investigations" Chapter 2, Academic Press,London, New York 1966.
16. Holland L. Electronic Components P. 181, 1970.
17. Redhead P.A., Hobson J.P. & Kornelson E.V. "The Physical Basis of Ultra-High Vacuum "Part C., Chapman and Hall Publ. Co., London 1968.

18. Pirani M. Yarwood J. "Principle of Vacuum Engineering" Chapter 2, Chapman and Hall Publ. Co. London 1961.

19. Hoffman V., Solid State Technology, P.93, Dec 1973.

20. Verga J.E. Baily W.A., Solid State Technology P.79, Dec 1973.

21. Buckley D., Spalvins T. NASA Special Publ. SP 5111 March 1972.

22. Wehner G. Ibid, P.59, March 1972.

23. Lamont L. Ibid, P.139, March 1972.

24. Holland L. Electronic Components P. 285 March 1970.

25. Coburn J.W., Kay E. Appl. Phys. Letters 18 P.435, 1971.

26. Coburn J.W. Kay E. Ibid, 12, P. 4965 1972.

27. Brown S.C. Introduction to Electrical Discharges, Wiley, New York and London 1966.

28. Nasser E, Foundamentals of Gaseous Ionisation and Plasma Electronics, Wiley - Interscience, New York, London, Sydney, Tronto 1971.

29. Westwood W.D., J.Vac. Sci. Technol. 15, No. 1, P.1, Jan 1978.

30. Wehner G., Sputtering Science and Technol. Sep. 1968.

31. Anderson J.C. Ref. 15 Chapter 3,

32. Tisone T.C., Cruzon P.D., J.Vac. Sci. and Technol. 12, P.1058, 1975.

33. Ryden W.D., Bindell J.B., Holschwender L.H. & Labuda E.F. J.Vac. Sci, and Technol. 15, No. 2, P.290, 1978.

34. Gaweh H., Agnew Z, Phys. Rev. 14, P.126 1962.

35. Anderson G.S., Mayer W.N. & Wehner G.K., J. Appl. Phys. 33, P.2991 .962.

36. Holland L., Electronic Components, P. 429, April 1970.

37. Maissel L.I., Schaible P.M., J. Appl. Phys. 36 No. 1, P.237, 1965.

38. Ferichs R., J. Appl. Phys. 33, P.1898, 1962.

39. Schwartz N. American Vac. Soc., 10th National Vac. Symp. P.325, MacMillan, New York, 1963.

40. Krikorian E. and Sneed R.J., J. Appl. Phys., 37, P.3674, 1966.

41. Holland L., Electronic Components, P.533 May 1970.

42. Mattox D.M. J. Appl. Phys. 34, P.2403, 1963.

43. Teer D.G. Tribology International P. 247, 1975.

44. Mattox D.M. J. Electrochem. Technol. 2, P.295, 1965.

45. Mattox, D.M. J. Vac. Sci. and Technol 10, P.47, 1973.

46. Mattox D.M. Sandia Lab. Report No. SLA. 73 - 0619 June 1973.

47. Spalvins T. Pamphlet No. 438, Corp. Develop. Lab. Brit. Steel Corp. Sheffield Feb. 1975.

48. Chambers D.L., Carmichael D.C., Research/Development, Airco Temescal May 1971.

49. Mattox D.M., Sandia Corp. Monograph SC - R.65 - 852.

50. Davis W.D., Vanderslice, T.A., Phys. Rev. 131, No. 1, P.219, 1963.

51. Teer. E.G, Delcea B.L., Proc. Int. Conf. on Ion Plating and Allied Techniques(IPAT) P.58 Edinburgh 1977.

52. Teer D.G Conf. on Ion Plating Oct. 1980.

53. Harwell Ceramic Centre, Commercial Office, Harwell Design Studio 19/1977.

54. Ahmad. N.A.G.M.Sc. Dessertation, Electrical Engineering Department, University of Salford, 1974.

CHAPTER III

THEORY OF ION PLATING

CHAPTER 3

THEORY OF ION PLATING

3.1 Introduction

3.2 Formation of Ions and Ionisation Efficiency in a Typical Ion Plating Discharge

3.3 Energy Distributions of Particles Impinging on the Substrate.

- 3.3.1 Nature of the Impinging Particles
- 3.3.2 Energy Distributions of Ions
- 3.3.3 Energy Distributions of Neutrals
- 3.3.4 Reported Experimental Observations

3.4 Surface Impact Phenomena

- 3.4.1 Sputtering
- 3.4.2 Surface Cleaning
- 3.4.3 Sputter-Redeposition
- 3.4.4 Cascade Mixing
- 3.4.5 Radiation Damage
  - 3.4.5(a) Irradiation Enhanced Diffusion
  - 3.4.5(b) Carrier Gas Entrapment
- 3.4.6 Recoil Implantation
- 3.4.7 Thermal Diffusion
- 3.4.8 Summary of Interface Broadening Effects.

3.5 Factors Affecting Characteristics of Ion-Plated Films

- 3.5.1 Adhesion
- 3.5.2 Throwing Power
- 3.5.3 Purity

3.1 Introduction

As briefly discussed in Chapter 2, ion plating is a generic term applied to a film deposition process in which part of the vapourised film material is ionised before it makes contact with the surface being coated. The substrate, in this technique, forms the cathode of an abnormal glow discharge (discussed in Section 2.3) in which the current density is a function of voltage at constant pressure. The ionisation mechanism of the gas in the glow discharge is briefly discussed in Section 2.5.

The substrate is sputter cleaned, i.e. surface contaminants and barrier layers are removed, by inert gas ion (and neutral particle) bombardment prior to deposition of the film material. The deposition then starts with the evaporation of film material into the discharge without interruption of the bombardment. The high electrical potential of the discharge accelerates the ionised inert gas and film material particles towards the biased cathode. The collision between particles in the discharge also results in knocking a number of unionised film material particles towards the cathode and results in the production of dense, porefree and adherent coatings. The technique exhibits higher throwing power (i.e. all sides of the substrate, including cavities, to a certain extent, are covered) than the simple evaporation. The high throwing power and adhesion of ion-plated films are two important characteristics of the ion plating technique which have received considerable attention.

To optimise the film characteristics (in ion plating) it is obviously essential to optimise deposition parameters such as discharge pressure, carrier gas species, evaporation rate, substrate surface condition, and substrate temperature. It is thus necessary to understand the way in which the plating mechanisms depend on both the gaseous discharge and ion surface interaction phenomena. A study of the energy and mass distributions and charge state of the atomic particles arriving at the substrate, together with an investigation of the composition and

structure of the film and film-substrate interface is therefore essential if the basic ion plating mechanisms are to be understood.

In this Chapter, a brief review of ionisation efficiency in a typical ion plating discharge and the basic processes involved in ion plating are discussed. Also, simplified theoretical expressions for the energy distributions of particles impinging on the substrate, together with a theoretical treatment of film-substrate interface broadening in ion plating are presented.

3.2 Formation of Ions and Ionisation Efficiency in a Typical Ion Plating Discharge.

As has been discussed earlier, ion plating is carried out in an abnormal glow discharge with an inert gas pressure of about 1×10^{-2} torr. The ionisation processes occurring in glow discharges are briefly discussed in Section 2.5.

Of particular interest in ion plating is the ionisation efficiency and a number of estimates have been made of this parameter for typical plating discharges. Lundin,[1] for example, estimated an ionisation efficiency of about 30%. This estimate was based on the fact that the thickness of the coating on the back surface of a flat ion-plated substrate was about 30% of the thickness on the front surface. The assumption that Lundin[1] made was that the back surface coating was due to ions only whereas that on the front surface was due to both ions and netural particles. However, referring to mechanisms of transport of particles to the cathode of ion plating discharge, discussed in Section 3.5, it can be seen that this assumption is incorrect and that this estimate of ionisation efficiency can be discounted as being excessively high. Aisenberg,[2] on the other hand, claimed that the ionisation efficiency under typical ion plating conditions cannot be more than 1%. Teer[3] performed two different experiments to measure the ionisation efficiency. In one of the experiments he worked out the

sum of the total number of ions arriving at the cathode, during the actual deposition period of the process , from the measured current and compared this figure with the total number of atoms deposited as calculated from film thickness measurement. An ionisation efficiency of about 1% was calculated based on the assumption that all the ions arriving at the cathode were those of the coating material. As can be seen (regarding the assumption made) this estimate is more than the actual value. This is because it is highly probable that many of the ions arriving at the cathode would be inert gas ions. In the second approach, Teer[3] measured the total current to the substrate. The current, of course, consists of ions arriving at, and electrons leaving the cathode. The current was compared with the number of atoms striking the cathode, per second, at the gas pressure in which the discharge was struck. Such comparison gave ionisation efficiency figures of about 0.1%. Although it is clear that reliable measurements have not yet been carried out, these comparatively crude estimates have shown quite convincingly that under typical ion plating conditions the ionisation efficiency is less than 1%.

3.3 Energy Distributions of Particles Impinging on the Substrate

One of the important quantities associated with discharge plating is the energy distribution of the particles striking the cathode. A knowledge of this distribution will be relevant to any understanding of the surface phenomena occurring at the cathode. This, in turn, will shed more light on the reasons for the good adhesion obtained in ion plating. The energy distributions of ions and neutrals in a glow discharge are discussed, separately, in this Section.

3.3.1 Nature of the Impinging Particles

In the early years of ion plating, the film growth was mainly

attributed to the substrate being coated only with ions of the coating material. However, the very low ionisation efficiency (see Section 3.2) in a typical ion plating discharge, raised the question as to how the properties of the deposited film could be affected so strongly by the impingement of a small number of energetic ions?. As further studies were carried out it became increasingly apparent that the energetic film material ions made a relatively minor contribution to the primary deposition process.

Under typical ion plating conditions (an inert carrier gas pressure of 10μ and a discharge voltage of about 3kV) mean free paths are of the order of 0.5cm and the cathode dark space is a few centimetres wide. Under these conditions the particles leaving the negative glow suffer collisions in the dark space region. For the energies in question, the cross-section for charge transfer collisions (certainly for the resonant reactions involving carrier gas ions in the carrier gas) are very high and hence both the energy and charge state of the particles actually reaching the cathode will be determined, to a large extent, by charge exchange collisions in the dark space as well as elastic scattering. In fact, it is probably reasonable to assume that charge exchange reactions of the form

$$\underset{\text{fast}}{X^+} + \underset{\text{slow}}{X^o} \longrightarrow \underset{\text{fast}}{X^o} + \underset{\text{slow}}{X^+}$$

described by the cross-section σ_{10} completely dominate the collision process. Since the slow ions produced in these reactions are subsequently accelerated towards the cathode and suffer further charge exchanging collisions it is clear that production of the ultimate energy distributions of both ionised and neutral particles must involve a detailed knowledge of the atomic collisions processes occurring in the dark space.

3.3.2 Energy Distribution of Ions

An expression describing the distribution of ion energies in a glow discharge has been derived by Davis and Vanderslice[9] on the basis of a number of simplifying assumptions. The assumptions are that all ions originate in the negative glow, that the electric field varies linearly from the cathode to the edge of the negative glow, that only symmetrical charge transfer collisions are responsible for the energy spectrum, and that the collision cross-section does not change with energy. Teer[10] followed the approach used by Davice and Vanderslice but with different boundary conditions such that equivalent, but simpler, expressions were obtained. The derivation of these expressions are as follows:-

Referring to Figure 3.1 the boundary conditions are:

$V = 0$ $\quad x = 0$ at the edge of the negative glow

$V = V_c$ $\quad x = L$ at the cathode.

The field strength varies linearly, thus

$$\frac{dV}{dx} = K \frac{x}{L} \qquad 3.3.1.$$

and

$$V = \frac{K}{2L} x^2 + A \qquad 3.3.2.$$

From the boundary conditions $A = 0$ and $K = \frac{2V_c}{L}$, thus

$$V = \frac{V_c}{L^2} x^2 \qquad 3.3.3$$

If N_o is the number of ions leaving negative glow, then the number

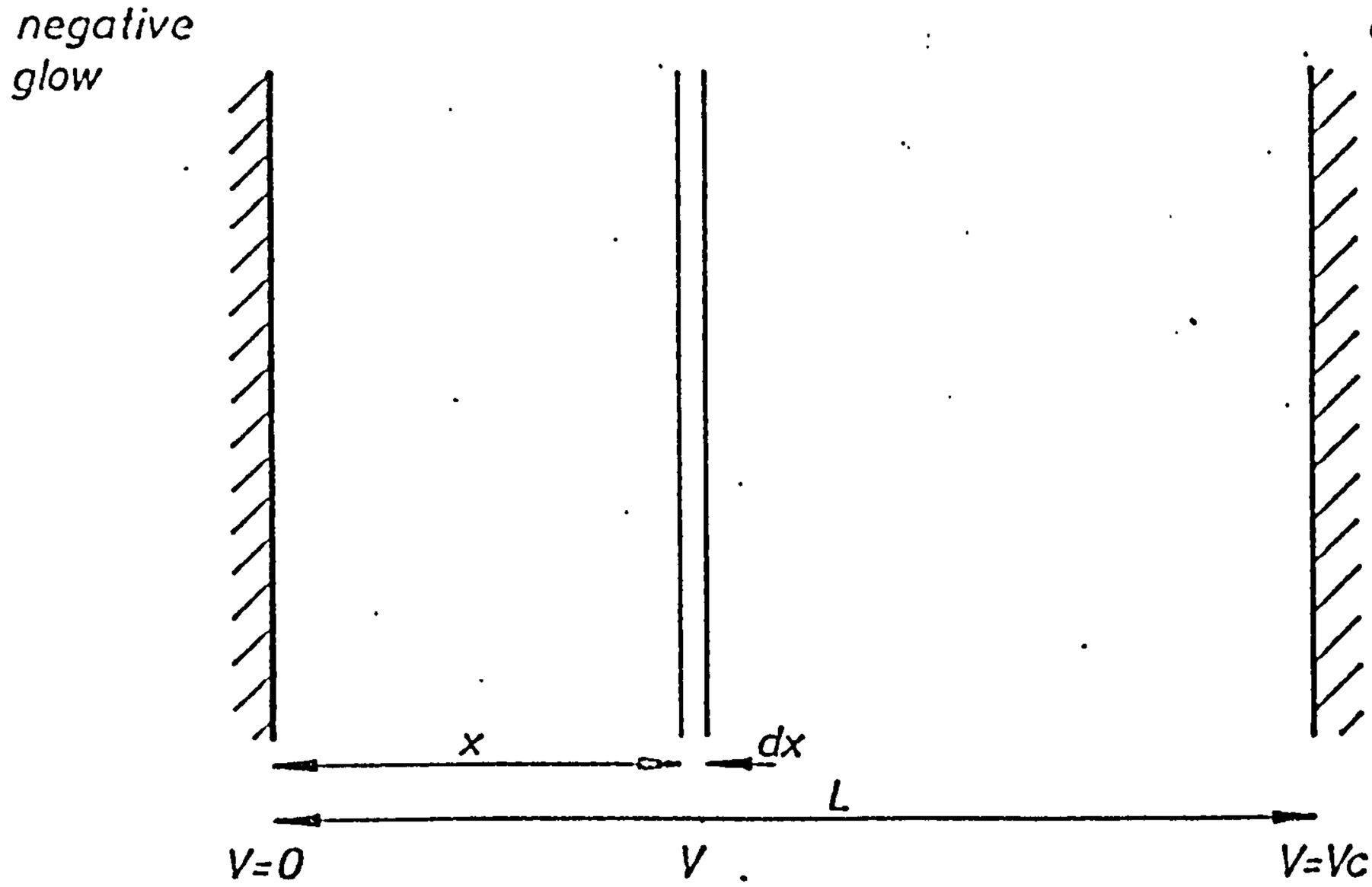

Figure 3,1 *Representation of cathode dark space used in the calculation of ion energies*

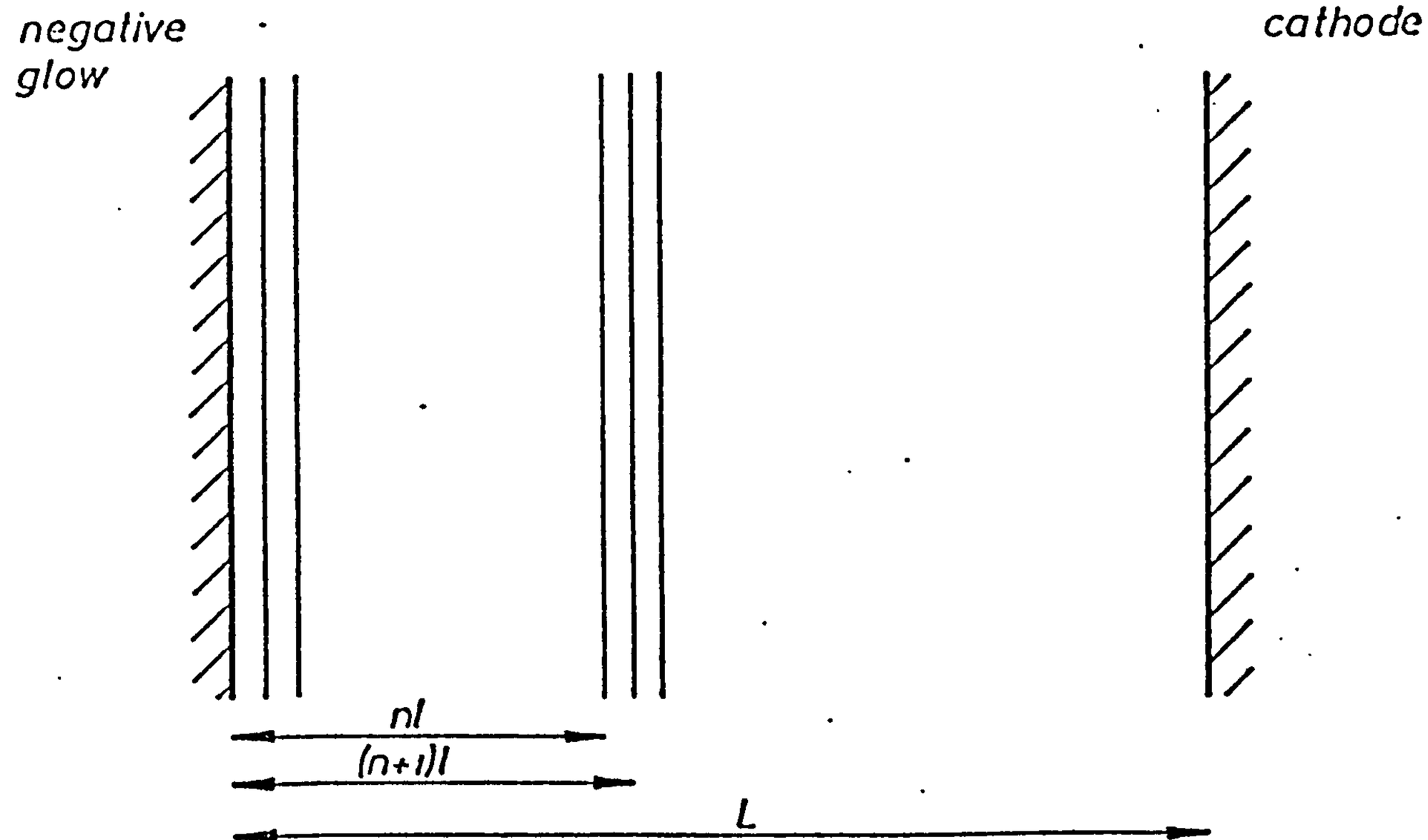

Figure 3, 2 *Representation of cathode dark space used in the calculation of neutral energies*

of collisions between x and x+dx is $N_o \frac{dx}{d\ell}$ where , ℓ , is the mean free path for the charge transfer collisions.

Now, the probability of any ion resulting from collisions, between x and x + dx, reaching the cathode without further collisions is given by by $e^{-\frac{L - x}{\ell}}$. Hence the number of ions arriving at cathode with energy of $(V_c - V)$ electron volt is:-

$$dN = \frac{N_o}{\ell} \exp\left(-\frac{L - x}{\ell}\right) dx \qquad 3.3.4$$

Substitutiong from expression 3.3.3

$$dN = \frac{N_o \cdot L}{2\ell\sqrt{V\, V_c}} \exp\left(-\frac{L - L\sqrt{\frac{V}{Vc}}}{\ell}\right) dV \qquad 3.3.5$$

This is equivalent to the expression derived by Davis and Vanderslice[9]

The total ion energy, E_{ti}, arriving at the cathode is given by:-

$$E_{ti} = \int_{V=0}^{V=V_c} (V_c - V)\, dN \qquad 3.3.6$$

Evaluation of this integral results in:-

$$E_{ti} = N_o V_o \left(\frac{2\ell}{L} - \frac{2\ell^2}{L^2} + \frac{2\ell^2}{L^2} \cdot e^{\frac{-L}{\ell}} - e^{\frac{-L}{\ell}}\right) \qquad 3.3.7$$

If no collision occurs, the ions leaving the glow would be responsible for the total energy deposited at the substrate. Since the

energy of each ion is e V_c the total energy is N_o e V_c. However, because of collisions, the actual ion flux reaching the cathode contains particles with widely differing energies, depending on the position of the final charge exchange in which they are involved. At the same time, fast neutrals formed in these collisions also make a contribution to the energy deposition and this contibution increases as $\frac{\ell}{L}$ decreases i.e. as the number of collisions increases.

When a single fast particle moves through a small distance dx the probability of a collision in this distance is given by:

$$P = \frac{dx}{\ell} = n \sigma dx \qquad 3.3.8$$

where , ℓ , is mean free path, n is density and σ, in our case, is the cross-section for charge exchange. The number of moving particles at a distance x is:

$$N = N_o \exp(-n \sigma x). \qquad 3.3.9$$

and when x = L

$$N = N_o \exp\left(-\frac{L}{\ell}\right) \qquad 3.3.10$$

3.3.3 Energy Distribution of Neutrals

Delcea and Teer[8,11] worked out expression for energy distribution of neutrals in a glow discharge after making a number of simplifying assumptions. The assumptions are that the space between the negative glow and the cathode is divided into $\frac{L}{\ell}$ equal regions, that the charge

transfer collisions occur only at the boundaries between these regions, i.e. all collisions take place after an ion has travelled a distance ℓ (the mean free path), and that the neutrals so formed travel to the cathode without further collision. These assumptions of course, are very crude and the latter, in particular, is seriously in error, in view of the large scattering cross-section, but it does not affect[8,11] the overall result for the calculation of the total energy of the neutrals, reaching the cathode, which can be estimated from experimental measurements[8,11] since stripping cross-sections are very low at these energies.

Referring to Figure 3.2, the voltage at $n\ell$ is $V_c \frac{n^2\ell^2}{L^2}$ and the voltage at $(n+1)\ell$ is $V_c \frac{\ell^2}{L^2}(n+1)^2$. Thus the energy of ions at $(n+1)\ell$ is $V_c \frac{\ell^2}{L^2}(n+1)^2$. These ions undergo charge transfer collisions at $(n+1)\ell$ producing neutrals of equal energy. The number of collisions at each plane is N_o and, therefore, there are N_o neutrals formed at $(n+1)\ell$ with energy of $V_c \frac{\ell^2}{L^2}(2n+1)$ and this gives the energy distribution of neutrals. The total energy contained in neutrals, $E_{t,n}$, is:-

$$E_{t,n} = \frac{N_o V_c \ell^2}{L^2} \sum_{o}^{\frac{L}{\ell}-2} (2n+1) = N_o V_c \left(1 - \frac{2\ell}{L} + \frac{\ell^2}{L^2}\right) \qquad 3.3.11$$

Referring to Section 3.3.1 the energy of ions arriving at cathode, after travelling distance ℓ, is given by $V_c \left(\frac{2\ell}{L} - \frac{\ell^2}{L^2}\right)$ and the total energy of ions is $N_o V_c \left(\frac{2\ell}{L} - \frac{\ell^2}{L^2}\right)$. This, when added to total energy of neutrals, equals $N_o V_c$

Considering now the energy of neutrals. The maximum possible energy of a neutral, from the expression 3.3.11, is obtained by substituting $n = \frac{L}{\ell} - 2$ and equals $\frac{V_c^{\,2}}{L^2}\left(\frac{2L}{\ell} - 3\right)$. However it should be pointed out that this treatment is seriously in error as it depends on the arbitrarily chosen origin i.e. the final plane where collisions occur has been arbitrarily chosen as being at a distance ℓ from the cathode. But, of course, collisions can occur and energetic neutrals formed at any plane up to the cathode surface.

3.3.4 Reported Experimental Observations

The theoretical predictions of Davis and Vanderslice[9] have been tested by themselves, Houston and Uhl[12] and Ahmad.[13] The results indicate that the theory can explain the main features of the measured energy distributions. The validity of the theoretical predictions has also been extensively investigated in the present work and the results are presented in Section 5.3

3.4 Surface Impact Phenomena

When the various particles from the discharge impinge on the cathode prior to and during plating, a variety of atomic collision processes occur within the surface layers. In fact, the energetic particles (ions and neutrals) incident on the surface(s) of the cathode experience mutual forces of attraction and repulsion with atoms of the solid particularly those in the near surface layers. In principle, an energetic ion may be treated as an atom since charge neutralisation is generally a very effective process near a surface[14,15]. It is an understanding of these projectile - target interactions that is required if the properties of ion-plated films are to be explained. The phenomena involved are:-

(i) Sputtering

(ii) Surface cleaning

(iii) Sputter - redeposition

(iv) Cascade mixing

(v) Radiation damage

(vi) Recoil implantation

(vii) Thermal diffusion

3.4.1 Sputtering

Sputtering was originally defined as the removal of atoms from a surface by the impact of an ion. The definition is often broadened to include the removal of atoms by the impact of incident neutral atoms, neutrons and electrons. One may also define sputtering as the emission of atomic particles from surfaces under energetic particle bombardment. The definition stresses the dynamical aspects of the sputtering process, i.ê., the atomic collision processes that are initiated by an impinging particle to the extent that they may lead to sputtering. Sputtering has been a very widely investigated subject and there have been many reviews and articles.[15-23]

In ion plating too, the impingement of ions, neutral atoms, etc. (see Chapter 5) on the target (substrate) causes atoms to be ejected from the surfaces of the substrate.[18] The sputtering or more appropriately at lower energies, ion impact desorption has been widely used in ion plating applications to clean the substrate, prior to film deposition, and also to maintain low active gas coverage during film deposition (see Chapter 2). Of course a further result of the sputtering of atoms from the substrate surfaces is erosion of the "growing" film and it is obvious that for a film to be produced in ion plating, the arrival rate of the film material particles at the substrate must exceed the rate at which they are sputtered.

The theoretical treatment of sputtering phenomenon in ion plating must, therefore, be concerned with the prediction of the rate at which ion-plated films are eroded as a result of sputtering. The prediction can then be used

to control the growth rate of films in ion plating.

Generally, the erosion of a bombarded surface is measured in terms of the sputtering yield, S, which is the average number of sputtered target atoms per incident particle. As can be seen from the many reviews[15,19-23] of the sputtering phenomenon yields depend on a number of factors such as the energy and mass of the incident particle, the structure of the target, the mass of the target atoms, and the binding energy of the target atoms in the solid.

Of the many theories of sputtering which have been proposed to date, several have met with considerable success in the prediction of sputtering yields for various ion - target combinations at various energies for amorphous or polycrystalline targets. Perhaps the most elegant treatment is that of Sigmund.[24] In this treatment which is applicable at not too high energy deposition densities, a collision cascade is considered to be initiated by an atom which starts the motion in a plane $x = 0$ at time $t = 0$ with an arbitrary velocity vector $\vec{v}$. In deriving an expression for sputtering yield an expression giving the distribution in energy of moving atoms, averaged over time, was derived[24] and, assuming an isotropic angular distribution for the atoms set in motion by a projectile, it was shown[24-26] that in the asymptotic limit of $E \ll E_o$ (where E_o is the projectile energy and E is the energy of moving atom) the energy spectrum of the moving atoms is of the form:-

$$f(E) \cdot dE \propto \frac{1}{E^2} dE \qquad 3.4.1$$

By finding the average number of atoms moving in the layer (x,dx) into the solids angle (Ω , $d\Omega$) with energy (E,dE), it becomes possible to calculate the flux of atoms H(E)dE through the target surface. Carter et al[27] summed up the works of Sigmund[24] and Thompson[26,28] and came up with the expression:-

$$H(E)dE\ 2\pi\ \text{Sin}\ \theta.\ \ \text{Cos}\ \theta\ = \frac{C}{E^2} dE.\ \ \text{Cos}\ \theta.\ \ \text{Sin}\ \theta\ \ d\theta \qquad 3.4.2$$

for the number of atoms recoiling from surface positions in the energy range

dE about E and in the angular range dθ about θ to the surface normal. In this expression C is a constant for a particular ion energy and substrate material. It includes a term describing the total energy deposited by the projectile near the surface. Both the $\frac{1}{E^2}$ and Cos θ dependencies of the ejected atoms must be subject to modification by the surface binding forces acting in the actual ejection process[28]. For the simplest possible estimate, Sigmund[24,29] assumed a plane target surface and a planar potential barrier U_o. Subject to these conditions, integration of expression 4.3.2 over angles from 0 to $\pi/2$ and energies up the projectile energy E_o results in the total number of atoms sputtered from the surface. Sigmund, then, found the total number of atoms with sufficient energy to overcome the surface barrier, for each projectile ion, to be[24,29,30]

$$S = \frac{1}{\pi^2} \cdot \frac{F_{D(x,E,\ Cos\ \theta_o)}}{U_o} \Delta x \qquad 3.4.3$$

In this expression $F_D(x,E,\ Cos\ \theta_o)$ is the energy deposited in a layer (x,dx) by a projectile, θ_o is the angle which the trajectory of the recoiled atom makes with respect to surface normal negative, and Δx is the effective depth of origin of the sputtered atoms. For the case of $Kr^+ \longrightarrow$ Cu, Sigmund[31] compared measured sputtering yield with the nuclear stopping power, and by considering that the overwhelming majority of sputtered atoms have energies of about 10eV, found that the effective thickness involved in sputtering is about 25 Å. He (Sigmund) then declared that this value is not only unique to $Kr^+ \longrightarrow$ Cu.

A more detailed calculation[30,32] yields

$$S = \frac{3}{4\pi^2} \cdot \frac{F_D(x,\ E,\ Cos\ \theta_o)}{NC_oU_o} \qquad 3.4.4$$

where N is the target atomic density and C_o a cross-section constant. The function F_D (x,E, Cos θ_o) has been calculated by Winterbon et al[24] for different energy ranges. For projectile ions with energies of up to 1 keV, which is the range of energies of the particles impinging on the cathode

under typical ion plating conditions (see Chapter 5), the normal yield reduces to;

$$S = \frac{3}{4\pi^2} \cdot \alpha \cdot \frac{4M_1 M_2}{(M_1 + M_2)^2} \cdot \frac{E_o}{U_o} \qquad 3.4.5$$

In this expression M_1 and M_2 are the masses of the projectile and target atoms, respectively, and α is a dimensionless quantity depending on the ratio M_2/M_1. Sigmund[31] reported that for normal incident ions α, varies between 0.2 to 0.8 for the mass ratio M_2/M_1 of 0.1 to 10, respectively. At this stage, it must be pointed out that expression 3.4.5 is somewhat inaccurate[32,33] for the case of light ions incident upon heavy targets in which significant cascade generation does not occur. A large fraction of yield is thus derived from backscattered ions as suggested by theoretical work of Weissman and Sigmund[34] and the experimental work of Weissman and Behrisch[35]. However, this restriction does not apply for the case ion plating for which the impinging particles (the majority of which are the atoms and ions of the carrier gas) are argon or krypton.

In terms of yield dependence on the angle of beam incidence, γ, Sigmund's theory suggests that for angles of incidence which are not too oblique the sputtering ratio may be approximated as;

$$\frac{S(E_o, \cos\gamma)}{S(E_o, 1)} = (\cos\gamma)^{-f} \qquad 3.4.6$$

For the cases applicable to ion plating, i.e. the energies of the incident particles are below 2.5keV, f can be obtained from the work of Sigmund[24,29] presented in the graph of Figure 3.3 for a wide range of the mass ratio M_2/M_1. The sputtering yield has been reported[24,29-31] to increase with the angle of incidence for the range: 0^o - 70^o, and drop sharply when the angle of incidence exceeds 70^o.

In ion plating, since the movement of the energetic particles impinging on the cathode are initiated by the movement of ions which follow the electric

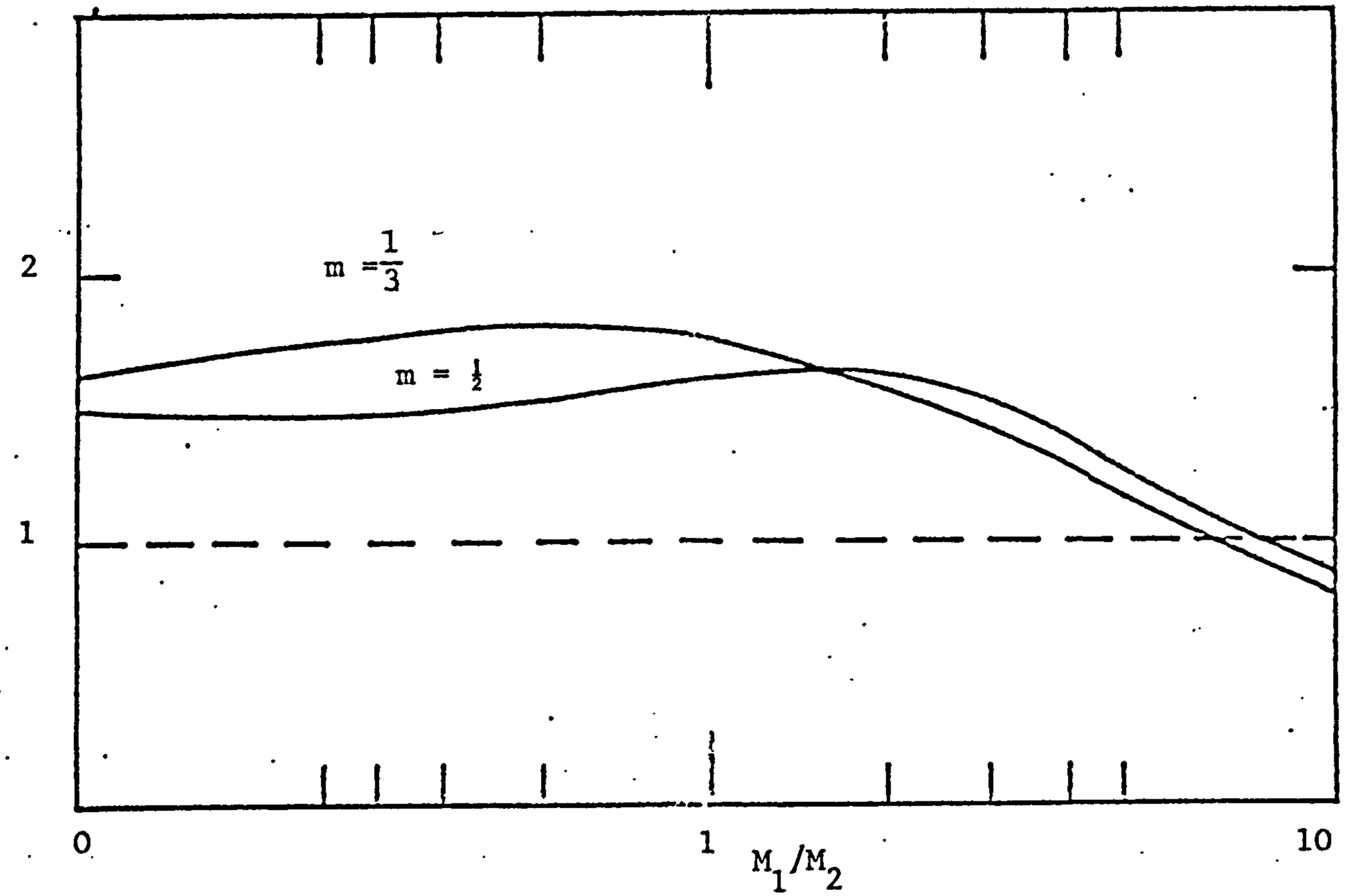

FIGURE 3.3. FACTOR f DETERMINING THE DEPENDENCE OF SPUTTERING RATIO ON ANGLE OF INCIDENCE[29,30] FOR TWO VALUES OF POWER POTENTIAL m

field lines (see Chapter 2), it seems reasonable to assume that the majority of the impinging particles arrive at the cathode at right angles to the surface. Hence, the prediction given by expression 3.4.5 can be used for the majority of ion plating situations. The predictions are found to be in good agreement with the experimental results reported by Henschke et al[36], Bader et al[37], Laegreid et al[38] and Keywell[39] for the sputtering yields from the surface of a copper target bombarded by argon ions with energies from a few eV up to about 1 keV. The results of all these experimental observations have been presented by Carter and Colligon[14] and are reproduced for completeness in Figure 3.4. As can been seen for argon ions impinging with energy of about 500 eV, the sputtering yield is about 2 atoms per incident ion. Since the energies of most of the particles impinging on the cathode in a typical ion plating discharge are in this range (see Chapter 5) this graph (Figure 3.4) and the above expressions are most appropriate for calculating, roughly, the film growth rate in ion plating.

Under normal plating conditions, the current density is about 10^{-4} amps/cm^2. The contribution of ion current can, roughly, be taken to be about say 5×10^{-5} amps/cm^2. Thus the flux-density of the ions is about $6\text{x}10^{18} \times 2\text{x}10^{-5}$ ions/cm^2/sec $\approx 1.2\text{x}10^{14}$ ions/cm^2/sec. Referring to the expression 3.4.5 (or Figure 3.4)the sputtering yield (for argon incident on copper.) is about 2 atoms/ion. Thus the total number of atoms sputtered from the target is $2.4\text{x}10^{14}$ atoms/cm^2/sec. which corresponds to a removal rate of about 1 monolayer/sec. or 3Å/sec.

This is, of course, a highly simplistic calculation since a very wide range of ion and neutral energies are involved and at the lower end of the energy range the relationship between sticking probabilities and sputtering rates plays an important role. It does, however, give an indication of the order of the rate of sputter removal.

Results of measuremenets by Teer and Sharbiney[40] on relative rates of deposition and removal by sputtering under typical ion plating conditions (discharge pressures of 10-50μ and voltages 2 - 5k V), using filament evaporation indicate that the sputtering rate is less than 30% of deposition rate.

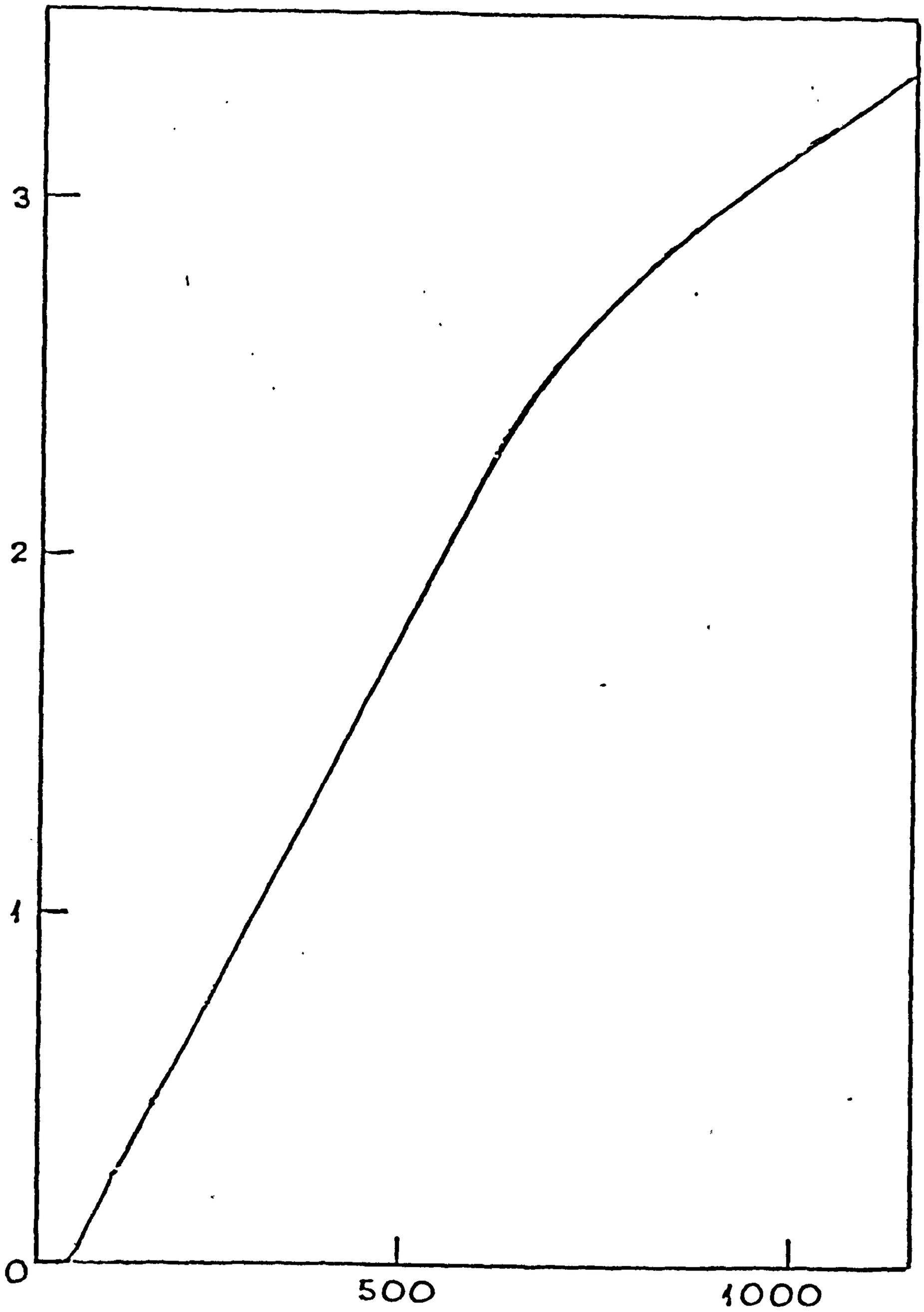

FIGURE 3.4 VARIATIONS OF SPUTTERING YIELD OF COPPER WITH ENERGY OF INCIDENT ION[14]

Although the method used was very crude the result does not appear to be too unrealistic. The most recent work[41] on deposition rates in ion plating indicates that growth rates of between about 100-25000 Å/min. are of practical interest. For the minimum rate in this range, an arrival rate of about 10^{15} atoms/cm^2/sec. is generally required.

3.4.2 Surface Cleaning

Sputter cleaning which is a convenient 'in situ' method of obtaining clean substrate surface both prior to and also during ion plating (see Section 2.6.1) is a technique based on the ability of the energetic particles incident on the surface(s) to cause the ejection of adsorbed atoms and molecules. Carter and Armour[15] used the ion-bombardment-induced desorption cross section, $\tilde{\sigma_d}$ which is defined in terms of the equation describing the rate of depletion of adsorbed atom areal density n due to bombardment with an ion beam flux density J i.e.

$$-\frac{dn}{dt} = J n \tilde{\sigma_d} \qquad 3.4.7$$

and then defined the equivalent sputtering yield S_d as

$$S_d = n_s \cdot \tilde{\sigma_d} \qquad 3.4.8$$

where n_s is the monolayer density.

In ion plating where the energies of the bombarding particles varies from about 100 eV or so up to 2.5 keV the low energy bombardment desorption processes can be associated with direct recoils and reflected recoils of substrate atoms and ejection of adsorbate atoms by reflected primary particles whereas for the higher energy bombardment range the adsorbed atoms are sputtered as part of general flux of sputtered substrate atoms[15]. The ion impact desorption cross-section of energies below those required to form a cascade are reasonably high and hence it is possible, to achieve high cleaning efficiency without significant substrate sputtering.

3.4.3 Sputter - Redeposition

An important difference between discharge and ion beam deposition processes is that in the former the sputtered particles have a high probability of returning to the substrate either as low energy neutrals or energetic ions following re-ionisation[46] in the discharge and subsequent acceleration across the dark space. The low particle densities in the vicinity of the target preclude these effects in ion beam systems. This sputter-redeposition or deposition of previously sputtered material is of potential importance from the point of view of mixed interface formation and the efficiency of the process has been investigated in the present work. The results are presented in Chapter 5.

3.4.4 Cascade Mixing

Cascade mixing is a process in which energetic flux bombardment can redistribute the atomic components of a binary or multielemental target, as a result of the cascade generated by the passage of the primary particles[42,43]. In cascade mixing it is assumed[42] that the collision between projectile and target atoms and mutual collisions between the target atoms themselves create atomic recoils which effectively mix the initial constituents of a complex target.

As discussed earlier (also in Chapter 5 of this thesis) in ion plating the substrate is bombarded with ions and neutral atoms of both the carrier gas and film material with a comparatively wide range of energies. The energetic bombardment in ion plating, by virtue of the deposited energy, can enable the film material, which is assumed to act as a plane source, to diffuse into the substrate. The diffusion coefficient D_x, which is therefore dependent on the energy deposited at the interface is[42,43]

$$D_x = \frac{0.42\ J\bar{\theta}(E,x)h^2}{6NE_d} \qquad 3.3.9$$

In this expression, J is the bombarding flux density. $\bar{\theta}(E,x)$ is the deposited energy per unit depth at the interface by particles arriving at the substrate surface with energy E, h is associated with atomic hop distance, N is the atomic density of the film and E_d is the effective displacement energy.

As will be seen, in Section 3.4.8, the effective diffusion coefficient D_x, is an essential factor for calculating interface broadening in ion plating.

As already indicated, in ion plating, the energies of the particles reaching the substrate are low (typically peaking below 1.5keV for a 3kV discharge) and the energy deposition depth distribution function $\bar{\theta}$ (E,x) is expected to be similar to, but closer to the incidence surface than, the atom penetration depth which at these low energies is of a decaying exponential nature. Hence to a reasonable approximation;

$$\bar{\theta}(E,x) = \bar{\theta}(E,0)\ \exp(^{-x}/\lambda) \qquad 3.4.10$$

where λ is some small characteristic distance and for any practical useful film thickness, $x \gg \lambda$. Substituting for $\bar{\theta}(E,x)$, in equation 3.4.9

$$D_x = \frac{0.42\ J\ell^2\ \bar{\theta}(E,0)}{6NE_d}\ \exp(^{-x}/\lambda) \qquad 3.4.11$$

It should be noted that this is an over simplified treatment of the diffusion coefficient since in reality the effective diffusion coefficient D_x will vary with depth into the substrate and within the film, as well as with time. A more detailed analysis allowing for such spatial-temporal variations of D_x is expected to give more accurate estimate. However, the present model should be expected to give reasonable order of magnitude estimates of the interface broadening.

3.4.5 Radiation Damage

During the deposition of energy by an ion slowing down in a solid, many of the atoms involved in the collision cascade may be permanently removed from their normal sites. In fact, the sputtering phenomenon in which

surface atoms are ejected when the cascade intersects the surface is essentially a special manifestation of radiation damage[44,45]. The type of defects produced after prolonged bombardment depend on a number of factors such as the relative masses of primary and substrate particles, the primary energy, substrate temperature and solubility of the bombarding species in target.

From the point of view of ion plating, the damaging process may play a significant role at a number of different stages in the process. The creation of"damage" sites e.g. atomic steps or pits or more macroscopic topographical features during the bombardment cleaning process may affect the initial sticking probabilities of the film atoms, the creation of vacancies and interstitials in the near surface region of the substrate may lead to enhanced diffusion and the incorporation of carrier gas atoms into the growing film may affect grain size. Since the actual desorption process involves energetic particles, the surface damage effect probably has little influence on the sticking and it is the enhanced diffusion and film growth factors which have the most significant implications.

3.4.5(a) Irradiation Enhanced Diffusion

In general, bombardment of a target with energetic flux of particles results in formation of defects within the bombarded region. A theoretical treatment of irradiation enhanced diffusion has been presented by Nelson[16] who separated defect losses to fixed sinks (e.g. dislocations) and mutual recombinations, independently. This is, in fact, reasonably justified as the temperature range over which each of the two phenomena dominates can be separated - e.g. mutual recombination dominates at lower temperature. In many circumstances ion plating is carried out at or near to ambient temperatures. It would, therefore, be reasonable to associate irradiation enhanced diffusion to the mutual recombination phenomenon. In fact, irradiation enhanced diffusion will only become significant where the vacancy becomes mobile. Hence it would depend on the bombarded target - e.g. around room temperature in Al, Au, and around 200^{o}C in nickel and steels[16]. However,

even at temperatures where the vacancy is immobile, limited enhanced diffusion occurs as a consequence of the mobility of interstitial atoms.

Irradiation enhanced diffusion in the coating (in ion plating) permits sufficient atomic mobility to result in the sintering or closure of small pores. Thus, if the substrate temperature is maintained at levels where irradiation-created vacancies are mobile the density of the film can be greatly improved.

3.4.5(b) Carrier Gas Entrapment

Entrapment of carrier gas atoms in ion-plated films occur if the kinetic energy of the carrier gas particle, incident on the surface of the growing film during deposition process, is sufficient to allow penetration of the atom beyond the surface plane. The gas enrapment mechanisms have been reviewed by Carter and Armour[15] according to which the entrapped particles come to rest in the solid with a Gaussian depth distribution $f(x)dx$. The trapping probability is then described by the integral over the depth distribution of positions in the semi-infinite solid i.e.

$$\eta(E) = \int_0^\infty dx\, f(E,x) \qquad 3.4.12$$

Carter and Armour then used the trapping probability measurements of Kornelson[46] for polycrystalline tungsten (carried out using a monoenergetic ion beam (shown in Figure 3.5)) and deduced that for many substrates $0.1 < \eta(E) < 1.0$ for argon in the energy range 100eV to 1kV and $\eta(E) < 0.1$ for $E < 100$eV. However, in ion plating where the energies of the carrier gas species incident on the substrate vary from about 100eV up to about 2.4 kV (see Chapter 5) very little information is available on the entrapment of the carrier gas in the deposited film. (This phenomenon has, in fact, been investigated as part of the present programme and the results are presented in Chapter 5).

In spite of the lack of knowledge concerning the density of carrier gas expected in films obtained, under normal operating conditions, it is worth

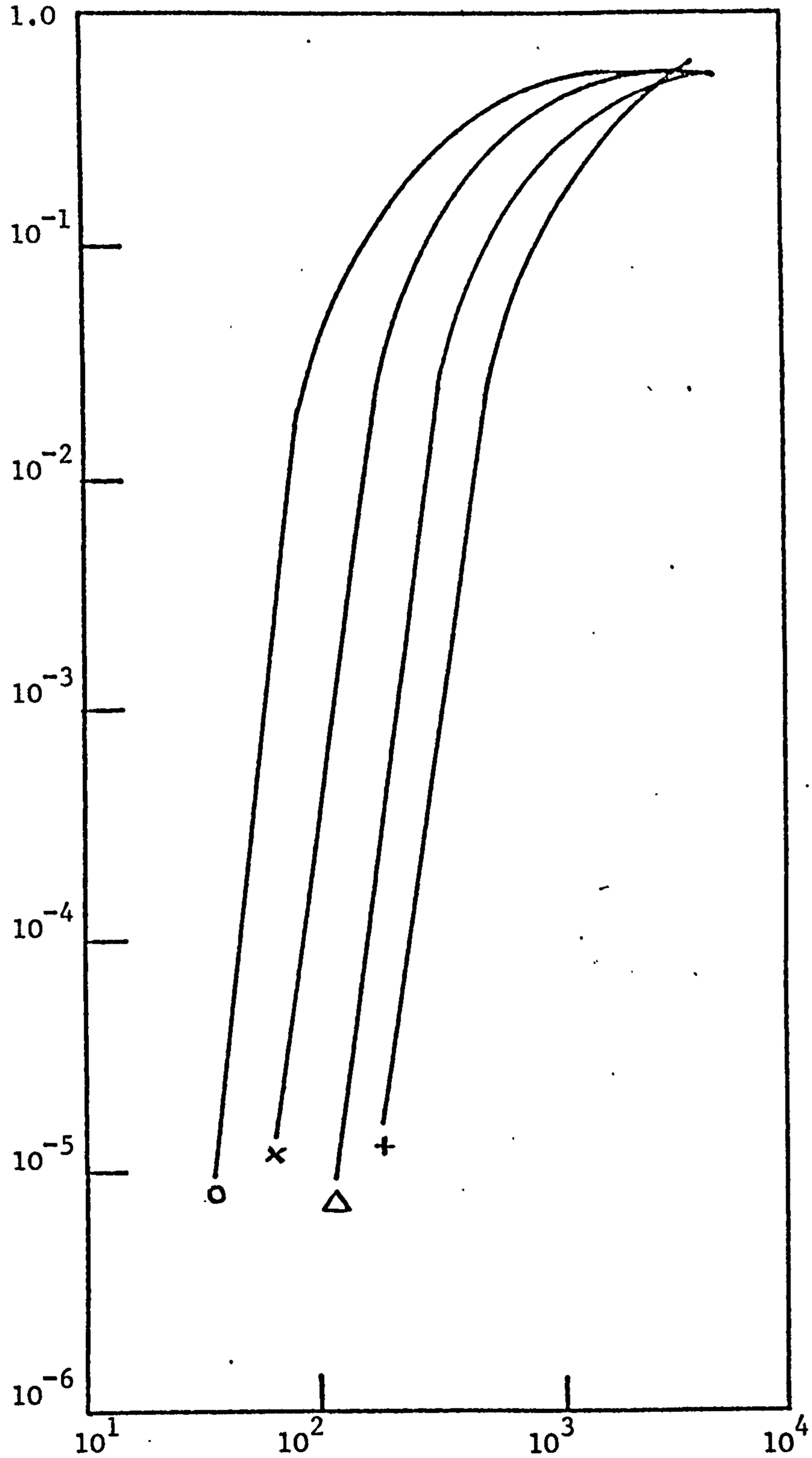

FIGURE 3.5 TRAPPING PROBABILITY AS A FUNCTION OF ENERGY FOR Ne^{+}(O), Ar^{+}(x), Kr^{+}(Δ), Xe^{+}(+) INCIDENT ON TUNGSTEN.[15]

pointing out that at concentrations greater than a few percent in materials such as nickel and copper, rare gas atoms, injected as energetic ions, tend to form into highly stable gas-vacancy agglomerates. The presence of such features would be expected to significantly affect the film growth characteristics.

3.4.6 Recoil Implantation

Recoil implantation is the introduction of foreign atoms into a solid by means of atomic recoil from a surface layer. Bombardment of a substrate, with a thin film on it, by energetic particles causes some of the bombarding particles to penetrate through the film layer into the substrate. In this process, some atoms within the film layer suffer elastic collisions with the bombarding particles and recoil with sufficient energy to penetrate into the substrate where they come to rest as an impurity. The penetration depth and the distribution of the recoil implanted particles, of course, depend on the energy and density of the incident beam and also on the thickness of the film layer.

A general mathematical treatment of the collision phenomena for finite film thickness has not yet been investigated. But it has been studied for two distinct cases. The first case is when the film layer is thin enough that there is virtually no energy loss of the incident beam during its transmission through the film[47-49]. The second case is when the film is thick and contains the main part of the energy deposition function[50,51], However, it should be pointed out that the latter case is less well documented. The works of Moline et al[50] give results which are in good agreement with experimental results up to thickness of $\sim$ 50Å, for SiO_2 on Si under Kr^+ bombardment. For higher thickness the theoretical predictions and experimental measurements were not in good agreement. Also the works of Fischer et al[51] on thick film recoil implantation is only valid for small irradiation fluences for which the film thickness remains approximately constant.

Regarding recoil implantation in ion plating it has already been pointed out that the substrate is subjected to uninterrupted bombardment of ions and

and neutral particles with a comparatively wide range of energies both before and during deposition. It can, therefore, be expected that film growth in ion plating is accompanied by recoil implantation of the film material into the substrate. Since the bombardment accompanies film growth on an essentially clean surface, then it is also clear that both the distinct cases of recoil implantation, discussed above, are applicable to ion plating.

Initially, when the coating is thin the energetic particles, impinging on the substrate, can penetrate the interface between coating and the substrate without significant loss of energy in this process. This particular phase has been claimed[16,45] to be particularly important in formation of a broad interface which is responsible for the good adhesion of ion-plated films. But, as will be seen in Section 3.4.8, the most important phenomenon in interface broadening is cascade mixing. The recoil across the interface can only occur if the damage profile spans across the interface. Essentially, the energy of the impinging particles, the sputtering rate of the coated surface, and the magnitude of the flux of the impinging particles are[16] the factors affecting the degree of irradiation damage at the interface. Nelson[16] used the thin film analysis for treatment of recoil implantation in ion plating and claimed that during an ion plating process with discharge voltage of 5kV up to $\sim$ 100 monolayers will undergo recoil mixing at the interface.

As the film grows thicker, a situation will be reached where the primary particles lose a significant fraction of their kinetic energy as they penetrate through the film. In this situation the so-called thin film approach for recoil implantation[16,48-50] is no longer applicable. In this case, the work of Fischer et al[51] may be used for treatment of the depth and concentration profile of the recoil-implanted atoms. However, it should be pointed out that this treatment can only be used when the damage profile is of the same order of the film thickness. Since the maximum energies of the particles impinging on the cathode in a typical ion-plating discharge is about 2.5k electron volts (see Chapter 5) the resulting damage profile is of the order of a few tens of monolayers[52] thus the above treatment will only be useful for film

thickness of this order. It can, therefore, be claimed that the major contribution of recoil implantation to the characteristic of ion-plated films will occur during the early stages of growth. The significance of energetic particle implantation in ion plating has been investigated as part of the present work and the result is presented in Chapter 5.

3.4.7 Thermal Diffusion

The bombardment of the substrate in ion plating generates local heat at the substrate surface. The heat is generated as a result of energy transfer from the impinging particles to the surface atoms. A surface temperature rise of 150^{o} has been reported[53] at the substrate of an ion plating discharge, struck in argon, in a time interval of ten minutes, at a discharge voltage of 4kV with current density of $0.35mA.cm^{-2}$. The heat aids diffusion between the film and the substrate. Diffusion of this nature has been reported for gold on aluminium[54], aluminium on titanium and indium on copper[3,7]. This type of diffusion is particularly important when the substrate and the coating material are metallurgically compatible i.e. they form alloy.

3.4.8 Summary of Interface Broadening Effects

As will be discussed later in Chapter 5, most of the particles bombarding the substrate have energies below about 50% of the discharge voltage for a plane substrate. In such circumstances the production of a broad interface[13] region cannot be satisfactorily explained in terms of either direct[55] or recoil implantation[14]. The role of sputter redeposition mixing, where substrate atoms are sputtered into the discharge, and subsequently redeposited on the growing film has also been found to play a minor role (see Chapter 5) under typical discharge and deposition rate conditions.

In the treatment, presented in this Section, it is suggested that the extent to which interface broadening occurs is fundamentally dependent on the energetic particle bombardment in two ways:-

1) Atoms of film material not normally compatible with the substrate are

able to penetrate beneath the surface where, in some cases, they may diffuse rapidly, and

2) The diffusion effects at the interface are enhanced for those atoms which do not readily diffuse normally, by virtue of the deposited energy which leads to cascade mixing of the components. Calculation of the broadening[42,43] due the latter effect gives a measure of the minimum interface broadening to be expected in ion plating.

Using the diffusion approximation, used by Armour et al[43], essentially the solution of the diffusion equation for Planar boundary conditions, it is possible to calculate the broadening width, $\delta(\Delta x)$, of a delta function plane source in time δt in terms of the diffusion coefficient. For the present situation,

$$\delta(\Delta x)^2 = 4D_x\,\delta t \qquad 3.4.13$$

Thus, as the film grows from thickness 0 to x, the inward broadening (of the film) into the substrate is given by[43]

$$(\Delta x)^2\Big|_x = \int_0^t 4D_x dt \qquad 3.4.14$$

If it is assumed that the film grows at a uniform rate

$$\rho = \frac{dx}{dt}, \quad \text{then} \quad dt = \frac{dx}{\rho}.$$ Substituting for D_x and dt in equation 3.4.14 and integrating gives

$$(\Delta x)^2\Big|_x = \frac{-0.3J^2}{NE_d\rho}\left\{\exp(^{-x}/\lambda) - 1\right\}.\ \bar{\theta}(E,0) \qquad 3.4.15$$

For any practically useful film thickness, $x \gg \lambda$ the exponential term becomes negligible. Hence

$$(\Delta x)^2\Big|_\infty \approx \frac{0.3J\ell^2.\ \bar{\theta}(E,0)}{NE_d\rho} \qquad 3.4.16$$

This broadening, however does not represent the entire effect since outward

able to penetrate beneath the surface where, in some cases, they may diffuse rapidly, and

2) The diffusion effects at the interface are enhanced for those atoms which do not readily diffuse normally, by virtue of the deposited energy which leads to cascade mixing of the components. Calculation of the broadening[42,43] due the latter effect gives a measure of the minimum interface broadening to be expected in ion plating.

Using the diffusion approximation, used by Armour et al[43], essentially the solution of the diffusion equation for Planar boundary conditions, it is possible to calculate the broadening width, $\delta(\Delta x)$, of a delta function plane source in time δt in terms of the diffusion coefficient. For the present situation,

$$\delta(\Delta x)^2 = 4D_x\,\delta t \qquad 3.4.13$$

Thus, as the film grows from thickness 0 to x, the inward broadening (of the film) into the substrate is given by[43]

$$(\Delta x)^2\Big|_x = \int_0^t 4D_x dt \qquad 3.4.14$$

If it is assumed that the film grows at a uniform rate

$$\rho = \frac{dx}{dt}, \quad \text{then} \quad dt = \frac{dx}{\rho}.$$ Substituting for D_x and dt in equation 3.4.14 and integrating gives

$$(\Delta x)^2\Big|_x = \frac{-0.3J^2}{NE_d\rho}\left\{\exp(^{-x}/\lambda) - 1\right\}.\ \bar{\theta}(E,0) \qquad 3.4.15$$

For any practically useful film thickness, $x \gg \lambda$ the exponential term becomes negligible. Hence

$$(\Delta x)^2\Big|_\infty \approx \frac{0.3J\ell^2.\ \bar{\theta}(E,0)}{NE_d\rho} \qquad 3.4.16$$

This broadening, however does not represent the entire effect since outward

diffusion coefficient will depend not only on the energy deposition but also on the structure of the film. For simplicity, therefore, in order to obtain an 'order of magnitude' estimate of the overall broadening, it is assumed that the outward broadening of the substrate into the film is the same as the inward broadening of the film into the substrate.

For a typical plating situation employing an argon discharge operating at a voltage 2 kV and a current density of 1 ma/cm^2 of substrate surface area, the total broadening width, ΔX_T is

$$\Delta X_T \sim 6b \qquad 3.4.17$$

where b is the interatomic spacing.

The cascade mixing model predicts that the film-substrate interface may typically be broadened by approximately 6 lattice spacing or about 20-30 Å and interface regions of this order of magnitude have been measured[13] experimentally for some film substrate combinations.

3.5 Factors Affecting Characteristics of Ion-Plated Films

It has been discussed earlier in this thesis that ion-plated films exhibit a number of desirable characteristics. In this Section the factors affecting those characteristics which have received most attention are discussed.

3.5.1 Adhesion

The high adhesion between the substrate and the film is one of the most important properties of ion-plated films. Mattox[54] considered the factors affecting the adhesion in some detail. Teer[11] summarised the works of Mattox[54] in terms of the following criterion: the substrate surface must be clean and there must be penetration and mixing of film material into the substrate and vice versa.

As discussed earlier, bombardment of the substrate surface with ions and nuetrals sputters away contaminants from the surface. It is believed that, as a result of this sputter cleaning, films do not form weak interlayers with the substrate. Also, when the substrate surface is clean, penetration and

mixing of the film material into the substrate (which is a major contirb-utary factor for adhesion between the coating and the substrate) will be greatly improved.

In an attempt to investigate the effect of surface cleanliness on film-substrate adhesion Teer[11] compared adhesion of an ion-plated film and that of a film produced by evaporation, immediately after sputter cleaning and observed that the film produced by evaporation did not exhibit good adhesion. He then concluded that for good adhesion, deposition in a discharge is essential. However, at background pressures typical of standard evaporators ($\sim 10^{-5}$ torr) monolayer formation times are very short (0.1` second at 10^{-5}torr assuming unity sticking coefficient). Hence these experiments cannot be regarded as conclusive. The effect of surface cleanliness on film - substrate adhesion has been thoroughly investigated here and the result is presented in Section 5.2

When films are depostied in a discharge a number of important phenomena take place which, particularly during the early stages of film growth, lead to the formation of a graded interface in a way which cannot be reproduced by simple evaporation following discharge cleaning. For example sputtered substrate atoms may return to the substrate as energetic ions or neutrals and be accommodated in the first layers of the coating. This phenomenon, which is in practice considered to be a minor contributor (see Chapter 5) together with energetic particle implantation, energy deposition,recoil implantation of the film material into the substrate, cascade mixing, irradiation enhanced diffusion, and thermal diffusion, results in the production of a graded interface between the film and the substrate[54-56]. The presence of such an interface is believed to be the major factor in improving the adhesion since it reduces the stress gradient across the interface caused by differences in the thermal expansion coefficients[11] of the two materials.

Although in some cases very broad interface have been observed, there is little reliable evidence for the existance of a graded interface in all cases and there is no real knowledge concerning the minimum interface thickness

required to produce the observed adhesion properties.

3.5.2 Throwing Power

The high throwing power of ion plating i.e. it can give good coverage on surfaces out of line of sight of the vapour source (not, however, down holes) is a well established feature of the technique. Earlier work[1,4,57] on ion plating attributed the good throwing power to the ionised portion of the coating material following the electric field lines to all parts of the substrate surface. This suggestion was later discounted after the works on ionisation efficiency under typical ion plating condition (see Section 3.2). The first successful attempt to obtain an understanding of the throwing power characteristics of ion plating was that of Chambers and Carmichael[58]. They studied the dependence of the coating deposition rate on gas pressure for the front and back surfaces of a flat plate, for a solid cylinder, and for the outer and inner surfaces of a hollow tube. Teer[59] repeated the work of Chambers and Carmichael[58] and measured the thickness of ion-plated film on the front and back surfaces of a flat specimen as a function of the pressure of inert gas (argon) in the discharge. The results of this investigation, which are also given in another paper by Teer[11] are presented in Figure 3.6. It can be seen that the ratio of the film thickness on the front and back surface approaches unity at higher inert gas pressures. It is thus concluded that the suggestion, by Aisenbert and Chabot[60], that 'throwing power in ion plating is mainly due to gas scattering and the field has a minor effect' is substantiated.

3.5.3 Purity

One of the main points to be considered concerning both the purity and mechanical properties of ion-plated films is the trapping of the gases present in the discharge chamber, in the growing films. The effects of partial pressures of various gases in the deposition chamber on some of the physical properties (other than purity) of sputter deposited films have been studied

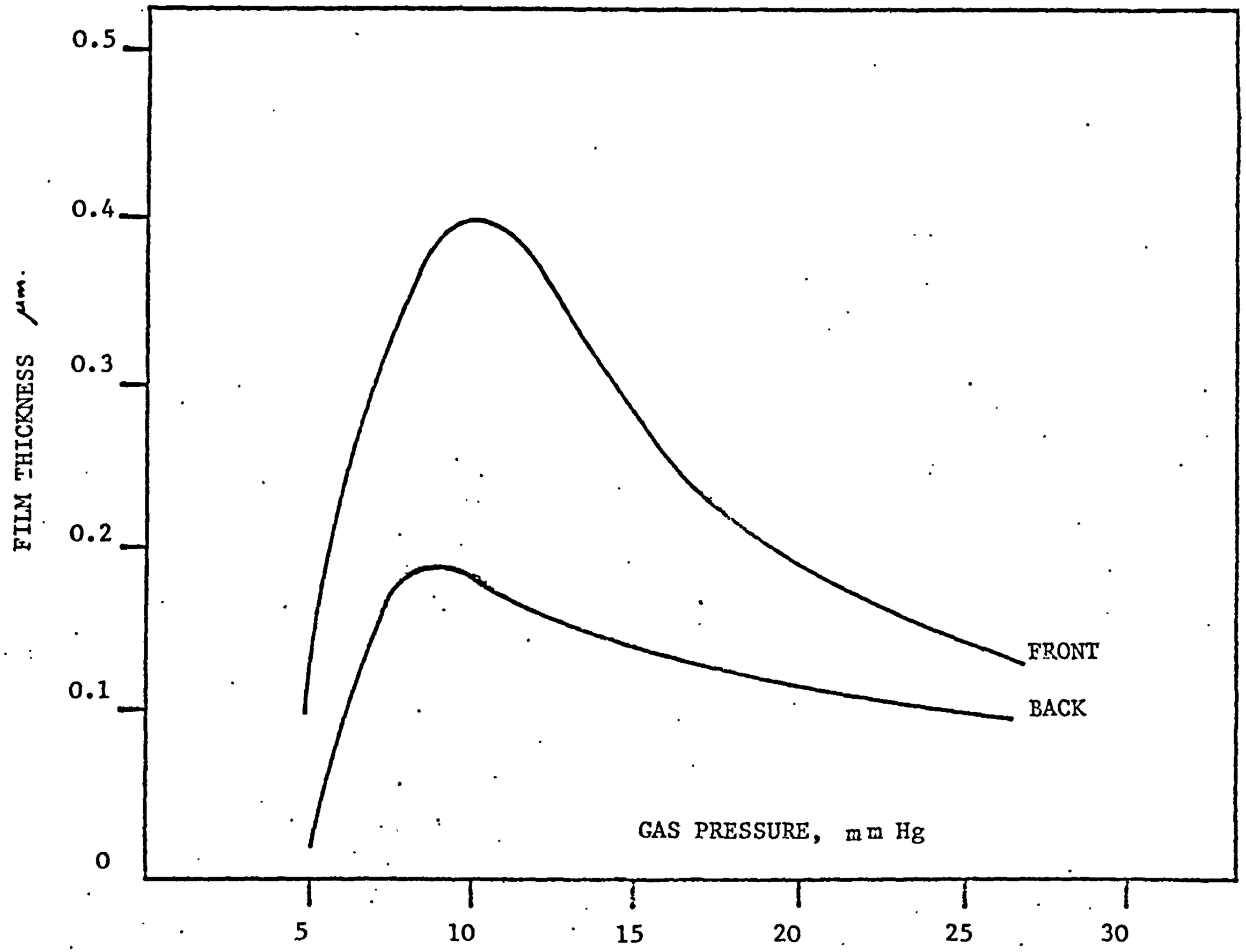

FIGURE 3.6 FILM THICKNESS ON FRONT AND BACK SURFACES OF A FLAT PLATE AS A FUNCTION OF ARGON PRESSURE[59]

by a number of investigators[61-64]. Although these works do not discuss the effect of gas trapping on the purity of the sputter-deposited films, there is clear evidence that gases do get trapped in the films. Winters and Kay[65] measured the concentration of argon in sputter - deposited nickel films as a function of the film growth rate, temperature, discharge pressure, and bias voltage.

So far as ion-plated films are concerned very little work has been reported in connection with the incorporation of the various gases, present in discharge chamber, into the deposited films. However, the fact that the substrate is subjected to continuous energetic particle bombardment both prior and during deposition makes some gas occlusion inevitable. A knowledge of the concentration of gas in the films, particularly rare gases which are known to be highly insoluble in most materials, is thus of considerable importance and this aspect of plating process was also investigated as part of the present research programme.

3.5.4 Grain Structure

Compared to the amount of works reported in studying the factors affecting adhesion and throwing power only limited work has been done in connection with grain structure of ion-plated films. In general, coatings formed by physical vapour deposition techniques consist of tapered, nodular or columnar grwoths with porous boundaries of low cohesive strength when the depositing atoms have limited mobility[66]. Sharbiney[7] compared the grain structure of thin (<200 Å) films produced by vacuum evaporation and ion plating and found that ion-plated films have finer grain size structure. He then attributed this effect to more homogeneous nucleation of ion-plated films which he found to have a much greater density of nucleii compared to films produced by vacuum evaporation technique. Mattox and Kominiak[67] studied the effect of ion bombardment during film growth and reported improved grain structure by intense ion bombardment and Bunshah and Juntz[68] reported that at high temperatures ion bombardment causes grain refinement of beryllium coating. Teer and

Delcea[69] investigated structures of ion-plated copper films and related them to plating parameters. The result of their investigations revealed that denser structures can be obtained by increasing discharge voltage, and pressure. Since both these factors tend to increase the surface temperature it can be concluded that improved grain structure of ion-plated film may be attirbuted to high surface temperature which increases the mobility of the depositing atoms.

3.6 Discussion

Various physical phenomena occurring, both prior to and during the ion plating process, have been reviewed in this Chapter. Regarding the particles arriving at the substrate, it has been shown that neutrals constitute the major portion of the impinging particles. The adhesion between the film and substrate is believed to be due to penetration of the coating material particles into the substrate lattice, recoil implantation, cascade mixing, physical mixing of the depositing atoms and the sputtered substrate atoms, preferential removal of any poorly adherent particles by sputtering, diffusion enhanced by elevated surface temperature, and diffusion enhanced by irradiation. The high throwing power of the ion plating process is attributed, mainly, to gas scattering. The grain structure of ion-plated film is related to bias voltage deposition rate, gas pressure, and substrate surface temperature. Although energetic flux bombardment was found to be responsible for the mixing process of the film material atoms and the substrate atoms, the major contribution to film growth is believed to come, in general, from flux of more or less thermal energy particles.

However, there is still no detailed understanding of the effects of these various parameters on the properties of the deposited films. Although the predictions of Davis and Vanderslice have been tested, to some extent, by a number of investigators (including themselves) it should be pointed out that the experimental apparatus used was comparatively crude and lacked mass analysis facilities. Thus the design and construction of experimental apparatus allow-

ing both energy and mass analysis is considered to be an essential step in improving our understanding of the ion plating process. This, combined with investigations of the effect of substrate surface conditions and the incorporation of gases into the deposited films represents the programme of research described in this thesis.

3.7 References - Chapter 3

1. Lundin B.T. NASA report 'SP-5111 1972 (Editorial)
2. Aisemberg A. NASA report 'SP-5111' P.171, I972
3. Teer D.G. Proc. Int. Conf. on Ion Plating and Allied Techniques Edinburgh1977.
4. Mattox D.M. Sandia Corportation Report "SC-DR-281-63; Electrochem. Technol. 2 P.295 1964
5. Mattox D.M. J. Electrochem.Soc. 12 P.1255, 1968
6. Mattox D.M. U.S. Patent No. 3329601, 1967.
7. Sharbiney M.G. Ph.D. Thesis. University of Salford 1975.
8. Teer D.G., Delcea B.L. Proc. Int. Conf. on Ion Plating and Allied Techniques, Edinburgh 1977.
9. Davis W.D., Vanderslice T.A. Physics Rev. 131 P.219 1963.
10. Teer D.G. J. Phys. D; Appl. Phys. 9, P. L187, 1976.
11. Teer D.G. J. Adhesion 8, P.284 1977.
12. Houston J.E., Uhl, J.E. Sandia Corporation Report SC-RR-710122, 1971
13. Ahmad N.A.G. M.Sc. Dessertation. University of Salford 1974.
14. Carter G., Colligon J.S. Ion Bombardment of Surfaces, Chapt. 7,(London: Heinemann) 1968.
15. Carter G., Armour D.G. Thin Solid Films. 80, P.13, 1981.
16. Nelson S. Proc. Int. Conf. on Ion Plating and Allied Techniques, Edinburgh 1977.
17. Mattox D.M. J.Vac. Sci. and Technol. 10, no. 1, P.47, 1973.
18. Mattox D.M. Sandia. Corp. Report 1973.
19. Behrisch R. Ergebn. Exakt. Naturw. 35, P. 295, 1964 - Can. J. Phys. 46, P.527, 1968.
20. Kaminshy M. Atomic and Ionic Impact Phenomena on Metal Surfaces (Berlin: Springer - Verlag) 1965.
21. Pleshivetsev N.V. Cathode Sputtering (Moscow: Atomizdat) 1968.
22. McDonald R.J. Adv. Phys. 19 P.457, 1970
23. Sigmund. P. Rev. Roum . Phys. 17, P. 1079, 1972
24. Sigmund P. Phys. Rev. 184 , P. 383, 1969
25. Robinson M.T. Phil1. Mag. 17, P.121, 1972.

26. Thompson M.W. Proc. 5th, Int. Conf. on Ioniz. Phenomena in Gases, North Holland Publ. Co. Amsterdam, 1962.

27. Carter G., Armout D.G., Snowdon K.J. Rad. Eff. 35, P. 175, 1977

28. Thompson M.W. Phill. Mag. 18 P 377, 1968.

29. Sigmund P. Lecture notes presented at Int. Summer School on Interaction of Radiation with Matter, Predeal, Rumania, July 1971.

30. McCracken. G. Behaviour of Surfaces Under Ion Bombardment. London 1975.

31. Sigmund P. Sputtering Processes: Collision cascades and spikes. Monograph N. 77-07, H.C. Ørsted Inst. Københavns Universitet.

32. Nobes M.J. Theory of Topographic Changes at Sputtered Surfaces Ph.D. Thesis University of Salford, 1976.

33. Winterbon K.B., Sigmund P., Sanders J.B., Dan. Vid. Selsk., Mat. Phys. Medd 36 no. 10 1968

34. Weissman R., Sigmunc P., Rad. Effects, 19, P.7 1972.

35. Weissman R., Behrisch R., Rad. Effects, 19, P.69, 1972

36. Henschkle, E.B. and Derby S.E. J. Appl. Phys. 34, P. 2458, 1963

37. Bader M. Witterborn F.C. and Snouse T.W. NASA Rep. No. TR-R-105

38. Laegreid N. and Wehner G.K. J. Appl. Phys. 32, P.365, 1961

39. Keywell F. Phys. Rev. 97, P.1611, 1955

40. Teer D.G. and Sherbiney M.G. Department of Aeronautical and Mechanical Engineering, University of Salford (private communication).

41. AGARAD Lecture Series No. 106, Met. Coating Techniques, Lisbon, Athens, Ankara, March 1980.

42. Carter G., Armour D.G., Ingram D.C., Webb. R.P. Newcombe R. Rad. Effect Let. 54, P.217, 1979.

43. Armour D.G., Carter G., Webb R.P. Ingram D.C. Newcombe R., Rad. Eff. Let. 50, P.45 1980.

44. Nelson R.S. Ion Implantatoin Chapt. 3, North Holland Publ. Co. 1973.

45. Nelson R.S. Rad. Effects 2 P.47 1969.

46. Kornelson E.V., Can. J. Phys. 42, P.364, 1964

47. Ishitani T., Shimizu R., J. Appl. Phys. 6, P.241, 1975

48. Grötzschel R., Klabes R., Greissig V. Schmidt A. Rad. Eff. 36, P. 129, 1978.

49. Kelly R., Sanders J.B. Surface Science, 57, P. 143, 1976.

50. Moline R.A., Reutlinger G.W. North J.C. "Atomic Collisions in Solids" Edited by Datz S., Appleton B.R., Moak C.D. P. 159. (Plenum N.Y.) 1975

51. Fischer G., Carter G. & Webb R.P. Rad. Eff. 38, P.41, 1978.

52. Webb R.P. Ph. D. Thesis University of Salford, 1980.

53. Teubner W., Schulze, D. Wilberg R. VEB Hockvakuum Dresden Fortschritte der Physik 16, P. 419, 1968.

54. Mattox D.M. Sandia Corp. Monograph SC-R-65-852, 1965

55. Walls J.M., Hall D.D., Teer D.G. & Delcea B.L. Thin Solid Films 54, P. 303, 1978.

56. Teer D.G. & Salem F. Thin Solid Films 45, P. 583, 1977

57. Spalvins T. Przybyszewski J.S., & Buckley D.M., NASA TND - 3707 1966

58. Chambers D.L. & Carmichael D.C. Research / Development 22 P. 32, 1971

59. Teer D.G. Tribology International P. 247, Dec. 1975.

60. Aisenberg S. & Chabot R.W. J. Vac. Sci. & Technol. 10, no. 1, P. 104, 1973.

61. Melmed A.J., J. Appl. Phys. 37, P. 275, 1960

62. Bundik J. I., J. Appl. Phys. 119, P. 1578, 1960

63. Caswell H.L., J. Appl. Phys. 32, P. 105, 1961

64. Gaestenberg D. & Calbick C.J. J. Appl. Phys. 35, P. 402, 1964.

65. Winters H.F. and Kay E. J. Appl. Phys. 43, P. 789, 1972.

66. Thornton J.A. Annu. Rev. Mater. Sci. 7, P. 239, 1977

67. Mattox D.M., Kominiak G.J., J. Vac. Sci. Technol 9, P. 528, 1972

68. Bunshah R.F., Juntz R.S., J. Vac. Sci. Technol 9 P. 1404, 1972.

69. Teer D.G., Delcea B.L. Thin Solid Films, 54, P. 295, 1978.

CHAPTER IV

INSTRUMENTATION

CHAPTER 4

INSTRUMENTATION

4.1 Introduction

4.2 Experimental Apparatus for the Measurement of Energy Distributions of the Ionic and the Neutral Species Impinging on the Cathode of a Typical Ion Plating Discharge.

4.2.1 Overall Vacuum System

4.2.1(a) Design Considerations

4.2.1(b) Performance

4.2.2 Discharge and Gas Handling System

4.2.2(a) The Discharge Chamber.

4.2.2(b) Gas Handling System

4.2.2(c) Measurements of the Conductance of Silicon Carbide Leak.

4.2.2(d) Constructional details.

4.2.2(e) Performance

4.2.3 The Analysis System

4.2.3(a) Ion Extractor

4.2.3(b) Deflection Lens

4.2.3(c) Ionisation Chamber

4.2.3(d) Retarding Lens

4.2.3(e) Energy Analyser

4.2.3(f) Mass Spectrometer

4.2.3(g) Detection System

4.2.4 The Overall Arrangement

4.2.5 Performance

4.3 UHV Ion Plating/Evaporator Apparatus

4.1 Introduction

The characteristic properties of ion-pated films have been discussed earlier in this thesis. However, the reasons why they possess these characteristics are not fully understood. In fact, the nature of the particles impinging on the substrate together with their energy distributions, the discharge conditions, the substrate surface conditions, the effect of carrier gas bombardment, and the impurities in the plating environment all appear to be of significance.

The overall experimental programme was to investigate these parameters and the following distinct studies were carried out:-

1. Measurement of the energy distributions of the ionic and neutral species impinging on the cathode of a typical ion plating discharge.
2. Investigation of the influence of the substrate surface conditions. on film-substrate adhesion.
3. Gas trapping and sputter - redeposition effects.

The work described in this Chapter is concerned with the design, constructional details, and performance of the apparatus required to facilitate these studies.

4.2 Experimental Apparatus for the Measurement of the Energy Distributions of the Ionic and Neutral species Impinging on the Cathode of a Typical Ion Ion Plating Discharge.

The overall apparatus consists of a pumping system, vacuum chamber, discharge chamber, evaporation source, and analysis system. The basic requirements of the apparatus are:-

(i) the absolute pressure (in the 10^{2}-10^{-1} torr range) in the discharge chamber must be known,

(ii) the analysis system must have constant transmission up to a maximum pressure of 10^{-4} torr for energy and mass analysis of the species leaving a cathode pinhole during operation of the plating discharge,

(iii) the analysis system must have a facility for ionising neutral particles impinging on the cathode (i.e. leaving the cathode pinhole) during discharge so that their energy and mass distributions can be measured.

(iv) an evaporation source to evaporate the film material into the discharge, and

(v) a clean experimental environment for both film deposition and analysis.

Regarding the clean environment, the design criteria must include capability of operation at ultra-high vacuum (u.h.v.). To this end, all the materials used in the fabrication of the main vacuum chamber, evaporation system, analysis system, and all the electrical connections inside the vacuum chamber must be ultra-high vacuum compatible.

A detailed description of the design, fabrication and performance of

the components of the apparatus is given in this Section.

4.2.1 Overall Vacuum System

The overall vacuum system is composed of two main units; the main vacuum chamber and the pumping unit. In view of the requirements for investigating the effects of the degree of cleanliness of the substrate and discharge on parameters such as adhesion of ion-plated films, a system capable of producing well-defined environmental conditions had to be designed. Thus the system had to serve the dual purpose of attaining pressures of in the u.h.v. range, prior to ion plating operation, and of allowing pressures less than $1x10^{-4}$ torr to be maintained in the analysis region when operating the discharge at pressures up to $5x10^{-2}$ torr.

4.2.1(a) Design Considerations

The choice of minimum dimensions of the main vacuum chamber was based on the need to accommodate a 4" diameter discharge chamber (discussed in Section 4.2.2(a)), a 6" diameter spherical energy analyser (discussed in Section 4.2.4(e)), and a 4" long quadrupole mass spectrometer (discussed in Section 4.2.4(f)). In view of the u.h.v. requirements, for both clean substrate and deposition environment, stainless steel was used to fabricate the main vacuum chamber. A 12" diameter stainless chamber was designed following the standard practice used in evaporator systems in that it comprised a service collar combined with a bell - jar. However, u.h.v. technology was used throughout and all the flanges were designed to seal using metal gaskets. The main vacuum chamber, therefore comprised a cylinderical collar, 12" diameter 20" height, which incorporated all the parts necessary for electrical and mechanical feed through connections to the analysis system, the main and rough pumping systems, and the gas inlet system. A conventional stainless bell-jar style cover, 12" diameter 13" height, served as the top cover. The layout of the complete discharge chamber, and the analysis system, as originally

designed, is shown in Figure 4.1.

The main consideration in the design of the pumping system was the choice of an appropriate pump with an adequate pumping speed in order to:-

(i) allow the required base pressure to be attained, and

(ii) provide adequate differential pumping so that the pressure in the analysis system would remain below 10^{-4} torr when operating the discharge at up to 5×10^{-2} torr

Because of speed requirements, cost consideration and factors such as reliability and convenience a diffusion pump, using Polyphenyl ether Oil as the pumping fluid, was selected.

The base pressure, which was intended to be in the u.h.v. range, was to be achieved after baking the overall vacuum chamber at a temperature of 200°C for about 12 hours. The choice of this baking temperature was decided partly on the basis of experience and partly on the limitation imposed by the viton 'O' ring which seals the valve of the combination cold trap (discussed later in this Section). For calculation of the ultimate pressure the relationship

$$V \frac{dP}{dt} = Q - SP \qquad 4.2.1$$

was used. In this expression

V is the volume in litres,

P is the pressure in torr

S is the effective pumping speed in $\ell \cdot sec^{-1}$ and

Q is the total gas load in torr $\ell \cdot sec^{-1} cm^{-2}$.

The gas load, Q, is given by the expression

$$Q = \sum_{n=1}^{n} q_n A_n \qquad 4.2.2$$

KEY TO FIGURE 4.1

a) Stainless steel vacuum collar,12", OD

b) Titanium sublimation pump filament

c) 2kW, water cooled, 270° electron gun

d) Machinable ceramic discharge tube with heating facility

e) Target or substrate for ion plating (movable in plane normal to paper)

f) Extractor

g) X-Y deflectors

i) Ioniser

j) Retarding Lens

k) Hemispherical energy analyser

l) Stainless steel bell jar

m) 100 mm quadrupole mass analyser

n) Electron Multiplier.

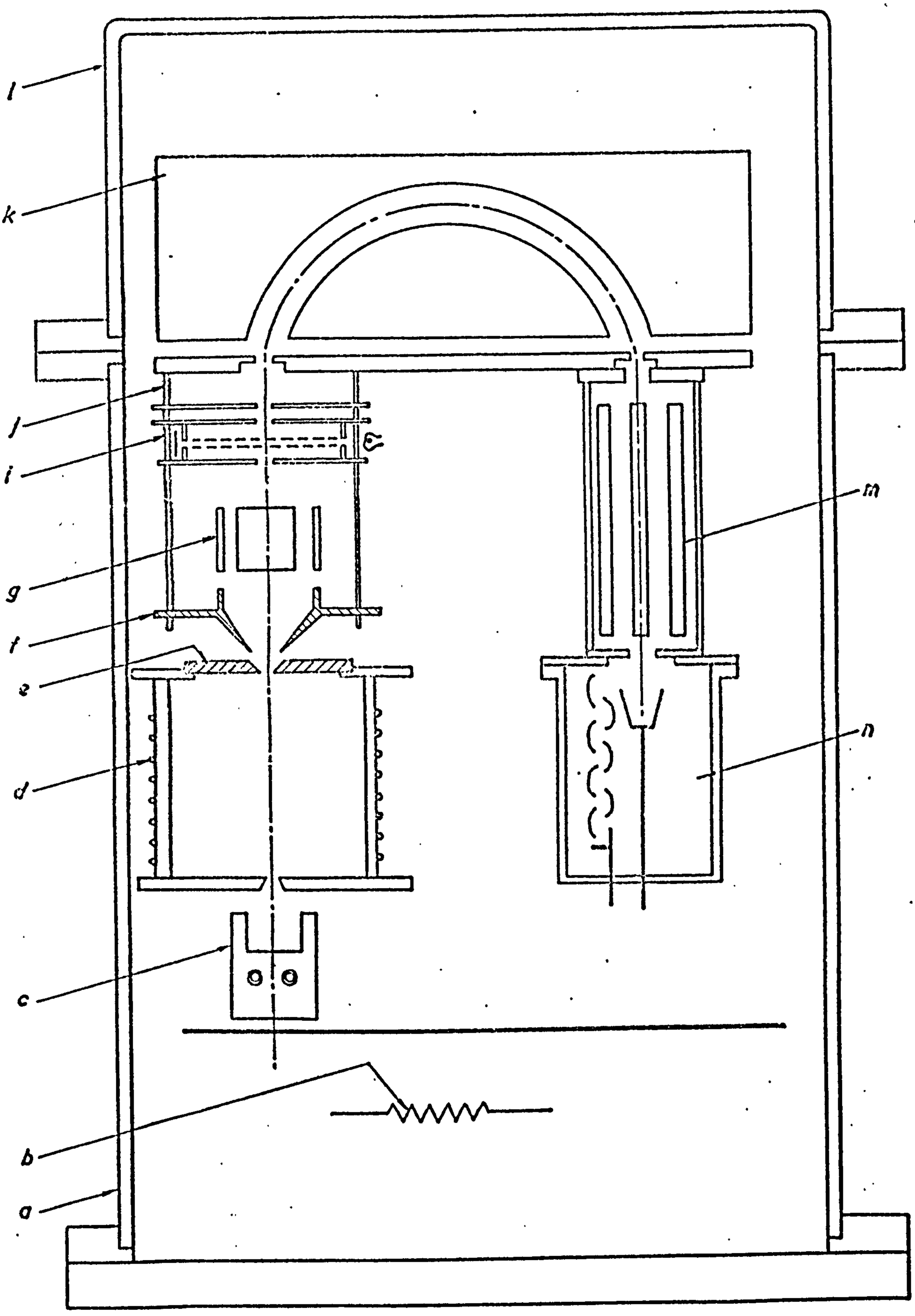

FIGURE 4.1 SCHEMATIC DIAGRAM OF THE ANALYSIS SYSTEM, AS ORIGINALLY DISIGNED.

where, q_n, is the outgassing rate of the materials exposed to the vacuum and, A_n, is the respective area. Since at the ultimate pressure $\frac{dP}{dt} = 0$ the ultimate pressure

$$P_{ultimate} = \frac{Q}{S} + P_o \qquad 4.2.3$$

where P_o is the pump contribution. Using this expression and taking the outgassing rate for stainless steel, after 12 hours of baking at 200°C to be $\approx 10^{-11}$ torr ℓ . sec.$^{-1}$ cm^{-2} a minimum pumping speed of about 150 ℓ . sec.$^{-1}$ at the main vacuum chamber was found to be necessary to pump the chamber down into the u.h.v. range.

To minimise the backstreaming of pump oil vapours into the vacuum chamber, a liquid nitrogen cooled cold trap was mounted in the pumping line. In practice, a series combination of a combination cold trap and a conventional cold trap was chosen. A short length of stainless steel bellows connected the combination cold trap to the chamber to simplify assembly of the complete system. The bellows was 200mm long, with 150mm inside diameter. In addition to minimisation of the backstreaming of pump oil into the vacuum chamber, the combination cold trap was used because it has, built into it, a high open conductance valve . This valve facilitates both throttling, and valving off the vacuum chamber from the pumping system should the need arise.

The pumping speed of the diffusion pump used in the pumping system was worked out using the expression:-

$$\frac{1}{S} + \frac{1}{C_{Tb}} + \frac{1}{C_{T1}} + \frac{1}{C_{T2}} = \frac{1}{S_p} \qquad 4.2.4$$

In this expression:

S_p is the effective pumping speed at the main vacuum chamber,

C_{Tb} is the conductance of the short flexible

bellows,

C_{T1} is the conductance of the combination cold trap,

C_{T2} is the conductance of the cold trap,

$S_{.}$ is the pumping speed at the top of the diffusion pump i.e. the effective pumping speed required

The conductances of the cold trap and the combination cold trap are given by the manufacturers[1] and the conductance, C_{Tb}, of the bellows was worked out using the expression:

$$C_{Tb} = 100 \frac{a^3}{\ell'} \ell \text{ .sec}^{-1}. \qquad 4.2.5$$

where ,a, is the inside radius (in cm) of the bellows and , ℓ' is its length (in cm). As a result of these calculations : minimum pumping speed of about 200 ℓ .sec^{-1} at top of the diffusion pump was found to be necessary. The diffusion pump chosen was a 4 inch Oil diffusion pump (Varian VHS , 600/SP utilising polyphenyl ether Oil, Convolex 10) with a pumping speed of 200 ℓ .sec.$^{-1}$. The diffusion pump, in fact, comprised part of a commercial evaporator (Nanotech Microprep 250 Coating Unit) on which the overall system was based. It was backed by a rotary pump having pumping speed of 50 ℓ. min^{-1}. A titanium sublimation pump, comprising three independent filaments, which was to be activated in the final stage of pumping (after baking) was mounted under a stainless steel shield in the main vacuum chamber. The three independent filaments were mounted onto a single high-current feedthrough flange for easy withdrawal.

A bakeable foreline trap, filled with alumina spheres, was mounted in the backing line of the diffusion pump to minimise contamination of the fine side of the pumping system following frictional dissociation of the rotary pump oil in the pump and subsequent backstreaming. A schematic diagram of the overall system is shown in Figure 4.2.

Key to Figure 4.2

1. Bell-jar cover
2. Main vacuum chamber
3. Semi-flexible stainless steel bellows.
4. Combination cold trap valve (V_{cct})
5. Combination cold trap
6. Cold Trap
7. Diffusion Pump
8. Backing line Pirani gauge (PG2)
9. Foreline Trap
10. Fine Valve (V_2)
11. Rotary Pump
12. Roughing Valve (V_1)
13. Roughing line Pirani gauge (P G1)
14. Roughing line u.h.v. valve (V_{u1})
15. Main chamber ionisation gauge (IG1)
16. Combination cold trap ionisation gauge (IG 2)
17. Valve connecting low pressure side of capacitance manometer of gas handling system to rotary pump (V_3)
18. Capacitance manometer.
19. Gas handling system u.h.v. valve (V_{u2})

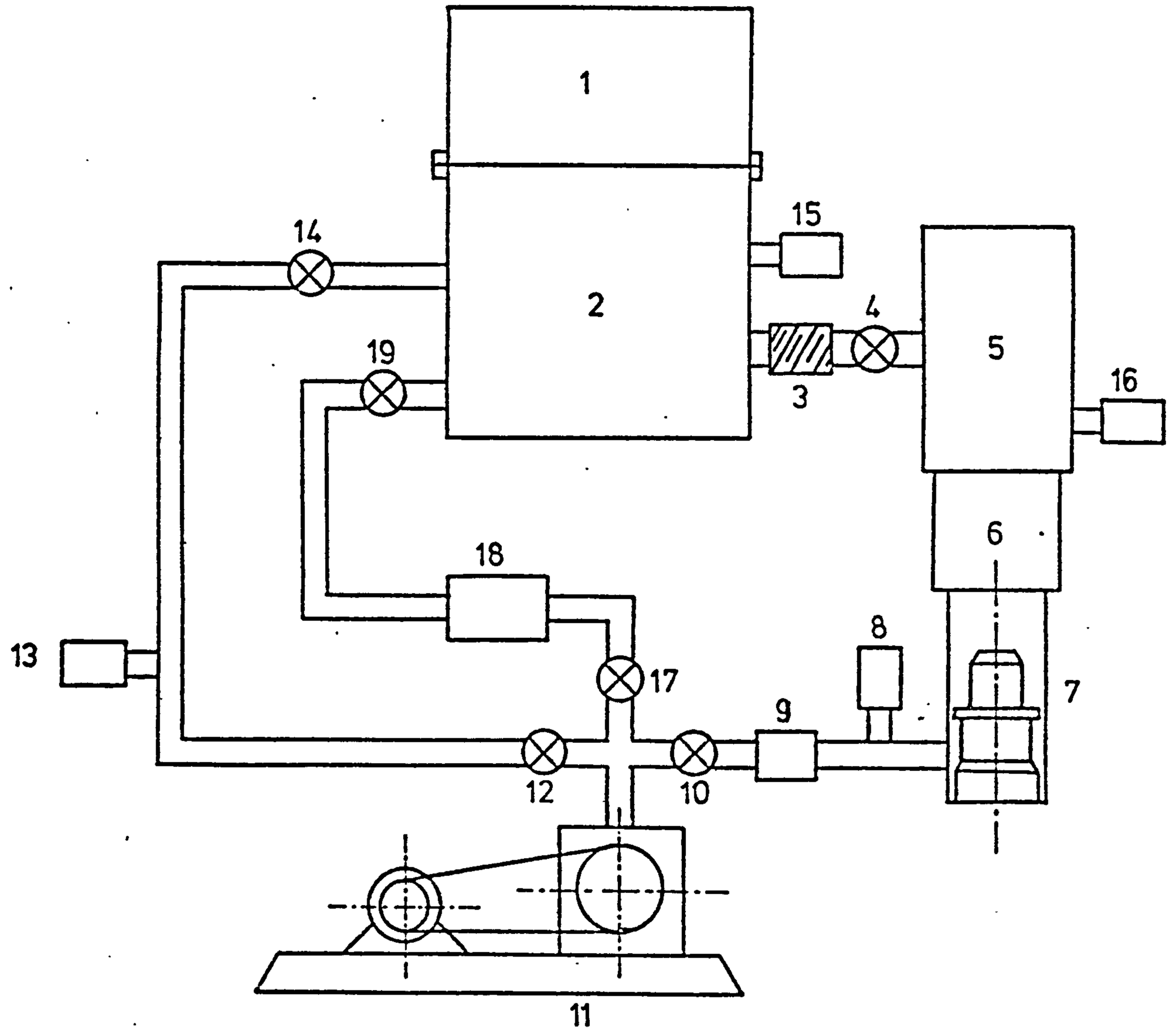

FIGURE 4, 2. LAYOUT OF THE OVERALL SYSTEM

4.2.1(b) Performance

The main pumping (fine pumping) is carried out via the valve Vcc_T, the combination cold trap and the cold trap. The rough pumping is used to pump the vacuum chamber, by the rotary pump only, via the uhv value, V_{ul} and the value, V_l . The main idea behind the deployment of the roughing line, together with the value, V_{CCT}, was to avoid breaking the vacuum above the diffusion pump (and hence switching the diffusion pump off) each time the vacuum chamber was opened to atmospheric pressure. Eventually, with the provision of the roughing facility, the system could be operated as a conventional evaporator. The pirani gauge, PG2, facilitated continuous monitoring of the pressure behind the diffusion pump to minimise the risk of incorrect operation.

From "design" considerations regarding the pumping speed of the diffusion pump, an ultimate unbaked pressure in the 10^{-8} torr range in the main vacuum chamber was expected to be achieved. After about five hours of pumping with both the liquid nitrogen cooled cold traps full, an ultimate pressure of 4×10^{-8} torr was achieved.

The system was then baked for about 12 hours at about $200^{o}C$ and, after outgassing the filaments of both the ionisation gauges, a pressure of 2×10^{-9} torr was achieved in the chamber. The titanium sublimation pump was then activated with a current of about 50A, and after a total activation time of about 15 minutes a pressure of about 3×10^{-10} torr was achieved in the chamber. Hence it was practically proved that the system was capable of pumping down into the u.h.v. range.

4.2.2 Discharge and Gas Handling System

As discussed earlier in this chapter, the evaporation source, discharge chamber, and analysis system were all mounted in the same vacuum chamber and it is therefore clear that the main pumping system must also be capable of maintaining the required differential between the pressure inside the discharge tube, typically about 2×10^{-2} torr, and that in the analysis region $< 10^{-4}$ torr.

The sytsem was designed to allow gas to be introduced into the discharge chamber to an accurately known pressure. The discharge system is composed of two parts. They are:-

(i) the discharge chamber, and

(ii) the gas handling system

4.2.2(a) <u>The Discharge Chamber</u>

On the basis of the work of Sharbiney[2], in determining the optimum parameters for a typical ion plating discharge, a cathode-anode distance of about 100mm was chosen. The cylinderical discharge chamber was thus fabricated using a machinable glass ceramic tube. It is 100mm long with outside and inside diameters of 100mm and 88mm, respectively, with stainless steel electrode plates at each end. A spiral groove was machined along the whole outside wall ofthe tube in order to accommodate a heating coil should the need for additional outgassing arise. The seals between the ends of the tube and the electrode plates were formed using gold wire. A detailed diagram of the discharge chamber is given in Figure 4.3. A 0.5mm sampling aperture, in the cathode, was used. The diameter of the aperture was later widened to 1mm. (see Section 4.2.6).

To prevent the build up of evaporant on the inside of the discharge chamber itself a thin-walled quartz tube, 94mm long, and a glass ceramic disc 4mm thick with a diameter equal to that of the outside diameter of thin-walled glass tube were mounted inside the main ceramic tube. A 15mm diameter hole was drilled through the glass ceramic disc. Consequently, the only part of the top stainless disc of the discharge chamber exposed to the discharge was the area immediately behind the 15mm diameter hole.

It has been indicated earlier that it is necessary to provide differential pumping in order to maintain an acceptable pressure in the analysis region when operating the discharge. The requirements (10^{-2} torr range in the discharge chamber and $< 10^{-4}$ torr in the analysing region) were the major factors in determining the size of the apertures in the electrodes. The apertures initially used, 0.5mm diameter in the cathode and 1mm diameter in the centre

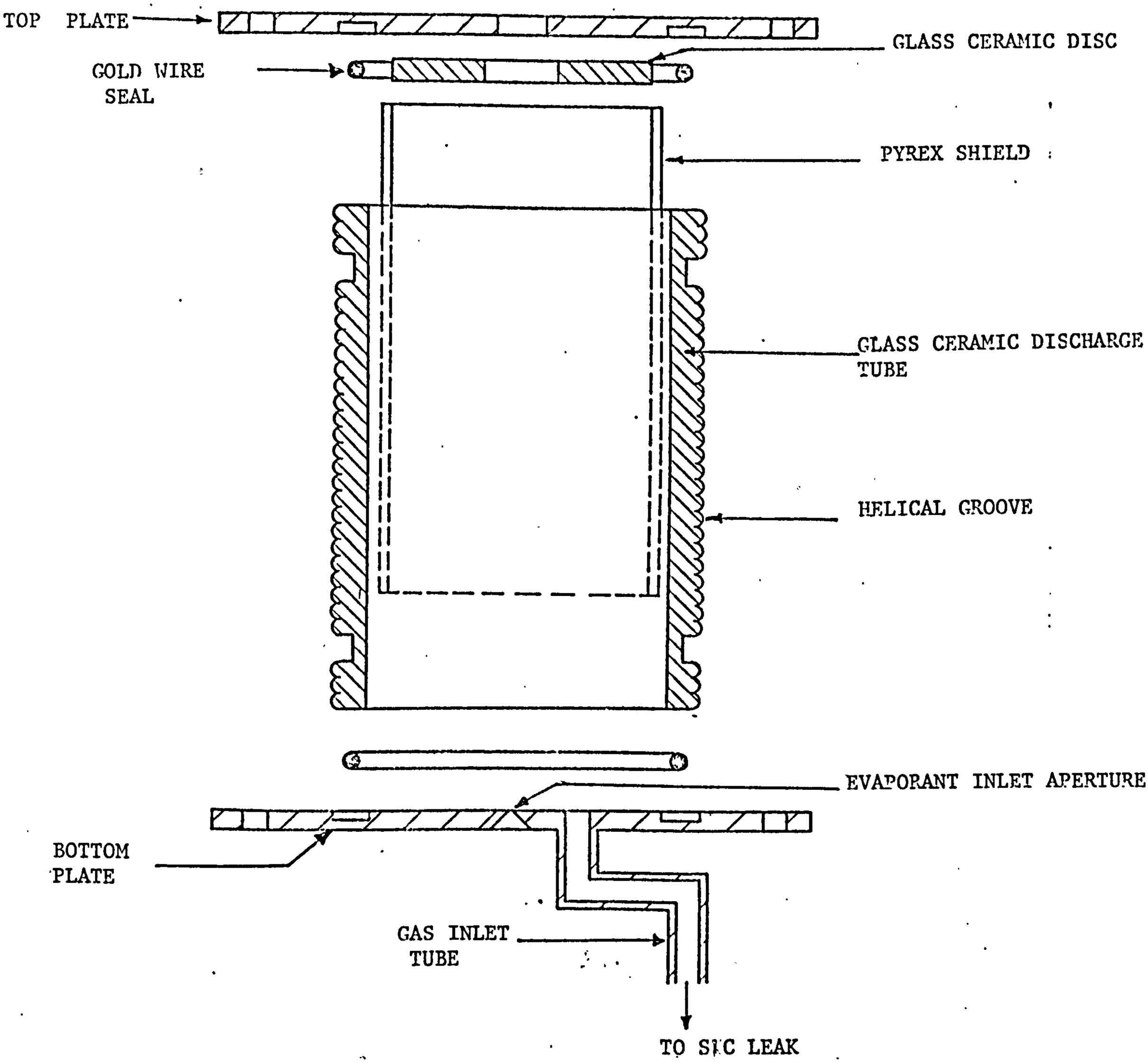

FIGURE 4.3 EXPLODED VIEW OF DISCHARGE CHAMBER

of the anode (bottom disc of the discharge tube) were found to allow a discharge chamber pressure of 9×10^{-2} torr with a rise of 10^{-5} torr in the analysing region. The 1mm diameter aperture in the bottom disc of the discharge chamber was to allow the evaporant originating in the hearth of the electron gun placed immediately underneath the discharge chamber to enter the discharge region. The size of the apertures represents a compromise between a number of conflicting factors. The aperture in the cathode must be large enough to allow reasonable sampling i.e. measurable signals in the detector system, but its presence should not perturb the discharge to any significant extent. Similarly, the aperture in the anode must be large enough to allow significant evaporant into the discharge without unacceptable load in the pumping system. However, this arrangement was found to be unsatisfactory and in that an adequate supply of evaporant could not be obtained within the discharge tube and an alternative arrangement was used. In this arrangement a boat evaporator was located inside the discharge tube itself rather than outside it as was required for the electron gun evaporator. This allowed a further improvement in sensitivity to be maintained since the size of the sampling aperture could be increased to 1mm without any increase in the differential pumping requirements. (the differential pumping requirements were maintained by blocking the anode aperture). The boat evaporator arrangement is shown in Figure 4.4.

4.2.2(b) Gas Handling System

Figure 4.5 shows the layout of the gas handling system. The system in which gas is introduced into the discharge region via a calibrated silicon carbide (SiC) leak was designed to be used in conjunction with a capacitance micromanometer (Furness Controls Ltd., MDC FC001) such that absolute measurements of the discharge pressure could be carried out using oil or mercury manometer without contaminating the gas. Carrier gas at known pressure, measured by the capacitance micromanometer, was leaked through the SiC leak into the discharge chamber. The pressure inside the discharge chamber, P, can be calculated using the expression:-

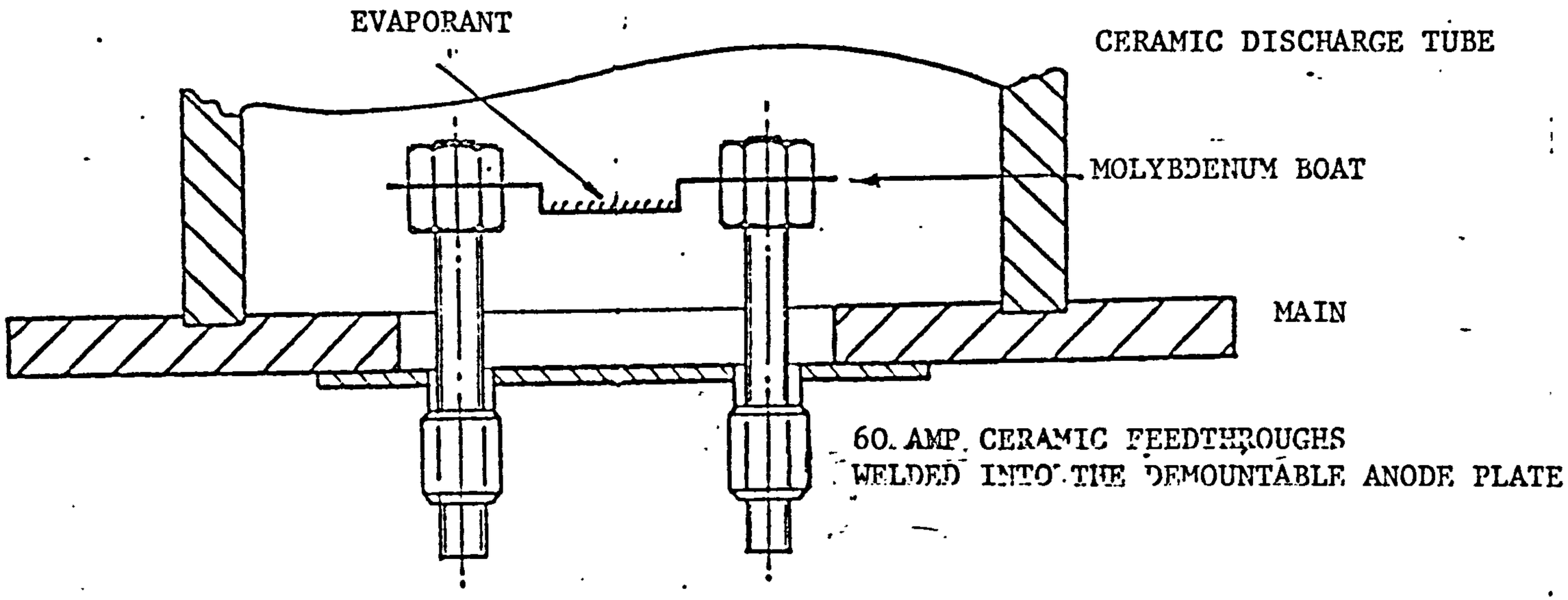

FIGURE 4.4 BOAT EVAPORATOR MOUNTED INSIDE THE DISCHARGE TUBE

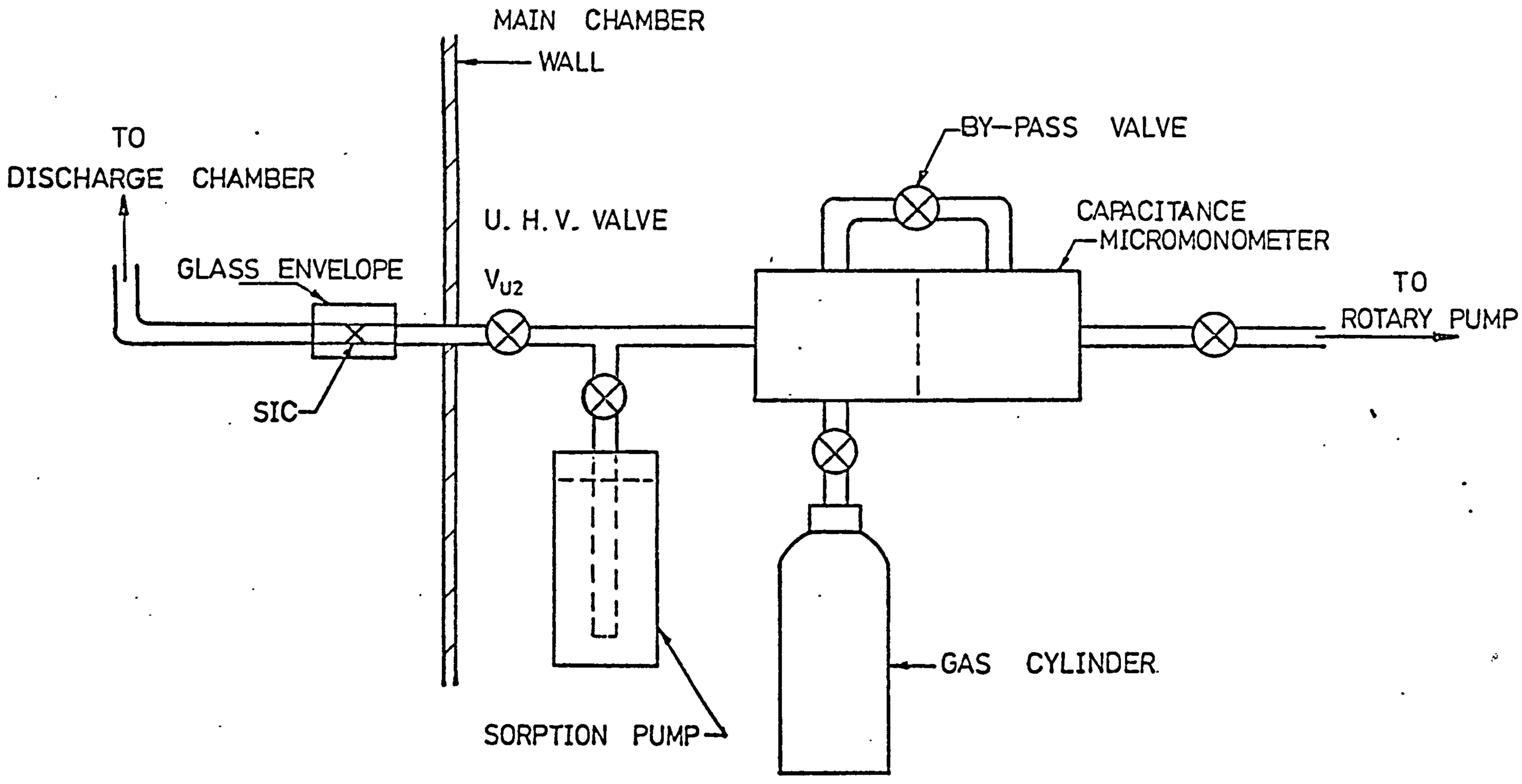

FIGURE 4, 5. LAYOUT OF GAS HANDLING SYSTEM

$$P \approx \frac{C_1C_L + C_bC_1P_c + P_gC_L}{C_LC_b + C_1C_L + C_bC_1} \qquad 4.2.6$$

In expression 4.2.6

C_1 is the conductance through the aperture in the cathode,

P_c is the pressure in the analysis region,

P_g is the pressure of the carrier gas behind the silicon carbide leak,

C_b is the conductance of the bellows and the pipe betwen the silicon carbide leak and the discharge chamber, and

C_L is the conductance through the silicon carbide leak.

The conductance C_1 and C_b can easily be calculated from the formalae given in Reference 1, P_g can be measured by the capacitance manometer and P_c, which does not need to be known accurately as long as it is much less than P, can be measured by the ionisation guage IGI in the vacuum chamber. Thus the only unknown parameter in the calculation of the pressure in the discharge region, in the above expression, is the conductance C_L, through the silicon carbide leak. However, this leak can be calibrated for different gases using the technique described in Section 4.2.2(c)

4.2.2(c) Measurement of the Conductance of Silicon Carbide Leak

The leak to be calibrated was sealed into a 5/8" O.D. glass tube which could be mounted directly into the calibration system. The approximate length of silicon carbide rod required to give the desired conductance was initially calculated using data supplied by the manufacturer (A.E.I. Scientific Apparatus Ltd.). The measuring technique may be best described with reference to Figure 4.6

The procedure adopted to measure the conductance C_L (of the silicon carbide leak) was to monitor the pump-down of a known volume (V) through the leak i.e. if P(t) is the continuous pressure in the volume V and C_L in the leak conductance.

$$P(t) = P_o \exp\left(-\frac{C_L}{V} t\right) \qquad 4.2.7$$

where P_o is the pressure in the known volume V at time t = 0. Expression 4.2.7 can be re-arranged as:-

$$\log_e\left(\frac{P}{P_o}\right) = -\frac{C_L}{V} t \qquad 4.2.8$$

A plot of $\text{Log}_e(\frac{P}{P_o})$ versus t is a straight line of gradient $-\frac{C_L}{V}$. Since V is known C_L can be deduced.

However, due to small C_L and relatively high outgassing rate of the test chamber no total pressure drop is expected and, in practice, it is necessary to use a partial pressure measuring system. Referring to Figure 4.6 the procedure adopted was, therefore, as follows:-

(a) The stainless steel test chamber (Volume V) and the mercury manometer were evacuated by the diffusion pump via the by-pass valves I and II. The minimum obtainable pressure was $\sim 10^{-5}$ torr.

(b) The by-pass valves were then shut and argon was admitted to the known volume on the high pressure side of the leak. The partial pressure

of argon, on the low pressure side of the leak, was monitored (using the mass spectrometer) as a function of gas pressure in the test chamber (measured with mercury manometer in conjunction with a capacitance bridge arrangement). This measurement yielded the expected linear relationship between the two pressure readings and allowed the argon pressure in the high pressure chamber to be measured using the mass spectrometer.

(c) Argon was admitted to a certain pressure (100 torr) and the known volume isolated from the gas supply. The decay of the mass spectrometer reading with time, as the volume was slowly evacuated via the leak, was recorded over a period of 15 hours. This decay was then converted to the corresponding decay of gas pressure with time using the linear relationship between the gas pressure, on the high pressure side and mass spectrometer reading, on low pressure side (obtained in stage b of this procedure).

(d) The decay was then plotted on a log./linear graph giving a straight line whose gradient is proportional to the conductance of the leak.

The procedure was repeated for Krypton and Xenon gases and conductances of 3.5×10^{-5} torr ℓ . sec^{-1}, 2.4×10^{-5} torr ℓ . sec^{-1} and 1.9×10^{-5} torr ℓ . sec^{-1} were found for Argon, Krypton, and Xenon respectively. It was, therefore, confirmed that as expected for molecular flow conditions C_L is proportional to $M^{-\frac{1}{2}}$ where M is the atomic weight of the gas.

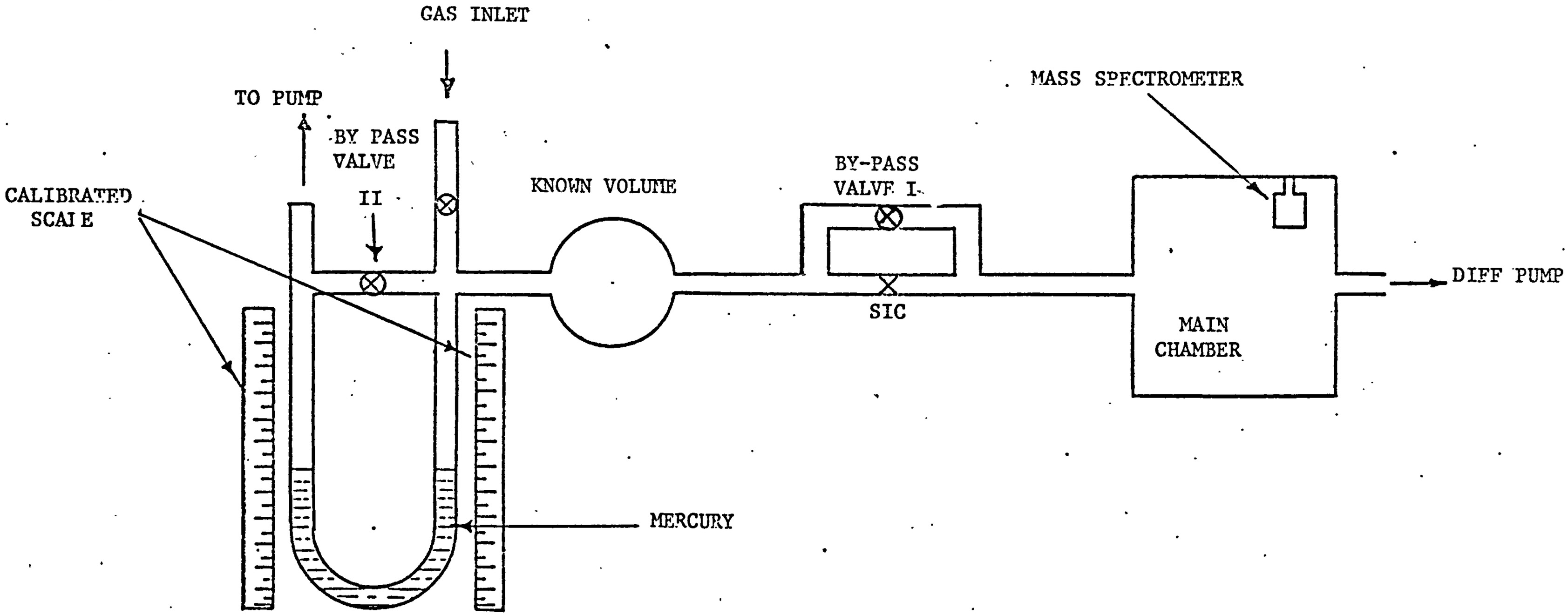

FIGURE 4.6 SCHEMATIC DIAGRAM OF THE SYSTEM USED IN CALIBRATION OF CONDUCTANCE OF THE SIC LEAK

4.2.2(d) Constructional Details

The discharge tube was constructed from machinable glass ceramic. This material was selected because it is insulating, machinable, bakable, and has (according to the manufacturer's specification) low outgassing rate even at high temperatures. The discharge carrier gas was fed into the chamber via the glass encapsultated SiC leak assembly, a stainless steel bellows, and a short length of machinable ceramic tube. (see Figure 4.5) Interference fits at both ends of the short glass ceramic pipe provided almost negligible leakage conductance and this pipe together with the glass envelope of the SiC leak allowed the stainless steel bellows to remain at a floating potential. This was necessary in order to ensure that the discharge struck only inside the discharge chamber, and not across the glass ceramic feed pipe, which would have occurred ,and in fact did occur, if the bellows touched earth when this arrangement was not in use.

4.2.2(e) Performance

The manometer can be used as a null reading instrument or as a straight-forward direct pressure measuring device by continuous pumping of one side of the diaphragm. When used in the latter mode it required regular adjustment and was zeroed initially by pumping out both sides of the diaphragm using the rotary pump in conjunction with a suitable by-pass valve. Following this procedure, and closure of the by-pass valve, the pressure of the gas admitted to the high pressure side of the SiC leak, to which region one side of the diaphragm is connected, could be measured directly. The u.h.v. valve, V_{u2} was then turned to 'open' position and the operation of the gas handling system started. The pressure in the vacuum chamber was measured for different readings of the carrier gas pressure behind the silicon carbide leak. The pressure inside the discharge chamber was deduced on the basis of the known rates of the introduction of the carrier gas and the conductances of the aperture in the discharge chamber. The calibration curve, i.e. discharge pressure versus

the pressure on the high pressure side of the SiC leak is shown in Figure 4.7. The validity of the results presented in Figure 4.7 was assessed by running discharges with different pressure readings on the high pressure side of the SiC leak and recording the discharge voltage current and pressure (the latter was obtained using the characteristic given in Figure 4.7) after the discharge reached its stable state. The results were observed to be in good agreement with the work done by Sharbiney[2] who measured voltage and current values of ion plating discharges at various pressures.

4.2.3 The Analysis System

One of the most important purposes of the work described in this thesis was to investigate the constituents of the particle flux impinging on the cathode of a typical ion plating discharge. In particular the mass and energy distribution were of interest. To fulfill these requirements an analysis system comprising:-

(i) ion extractor
(ii) deflection lens
(iii) post extraction ionisation chamber
(iv) retarding lens
(v) energy analyser
(vi) mass spectrometer, and
(vii) detector.

was designed and developed. These components are described in this Section. The materials used in the construction of all the elements of these components were ultra high vacuum (uhv) compatible.

4.2.3(a) Ion Extractor

In any plasma sampling system, it is essential that there is a known, and preferably constant relationship between the detected flux and the flux of particles impinging on the extractor aperture (in this case this aperture is in the

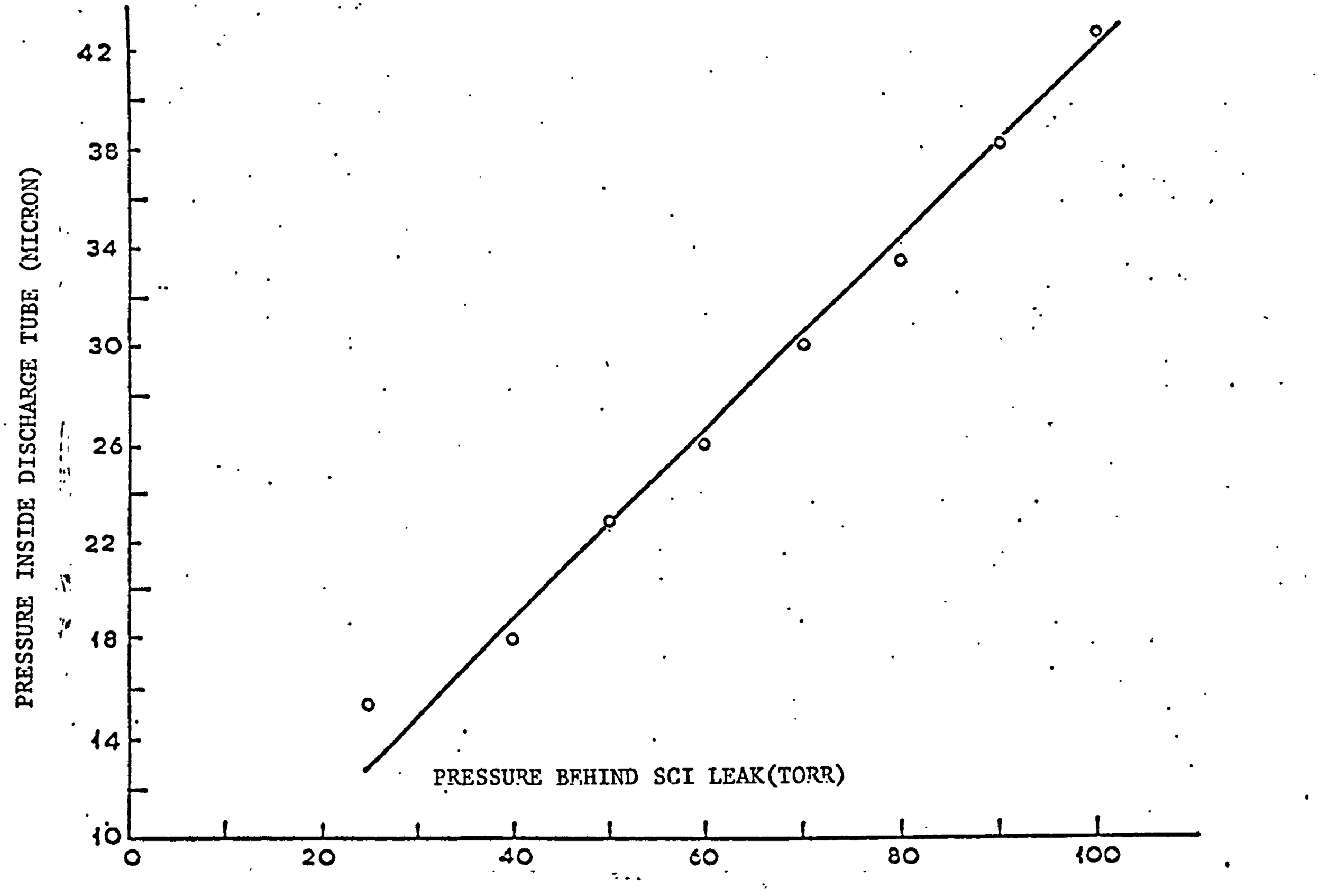

FIGURE 4.7 VARIATIONS OF THE PRESSURE IN THE DISCHARGE TUBE WITH PRESSURE BEHIND SIC LEAK

cathode). Hence the overall expreimental function of the analysis system must be known and the design of ion extractor system must be based on a number of fundamentally important considerations. These considerations have been thoroughly investigated by Armout[3] and they are briefly discussed here.

The final choice of the dimensions of the sampling aperture must represent a compromise between a number of conflicting requirements.

1. The diameter has to be large enough to allow accurately measurable current in the analysis system.

   For the plasma conditions considered in the present work and for the purpose of an order of magnitude calculations, ambipolor diffusion was assumed to be the controlling charged particle loss mechanism and an approximation to the current entering the analysis system, for the case of right circular cylinder with the origin of the co-ordinate system at the centre of the cylinder shown (Figure 4.8(a)), is

$$I_s = eN_o \left(\frac{D_a \pi}{\ell_o} \cdot \frac{\pi d^2}{4} \right) \qquad 4.2.9$$

   In this expression e is the electronic charge, N_o is the central density at the particular instant of time considered, D_a is the diffusion coefficient and d is the diameter of the sampling aperture.

2. The mean free paths for any of the possible ion production, conversion or loss processes have to be larger than the aperture diameter (assuming diameter $>$ length) so that perturbation of the sample during its transfer from the plasma into the extractoris is minimised.

3. In order to minimise the number of particle surface collisions within the aperture its length, ℓ is required to be less than its diameter d. Armour[3] reported that the ion transmission of a sampling aperture is extremely sensitive to changes in the ratio of d/ℓ and an increase in d/ℓ by a factor of 2, at a constant diameter, leads to an increase in the ion current, for similar plasma conditions, of more than an order of magnitude.

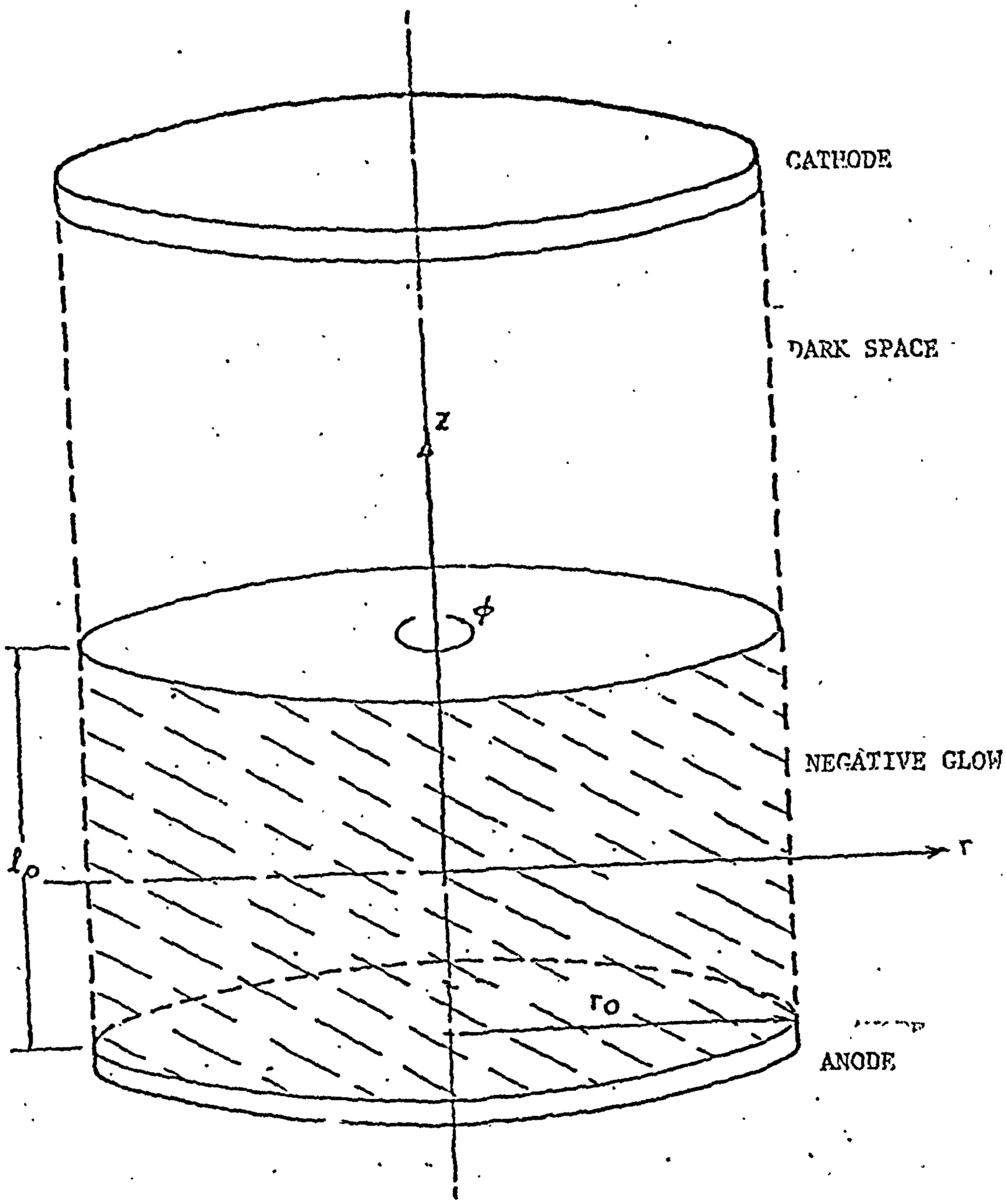

FIGURE 4.8(a) SIMPLIFIED MODEL OF DISCHARGE USED IN PLATING CALCULATIONS [3]

4. The diameter had to be small enough to ensure that:-

(a) the sampling process i.e. the flow of neutral and ionised species out of the discharge did not significantly perturb the stationary characteristics of the plasma.

(b) maintenance of the required pressure differential at the highest working pressures required pumping speeds that were practically feasible.

In fact the choice of the diameter of the aperture(s) in the cathode was based upon these considerations. The extraction electrode geometry was based upon the Pierce criterion but, as will be discussed later, the use of an accelerating field in the extraction region was actually avoided .. The extractor electrode was machined from a solid aluminium with a 5mm diameter aperture (Figure 4.8(b)) and was mounted 5mm. above the sampling aperture. This arrangement was found to fulfill the most important sampling considerations which were to avoid disturbing the discharge and to obtain species independent transmission.

4.2.3(b) Deflection Lens

The deflection system was incorporated for two reasons.

a) To optimise the alignment of the ion beam passing through the extractor, with the axis of entrance aperture of the analysis system.

b) To facilitate the mass and energy analysis of the neutral species which also pass through the cathode sampling aperture by deflecting the extracted ions off the axis to prevent them from reaching the analyser.

A diagram of the deflection system is shown in Figure 4.9. The material used in the construction of the deflector system was aluminium. A single D.C. power supply was used to provide D.C. voltage to opposite paris of deflector elements.

4.2.3(c) Ionisation Chamber

An important feature of the experiments reported in this thesis is the measurement of the mass and energy distribution of the neutral particles which

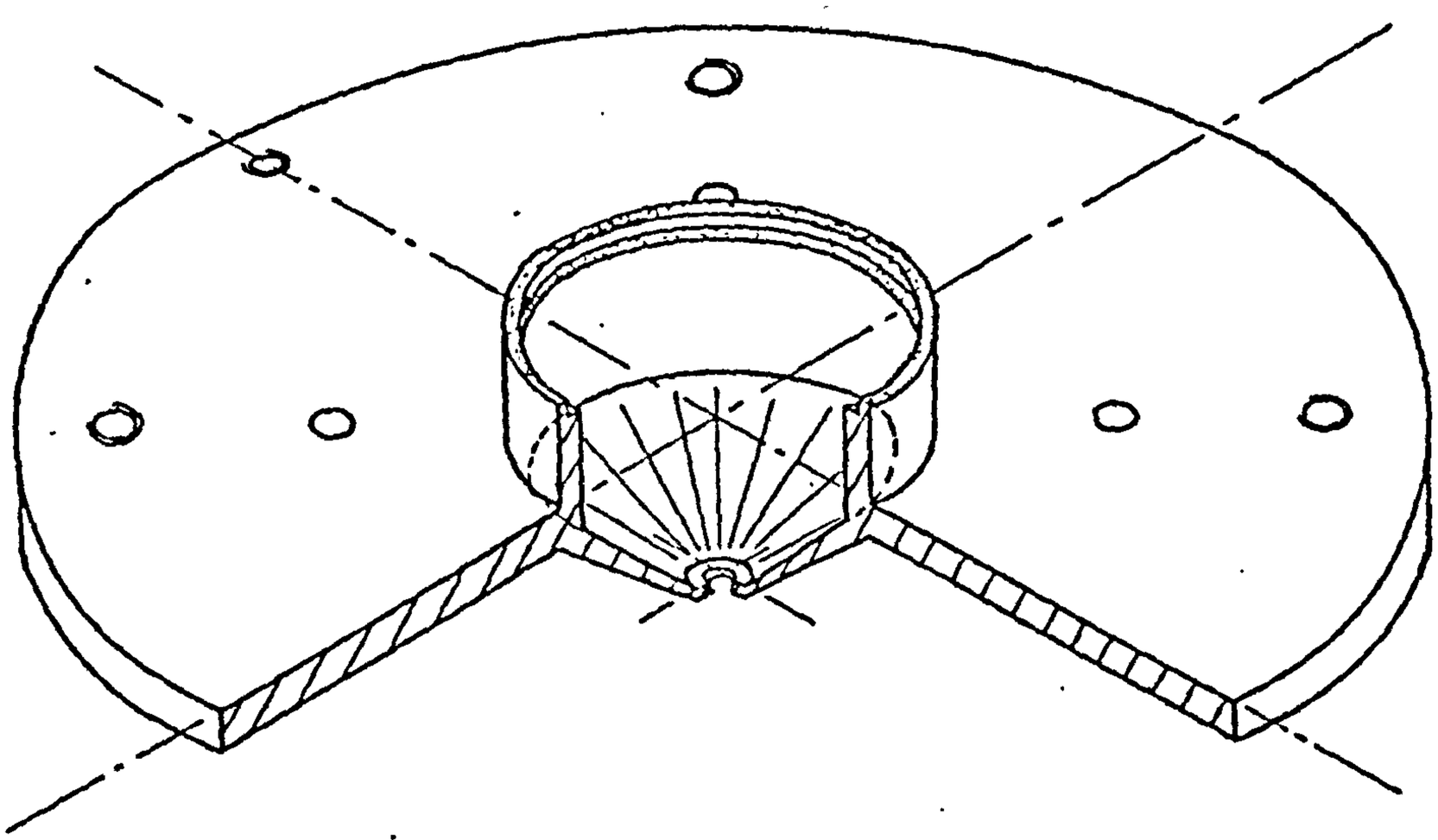

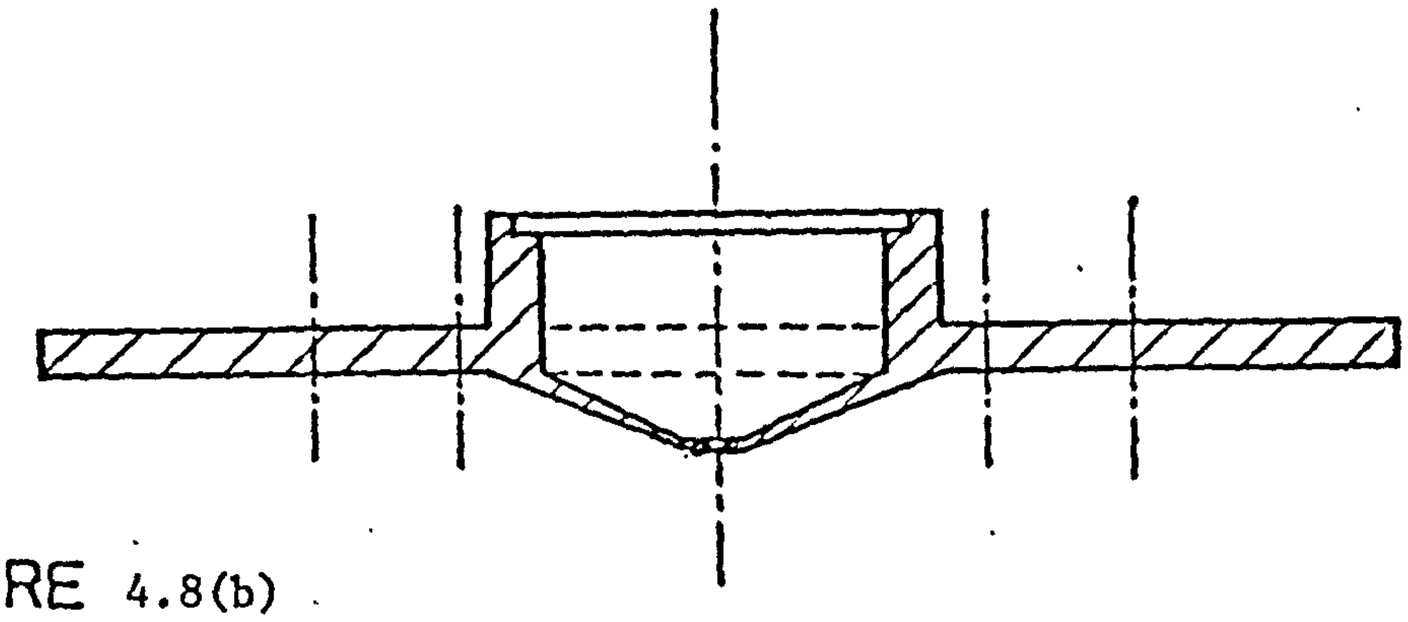

FIGURE 4.8(b)

SECTIONAL & PICTORIAL VIEWS OF THE ION EXTRACTION LENS

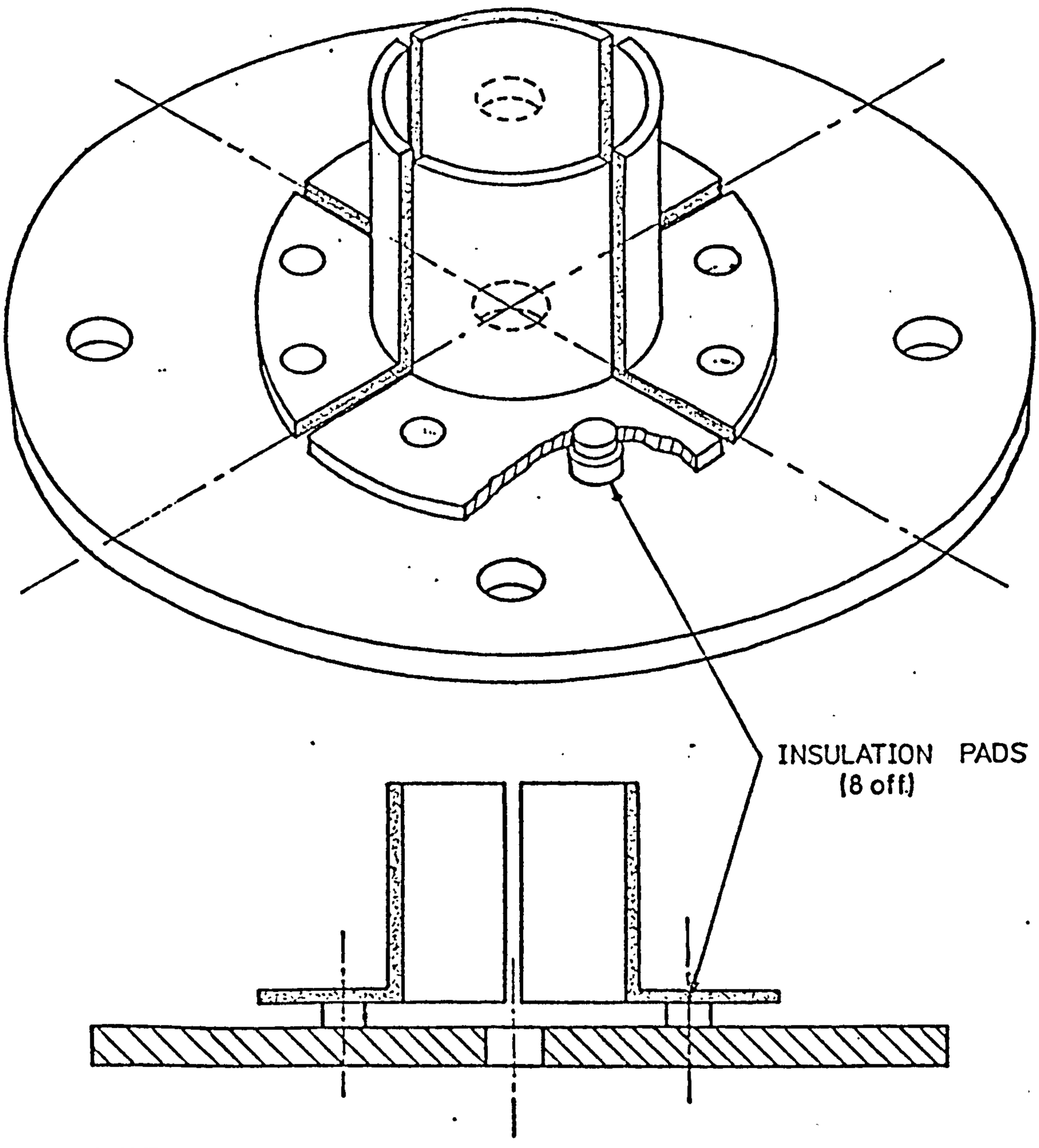

FIGURE 4.9

SECTIONAL & PICTORIAL VIEWS OF THE DEFLECTION LENS

also impinge on the cathode of plating discharge. To this end an ionisation chamber was mounted in the analysis system immediately in front of the retarding lens such that those neutral particles passing through the extractor and travelling along the axis of the cathode pinhole could be ionised and subsequently identified and energy analysed.

Figure 4.10 shows a diagram of this post-extraction ionisation system. Ionisation of neutral particles in the ionisation chamber took place as a result of electron impact. The material used in the construction of the ionisation chamber was stainless steel which was preferred on mechanical grounds to aluminium because of radiation heating from the filament. A potential difference of about 100V was applied between the filament and the ionisation chamber. This voltage was selected to optimise the ionisation efficiency since[4] electron impact ionisation cross-section in most materials peak in the 70-120V range.

4.2.3(d) Retarding Lens

Two main reasons necessitated the deployment of a retarding lens in the analysis system:-

(i) to operate the energy analyser with constant transmission and,

(ii) to enable the optimium acceptance energy for the mass spectrometer to be selected.

The constant transmission phenomenon has already been discussed in this Chapter. Regarding the second reason for the use of the retarding lens, as described in Section 4.2.3(f), the resolution in quadrupole mass spectrometers degrades when the transit time of the ions passing through it becomes so short that they cannot perform sufficient number of oscillations to allow adequate separation of particles following trajectories corresponding to stable and unstable oscillations.

An exploded view of the retarding lens is shown in Figure 4.11. The material used in construction of the lens was aluminium and its design was based on computer simulation work done by Beanland[5], The geometry of the lens was chosen such that the ion beam passing through it could be retarded over a wide

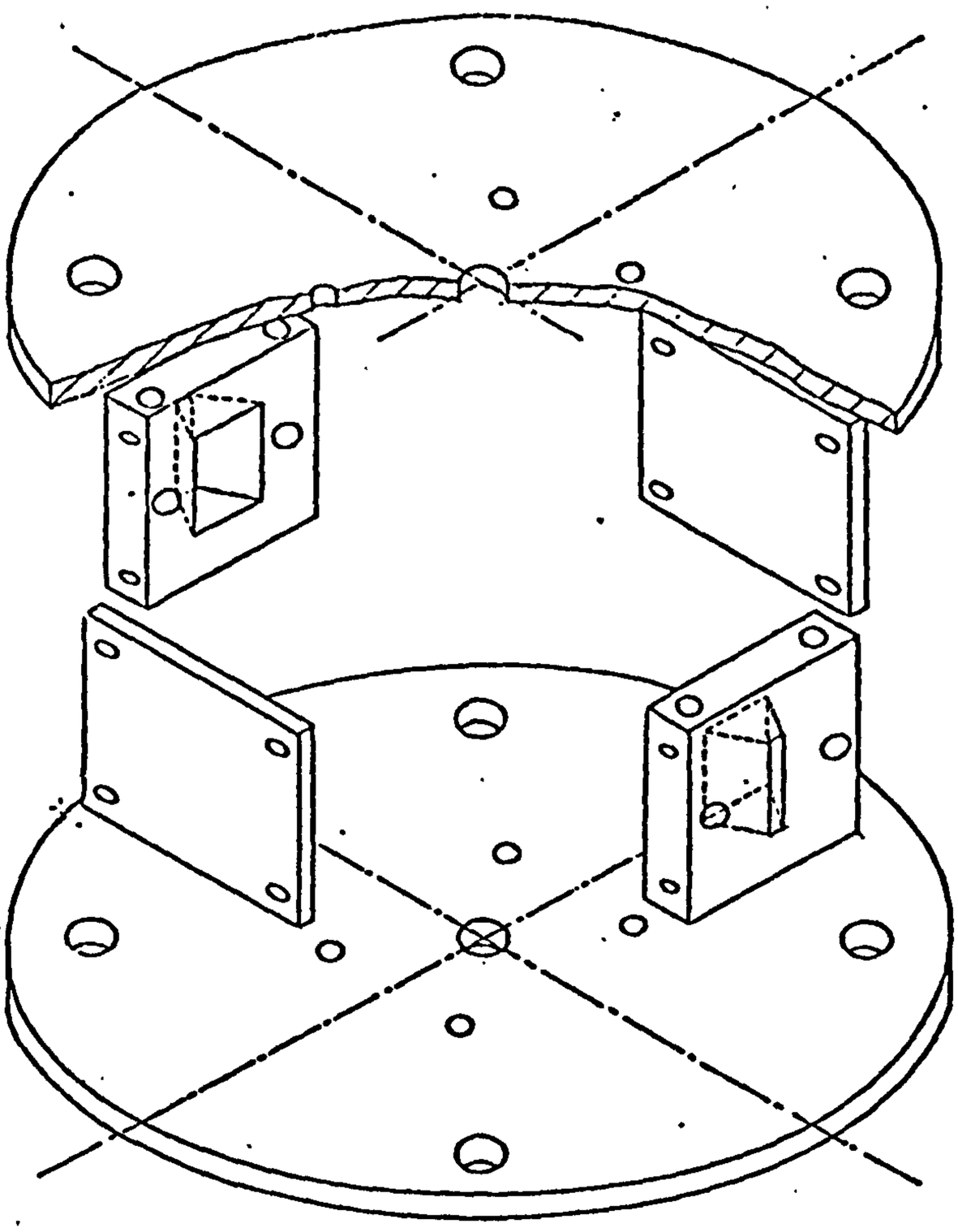

IONISATION CHAMBER

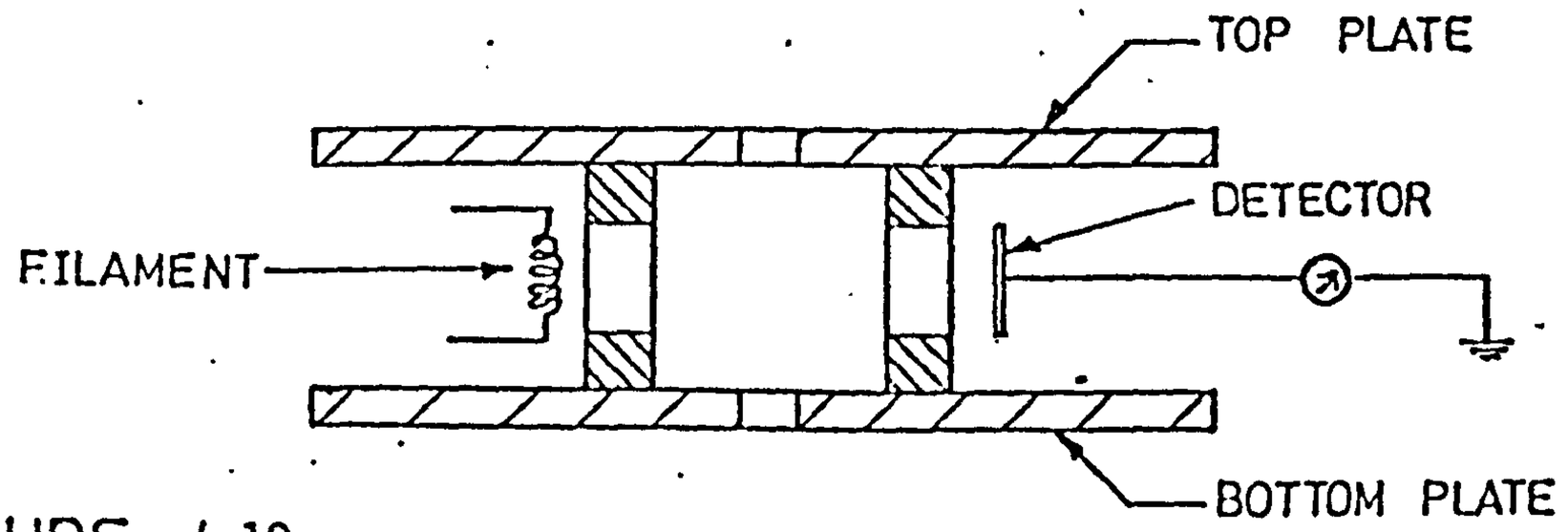

FIGURE 4.10

SECTIONAL & PICTORIAL VIEWS OF THE IONISATION CHAMBER

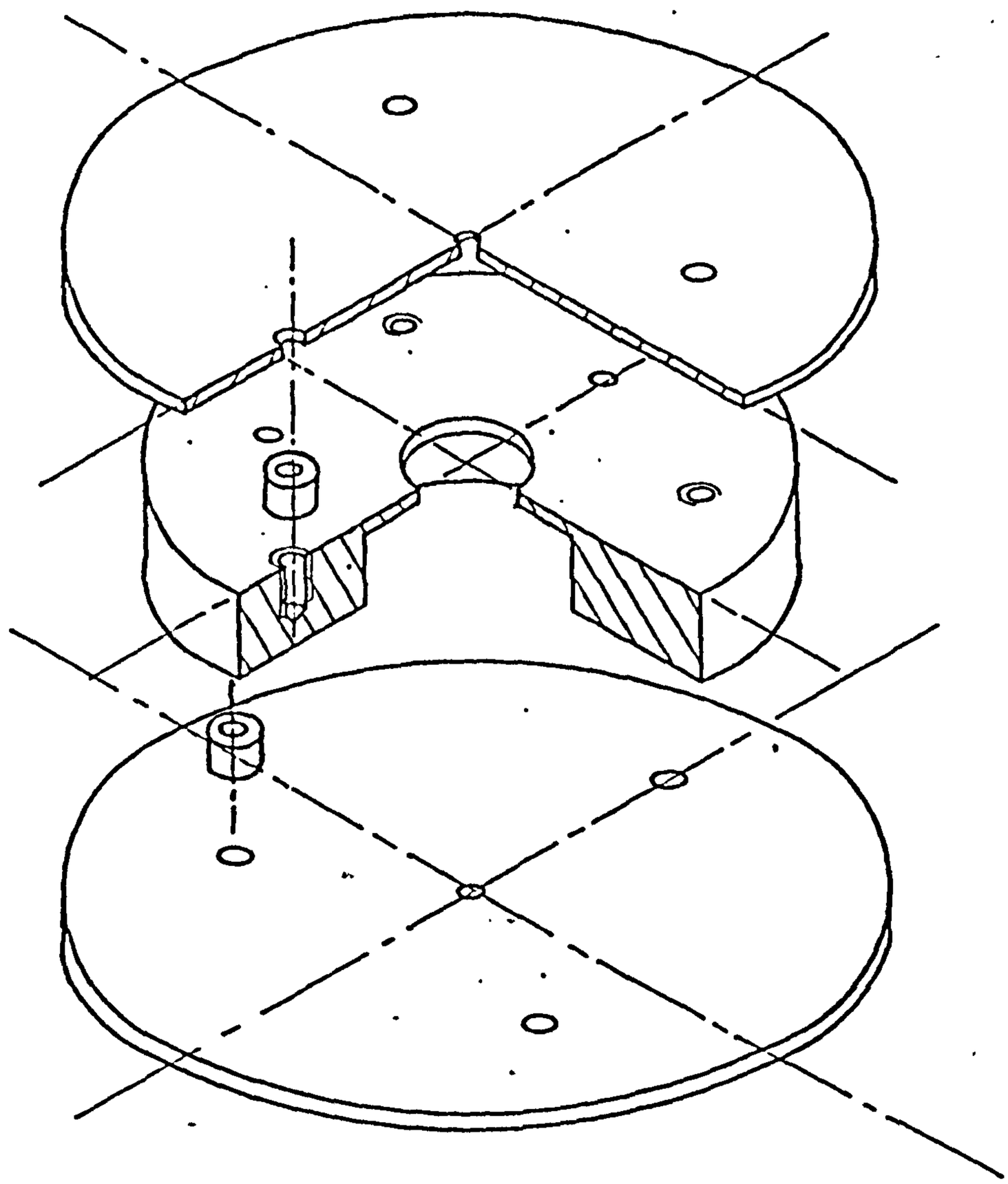

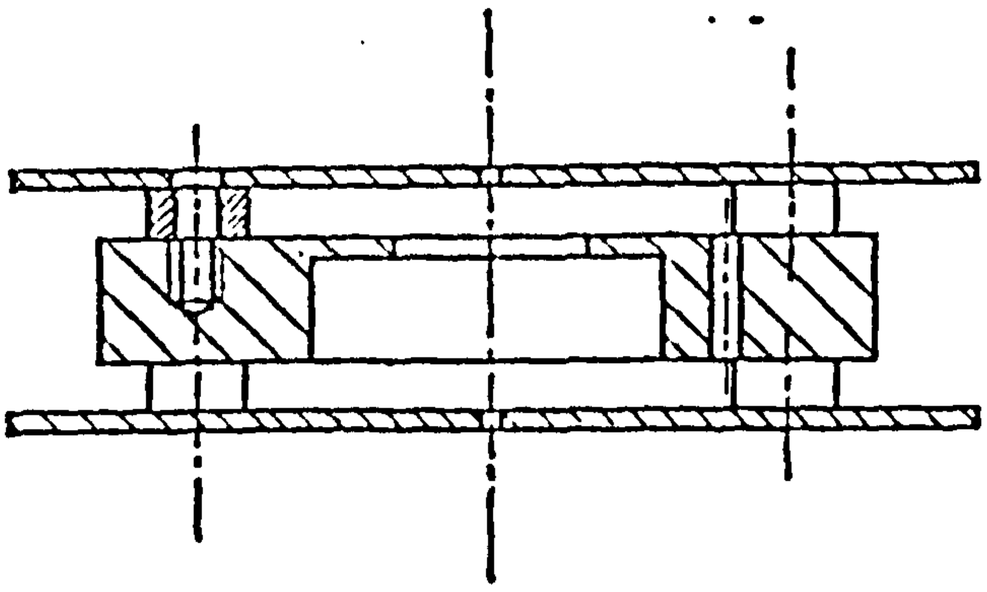

FIGURE 4.11

SECTIONAL & PICTORIAL VIEWS OF THE RETARDING LENS

range of retarding ratios E_f/E_i ratios (where E_i and E_f are initial and final energies, respectively) with minimum focusing. In the present application, the maximum incident energies were expected to be in the region of 2000-3000 eV and in order to obtain acceptable resolution with the 10cm rod, 2MHz quad. mass spectrometer the maximum entrance energy was 20eV (see Section 4.2.3(f)). Consequently retarding ratios up to about 150:1 were required. Figures 4.12 (a) - (d) show that for the lens used only minimal focusing is expected to occur up to a ratio of 200:1. For completeness the equipotential diagram for a 200:1 ratio is shown in Figure 4.12(e).

The use of this type of lens i.e. a single retarding stage in preference to a more sophisticated 3 or 4 element lens of the type used in electron spectroscopy enables an adequate experimental function to be obtained without the requirement of a sophisticated non-linear retarding voltage supply arrangement.

4.2.3(e) Energy Analyser

The need to measure the energy distributions of particles impinging on the cathode, in a typical ion plating discharge, necessitated the design of a suitable energy analyser. The analyser was required to have the following specifications:-

(a) the material of construction should be u.h.v. compatible.

(b) an ability to focus in two plains

(c) to have high transmission at low energies.

On the basis of these requirements the design of a hemispherical energy analyser was undertaken.

Following the work of Purcell[6] in 1938 considerable work on this type of electrostatic energy analyser has been done and the report of Simpson[7] contains most of the design information required. The design of the hemispher-

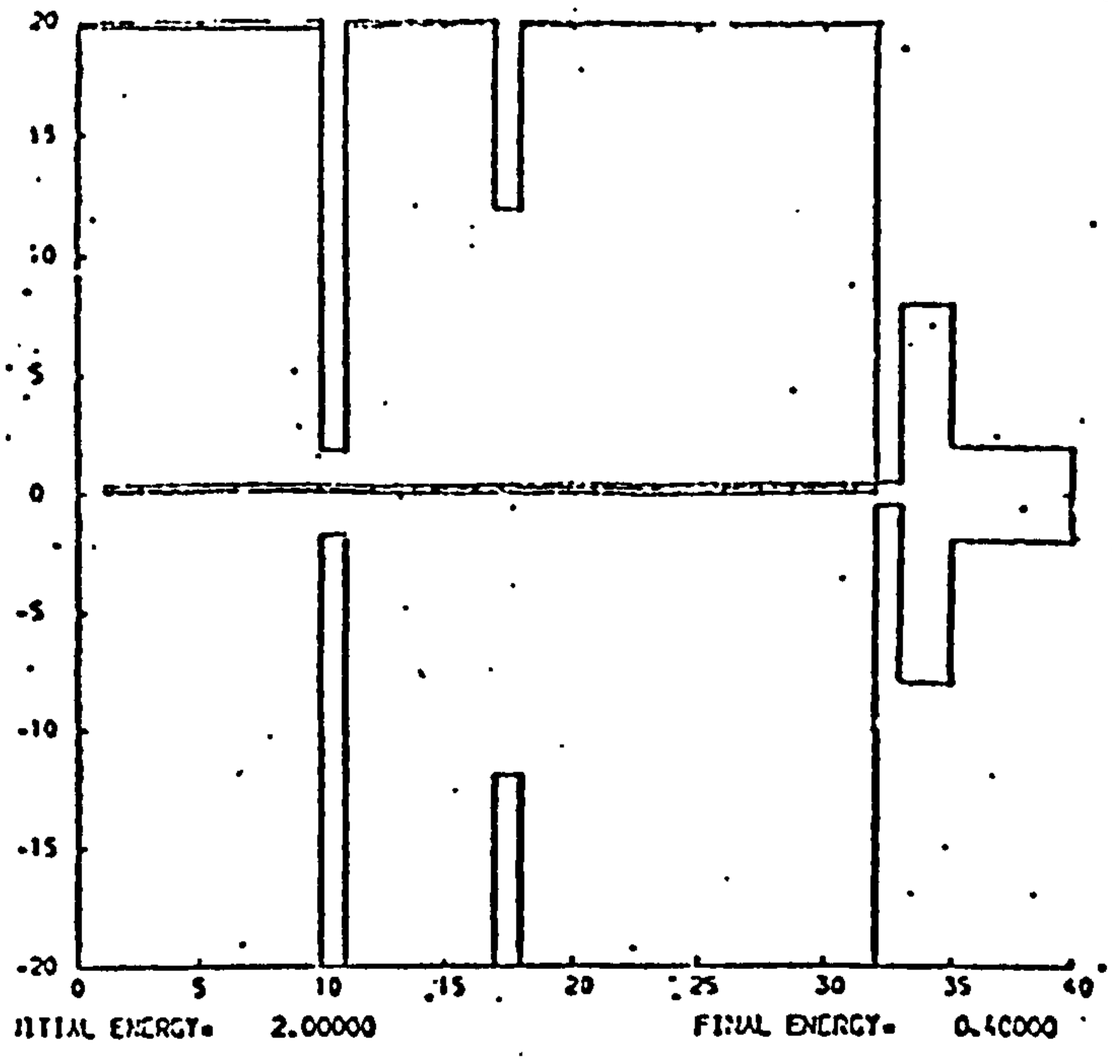

(a)

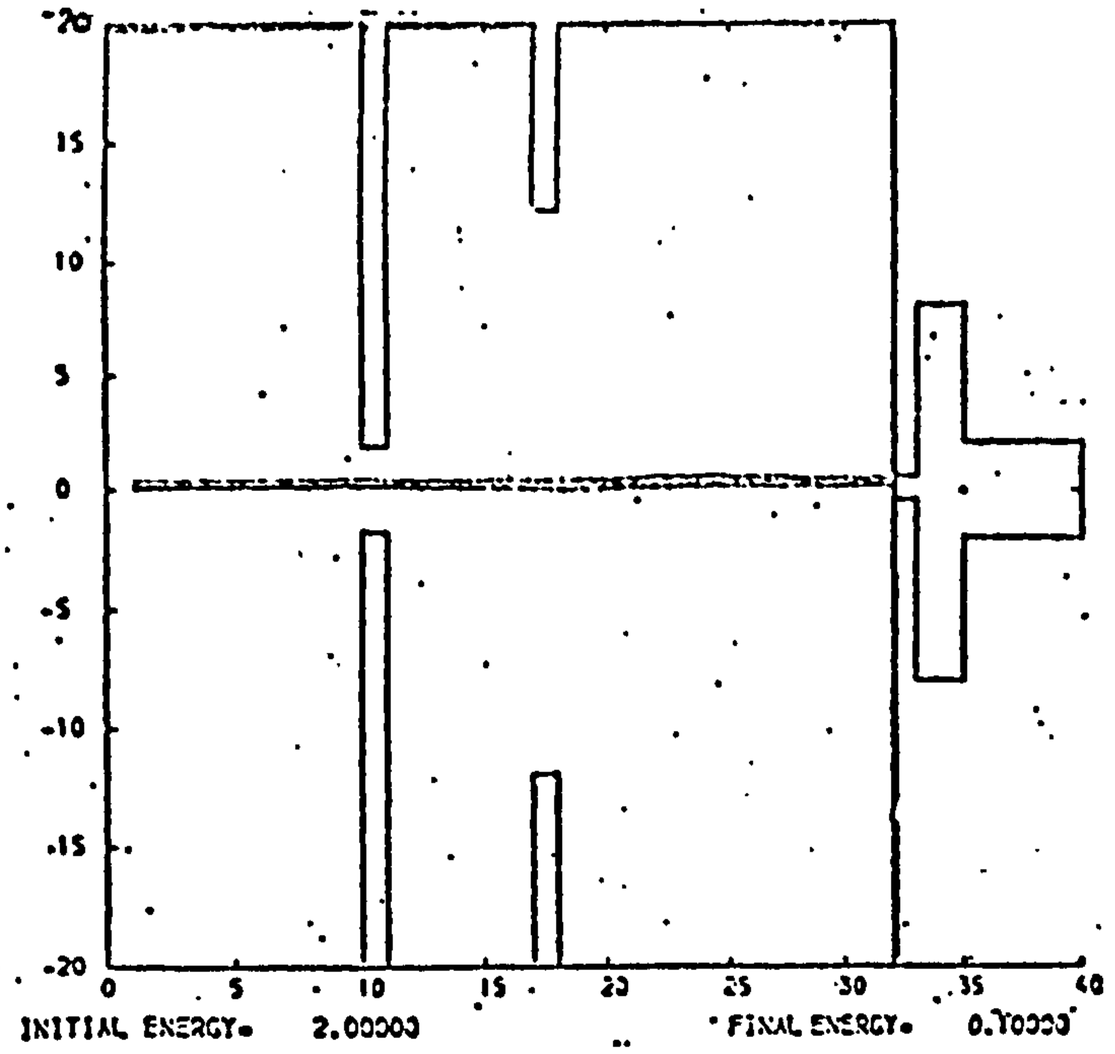

(b)

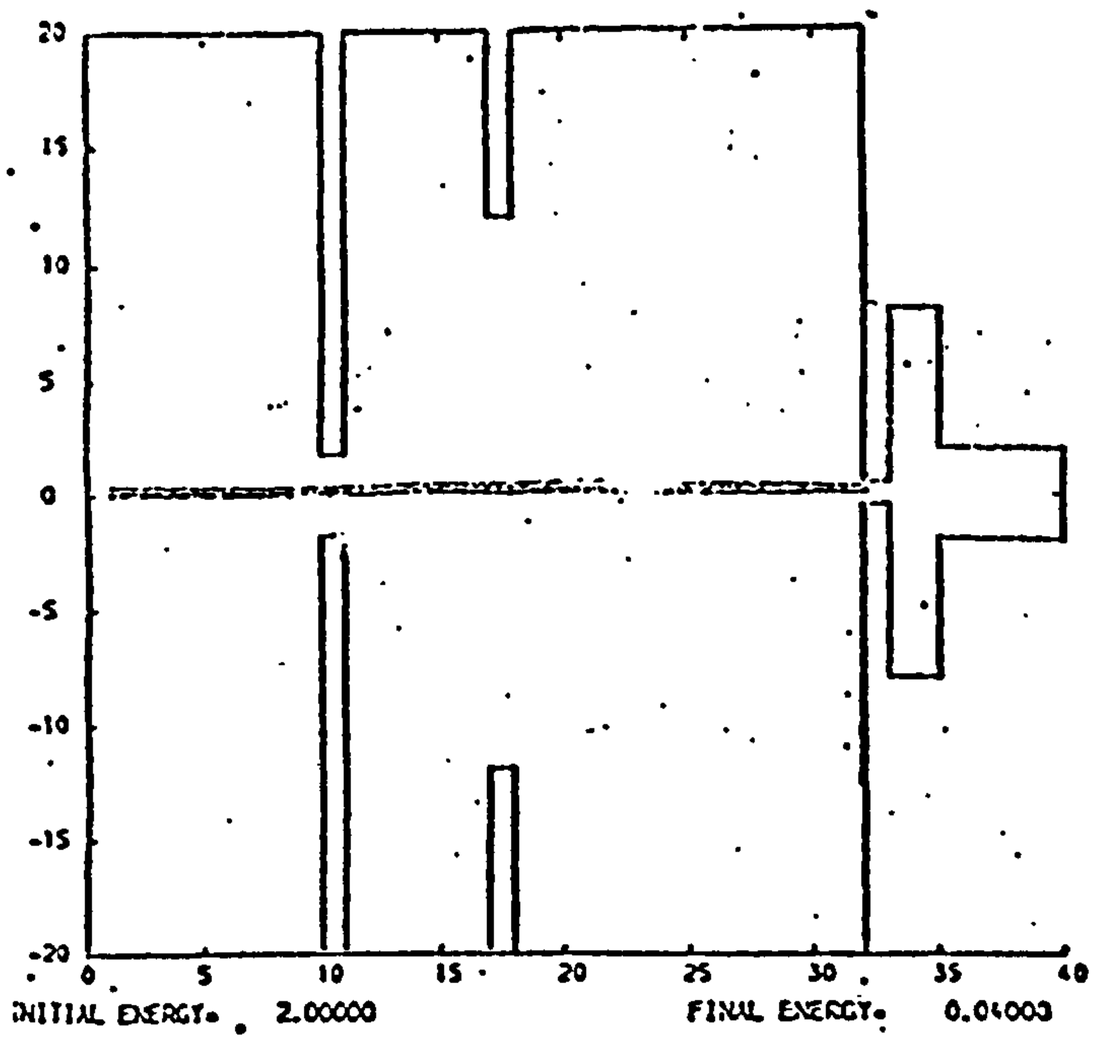

(c)

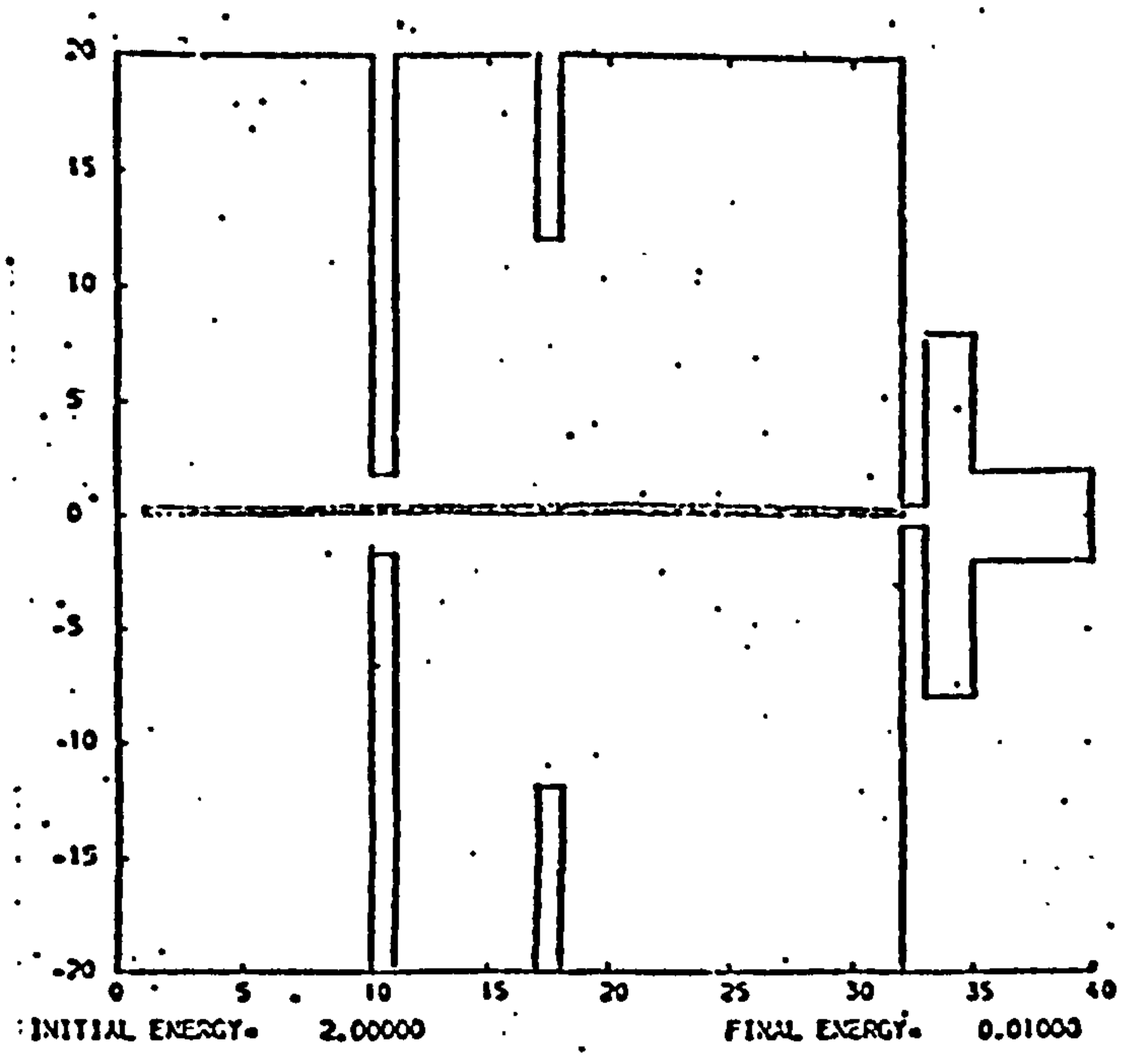

(d)

FIGURE 4.12 COMPUTER SIMULATION OF FOCUSING CHARACTERISTICS OF RETARDING LENS USED FOR VARIOUS RATIOS OF;

E_i/E_f . E_f/E_i =(a=5, b=20, C = 50, d = 200) [5]

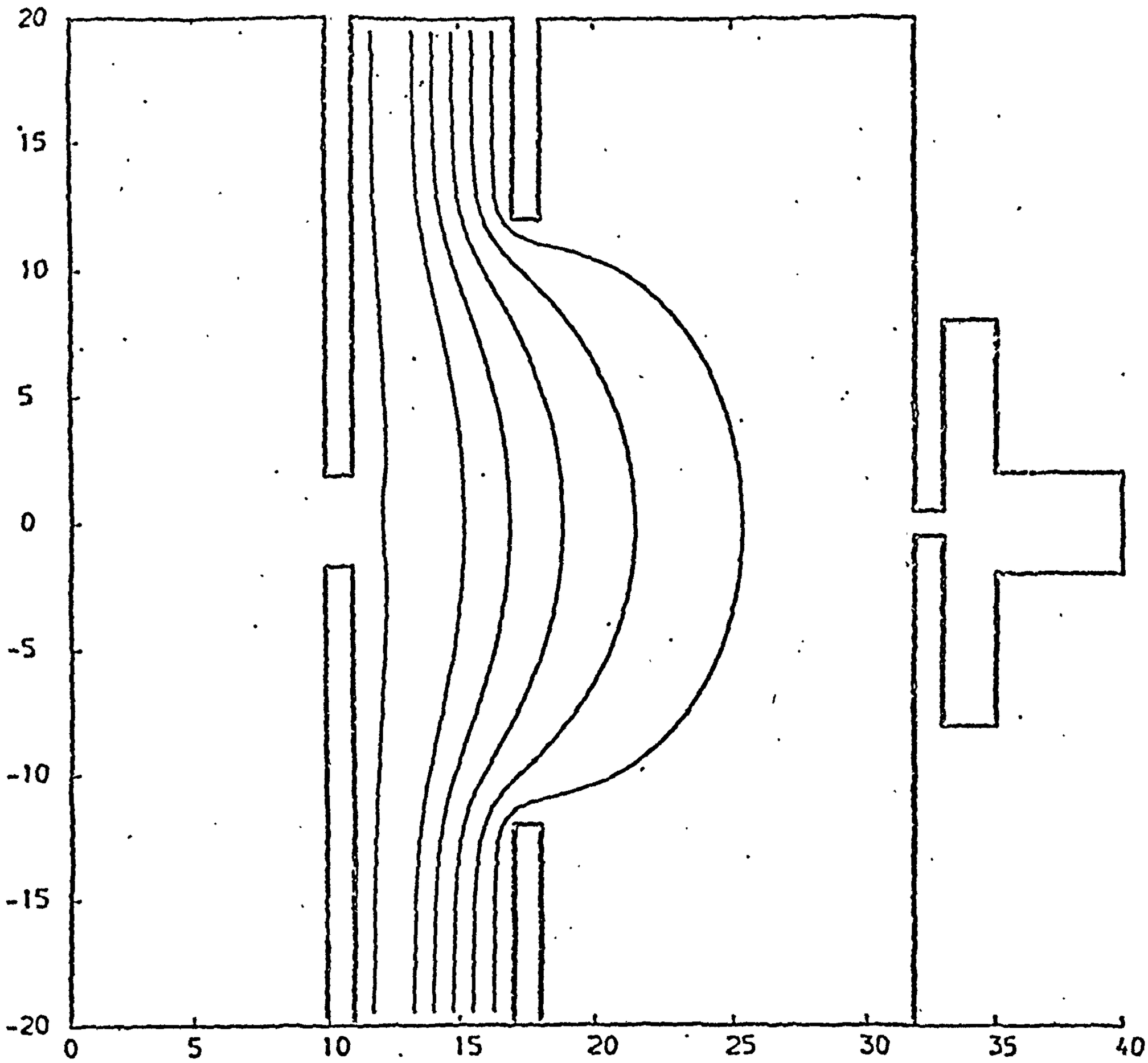

FIGURE 4.12(e) EQUIPOTENTIALS OF ELECTRODE CONFIGURATION FOR $E_i/E_f = 200$ [5]

charge chamber and the entire analysis system, as shown in Figure 4.1 could be removed from the main vacuum chamber in one piece. A mean trajectory radius of 65mm was found to satisfy all the requirements. The radial difference between the hemispheres was 5mm, and this was maintained by four ruby balls of high tolerance. The support plate, upon which the entire system was mounted, was conveniently insulated and located by means of eight more ruby balls positioned in accurately drilled indents.

The assembly of the analyser was facilitated by means of a jig comprising a 3mm. thick hemispherical shell the outer radius of which was equal to that of the outer hemisphere. The shell was cut into four segments such that the ruby balls could be placed in the crevices. This served as a simple method of locating the ruby balls until the inner hemisphere was in position, after which the segments were withdrawn. The weight of the inner hemisphere was sufficient to hold the balls in place and it then only remained to place the remaining balls in the locating indents, and clamp the support plate to the outer hemisphere block in order to obtain a rigid assembly. The hemispheres and the support were constructed from aluminium. Figure 4.13 shows the siting of ruby balls between the hemispheres using the assembly jig.

The basic requirement in the operation of this type of energy analyser without a retarding lens, is to vary the total voltage between the hemispheres while maintaining a constant ratio between the inner and outer electrode potentials. By this means the trajectory radius can be maintained at a fixed (zero volt) potential while the positive and negative voltages applied to the outer and inner hemispheres are varied. The fixed ratio for the anlayser described here is V_{in}/V_{out} =-1.08 and the relationship between the voltage applied to the inner hemisphere and the energy of the analysed beam is:-

$$V_{in} = -0.08E_N \qquad 4.2.10$$

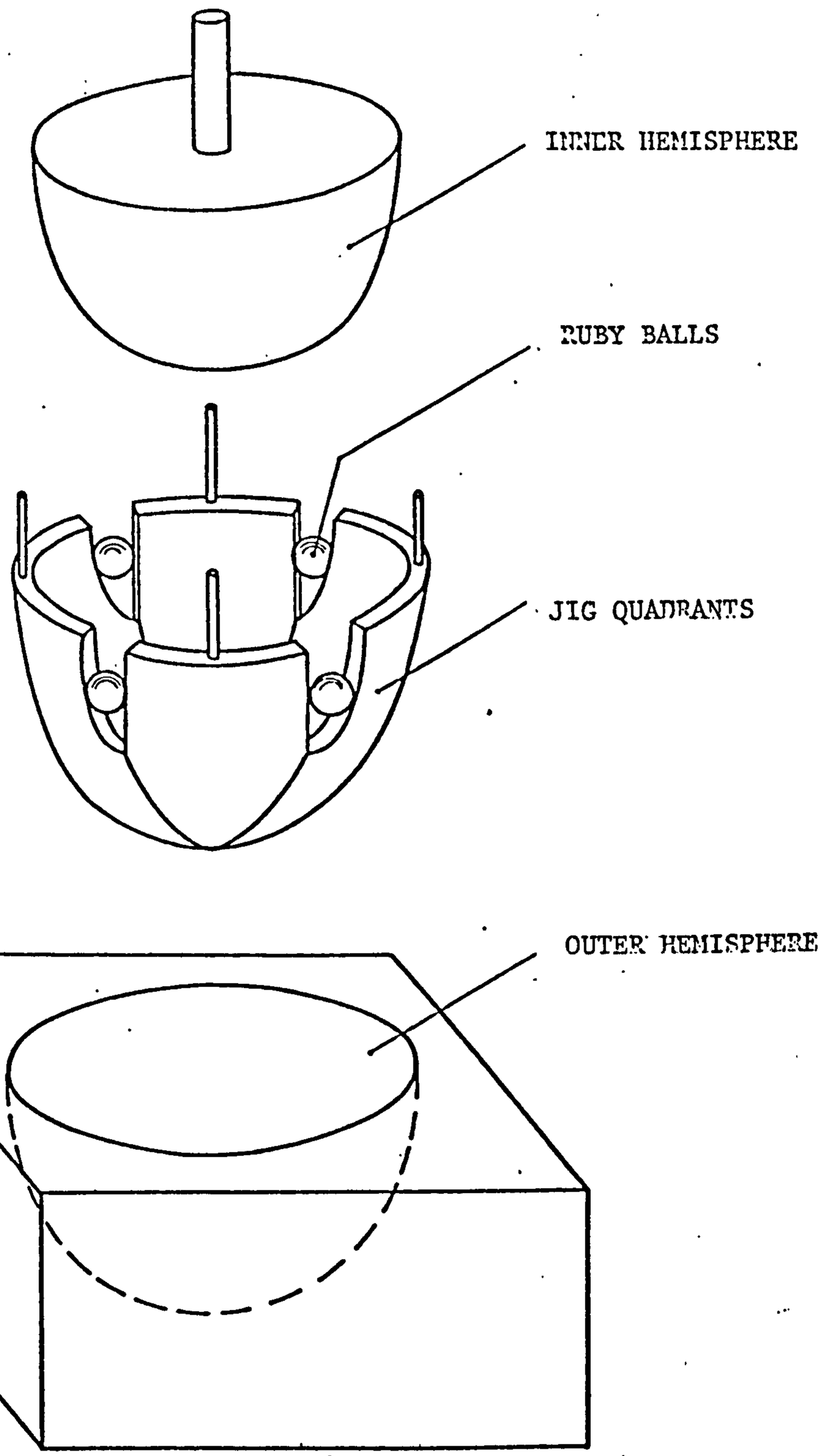

FIGURE 4.13 SITING OF RUBY BALLS BETWEEN HEMISPHERES USING ASSEMBLEY JIG

In this expression V_{in} is the voltage applied to the inner hemisphere and E_N is the energy of the analysed beam. The derivation of this expression together with the reason to the fixed ratio (discussed above) is given in Reference 8.

When a retarding lens is used, V_{in} and V_{out} are set to pass a prescribed energy. Under these circumstances, the support plate, through which entrance and exit apertures of the analyser protrude, is at the same potential as the final electrode of the retarding lens and the potential of the mean trajectory radius of the analyser, with respect to the support plate, defines the pass energy E_N. In the present application, this arrangement fulfills the constant transmission requirement (discussed earlier in this Chapter) of the analysis system and allows the most efficient operational energy regarding resolution, for the quadrupole mass spectrometer to be utilised. The energy of the analysed ion beam emerging from the exit aperture of the support plate, is obtained from the expression:-

$$E-V_R = E_N \qquad 4.2.11$$

In this expression E is the beam energy, V_R is the retarding voltage, and E_N is the pass energy of the analyser set by voltages V_{in} and V_{out} (or alternatively from expression 4.2.10).

The resolution of hemispherical energy analyser is given by the expression:-

$$\frac{\Delta E}{E} = \frac{W}{2R_o} \qquad 4.2.12$$

In this expression W is the width of the entrance aperture of the analyser and R_o is the main radius. It can, therefore, be said that the resolution of this type of analyser depends on its geometry hence is constant. The value of the resolution of analyser used is, therefore, 3.8% which, for a pass energy of 20eV corresponds to an energy window of 0.76eV.

4.2.3(f) Mass Spectrometer

Identification of the masses of the species leaving the discharge was a major part of the present research. To this end a mass spectrometer was used in the analysis system. In view of the requirements of the system, namely the need to operate at voltages of up to 3kV due to the use of the retarding lens, and unavoidable proximity of the mass spectrometer to the discharge chamber and extraction region a purely electrostatic instrument was considered to be more suitable than a magnetic analyser. The spectrometer chosen was, a 4"(10cm) quadrupole. It was placed in an aluminium housing (shown in Figure 4.14) and mounted immediately "behind" the exit aperture of the energy analyser.

4.2.3(g) Detection System

The detection unit initially used was a 10 dynode electron multiplier with a specified gain of about 10^5. However, in assessing the performance of the analysis system it was found that the signal level of the ion current (that of the neutrals species and the evaporant in particular) emerging from the quadrupole mass spectrometer was too low for reliable measurement using straight forward current amplification A closed ended channel electron multiplier (CCEM, Mullard B419/BL) with a gain of about 10^5-10^7 was used as detector with its output fed to a pulse counting system. The CCEM typically gives background count rates of less than 10cps compared with values closer to 100cps for a discrete dynode device. The higher gain and well defined pulse height distributions also allows more efficient discremination.

4.2.4 The Overall Arrangement

A schematic diagram together with a photograph of the system finally used is shown in Figure 4.15(a) and (b) respectively. It can be seen that the entire system i.e. the discharge chamber together with the analysis system was mounted in such a way that the assembly could be carried out prior to introduction

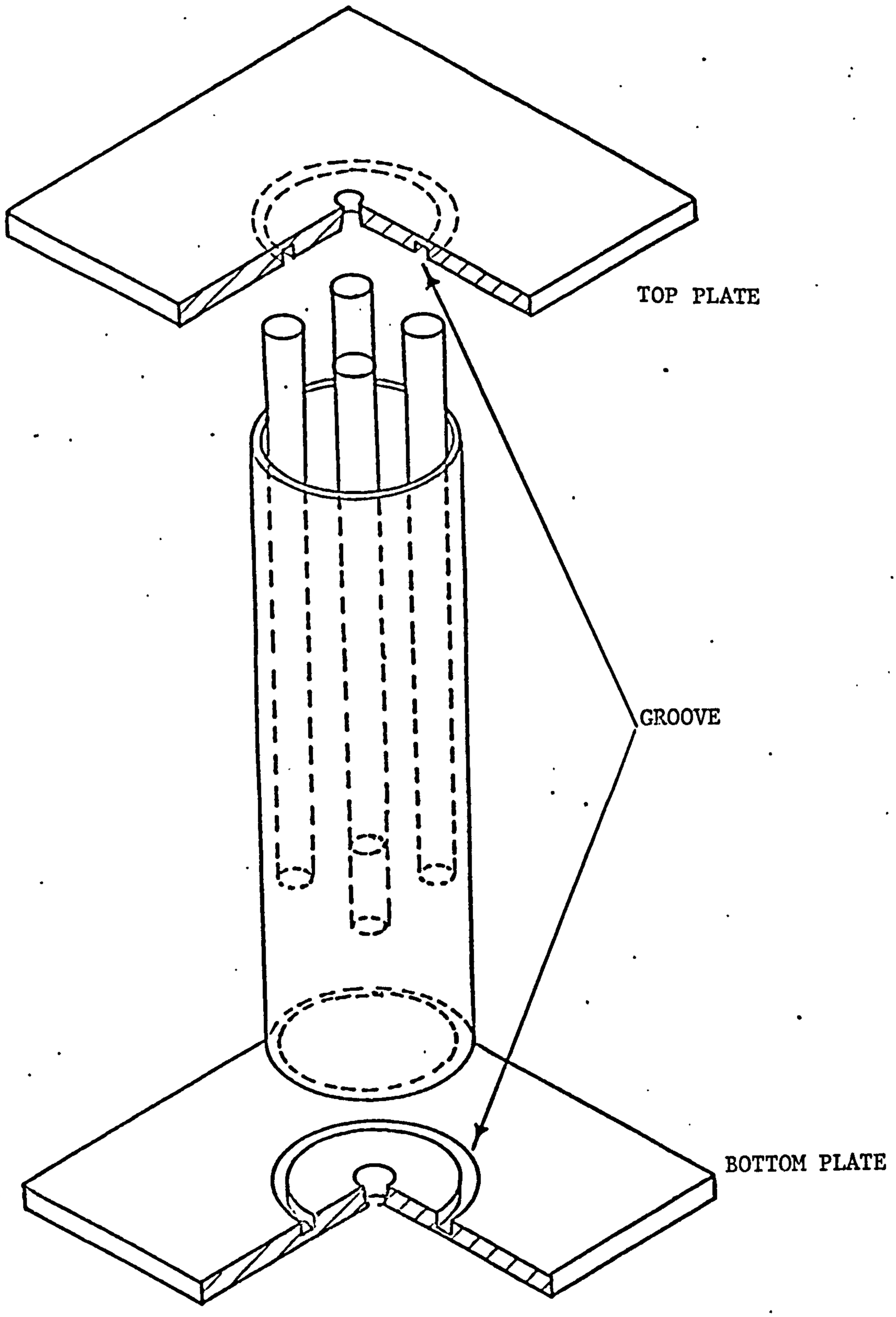

FIGURE 4.14 QUADRUPOLE MASS SPECTROMETER AND ITS HOUSING

KEY TO FIGURE 4.15(a)

a) Stainless steel vacuum collar, 12",OD

b) Titanium sublimation pump filament

c) Boat

d) Machinable ceramic discharge tube with heating facility

e) Target or substrate for ion plating (movable in plane normal to paper)

f) Extractor

g) X-Y deflectors

i) Ioniser

j) Retarding Lens

k) Hemispherical energy analyser

l) Stainless steel bell jar

m) 100 mm quadrupole mass spectrometer

n) Channel electron multiplier.

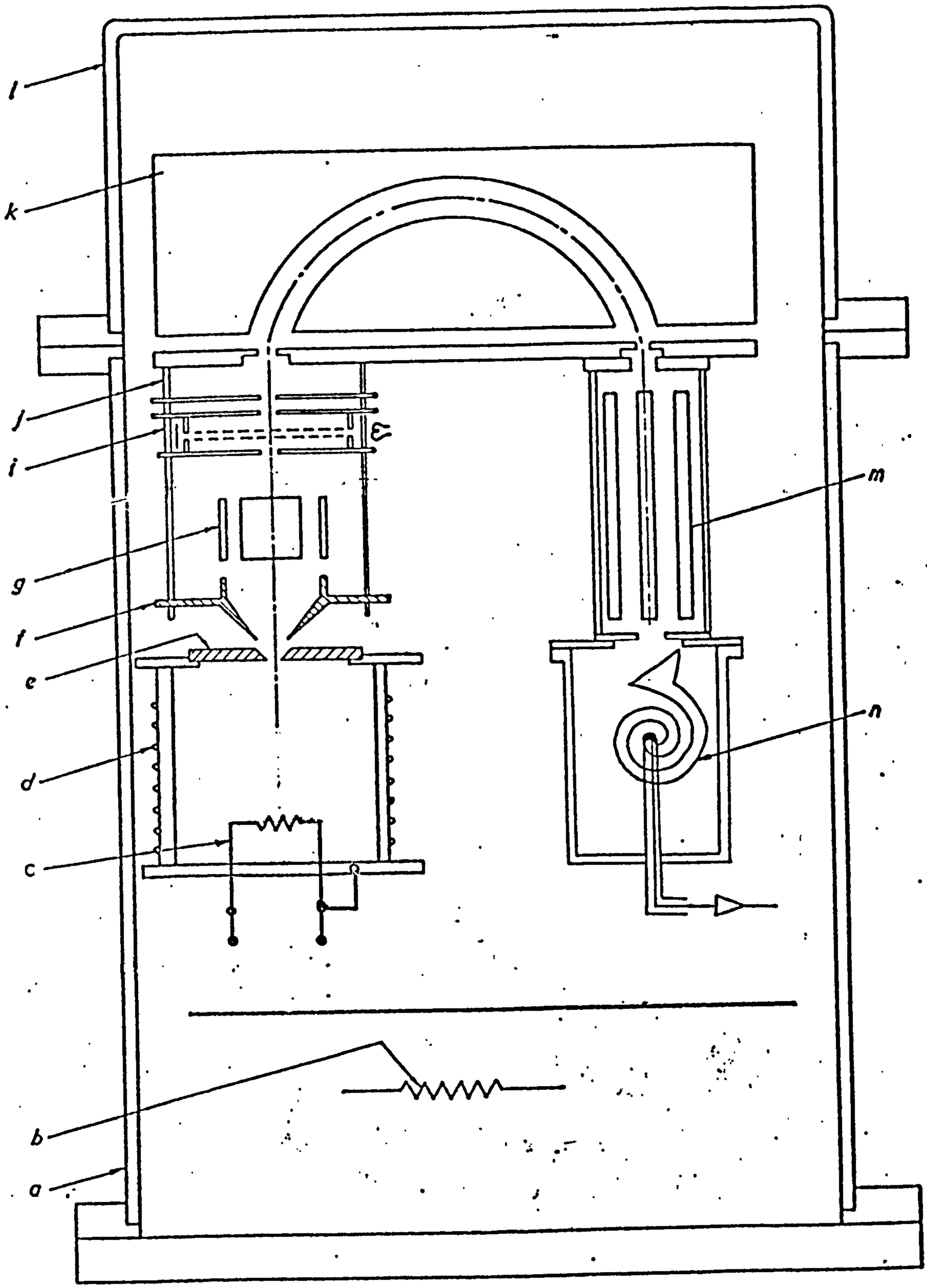

FIGURE 4.15(a) SCHEMATIC DIAGRAM OF THE SYSTEM EVENTUALLY USED.

FIGURE 5.15(b)

A PHOTOGRAPH OF THE DISCHARGE CHAMBER

AND THE ANALYSIS SYSTEM.

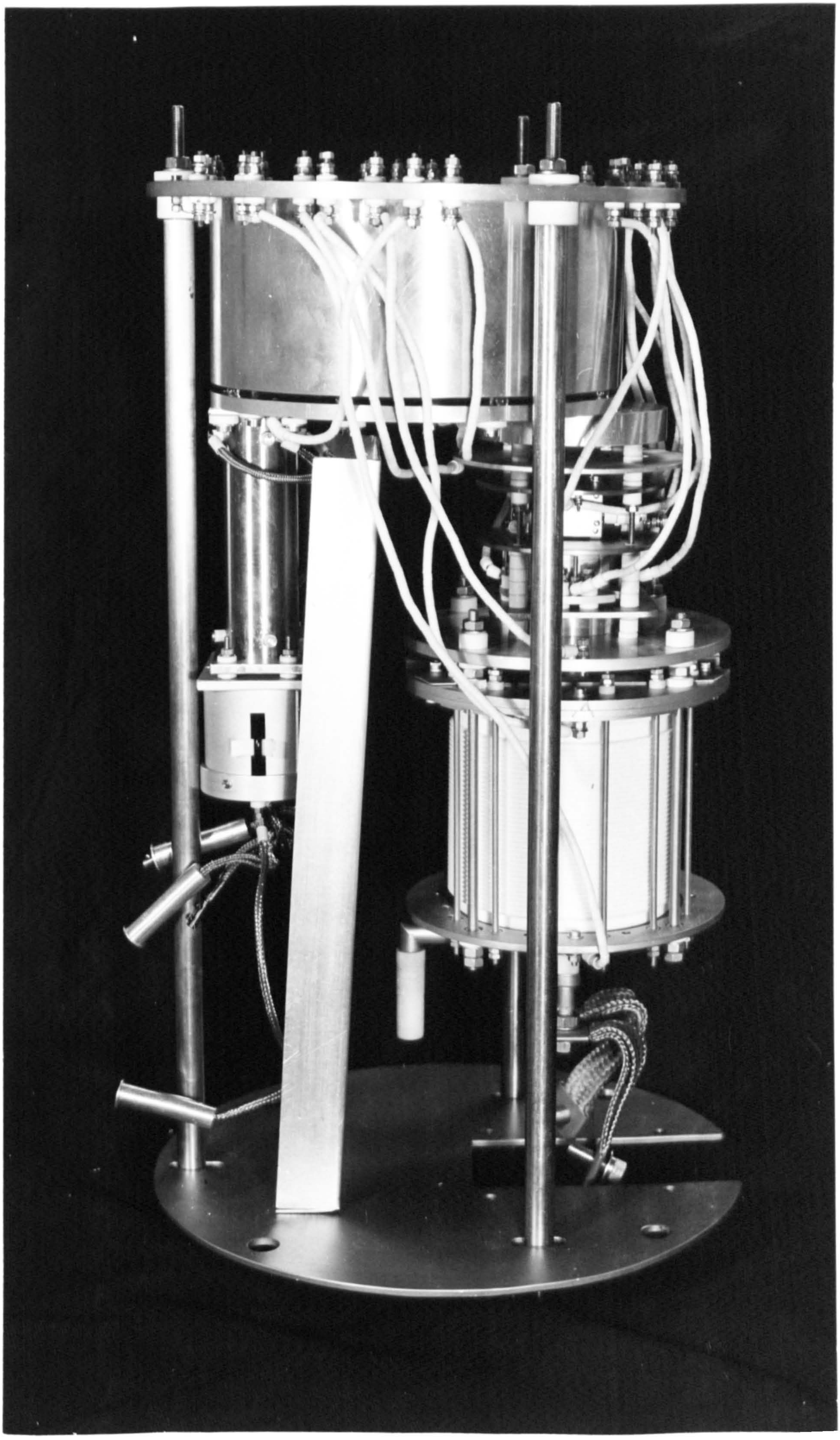

into the vacuum chamber. Finally, an over view of the overall vacuum system is shown in Figure 4.16.

4.2.5 Performance

The first step in testing the performance of the analysis system was to check the alignment of the cathode pinhole with the axis of the ion optical system. This was simply done by running the discharge and collecting the ions leaving the discharge on the outer hemisphere of the energy analyser. In this experiment all the ion optical components i.e. the extraction electrode, the deflector, ionisation chamber, retarding lens and the inner hemispheres of the energy analyser were earthed. It was found that about 10^{-9} amps of ion beam could be collected on the outer hemisphere. This value was close to the maximum value obtainable by varying the deflection voltages and hence alignment was confirmed. Also, in this experiment, it should be pointed out that the discharge cathode current density was about 0.16 ma/cm^2 and considering the diameter of the cathode sampling aperture, the distance between the aperture and the energy analyser, and the energy of the ion beam (see Chapter 5) the amount of ion current collected was close to that expected on the basis of simple theory.

To investigate the performance of the ion extractor, it was connected to a negative d.c. voltage while the rest of the electrical connections, described above, were left unchanged. The ion current measured on the outer hemisphere was recorded as a function of extraction voltage and the result of the measurements showed that an extraction voltage of about -5 volts resulted in the maximum extraction. However, the yield increase over that at zero volt was not significant and in order to retain similar sampling efficiencies for ions and neutrals, the major part of the experimental programme was carried out with less than 5V extraction. It should be pointed out that, as might be expected extraction voltages of hundreds of volts did give an increased yield but only at the risk of causing significant field perturbation in the extraction region of the discharge tube.

FIGURE 4.16 AN OVER VIEW OF THE OVERALL VACUUM SYSTEM


AMPERES
MICROMANOMETER MDC FC001
FURNESS CONTROLS LTD.

Regarding the deflector lens the prime purpose of its use in the analysis system, as already discussed, was to deflect the ions off the axis of the cathode pinhole such that they did not enter the energy analyser during neutral particles analysis. A voltage of about 20 volts was found to be adequate for this purpose.

The performance of the energy measurement facility of the system was assessed by performing two distinct sets of experiments:

1.- The first set of experiments were carried out in the preliminary testing of the analyser system while measuring the energy distributions of the ions leaving the discharge prior to evaporation. These measurements were carried out with the retarding potential and hence the mean potential of quadrupole mass spectrometer rods and its housing together with the post extraction ionisation box at earth potential while scanning the voltages applied to the analyser. The total ion yields for different discharge conditions were measured. The discharge voltage was varied from 1.5kV to 3.0kV. Typical energy distributions obtained for a discharge voltage of 2kV are shown in Figure 4.17(a). The same trends were observed at all discharge voltages studied. These figures do not, of course, represent the actual energy distributions of the ions impinging on the cathode since the transmission of the analyser used in this mode is energy dependent i.e. $\frac{\Delta E}{E}$ = constant or $\Delta E \propto E$. Hence the transmission increases with energy. The actual energy distribution can be obtained by taking the energy dependent transmission characteristic into consideration and dividing the spectra by energy. This correction for the spectra of Figure 4.17(a) is shown in Figure 4.17(b).

2.- The system was operated in the constant transmission mode i.e. the energy analyser was used in conjunction with the retarding lens such that a selected energy was transmitted through the analyser and the energy spectrum was obtained by scanning the retarding potential. The mean potential of the quadrupole mass spectrometer rods and its housing were held at the same potential as the retarding at all times. The spectra obtained using this mode of operation should be identical, in form, to the corrected variable pass energy spectra. However, for this

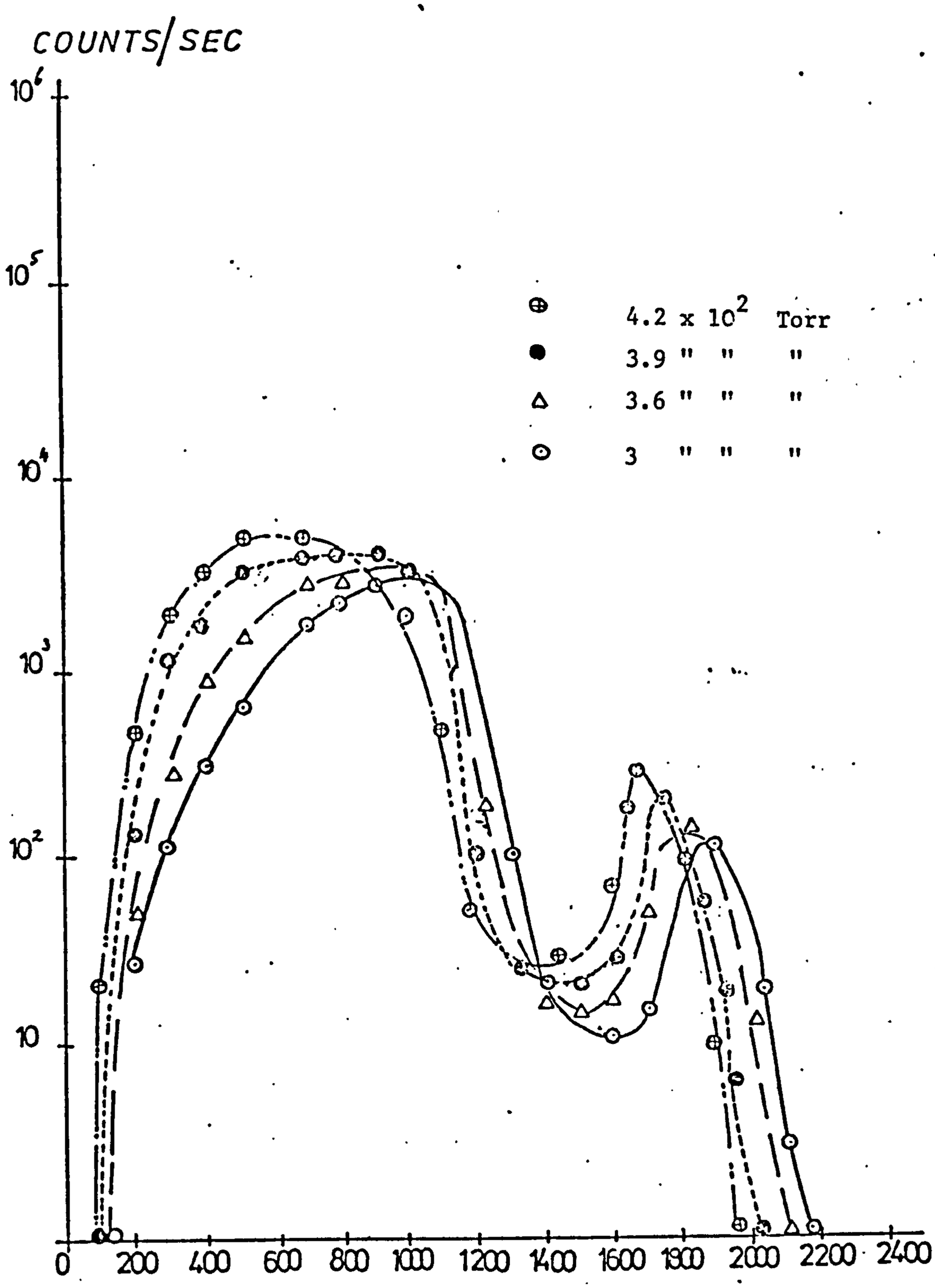

FIGURE 4.17(A) VARIATIONS OF THE OUTPUT YIELD OF THE ANALYSER WITH PASS ENERGY FOR A 2kV DISCHARGE AT VARIOUS PRESURES

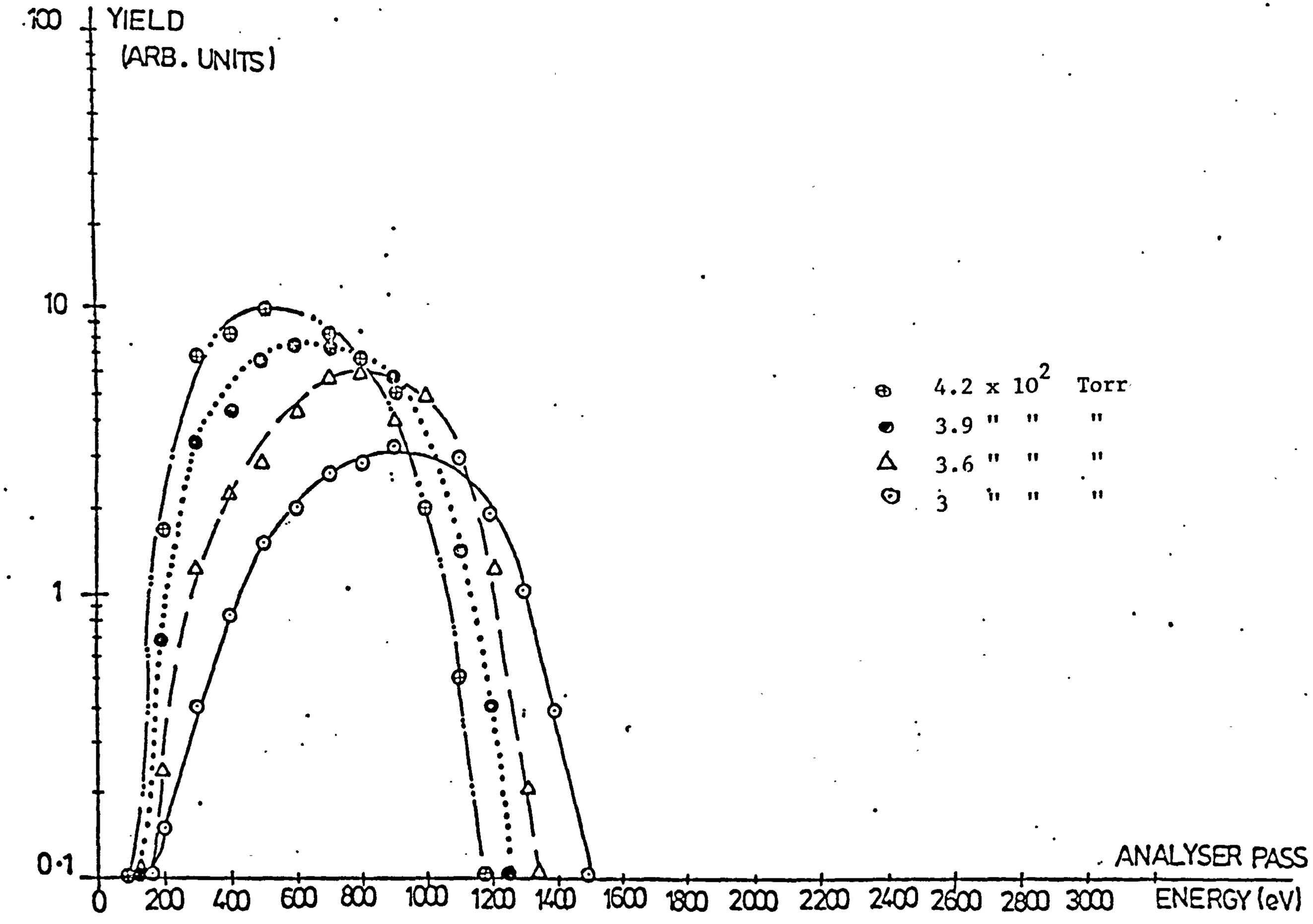

FIGURE 4.17(b) CORRECTED SPECTRA OF FIGURE 4.17(a)

to be so, the precise instrumental function of the analyser-retarding lens combination i.e. the transmission as a function of incident energy must be both well behaved and known. Hence, before attempting a comparison spectra, the analyser system must be calibrated.

The calibration was carried out by using the post extraction ionisation chamber as an ion source producing ions of known energies, obtained by applying known voltages V_B to the ion box and ionising the residual gas molecules. The energy of the ions leaving the box under these circumstances is given by the box potential minus a potential which depends on field penetration from electron collector and filament. This penetration typically leads to only small departures in energy from eV_B and hence the "source" was expected to provide input ionbeams of known energy suitable for analyser calibration. The actual calibration method employed was to set a pass energy E_p on the electrostatic analyser and then scan the retarding voltage to obtain an energy distribution for various values of V_B. Graphs of V_B versus the retarding voltage at which the distributions peaked V_{rp} were then plotted for various values of pass energy. These graphs are shown in Figure 4.18(a), and they demonstrate immediately that for ion energies above about 20eV ($V_B = 20_V$) there is the desired linear relationship between V_B and V_{rp}. At lower energies there are clearly transmission problems between the box and lens. The dash-dot line shows the ideal but unusable case of zero pass energy and the vertical displacement of the other lines should reflect the fact that $E_p + eV_{rp} = eV_B$. The extent to which this is obtained is shown in Figure 4.18(b) where $(E_p + V_{rp})$ is plotted against V_B. This figure indicates that there is a systematic "error" of approximately 7V but this is partly due, as already indicated, to field penetration into the ion box leading to a drop in the potential at which the ions are formed. Hence, these measurements confirm that analysis based on the retarding lens - constant transmission system is reliable and accurate to within less than 7V.

Following the calibration, the energy spectra of the total (non-mass analysed) ion flux leaving a 2kV argon discharge for various pressures were measured and the results are shown in Figure 4.19. Similar behaviour was observed

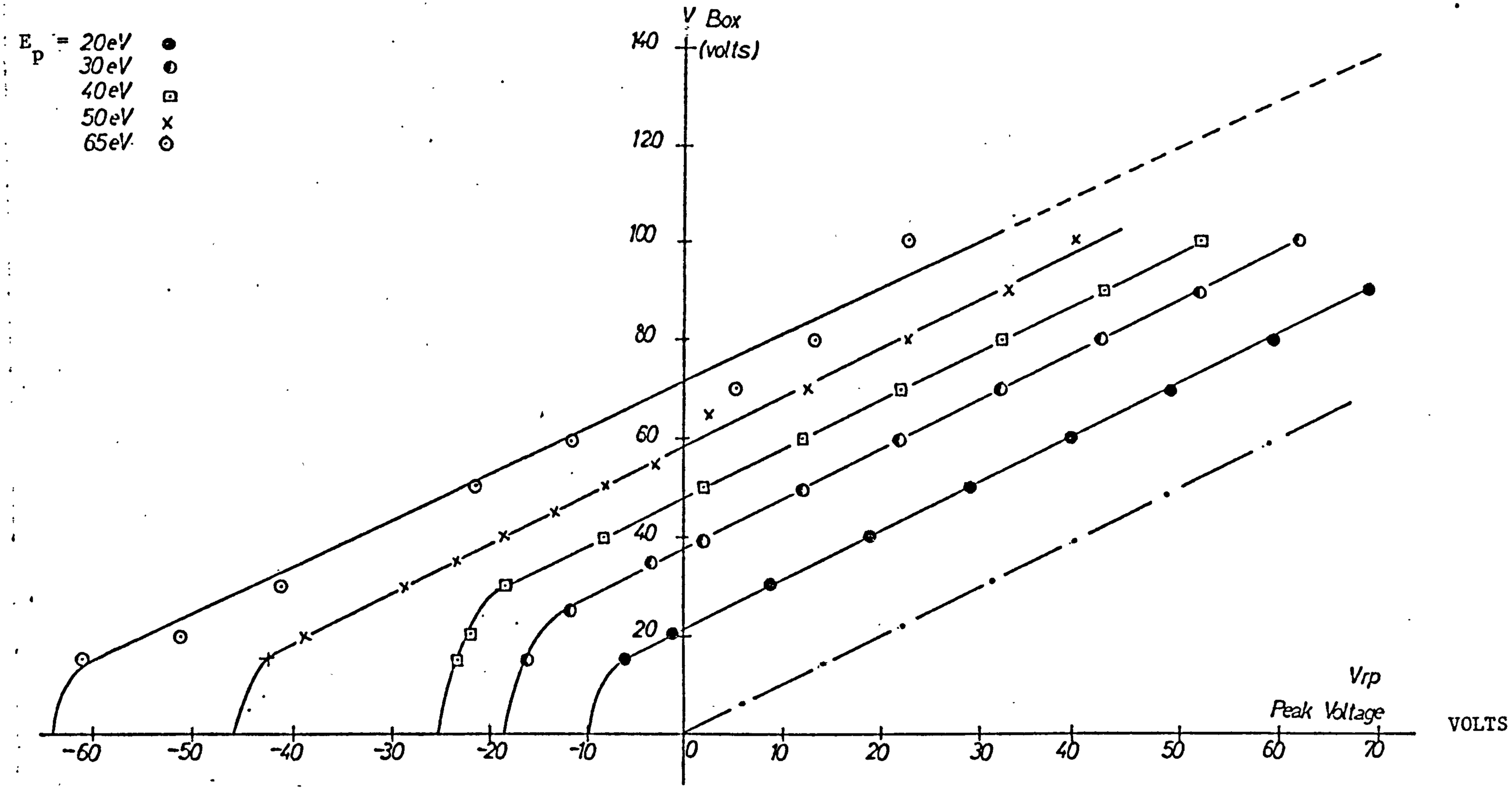

FIGURE 4.18(a) VARIATINS OF "SOURCE" POTENTIAL V_B VS. RETARDING POTENTIAL V_{rp} AT WHICH ENERGY DISTRIBUTION PEAKS FOR VARIOUS PASS ENERGY SETTING OF THE ENERGY ANALYSER.

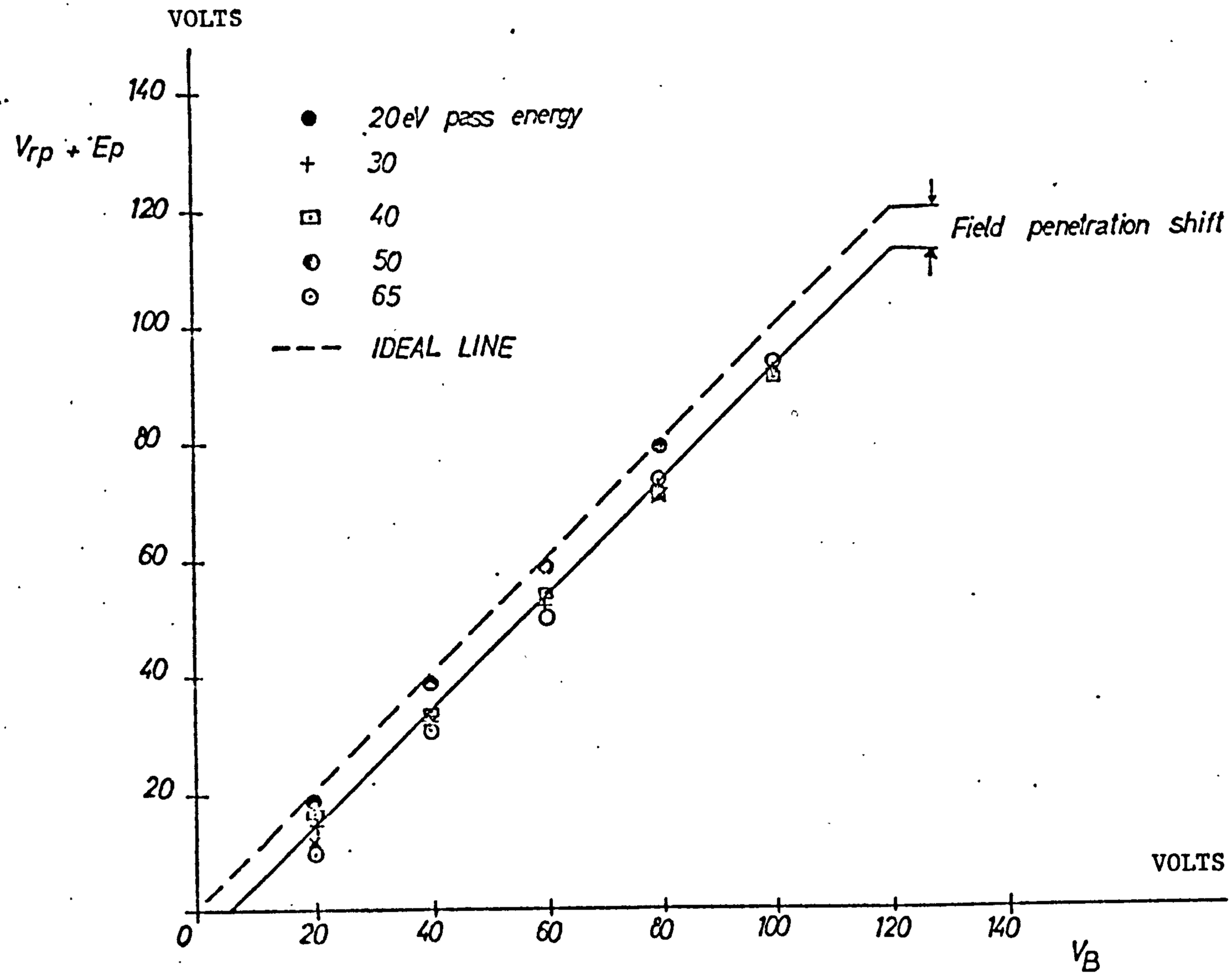

FIGURE 4.18(b) CHARACTERISTIC OF THE ENERGY ANALYSER WHEN USED IN CONJUNCTION WITH THE RETARDING LENS. VARIATIONS OF THE SUM OF THE PASS ENERGY OF THE ANALYSER AND THE RETARDING VOLTAGE AT WHICH THE ENERGY DISTRIBUTIONS PEAK ($E_p + V_{rp}$) VS. THE VOLTAGE OF THE ION BOX (V_B)

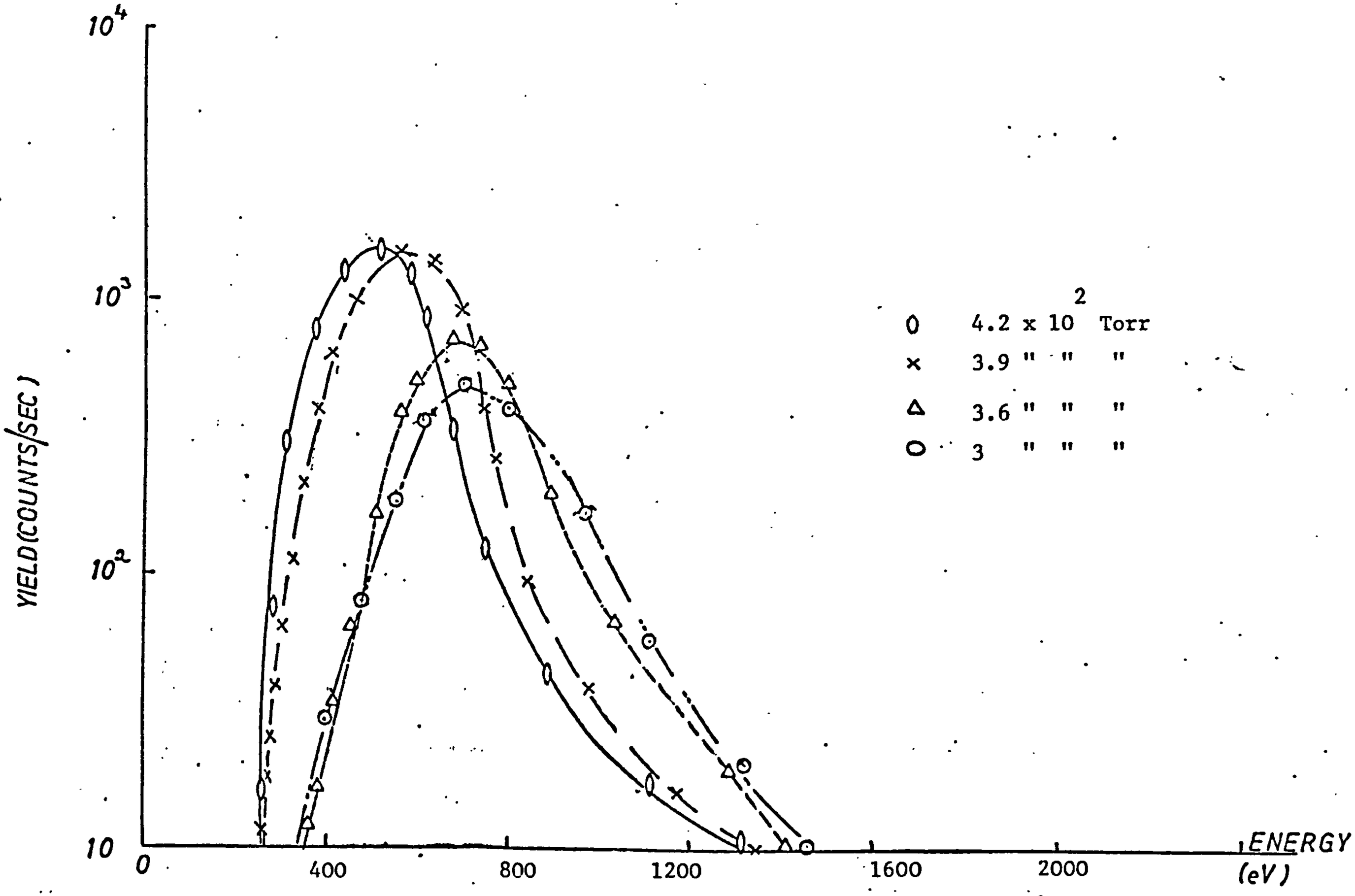

FIGURE 4.19 ENERGY DISTRIBUTIONS OF THE FLUX OF IONS LEAVING A 2kV ARGON DISCHARGE AT VARIOUS PRESSURES

for all the discharges voltages used. Comparison of these spectra with the "corrected" variable pass energy spectra shown in Figure 4.17 gives a further indication of the reliability of the energy measurements.

In order to completely characterise the instrumental function associated with the analysis system, it was necessary to check the transmission of the quadrupole mass spectrometer. In practice, in the present application it was sufficient to determine the resolution settings for which mass discrimination effects i.e. mass dependent transmission, were negligible. To carry out the necessary tests, the system was operated in the constant transmission mode with the quadrupole (operating at 2MHz) and its electronic control units raised to the retarding potential. As already indicated the constant transmission mode, in addition to its more satisfactory transmission characteristic, made it possible to select a pass energy for the hemispherical analyser which was acceptable to the 4" mass spectrometer. For this length of the instrument, entrance energies of between 5 and 10eV are typically employed but since only limited resolution was required for the present measurements higher energies of the order 20eV were used to increase the transmission efficiency of the analyser. The mass number readings of the mass spectrometer control unit was calibrated by relating the readings of the unit to the mass spectra obtained for ions leaving argon and nitrogen discharges of 2kV, $3x10^{-2}$ torr (see Figure 4.20). This type of instrument exhibits strong mass discrimination in that the transmission of the heavier ions falls off more rapidly than that for the faster moving light particles. This is clearly evidenced in Figure 4.21 where the ratio I^{40}/I^{28} is plotted against resolution setting. By employing a resolution setting of 5.8 adequate resolution with minimal mass discrimination was achieved. In order to measure the energy distributions of the neutral species impinging on the cathode the ions leaving the discharge were deflected off the entrance aperture of the energy analyser. This was achieved by monitoring the ion yield at the detector and applying voltages to the deflection lens elements until zero (noise level)counts were recorded. It was observed that potential differences of about 10-15 volts were enough to deflect all the ions off the axis. It was observed that no ion yield could be det-

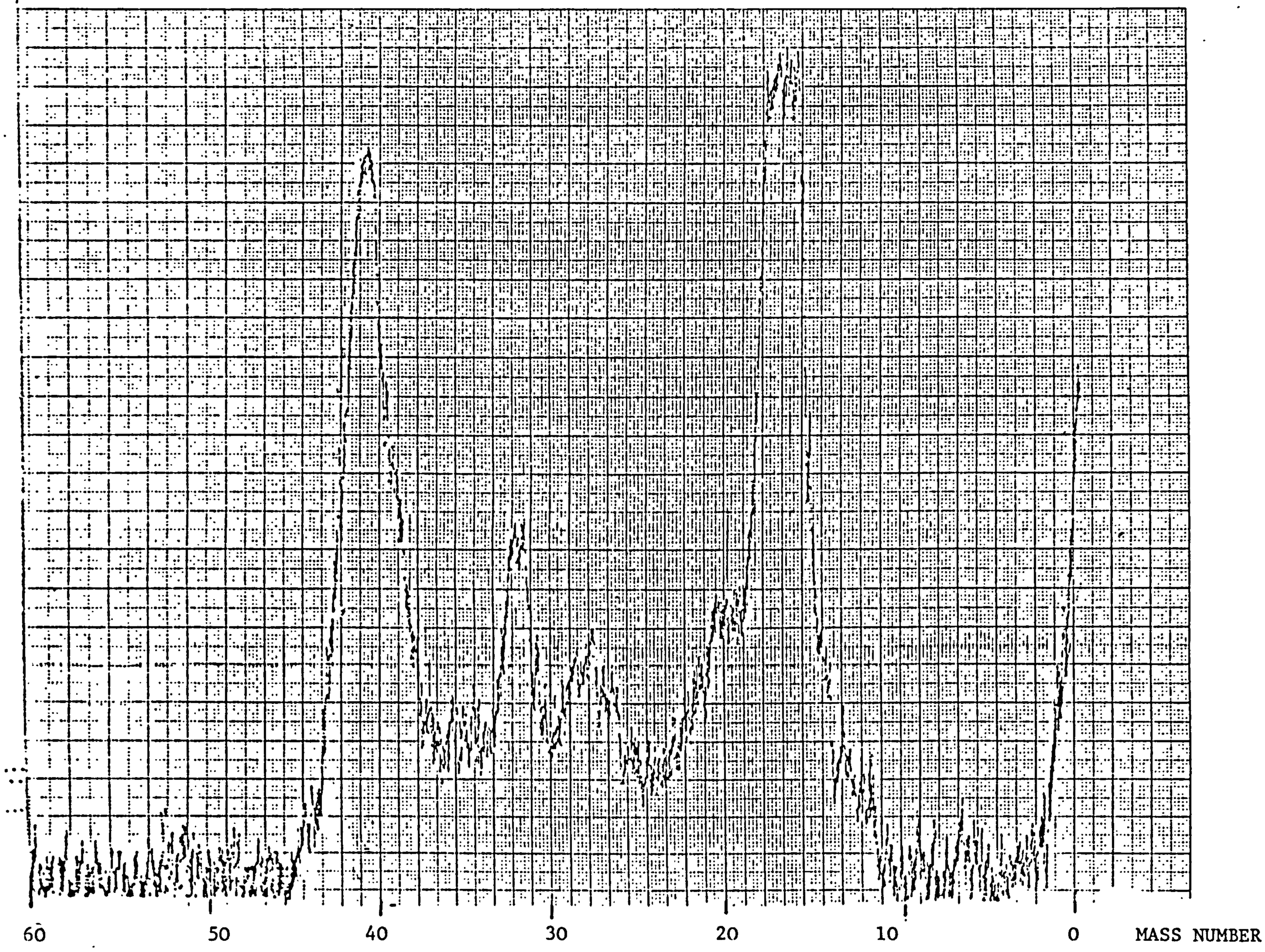

FIGRUE 4.20(a) MASS SPECTRUM OF THE FLUX OF ION LEAVING A 2kV, 3×10^{-2} TORR ARGON DISCHARGE, PRIOR TO EVAPORATION.

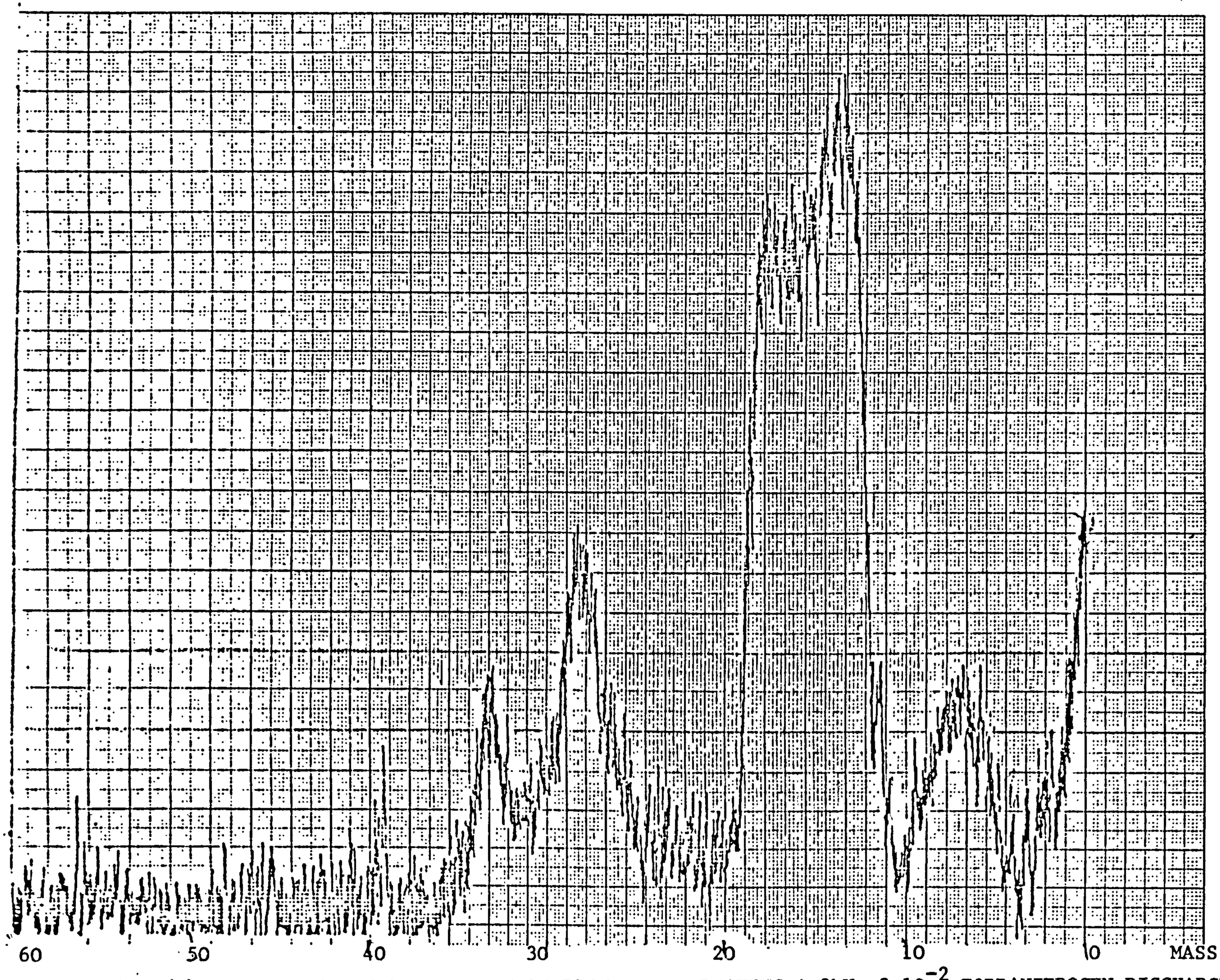

FIGURE 4.20(b) MASS SPECTRUM OF THE FLUX OF ION LEAVING A 2kV, 3×10^{-2} TORR NITROGEN DISCHARGE, PRIOR TO EVAPORATION

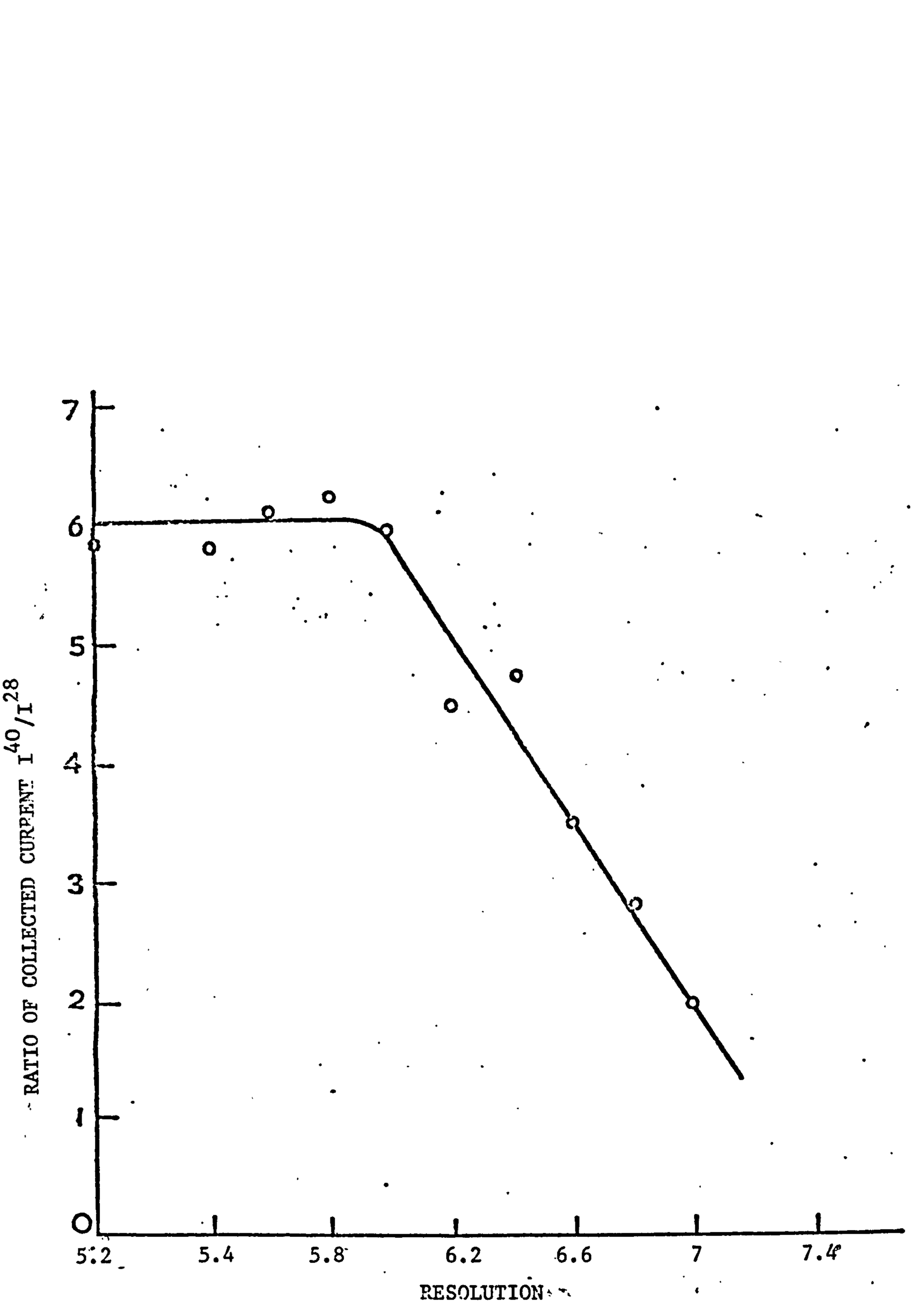

FIGURE 4.21 VARIATION OF SENSITIVITY OF THE QUADRUPOLE MASS SPECTROMETER WITH RESOLUTION.

ected even when the sensitivity of the detection system was increased by more than two order of magnitude. The filament of the ionisation chamber was then activated and the ionised neutral yield recorded. This yield was similar to the "ion"yield, and since an ionisation efficiency of 10^{-3} to 10^{-4} is typical for the type of ioniser used, the measurements give an immediate indication of the significance of energetic neutrals in ion plating. A current emission regulator was used to control the emission of the filament as measured on the trap to a specified value of 40 μA.

4.3 UHV Ion Plating / Evaporator Apparatus

An investigation of the validity of the hypothesis which attributes the strong film - substrate adhesions in ion plating to the cleanliness of the substrate was part of the present programme of research, and an apparatus for producing uhv ion - plated, uhv evaporated and conventionally evaporated films was designed and developed.

4.3.1 Description of the Apparatus

The simple apparatus consisted of three molybdenum boats connected in a star configuration, in which the star point was earthed, and the heating current could be supplied to any chosen boat. The assembly was surrounded by a 100mm diameter pyrex shield which had a 30mm hole in the top, above which was situated 30mm x 30mm nickel substrates. Three of these substrates were mounted on a movable holder which could be manipulated externally to expose a fresh substrate to the evaporant as required. In this way three films could be deposited without breaking vacuum. The complete assembly was installed in the u.h.v. chamber described in Section 4.2. A diagram and photograph of this simple apparatus is shown in Figures 4.22(a) and (b) respectively.

4.3.2 Performance

Using this apparatus films of gold were produced under uhv (10^{-9} torr press-

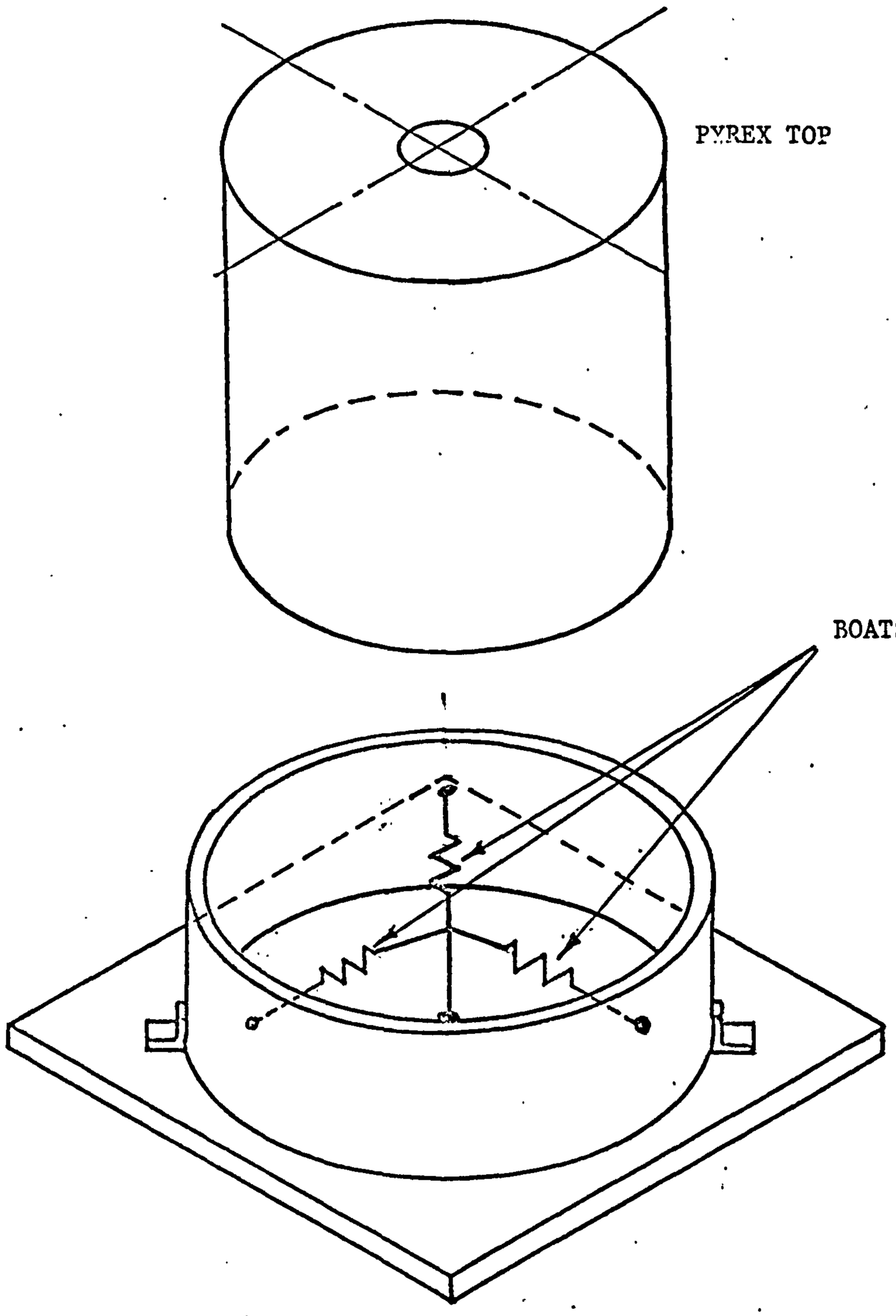

FIGURE 4.22(a) SCHEMATIC DIAGRAM OF THE UHV ION PLATING/EVAPORATOR APPARATUS

FIGURE 4.22 (b)

PHOTOGRAPH OF UHV ION PLATING/EVAPORATION APPARATUS.

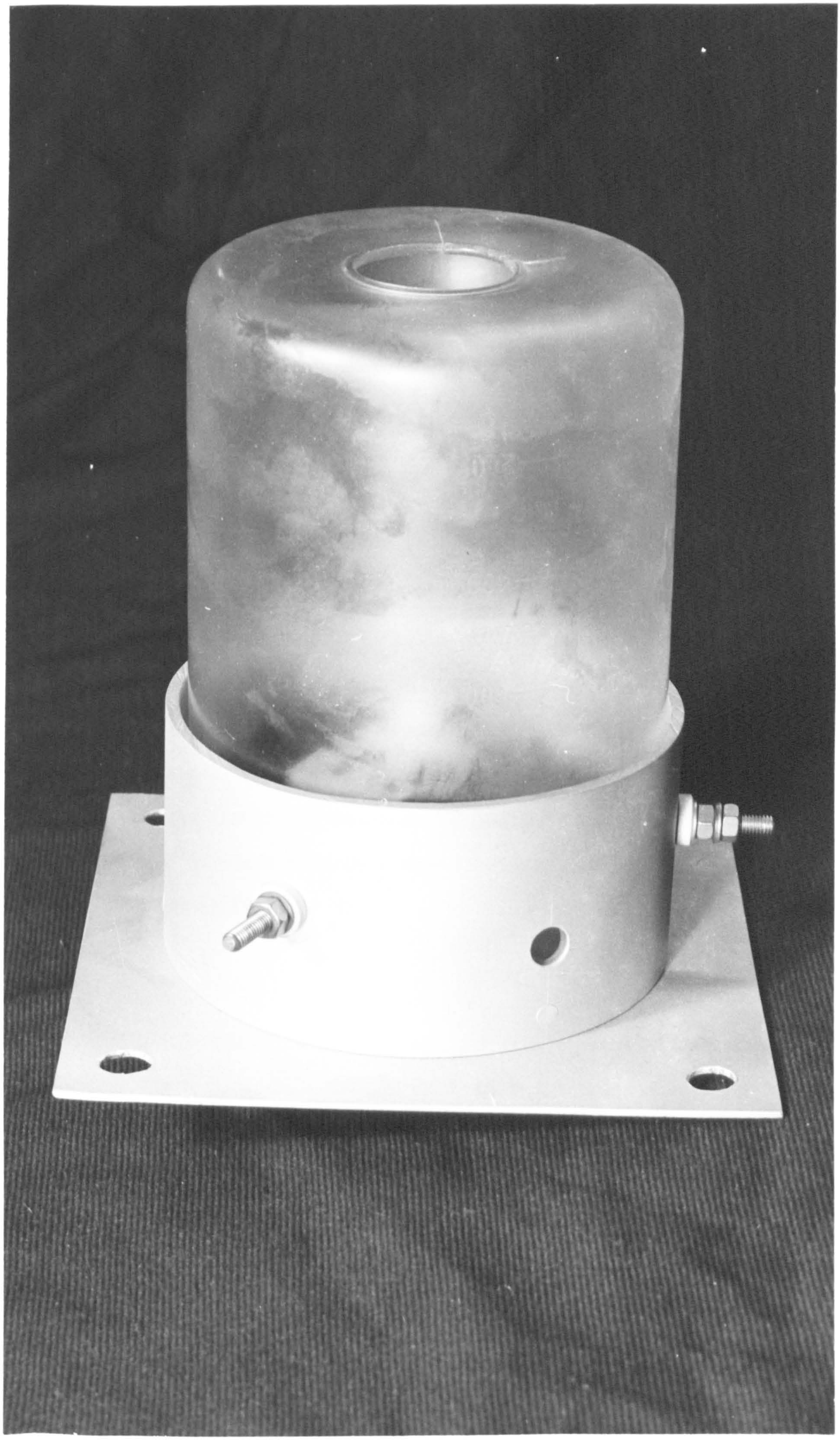

range ion plating, u.h.v. evaporation onto a sputter-cleaned surface and conventional evaporation. The result of these experiments are discussed in Section 5.2

4.4 Trapped Gas and Sputter-redeposition Apparatus

For the investigation of the amount of gas trapped in the deposited film during bombardment of the substrate surface with ions and neutrals from the plasms and for the investigation of sputter-redeposition effects on film-substrate interface formation, a separate piece of apparatus was utilised. This was a standard vacuum evaporation unit (Edwards, Type 12E), modified to allow ion plating to be carried out.

4.4.1 Modifications of Evaporator

The required modifications consisted of the introduction of an H.T. electrode system into the evaporator unit to allow straight-forward ion plating to be carried out. The substrate was mounted in a water cooled holder in order to allow some control of temperature during the deposition process. The holder insulation was protected by an earthed aluminium shield to prevent the build up of evaporated material and the inevitable increase in leakage current which occurs with inadequately shielded insulators in this type of system. A schematic diagram of the apparatus is given in Figure 4.23.

4.4.2 Substrate Holder

For the sputter-redeposition experiments two sample holders, one copper and one stainless steel were constructed. They were designed to hold 1mm thick substrates and were fabricated entirely from one material i.e. all components of copper or stainless holders were copper or stainless steel, respectively. A diagram and photograph showing the design of the substrate holder is shown in Figure 4.24. The reason for this design was to carry out sputter-redeposition experiments in which the source of the film material were the substrate holders themselves. These holders, together with a light substrate (i.e.lower atomic mass than the holder atoms to allow R.B.S. studies) were exposed to the discharge in

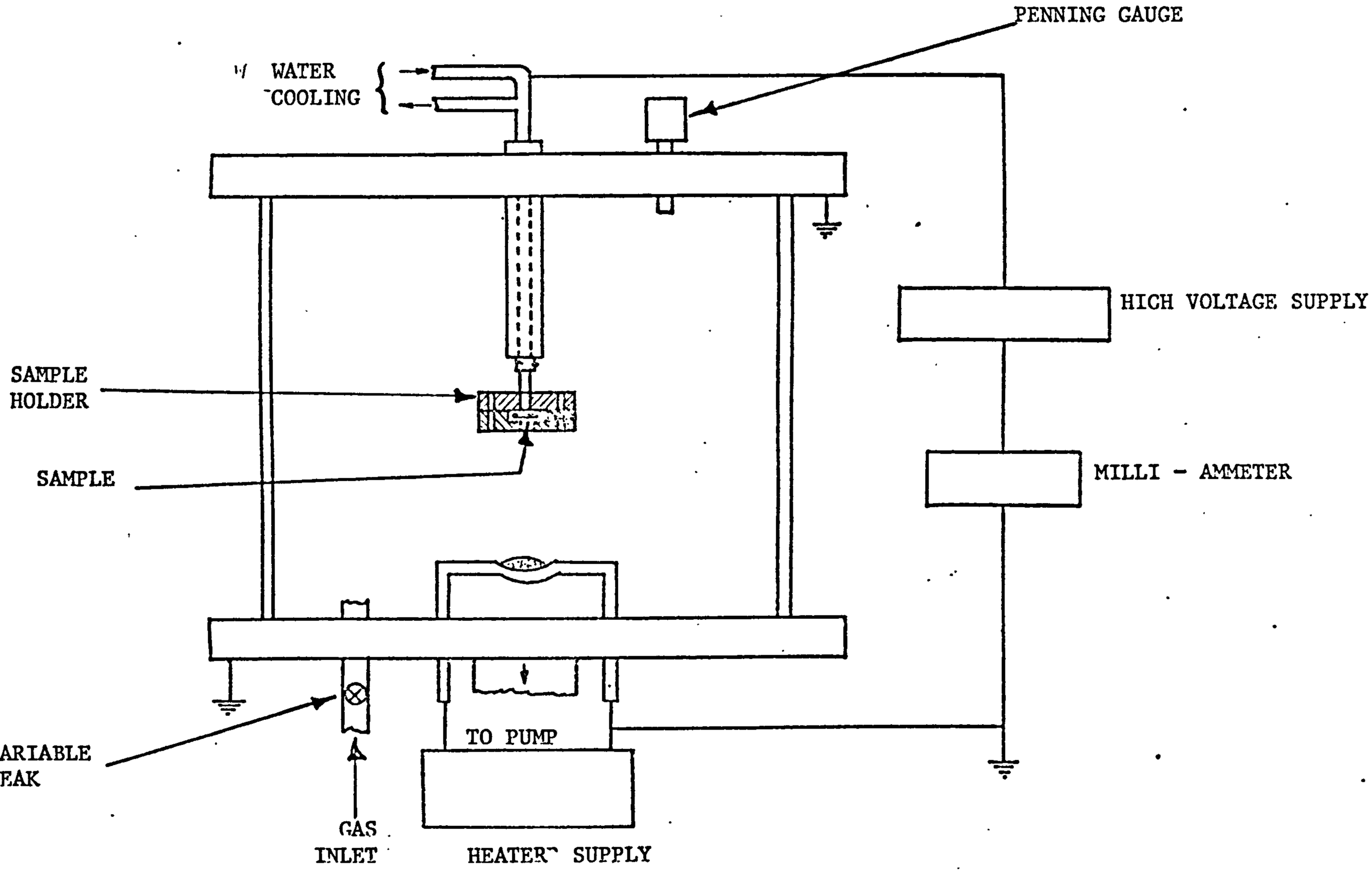

FIGURE 4.23 SCHEMATIC DIAGRAM OF THE EXPERIMENTAL APPARATUS USED IN SPUTTER-REDEPOSITION AND GAS TRAPPING EXPERIMENTS

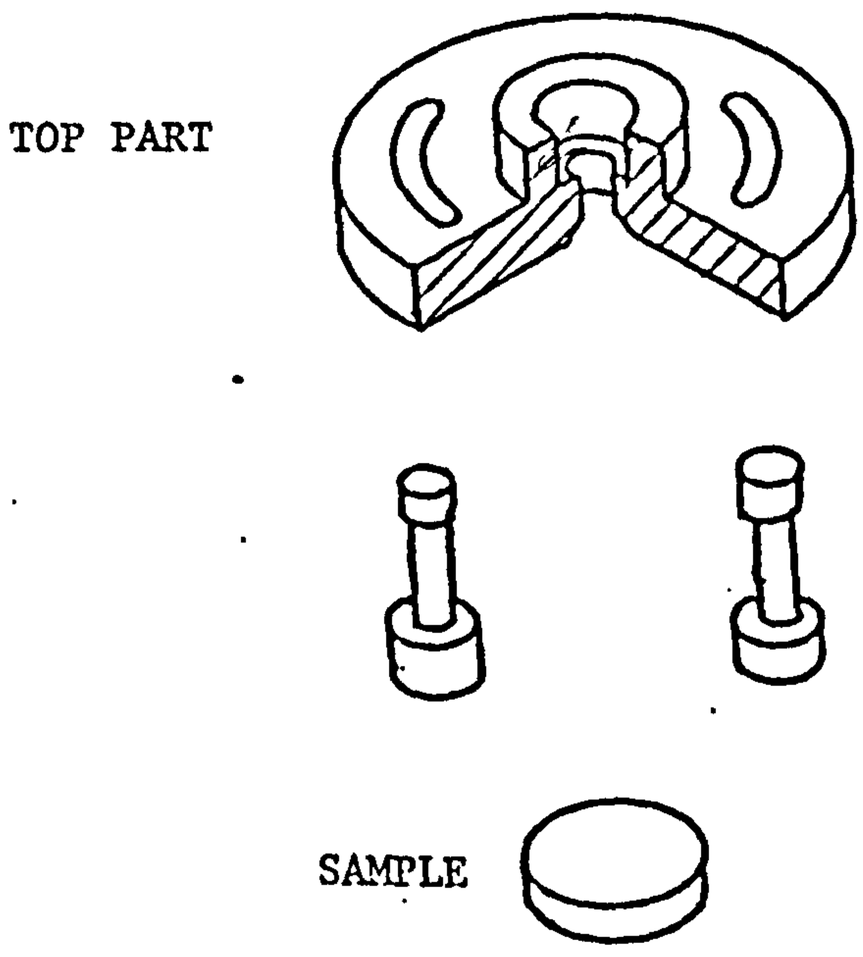

FIGURE 4.24(a) EXPLODED-PICTORIAL AND SECTIONAL VIEWS OF THE SAMPLE HOLDER.

FIGURE 4.24(b)

A PHOTOGRAPH OF THE SUBSTRATE HOLDER USED IN SPUTTER-REDEPOSITION AND CARRIER GAS ENTRAPMENT EXPERIMENTS.

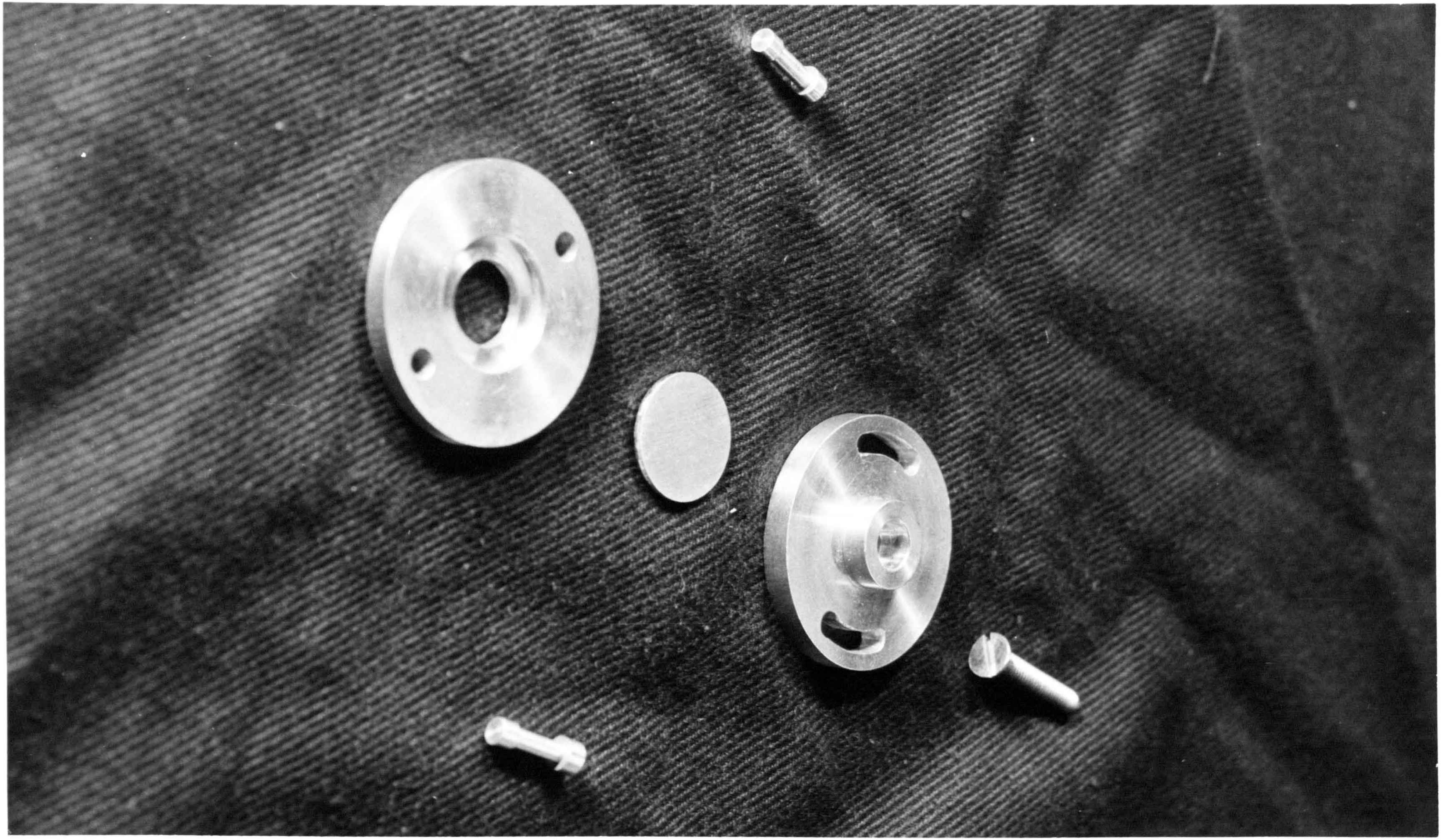

order to study the effect of the sputter-redeposition process.

4.4.3 Performance

The discharge voltage was supplied from a highly stablised power supply (Hewlett Packard) capable of supplying 6mA at 3kV. It was found that application of up to 3kV presented no problem concerning the electrical leakage through the cooling water and it was not necessary to incorporate a de-ioniser in the cooling water system. Sputter-redeposited films were produced using this apparatus and the results are shown in Section 5.4

4.5 References - Chatper 4

1 - V.G. Catalogue Published in 1977

2 - Sherbiney M.G. Ion Plating Ph.D. Thesis, University of Salford 1975

3 - Armour D.G. Studies of Decaying Plasmas, Ph.D. Thesis, University of Liverpool 1970.

4 - Rapp, D., Englander - Golden, P.J. Chem. Phys. 43, P. 1464; 1965

5 - Beanland, D. M.Sc. dissertation, University of Salford, 1974

6 - Purcell E.M., Phys. Rev. 54 1938

7 - Simpson J.A., Kuyatt C.E., Rev. Sci. Inst. 38 No. 1, 1967.

8 - Report on Hemispherical Analyser. Atomic Collisions in Solids, Department of Electrical Engineering, University of Salford, 1973.

CHAPTER V

RESULTS AND DISCUSSIONS

CHAPTER 5

RESULTS AND DISCUSSIONS

5.1 Introduction

5.2 Comparison of Film-Substrate Adhesion of Films produce under U.H.V. Ion Plating, U.H.V. Evaporation, and Conventional Evaporation

5.2.1 Preparation of Films

5.2.2 Adhesion Test

5.2.3 Comments

5.3 Energy Distributionsof the Particles Impinging on the Cathode

5.3.1 Energy Distributions of the Total Flux of Ions and Neutrals Leaving the Discharge prior to Evaporation.

5.3.2 Mass Analysis

5.3.3 Energy Distributions of the Ionic and Neutral Species of the Carrier Gas Leaving the Discharge

5.3.4 Energy Distributions of Film Material Species Leaving the Discharge

5.3.5 Comments

5.3.5(a) Contribution of Energetic Particles to Film Formation

5.3.5(b) Role of Energetic Particle Implantation.

5.3.5(c) Energy Deposition

5.3.5(d) Comparison with Davis and Vanderslice's Theory

5.4 Sputter-Redeposition

5.4.1 Preparation of Film

5.4.2 Quantity of Sputter-Redeposited Film

5.4.3 Comments

5.1 Introduction

There is now sufficient evidence to accept the superior properties of ion-plated films as an established fact. However, there has been little conclusive evidence presented to identify the mechanisms reponsible for the properties of ion-plated films. Basically, an ion plating system comprises the substrate which forms the cathode of an abnormal glow discharge and the plasma region in which there is a mixture of the gas species used to carry the discharge and the film species which is evaporated into it. Particles from the plasma impinge on the substrate and as a result of this bombardment a number of physical processes occur at, and close to, the surface. A diagram illustrating these processes is shown in Figure 5.1. It is clear that the explanation for the properties of ion-plated films is based on the mechanisms known to be associated with energetic bombardment of surfaces and hence the processes indicated in the diagram, namely ion implantation, recoil implantation, radiation enhanced diffusion, cascade mixing, thermal spikes, basic surface cleaning effects, trapping of carrier gas in the deposited film, surface damage effects, etc may all play a role. A comprehensive analysis of the mechanisms responsible for the properties of ion-plated films must, therefore, be based on a detailed investigation of all these effects in order to assess their respective contributions. In this connection the most important questions are:-

1. What is the effect of substrate surface cleanliness on film-substrate adhesion and is deposition in a discharge actually essential for good adhesion?
2. What are the constituents of the flux of particles bombarding the substrate surfaces, both prior to and during evaporation, and what are their energy distributions?
3. What mechanisms are responsible for the formation of a high binding film-substrate interface?
4. Is the formation of the film due to energetic particle impingement?
5. What is the concentration of trapped carrier gas atoms in the deposited

① INCIDENT PARTICLE

② FILM PARTICLE

③ SUBSTRATE PARTICLE

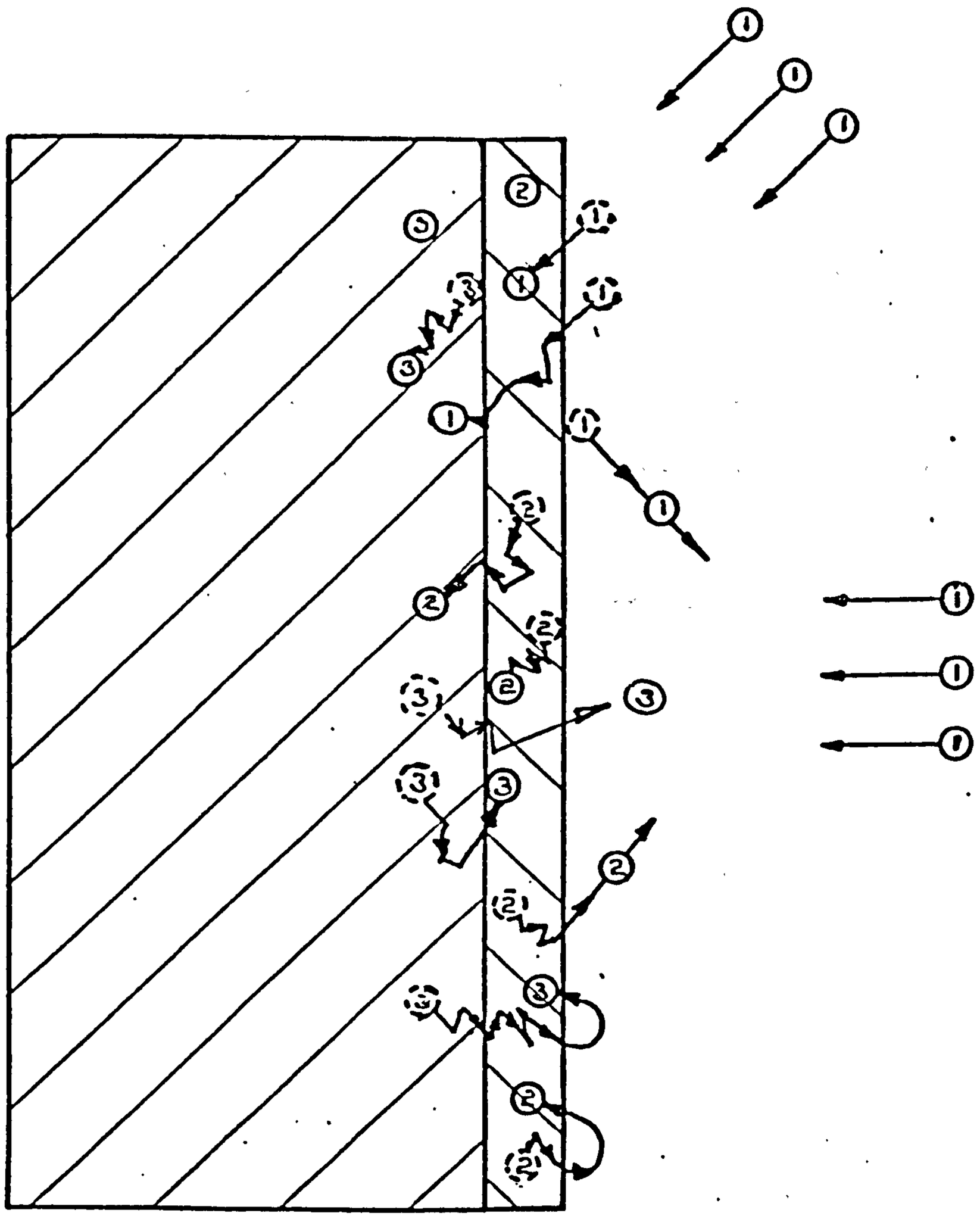

FIGURE 5.1 SCHEMATIC REPRESENTATION OF THE PROCESSES OCCURRING AT SURFACE/NEAR SURFACE LAYERS OF A TYPICAL ION PLATING DISCHARGE. DOTTED CIRCLES: INITIAL POSITION OF THE PARTICLE. SOLID CIRCLES: FINAL POSITION OF THE PARTICLE.

film and does the presence of this gas influence the structure of the film?

The work described in this Chapter is concerned with an attempt to consider all these questions by carrying out the following experiments:-

1. Comparison of film-substrate adhesion of films produced under u.h.v. ion plating, u.h.v. evaporation, and conventional evaporation.
2. Measurement of the energy distributions of total ion and neutral species (without mass analysis) impinging on the substrate, prior to evaporation.
3. Measurement of the energy distributions of carrier gas ions and neutral atoms prior to evaporation.
4. Measurement of the energy distributions of film material ions and neutral atoms.
5. Investigation of the role of Sputter - redeposition effects.
6. Investigation of the removal of pre-implanted gas atoms by exposure to the discharge using Rutherford backscattering (R.B.S.) analysis.
7. Measurement of the efficiency of carrier gas incorporation using R.B.S. analysis.

The result and discussion of these measurements are presented in this Chapter.

5.2 Comparison of Film-Substrate Adhesion of Films Produced under U.H.V. Ion Plating, U.H.V. Evaporation, and Conventional Evaporation.

As discussed earlier in this thesis the process of film deposition in ion plating is preceded and accompanied by sputter cleaning such that film material particles land on a clean substrate surface. This motivated some workers to attribute the strong film-substraet adhesion of ion-plated films to the clean substrate surface condition (see Chapter 2). To clarify this point films of gold . were produced on a nickel substrate under u.h.v. ion plating, u.h.v. evaporation, and conventional evaporation, and their adhesion to the substrate investigated by means of a scratch test technique.

5.2.1 Preparation of Films

The coating apparatus used for the preparation of films under the above mentioned conditions has been described in Section 4.4.1. The device was used in conjunction with the main vacuum chamber described in Section 4.2 Three nickel targets were mounted on the target holder which could be maniuplated from outside the chamber such that only one target at a time was aligned with the deposition aperture of the coating apparatus. This facilitated controlled coating of all three targets without breaking the vacuum in the chamber (see Section 4.4.1). Gold was used as film material and was evaporated by placing gold in the molybdenum boats of the apparatus shown in Figure 4.22. The positioning of the targets on top of the deposition aperture and the onset of evaporation were monitored by looking through the glass windows mounted on the wall of the main chamber. Since a quartz crystal was not available production of films with as near identical thicknesses as possible was achieved by passing identical currents through the filaments for identical periods of time (30 seconds) in each case. Obviously, this is not entirely satisfactory since evaporation rates vary under different vacuum conditions. However, this did not create serious problems in this particular investigation because the film-substrate adhesion,not thickness,was under study.

For the production of u.h.v. ion - plated films the chamber was first

pumped down to $9x10^{-10}$ torr then backfilled with research grade argon to a pressure of $1x10^{-2}$torr. A discharge (at 2.5kV) was then struck between the filament (the anode) and the target (the cathode) and after 30 minutes of sputter cleaning the boat was energised for 30 seconds. The sputter cleaning and evaporation procedure was repeated for the other two targets. The system was then opened to atmosphere and three more targets were mounted for production of three u.h.v. evaporated films. These films were deposited on sputter cleaned substrates at a base pressure of $9x10^{-10}$ torr. The boat was again energised for 30 second periods. Samples of films produced under conventional evaporation conditions were produced by applying a similar procedure with the exception that the operating vacuum was about $1x10^{-6}$ torr and sputter cleaning, which would have been irrelevant due to short monolayer formation times at this pressure, was not carried out.

5.2.2 Adhesion Test

The film-substrate adhesion of the samples produced under the above-mentioned conditions was tested by performing scratch tests. These were carried out at the Tribological Research Laboratory of the Department of Mechanical and Aeronautical Engineering of University of Salford. In these tests the deposited samples were subjected to scratches created under mechanical loads of 25gm, 50gm, and 100gm. The extent of the damage and hence the quality of the film-substrate adhesion was observed using a scanning electron microscope. The relevant micrographs are shown in Figure 5.2 It can be seen that although the u.h.v. evaporated films showed significantly better adhesion than those produced under normal evaporation condition, u.h.v. ion plating clearly produced the best adhesion.

5.2.3 Comments

The results shown in Figure 5.2 are consistent with the adhesion investigations of Teer[1] who discovered much superior film-substrate adhesion for

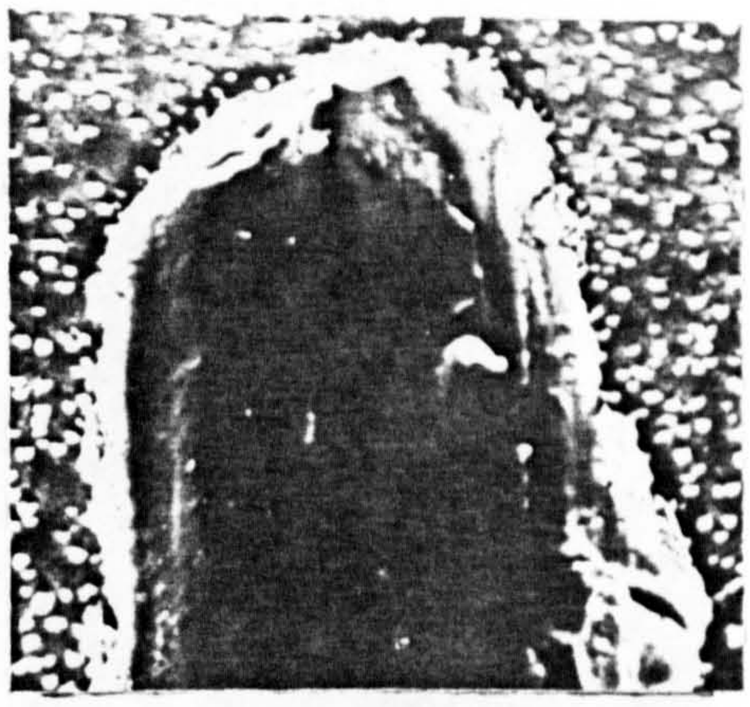

(a)

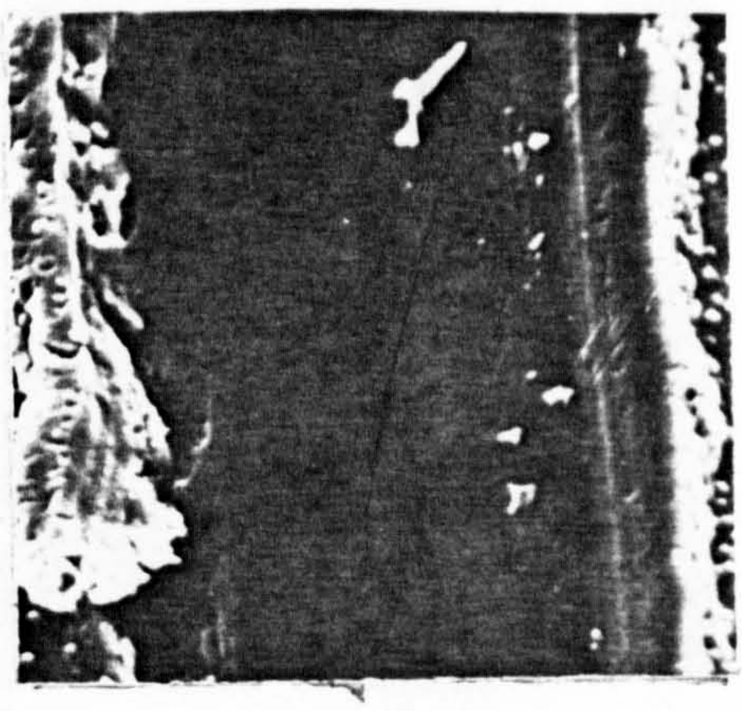

(b)

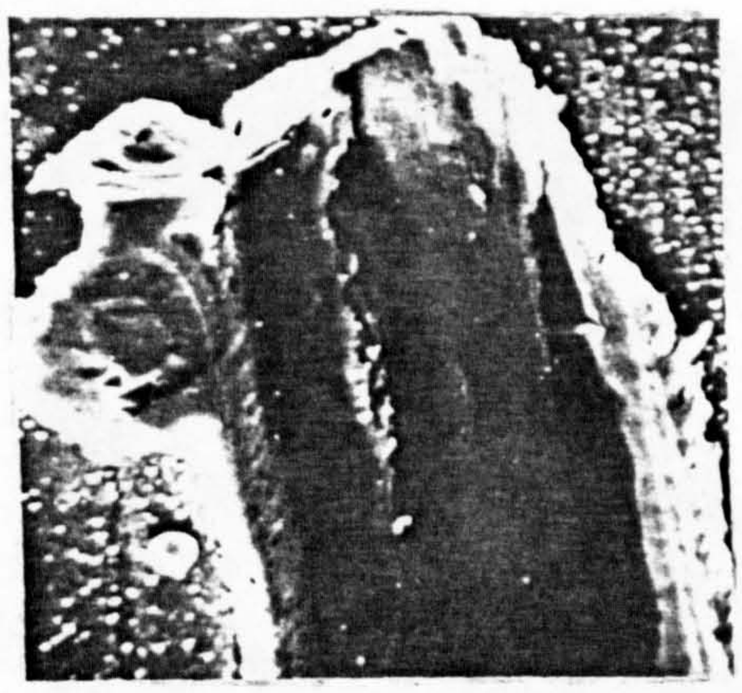

(c)

Figure 5.2 (a)

Micrographs of scratch tests, created under various mechanical loads, on gold films (produced on nickel substrates) under conventional evaporation conditions. Mechanical load: a - 25 g ; b - 50 g ; c - 100 g.

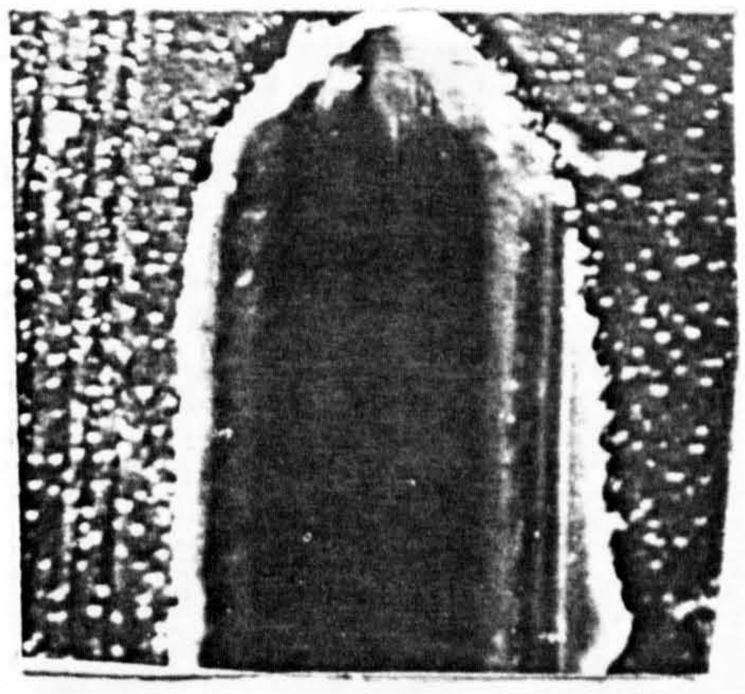

(a)

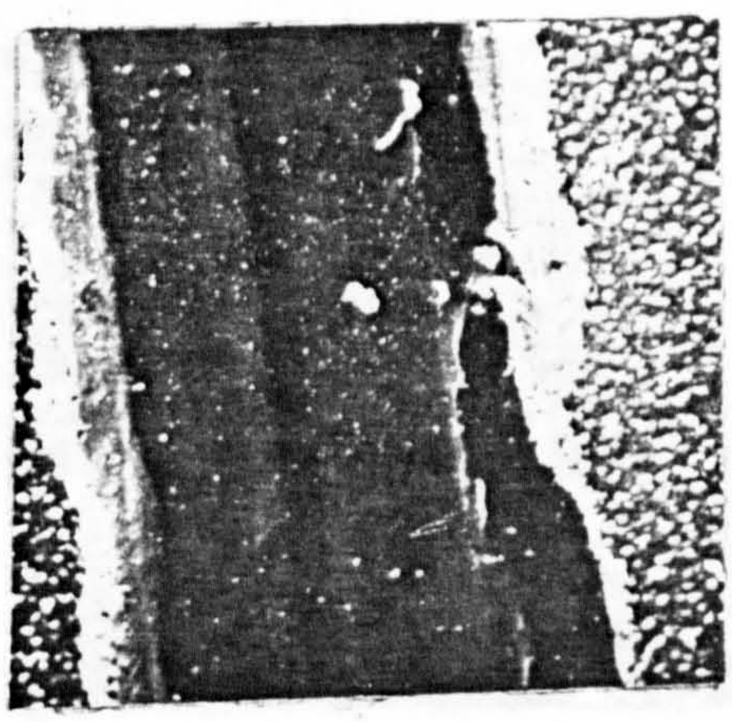

(b)

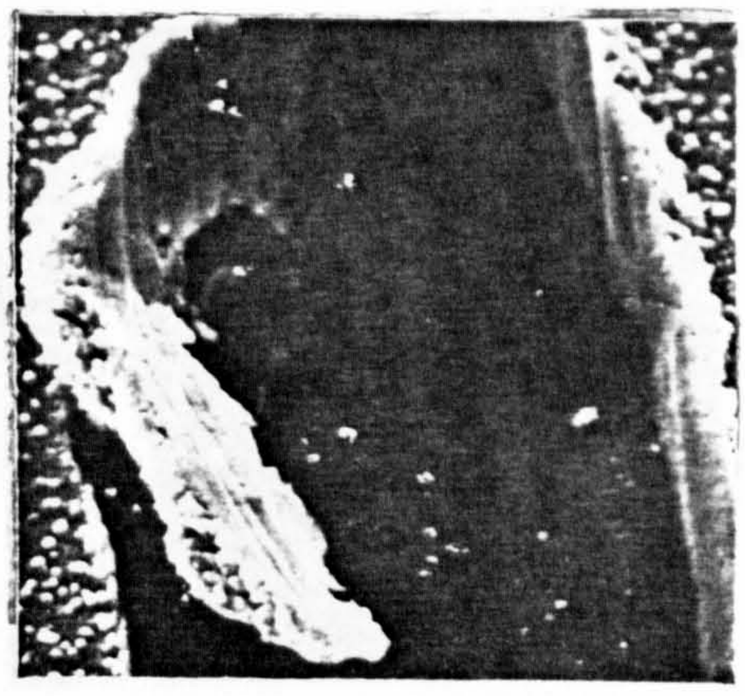

(c)

Figure 5.2 (b)

Micrographs of scratch tests, created under various mechanical loads on gold films (produced on sputter-cleaned nickel substrates) under u.h.v. base evaporation conditions. Mechanical loads: a - 25 g ; b - 50 g ; c - 100 g.

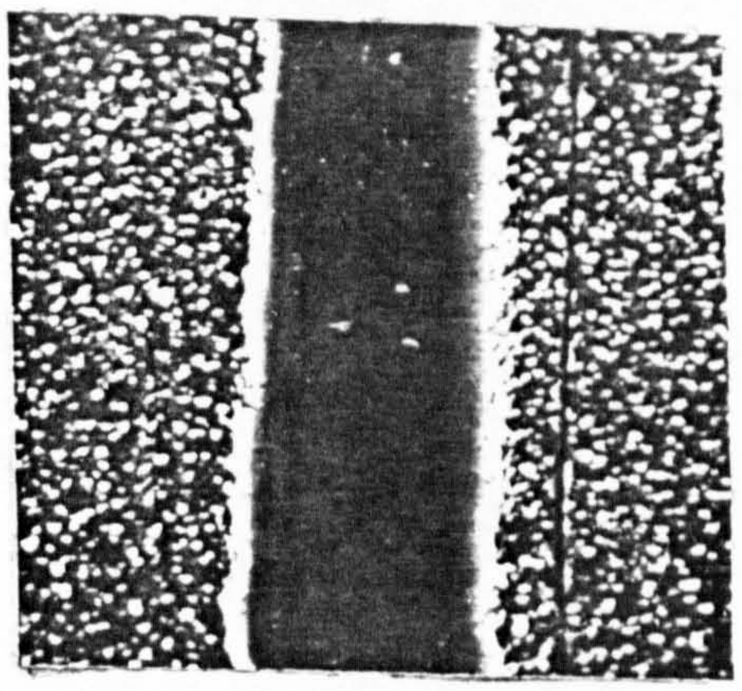

(a)

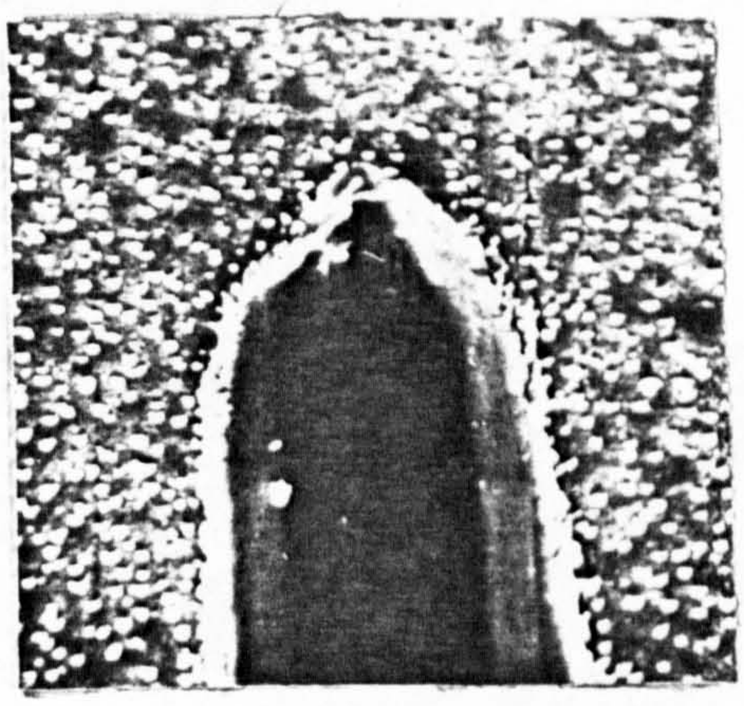

(b)

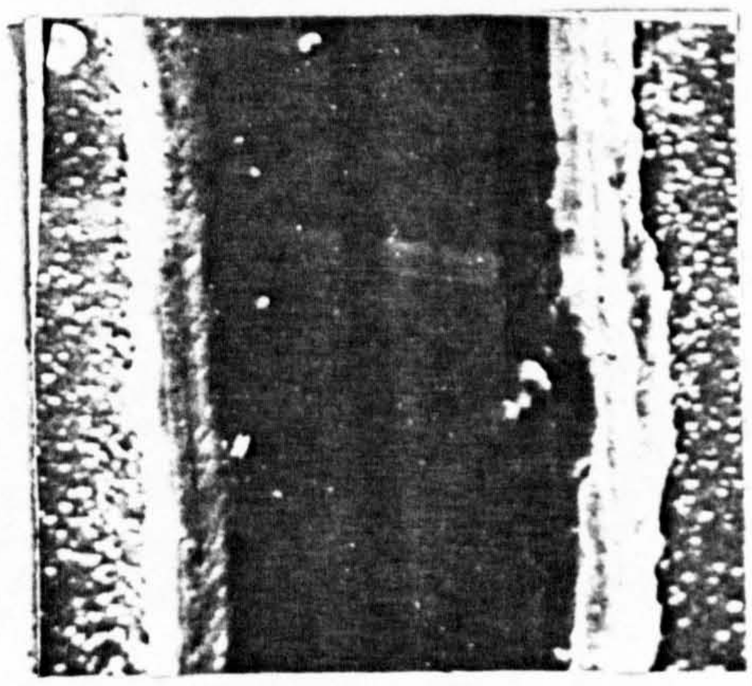

(c)

Figure 5.2 (c)

Micrographs of scratch tests, created under various mechanical loads, on gold films (produced on nickel substrates) under u.h.v. ion plating conditions. Mechanical loads: a - 25 g ; b - 50 g ; c - 100 g.

ion-plated films compared to vacuum evaporated films produced immediately after sputter cleaning of the substrate. From these results it can be concluded that for optimum adhesion, deposition in a discharge is essential. Hence, once again, the strong film-substrate adhesion must be attributed, in some way, to the deposition of energy during film formation and hence to the production of a graded film-substrate interface. However, this conclusion motivates interest in finding explanations for the mechanisms responsible for the formation of such an interface.

5.3 Energy Distributions of the Particles Impinging on the Cathode

So far, the pattern that has emerged is that deposition in a discharge is an essential factor in determining the strong adhesion of ion-plated films and that is this feature of ion plating which is responsible for the formation of the graded interface. This conclusion raises the following questions:-

What mechanism(s) associated with energetic flux bombardment of surfaces is (are) responsible for the film-substrate interface of ion - plated films. To this end the following measurements were carried out on the flux of particles impinging on the cathode of an ion plating discharge:-

1. Measurement of the energy distributions of the total ion and neutral fluxes prior to evaporation.
2. Mass analysis of the constituents of the total ion and neutral fluxes both prior to and during evaporation.
3. Measurement of the energy distributions of the carrier gas ions and neutrals.
4. Measurement of energy distributions of the film material ions and neutrals.

These measurements were carried out using the apparatus described in Section 4.2 in its constant transmission mode of operation with a pass energy of 20eV for the energy analyser.

5.3.1 Energy Distributions of Total Flux of Ions and Neutrals Leaving the Discharge Prior to Evaporation.

These measurements were carried out for argon and nitrogen discharges. The discharge voltage was varied from 1.5kV to 3kV. At each discharge voltage studied, energy spectra were obtained for discharge pressures in the range 3×10^{-2} torr to 4.2×10^{-2} torr (30μ - 42μ). Typical energy distributions for ions leaving argon and nitrogen discharges operating at 3×10^{-2} torr and various voltages prior to evaporation are shown in Figures 5.3(a) and (b). Similar trends were observed at all the discharge pressures studied with a consistent shift of the spectra to lower energies as the discharge pressure was increased. These variations have been characterised, for convenience, in terms of peak energies and, low and high energy cut-offs and are presented in Tables 5.1(a) and (b) for argon and nitrogen discharges, respectively. It can be seen that for discharge voltages, varying from 1.5 — 3kV, the peaks in the energy distributions for the ions leaving argon discharges vary from $\sim$ 350eV to $\sim$ 500 eV and for nitrogen discharges from $\sim$ 400eV to $\sim$ 625 eV.

Measurements of the energy distributions of the total flux of neutral particles leaving discharges struck in argon and nitrogen were carried out by deflecting the ions off the axis of the analysing sytem and operating the electron beam ioniser discussed in Section 4.2. These measurements were carried out under similar conditions to those used for the ion energy measurements and typical energy distributions obtained at various discharge voltages and a pressure of 3×10^{-2} torr for argon and nitrogen discharges are shown in Figures 5.4(a) and (b). The same trends were observed at all pressures studied with a cosistent shift of the spectra towards lower energies as the pressure was increased. The peaks in the spectra vary from $\sim$ 275eV to $\sim$ 350eV for argon and from $\sim$ 200eV to $\sim$ 400eV for nitrogen discharges. The results of these measurements characterised in the same way as the ion measurements are tabulated in Tables 5.2(a) and (b). In all cases, the neutral spectra are shifted to lower energies than the corresponding ion spectra, an effect which is illustrated in Figure 5.5. which compares the spectra for a 3×10^{-2} torr, 3kV argon discharge.

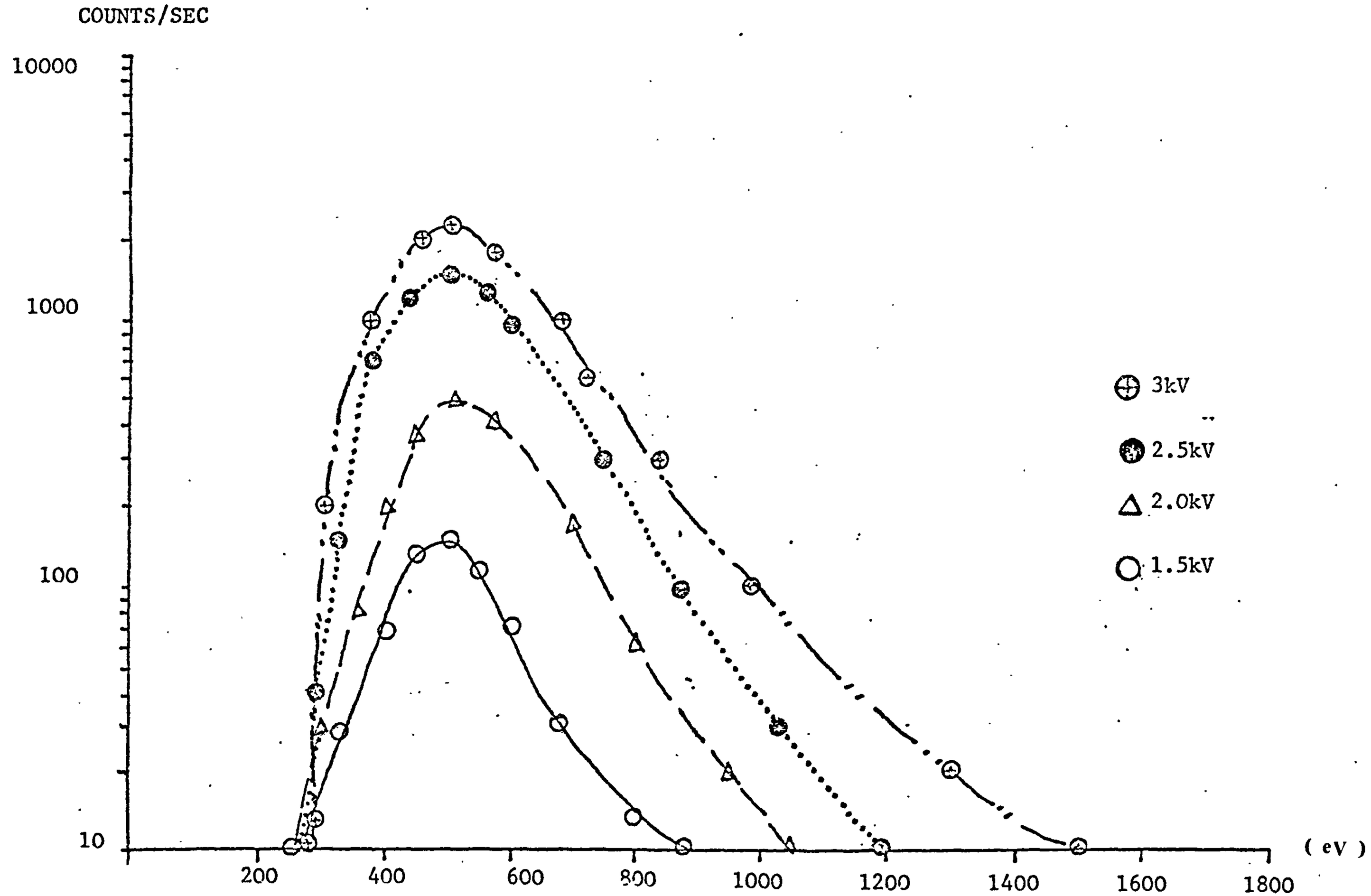

FIGURE 5.3(a) ENERGY DISTRIBUTIONS OF THE TOTAL FLUX OF IONS LEAVING ARGON DISCHARGE OF 3×10^{-2} TORR AT VARIOUS VOLTAGES

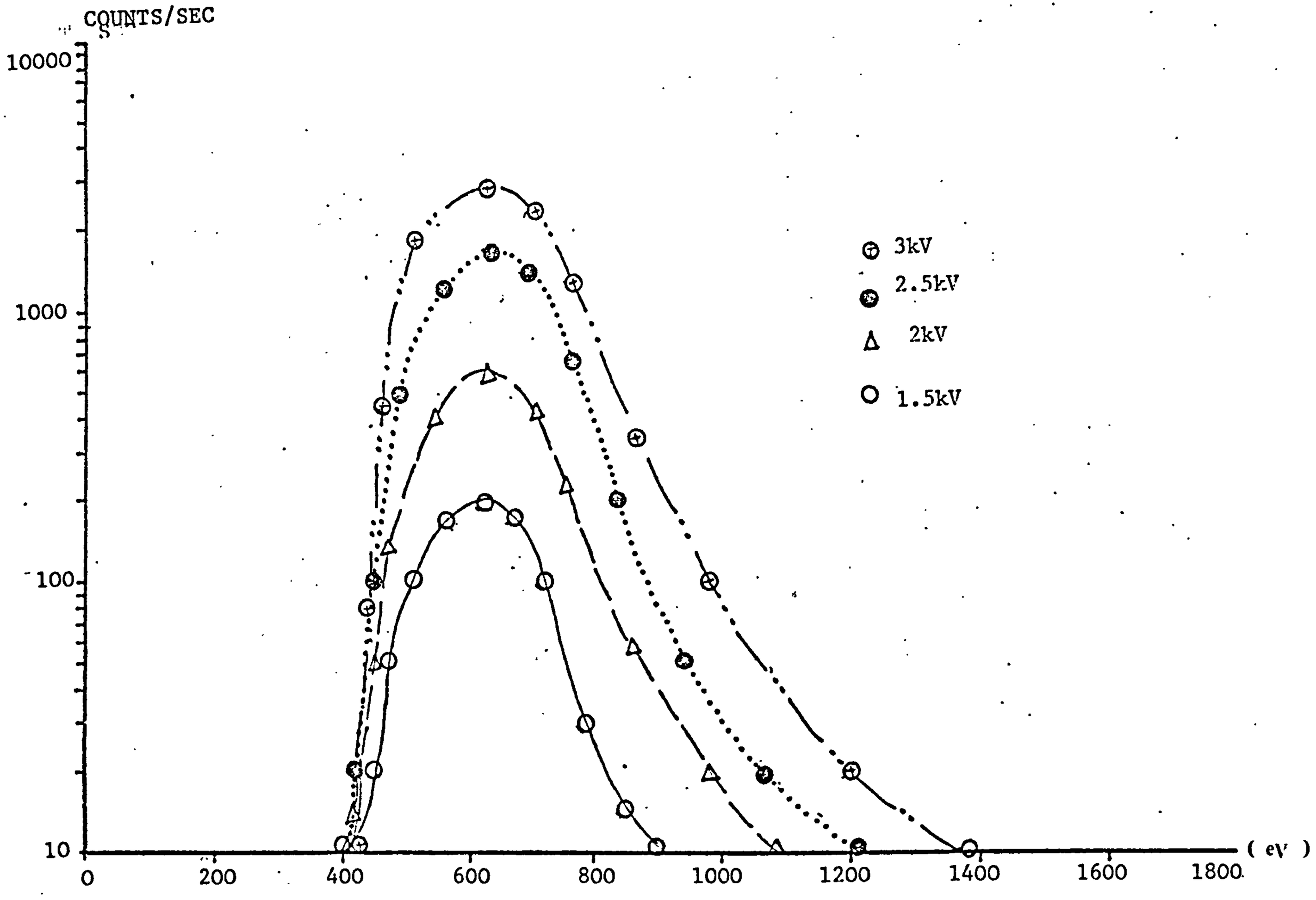

FIGURE 5.3(b) ENERGY DISTRIBUTIONS OF THE TOTAL FLUX OF IONS LEAVING NITROGEN DISCHARGE OF 3×10^{-2} TORR AT VARIOUS VOLTAGES.

Discharge Voltage (kV)	Discharge Pressure (/μ)	Low Energy (eV)	Peak (eV)	High Energy (eV)
1.5	30	260	500	875
	36	240	500	825
	39	210	450	780
	42	150	350	975
2.0	30	265	500	1050
	36	250	470	1100
	39	200	425	1025
	42	165	350	
2.5	30	270	520	1200
	36	260	500	1150
	39	210	420	1100
	42	165	350	1050
3.0	30	270	500	1500
	36	265	520	1375
	39	200	420	1350
	42	165	350	1300

(a)

Discharge Voltage (kV)	Discharge Pressure (/μ)	Low Energy (eV)	Peak (eV)	High Energy (eV)
1.5	30	400	625	900
	36	300	535	870
	39	200	500	865
	42	160	420	760
2.0	30	410	625	1100
	36	320	525	1000
	39	210	510	1000
	42	160	400	900
2.5	30	400	630	1200
	36	310	560	1175
	39	200	475	1025
	42	165	420	1050
3.0	30	410	625	1400
	36	320	550	1460
	39	210	475	1385
	42	170	360	1350

(b)

TABLE 5.1 TABULATED CHARACTERISATION OF ENERGY DISTRIBUTIONS OF THE TOTAL FLUX OF IONS LEAVING ION PLATING DISCHARGES.

a. ARGON DISCHARGE

b. NITROGEN DISCHARGE.

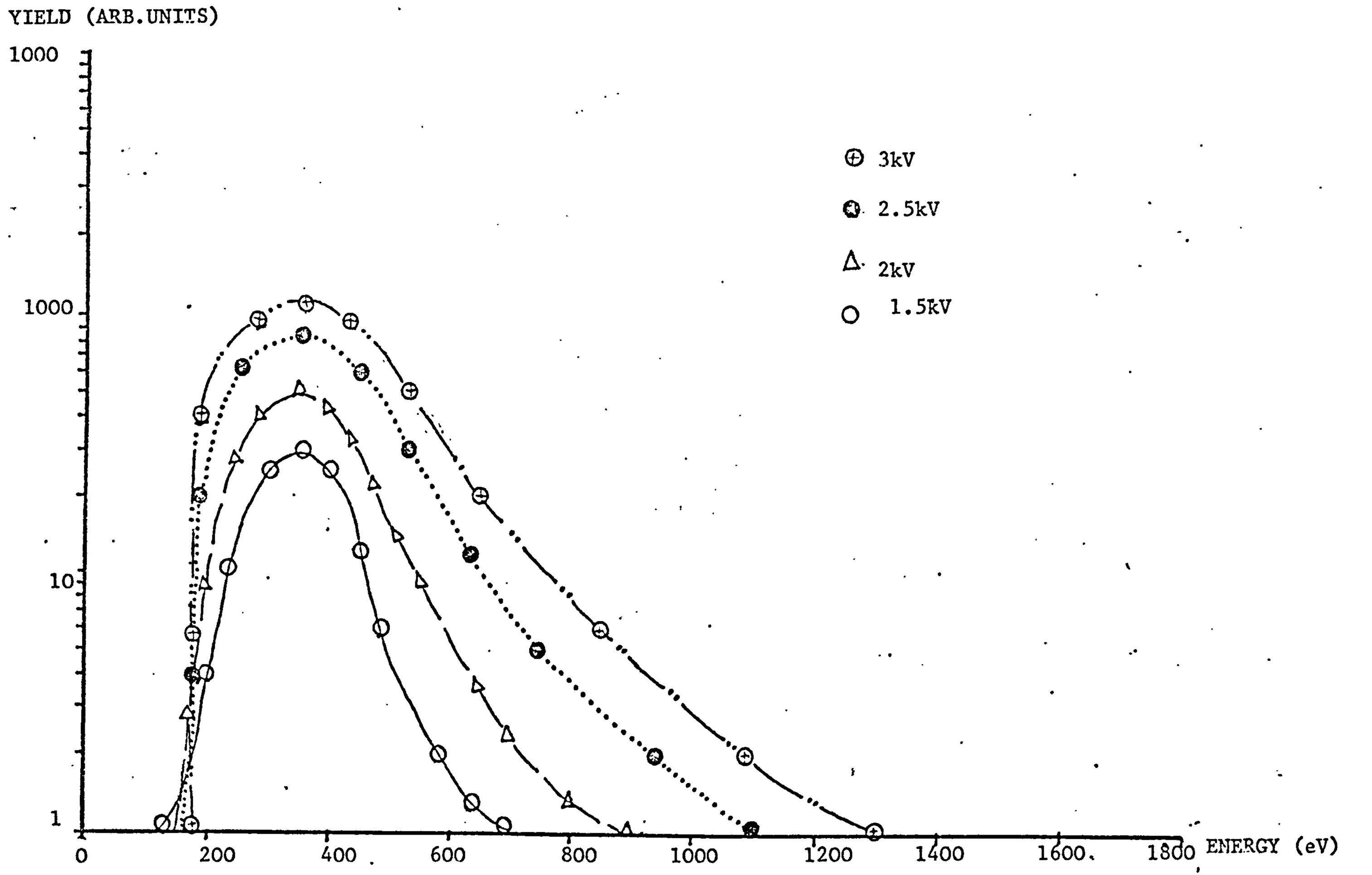

FIGURE 5.4(a) ENERGY DISTRIBUTIONS OF THE TOTAL FLUX OF NEUTRAL PARTICLES LEAVING ARGON DISCHARGE OF 3×10^{-2} AT VARIOUS VOLTAGES.

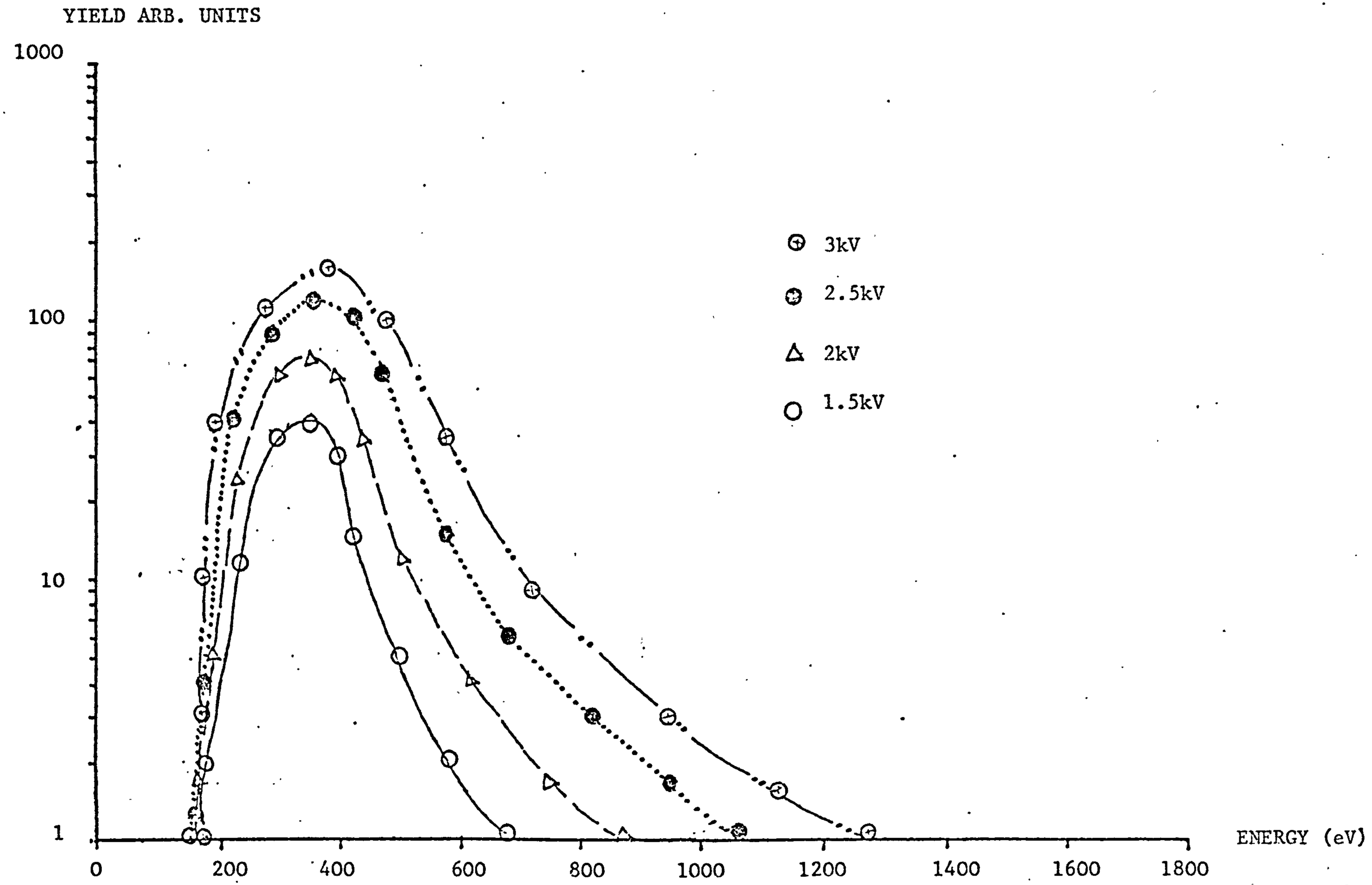

FIGURE 5.4(b) ENERGY DISTRIBUTIONS OF THE TOTAL FLUX OF NEUTRAL PARTICLES LEAVING NITROGEN DISCHARGE OF 3×10^{-2} TORR AT VARIOUS VOLTAGES.

Discharge Voltage (kV)	Discharge Pressure (μ)	Low Energy (eV)	Peak (eV)	High Energy (eV)
1.5	30	150	350	700
	36	125	300	630
	39	100	300	600
	42	100	250	600
2.0	30	155	350	900
	36	130	300	850
	39	120	300	800
	42	120	260	750
2.5	30	160	350	1100
	36	150	330	1050
	39	130	280	975
	42	125	260	975
3.0	30	160	350	1300
	36	160	340	1250
	39	150	300	1200
	42	140	270	1150

(a)

Discharge Voltage (kV)	Discharge Pressure (μ)	Low Energy (eV)	Peak (eV)	High Energy (eV)
1.5	30	140	350	675
	36	130	312	625
	39	100	260	560
	42	75	200	550
2.0	30	140	350	870
	36	125	315	825
	39	110	275	775
	42	75	210	725
2.5	30	150	350	1060
	36	130	320	975
	39	120	250	950
	42	80	220	900
3.0	30	160	375	1275
	36	135	325	1180
	39	120	250	1150
	42	85	220	1125

(b)

TABLE 5.2 TABULATED CHARACTERISATION OF ENERGY DISTRIBUTIONS OF THE TOTAL FLUX OF NEUTRAL PARTICLES LEAVING ION PLATING DISCHARGES.

a. ARGON DISCHARGE

b. NITROGEN DISCHARGE

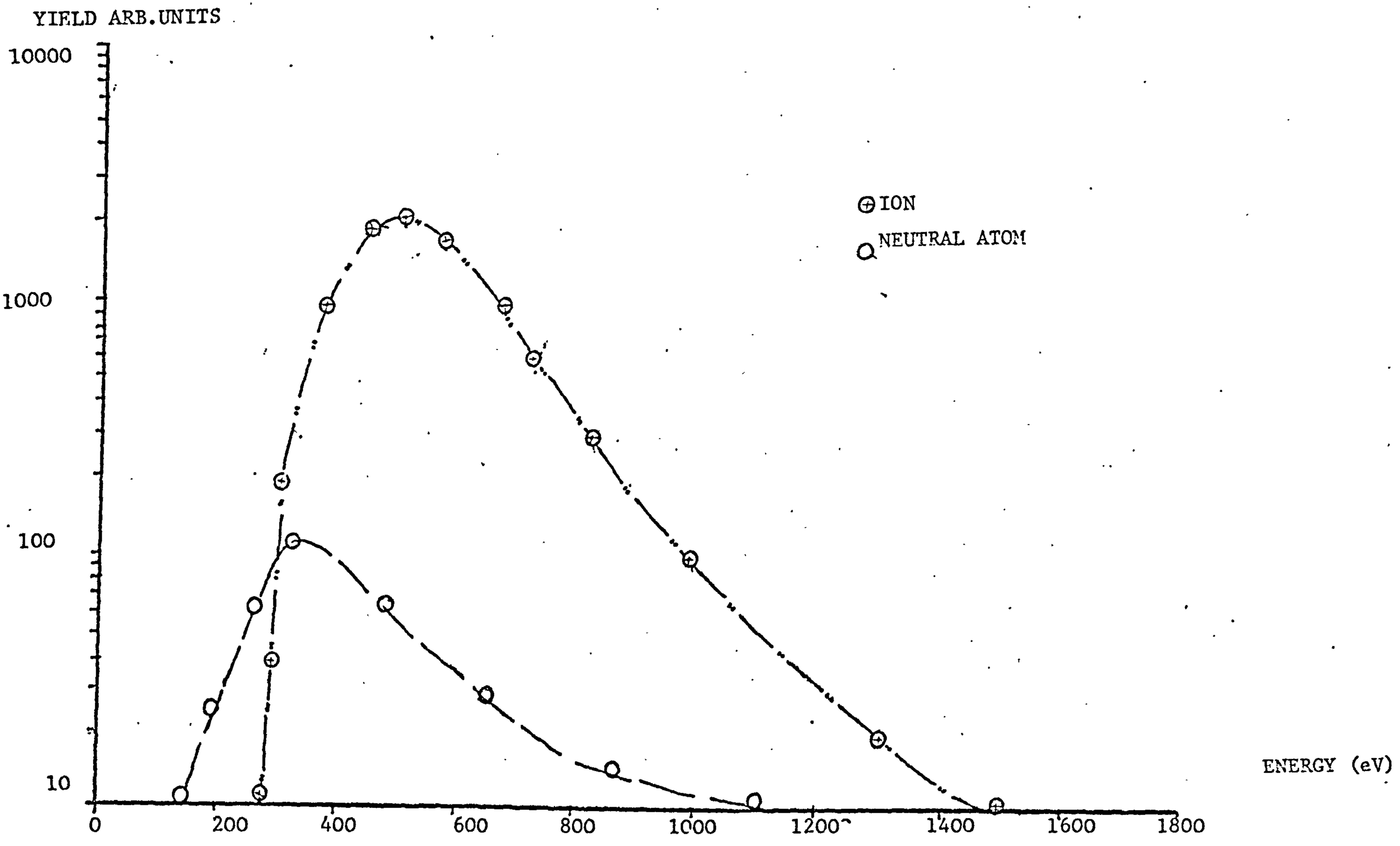

FIGURE 5.5 COMPARISON OF THE ENERGY SPECTRA OF THE TOTAL IONS AND NEUTRAL PARTICLES LEAVING ARGON DISCHARGE OF 3×10^{-2} TORR AT 3kV.

5.3.2 Mass Analysis

In order to further characterise the processes occurring during plating, the measurements described in the previous section were refined by the use of mass analysis such that the energy distributions of the various constituents of the plasma impinging on the cathode of the plating discharge could be measured. Mass analysis of the ionic and neutral species leaving argon and nitrogen discharges were carried out for the discharge conditions described in Section 5.3.1. Typical mass spectra obtained for ionic species leaving argon and nitrogen discharges, prior to evaporation, at 2kV and $3x10^{-2}$ torr are shown in Figures 5.6(a) and (b). Similar mass spectra were observed at all discharge conditions studied. The mass spectra for the neutral particles leaving the discharges studied followed similar trends without peaks at mass 20 (for argon discharge) and mass 7 (for nitrogen discharge). The results of these measurements indicate that ionic species are comprised of Ar^+, Ar^{++} (in argon discharge) and N_2^+, N^+ and N^{++} (in nitrogen discharge) together with water vapour, carbon mono-oxide and oxygen as the major impurities. Plasma induced outgassing from the walls of the machinable glass ceramic discharge tube probably accounts for the high impurity levels observed since even without baking, the partial pressures of these contaminant species prior to running the discharge were several order of magnitude lower than that of the carrier gas.

The mass spectra of the ionic species leaving the argon and nitrogen discharges, during evaporation with the carrier gas pressure set at $1.8x10^{-2}$ torr are shown in Figures 5.7(a) and (b). It can be seen that these spectra, apart from the copper peaks, are similar to those obtained prior to evaporation. At this stage it must be pointed out that accurate measurement of the discharge pressure during evaporation is impossible due to the limitations described in Section 5.3.4

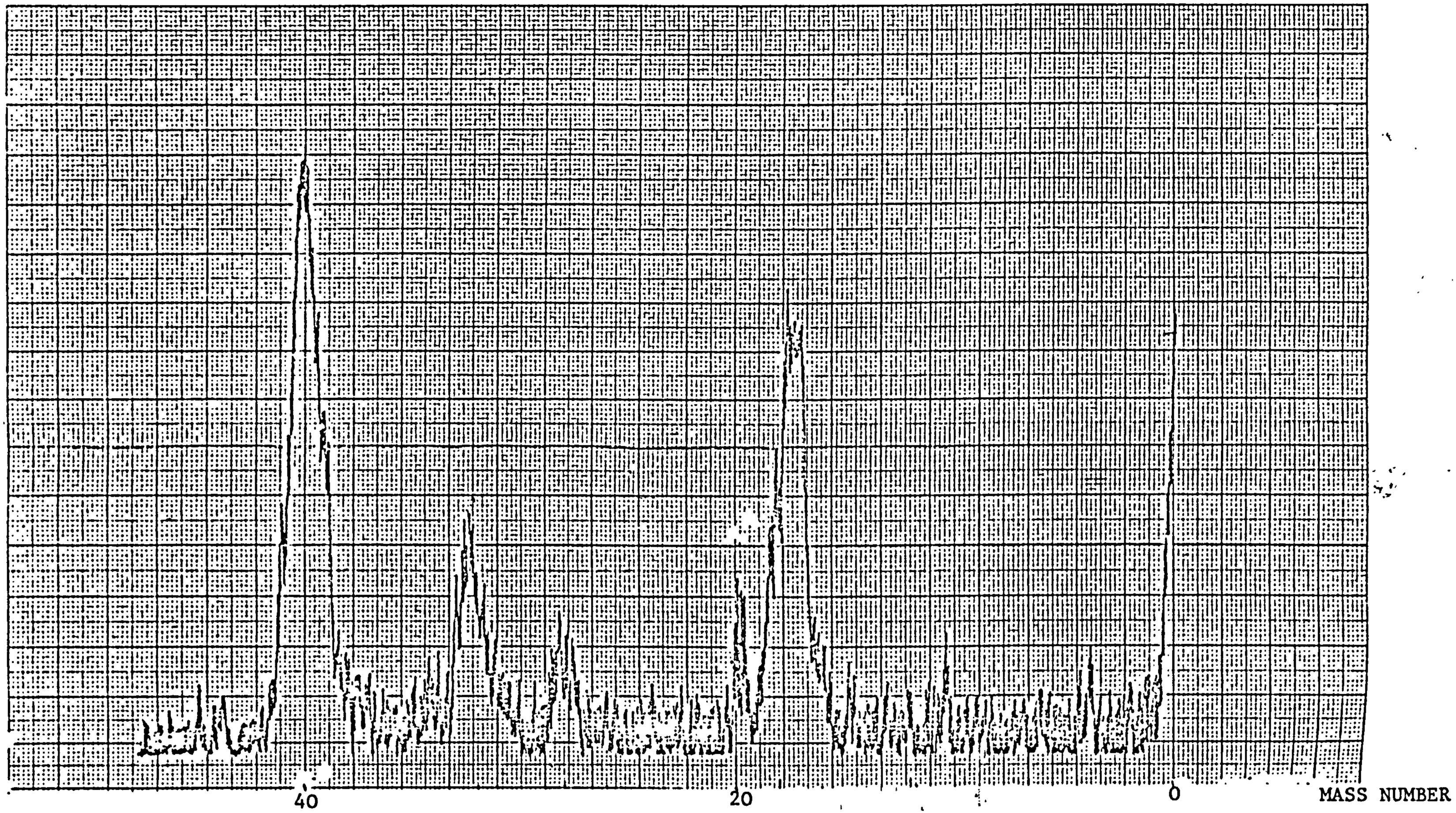

FIGURE 5.6 (a) MASS SPECTRUM OF THE FLUX OF ION LEAVING A 2kV, 3×10^{-2} TORR ARGON DISCHARGE, PRIOR TO EVAPORATION.

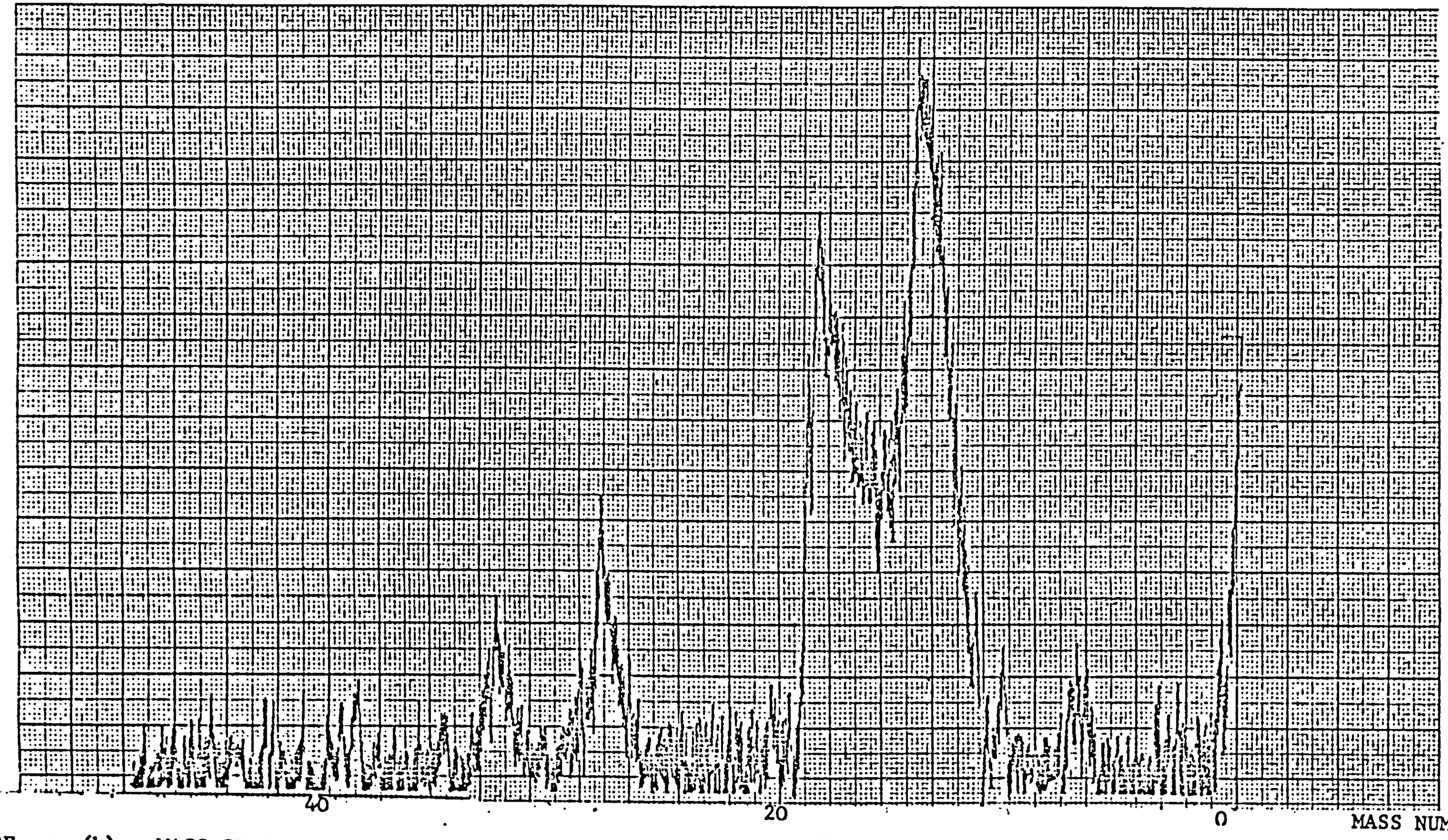

FIGURE 5.6(b) MASS SPECTRUM OF THE FLUX OF ION LEAVING 2kV, 3×10^{-2} torr NITROGEN DISCHARGE, PRIOR TO EVAPORATION OF FILM MATERIAL.

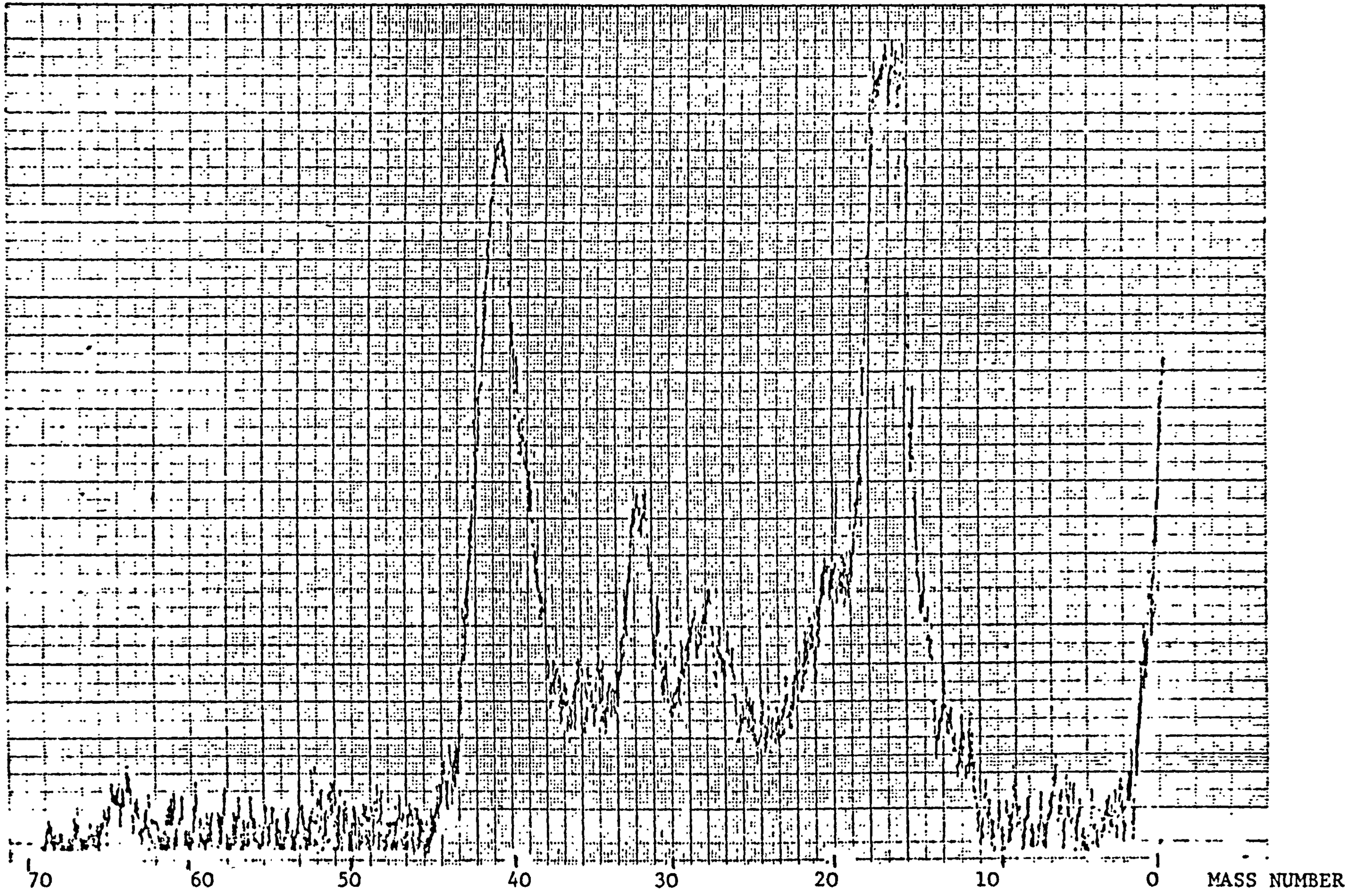

FIGURE 5.7(a) MASS SPECTRUM OF THE FLUX OF IONS LEAVING ION PLATING DISCHARGE DURING EVAPORATION OF THE FILM MATERIAL. DISCHARGE VOLTAGE = 1keV, CARRIER GAS (ARGON) PRESSURE SETTING 1.8×10^{-2} TORR.

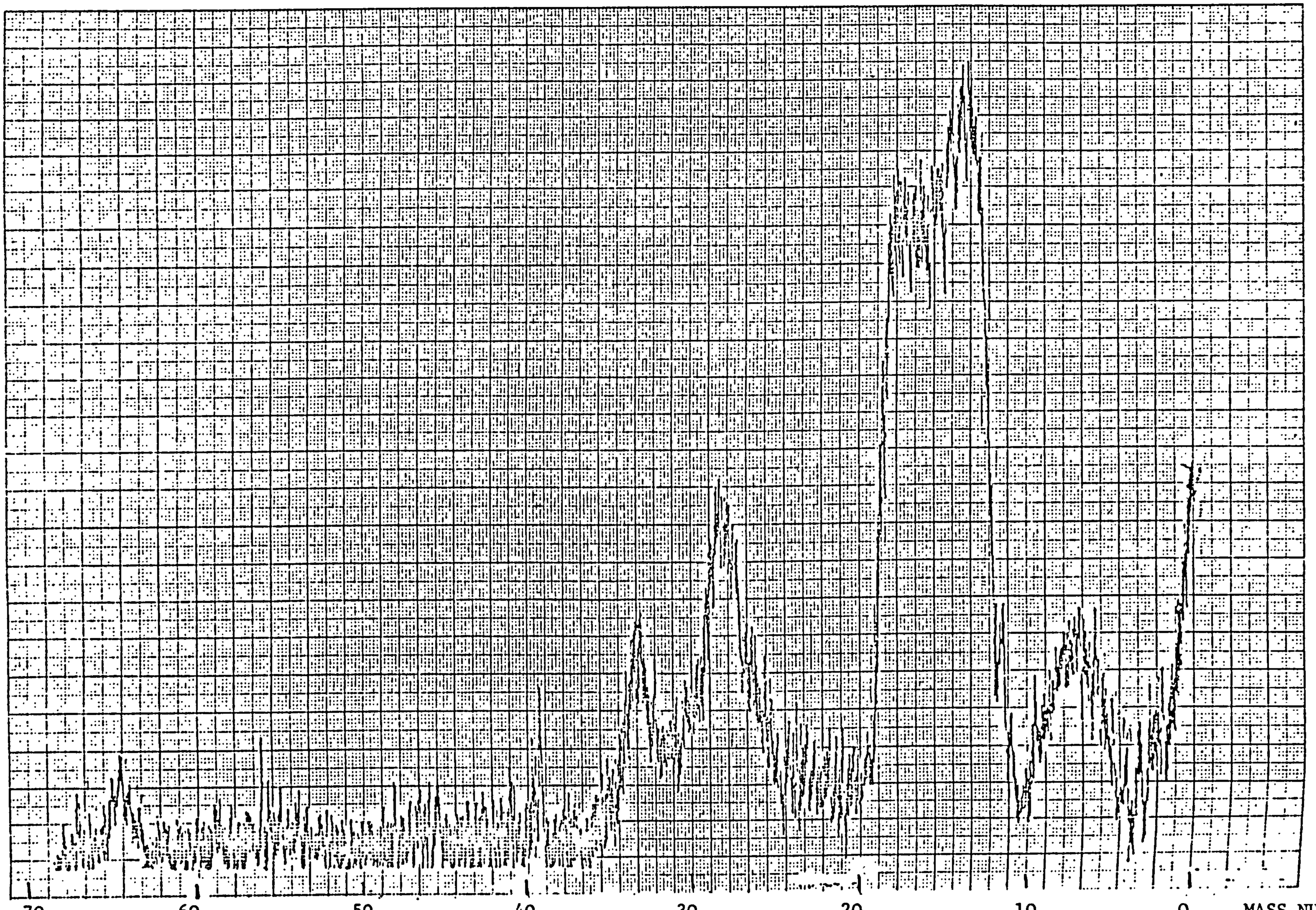

FIGURE 5.7(b) MASS SPECTRUM OF THE FLUX OF IONS LEAVING ION PLATING DISCHARGE DURING EVAPORATION OF FILM MATERIAL. DISCHARGE VOLTAGE = 1keV, CARRIER GAS (NITROGEN) PRESSURE SETTING 1.8×10^{-2} TORR.

5.3.3 Energy Distributions of the Ionic and Neutral Species of the Carrier Gas Leaving the Discharge.

The energy distributions of the carrier gas particles leaving the discharge were measured for argon and nitrogen discharges, prior to evaporation, under the conditions described in Section 5.3.1. As a result of the investigations described in Section 5.3.1, it was known that carrier gas particles in the neutral and singly and doubly charged states were impinging on the cathode of the plating discharge. The energy distribution measurements were carried out by tuning the mass spectrometer to the relevant mass number e.g. 40 for Ar^{+}, 20 for Ar^{++}, etc, and scanning the retarding potential. Typical energy spectra of the ionised particles obtained for argon and nitrogen discharges of $3x10^{-2}$ torr and various voltages are shown in Figures 5.8(a) and (b) (for Ar^{+} and Ar^{++}), and Figures 5.9(a) and (b) (for N^{+} and N^{++}). Similar trends were observed at all the discharge pressures studies but a consistent shift of the spectra towards lower energies as the pressure was increased was observed. This is illustrated in Figure 5.10 for the case of singly charged argon ions and, as far as the peak positions are concerned, in the summary graphs shown in Figures 5.11 and 5.12. Two peaks were consistently observed in the energy spectra corresponding to singly charged ion species. The mechanism responsible for the double peak structure in the energy distributions of the singly charged particles is possibly associated with the conversion of doubly charged ions extracted from the plasma into singly charged ions after some acceleration in the dark space.

The energy spectra of the neutral species of the carrier gas, leaving argon and nitrogen discharges, were also measured under the conditions described in Section 5.3.1. Typical spectra, obtained at $3x10^{-2}$ torr and various voltages are shown in Figures 5.13(a) and (b). Similar trends were observed at all discharge pressures studied with a consistent shift of the spectra to lower energies as the pressure is increased. Since these spectra were observed to be considerably more symmetrical than those obtained for the ions, it was considered reasonable to characterise them in terms of peak energy and full width half maximum (FWHM) and the variations of these quantities with pressure and discharge voltage are

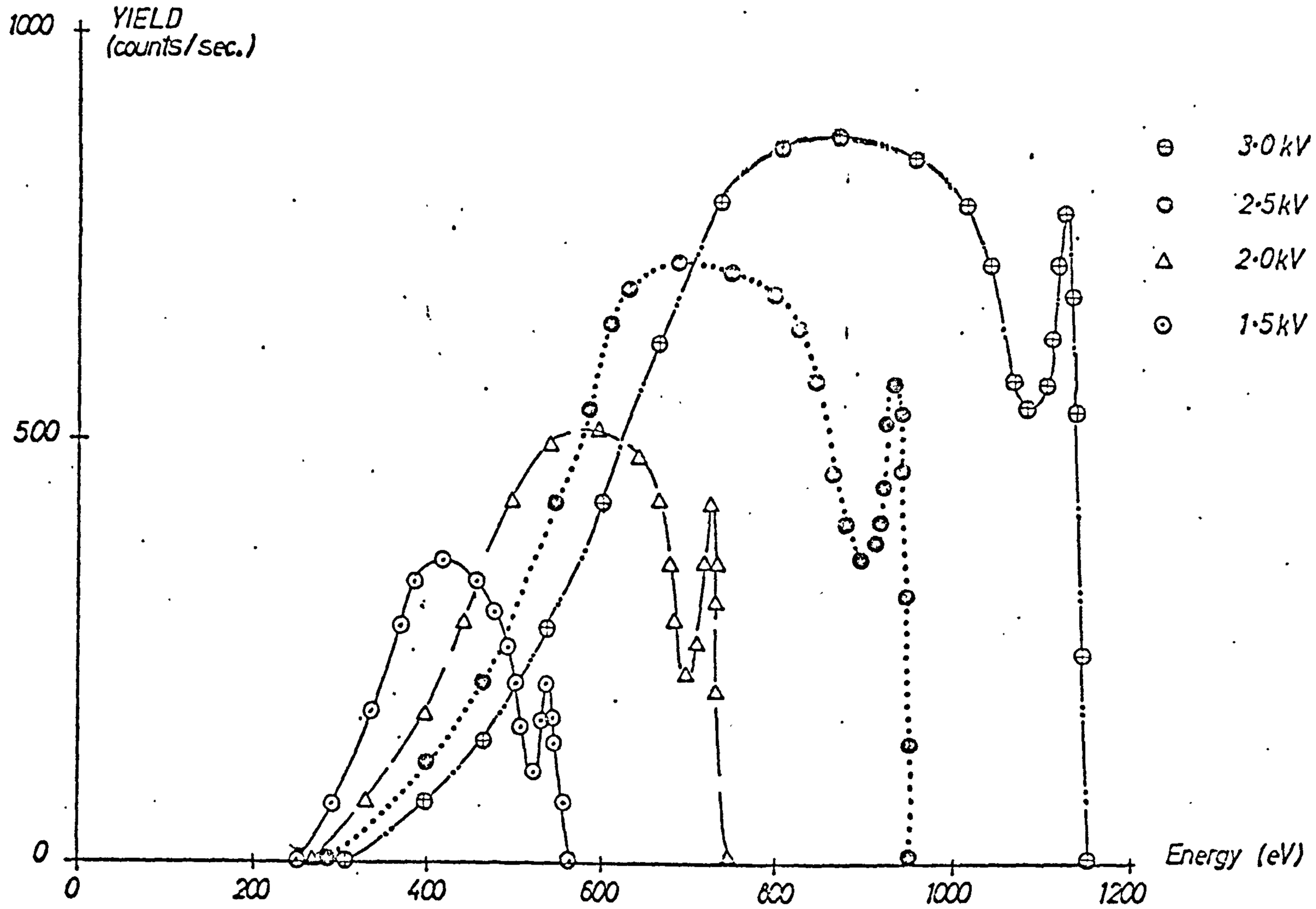

FIGURE 5.8(a) ENERGY DISTRIBUTIONS OF THE CARRIER GAS IONS (AR^+) LEAVING ION PLATING DISCHARGE OF $3x10^{-2}$ TORR AT VARIOUS VOLTAGES.

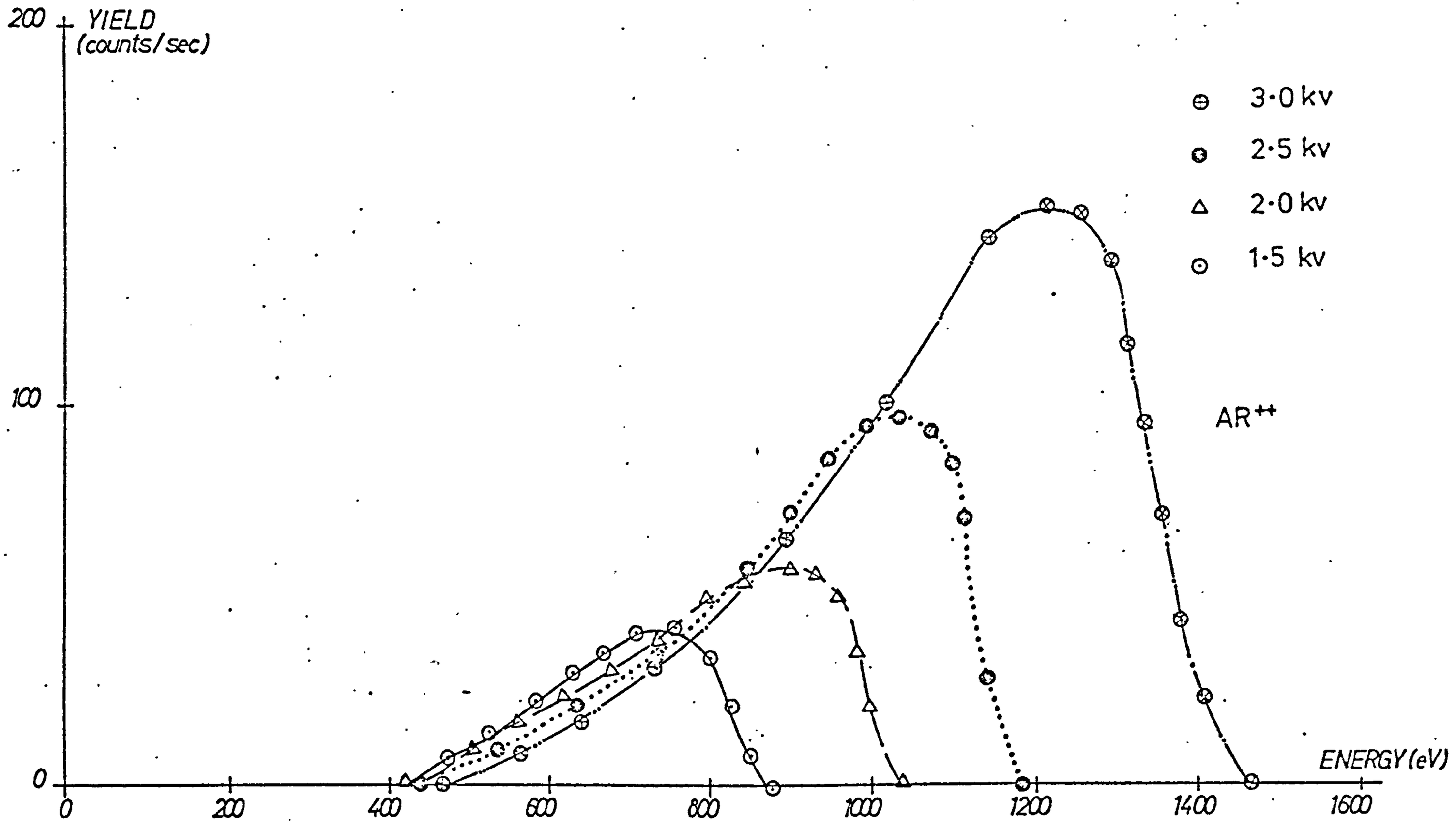

FIGURE 5.8(b) ENERGY DISTRIBUTIONS OF THE DOUBLY CHARGED CARRIER GAS IONS (AR^{++}) LEAVING ION PLATING DISCHARGE OF 3×10^{-2} TORR AT VARIOUS VOLTAGES.

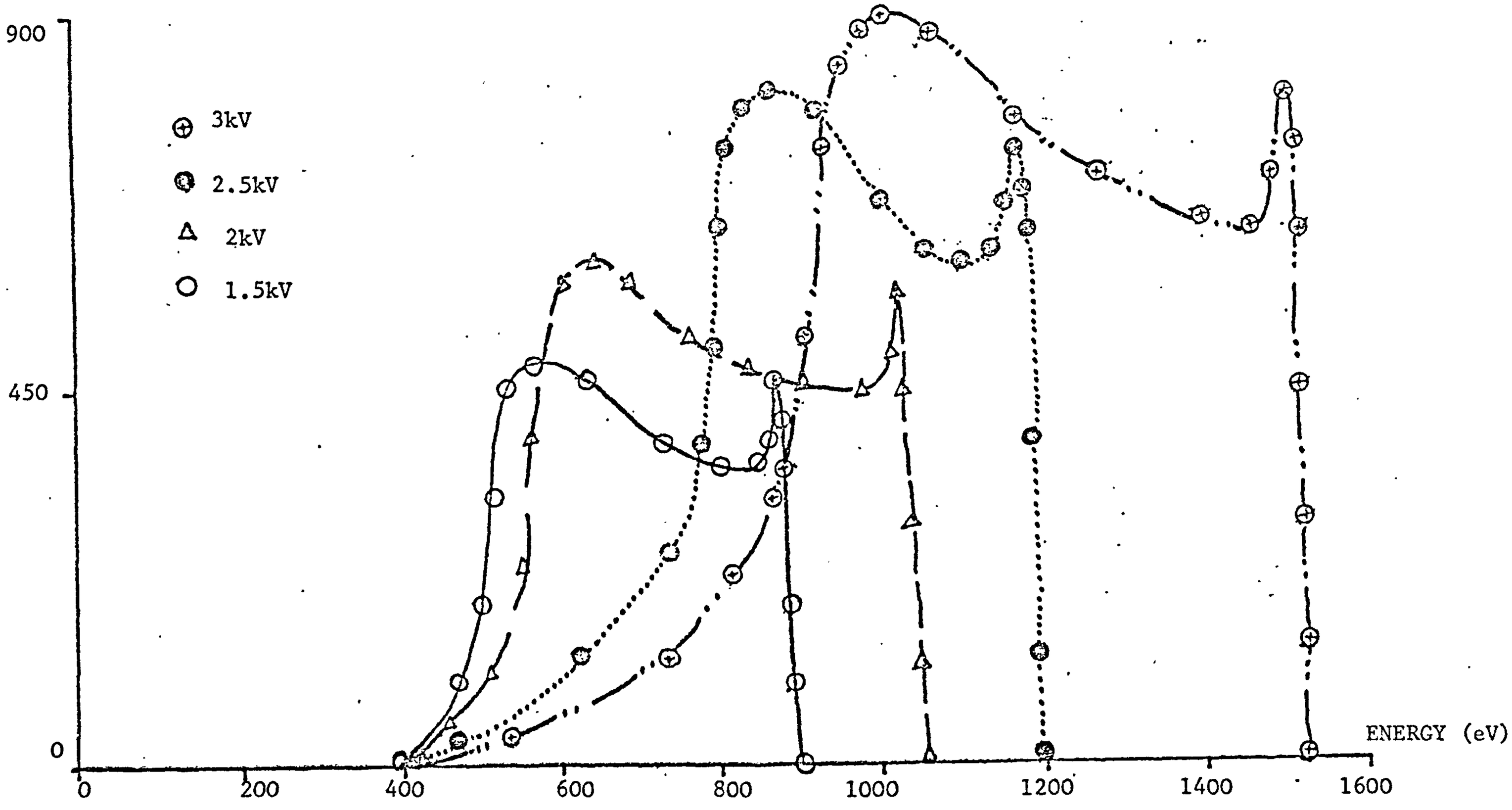

FIGURE 5.9(a) ENERGY DISTRIBUTIONS OF THE NITROGEN IONS (N^+) LEAVING ION PLATING DISCHARGE OF 3×10^{-2} TORR AT VARIOUS VOLTAGES.

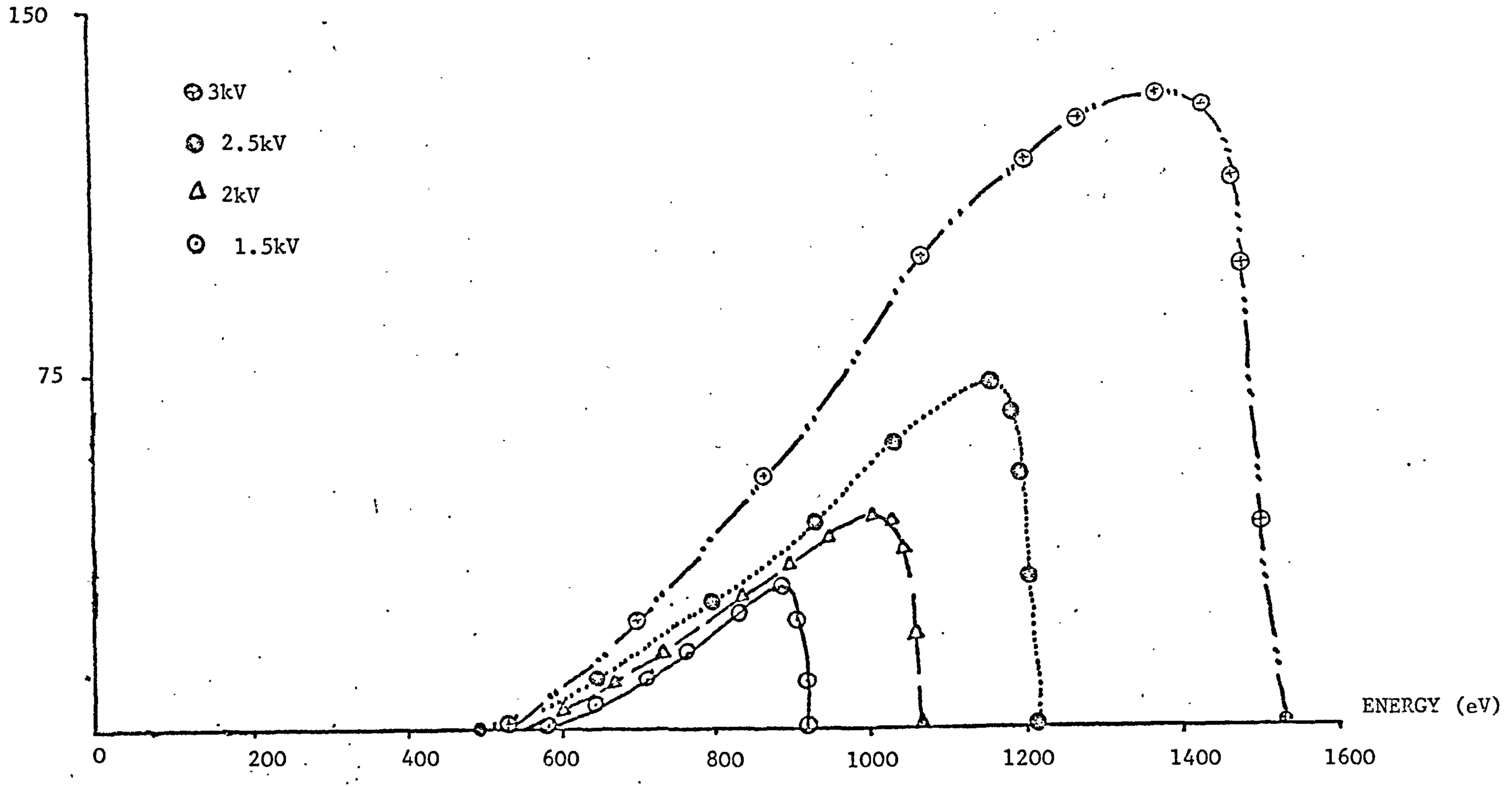

FIGURE 5.9(b) ENERGY DISTRIBUTIONS OF THE DOUBLY CHARGED CARRIER GAS ION (N^{++}) LEAVING NITROGEN DISCHARGE OF 3×10^{-2} TORR AT VARIOUS VOLTAGES.

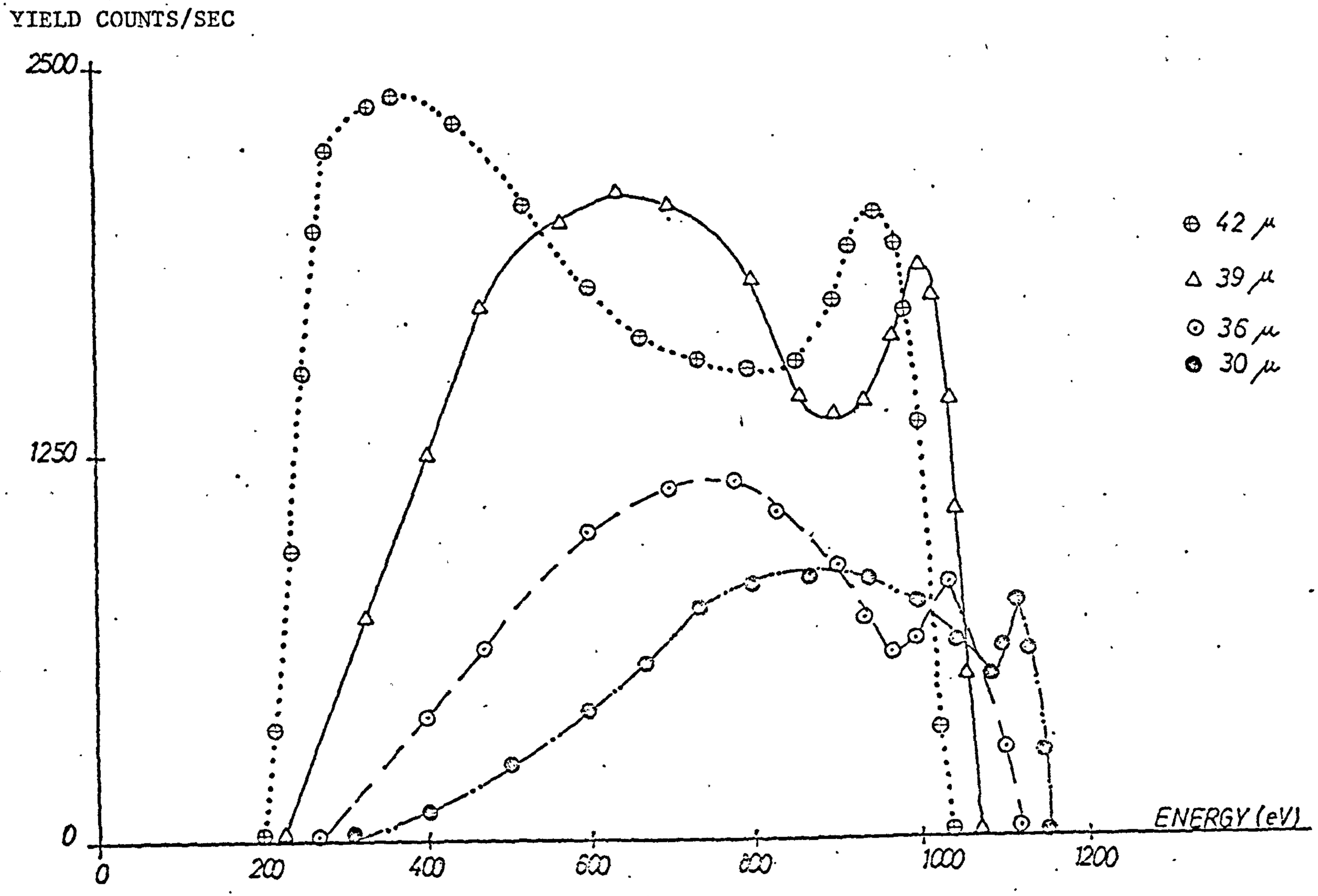

FIGURE 5.10 ENERGY DISTRIBUTIONS OF ARGON IONS (AR^+) LEAVING 3kV ARGON DISCHARGE AT VARIOUS PRESSURES.

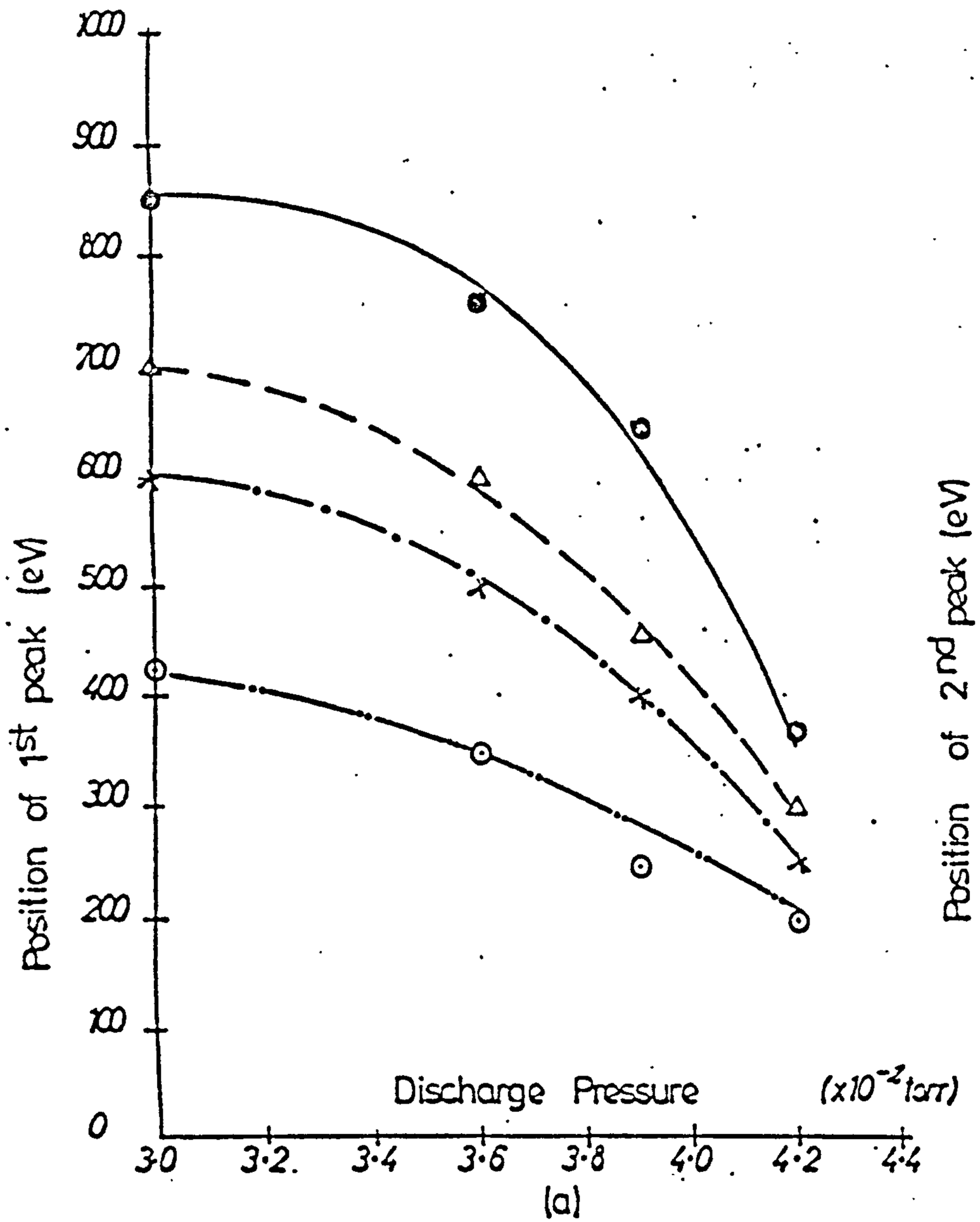

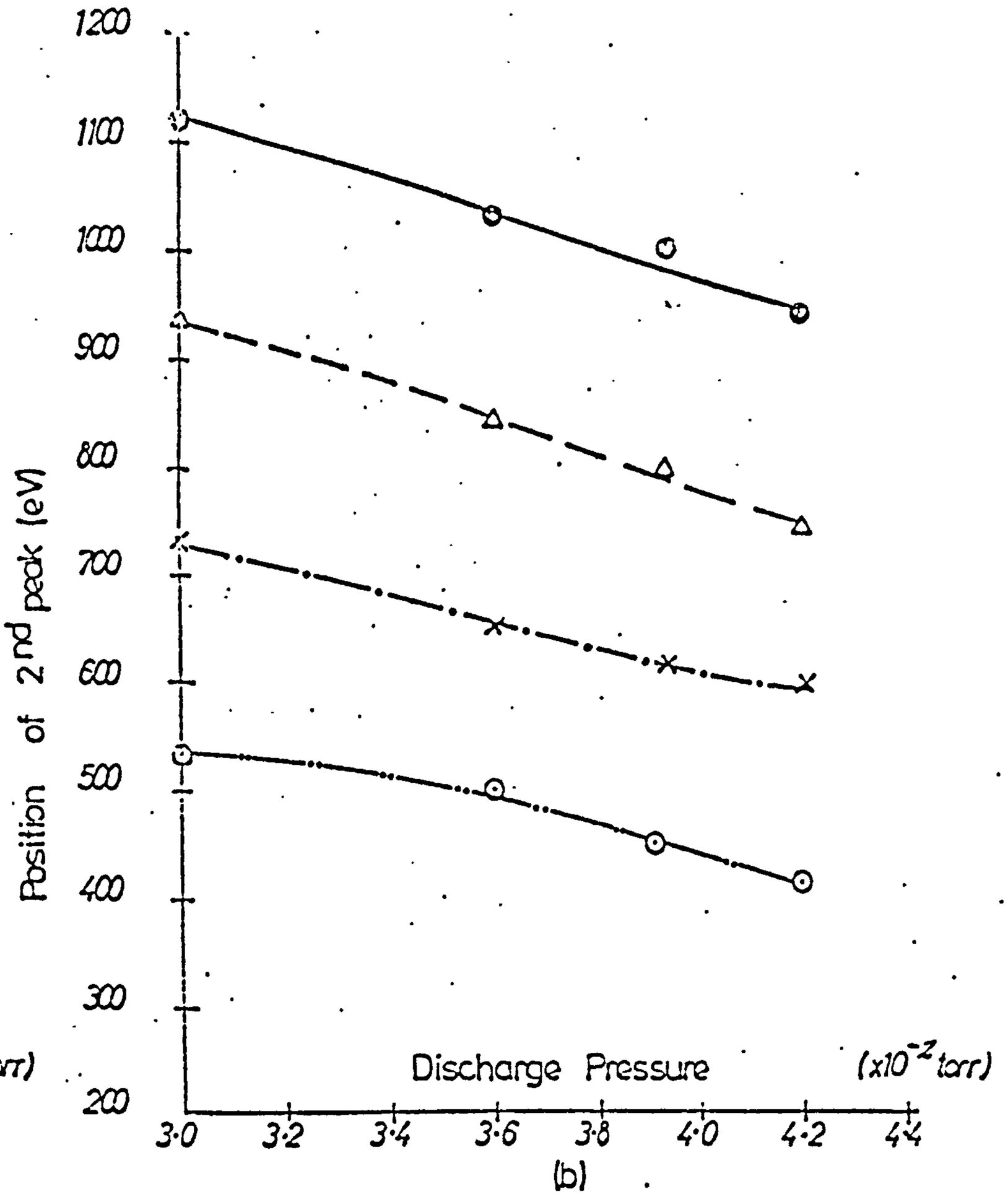

FIGURE 5.11 VARIATIONS OF THE POSITIONS OF THE 1st AND 2nd PEAKS, OF ENERGY DISTRIBUTIONS OF AR^+, WITH PRESSURE AT VARIOUS VOLTAGES.

(⊙ - 1.5kV, x - 2.0kV, △ - 2.5kV, ● - 3.0kV)

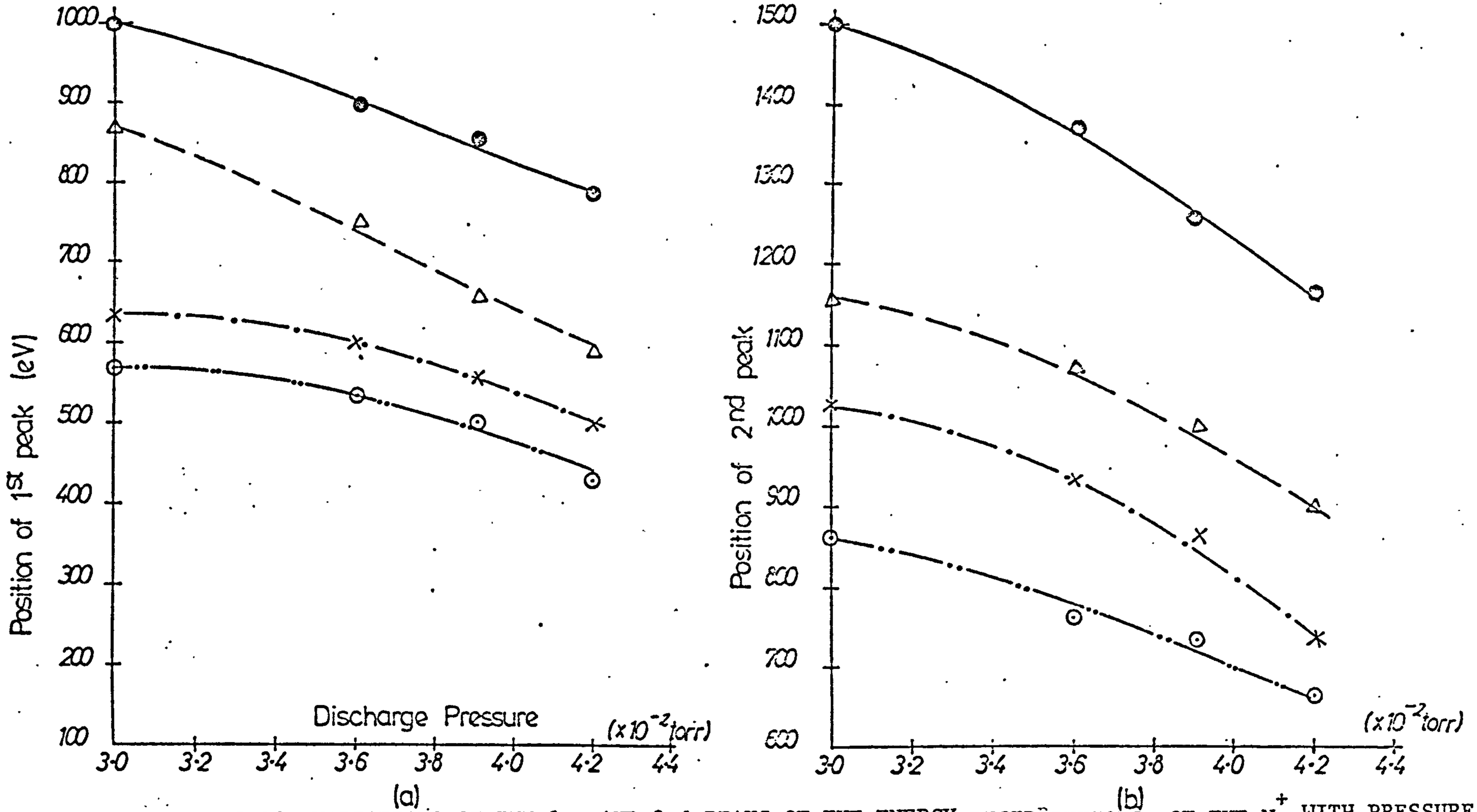

FIGURE 5.12 VARIATIONS OF THE 1st AND 2nd PEAKS OF THE ENERCY DISTRIBUTIONS OF THE N^+ WITH PRESSURE AT VARIOUS VOLTAGES

(○ — 1.5kV, × — 2 2.0kV, △ — 2.5kV , ● — 3kV)

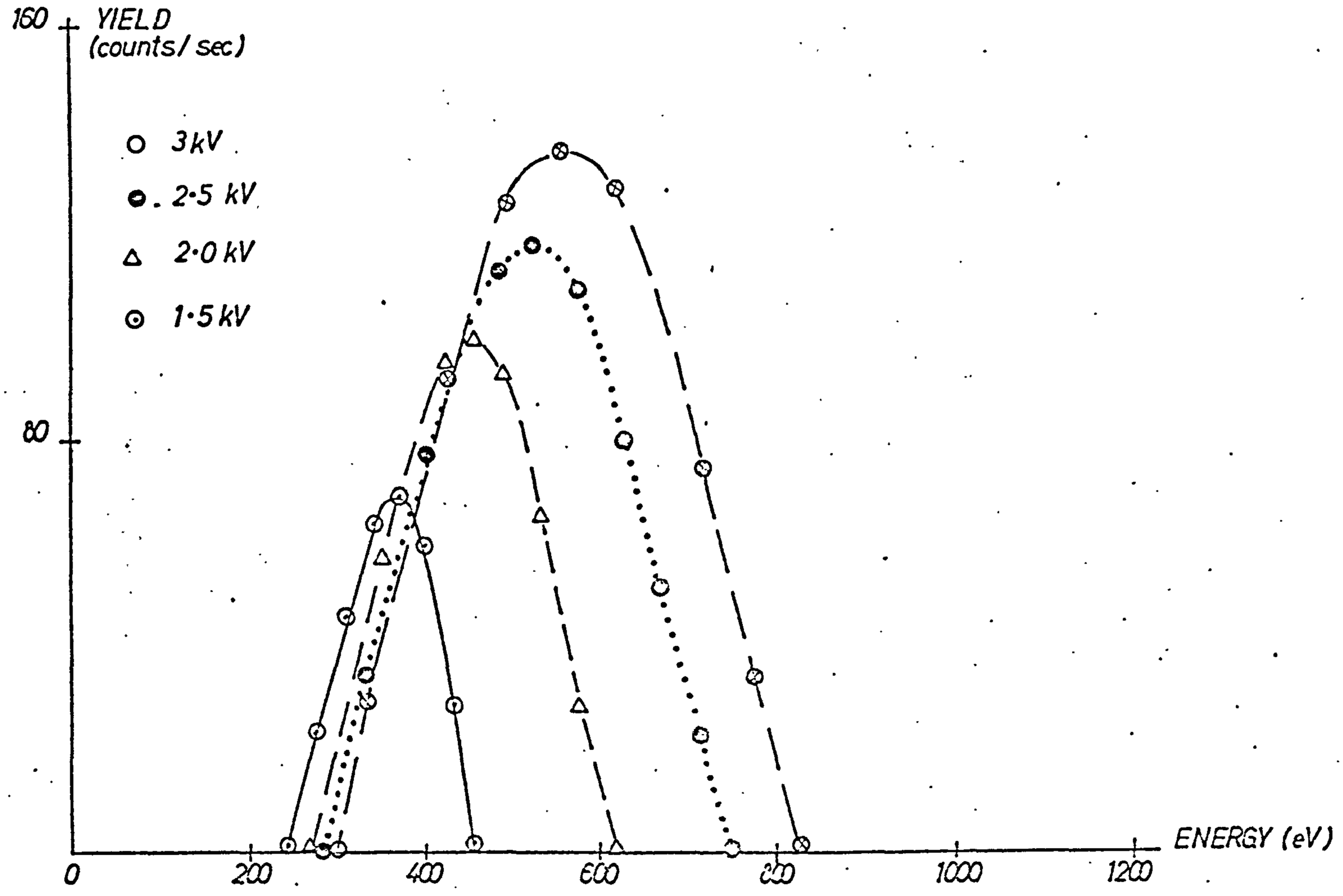

FIGURE 5.13(a) ENERGY DISTRIBUTIONS OF THE NEUTRAL PARTICLES OF THE CARRIER GAS (AR^{o}) LEAVING DISCHARGE OF $3x10^{-2}$ TORR AT VARIOUS VOLTAGES.

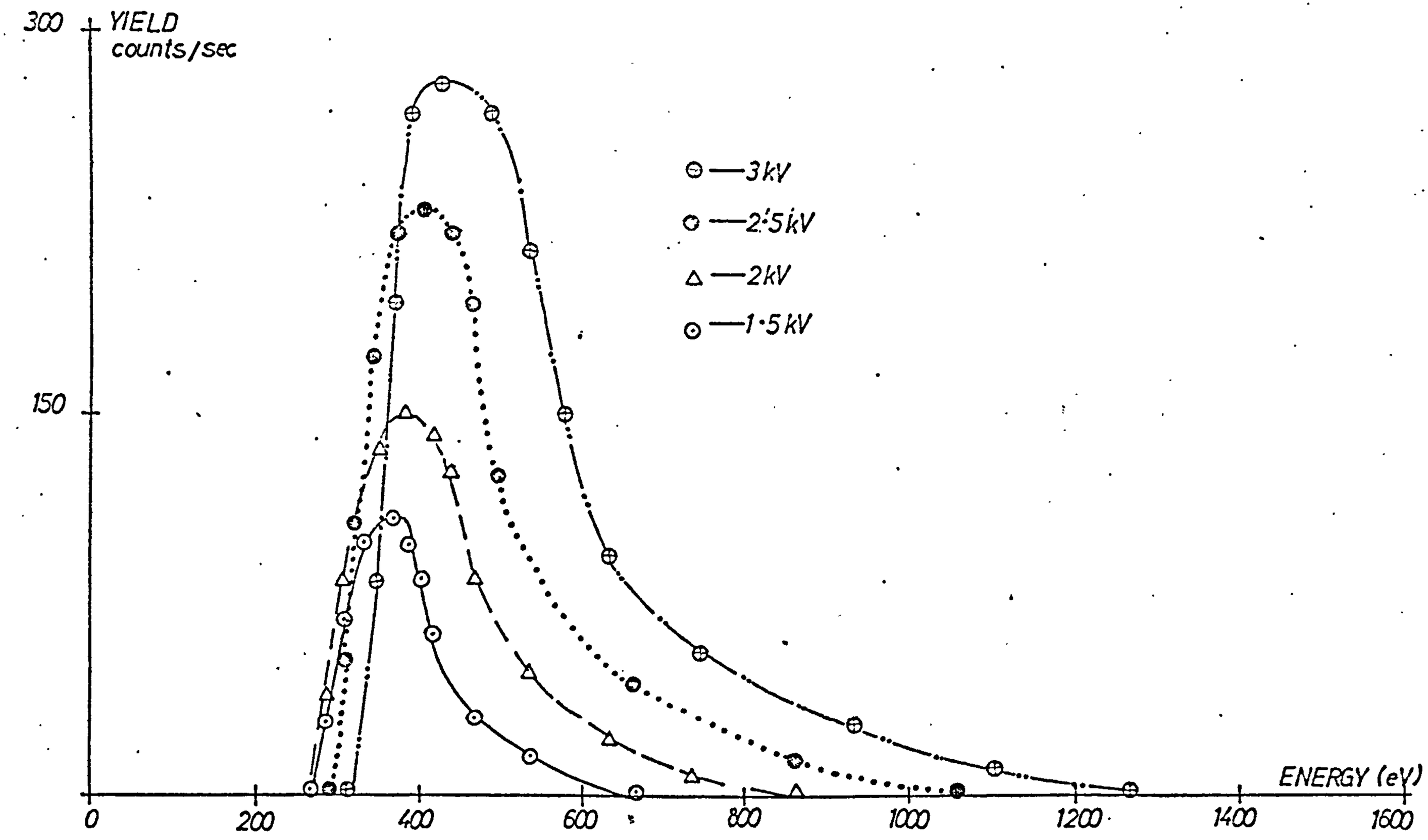

FIGURE 5.13(b) ENERGY DISTRIBUTIONS OF THE NEUTRAL PARTICLES OF THE CARRIER GAS (N°) LEAVING DISCHARGE OF 3×10^{-2} TORR AT VARIOUS VOLTAGES.

summarised in Figures 5.14(a) and (b) for Ar^{o} and N^{o}, respectively.

5.3.4 Energy Distributions of Film Material Species Leaving the Discharge

This investigation represents probably the most important, and the most difficult, set of measurements. The major problems were associated with the inability (in practice virtual impossibility) to actually specify the discharge pressure during evaporation and to control the impurity content. All the copper evaporated in the course of measurements was vacuum metled in a standard evaporator prior to being inserted into the discharge tube.

The pressure measurement problem, which would be significant in any system due to high sticking probability of the copper i.e. single shot measurements, was particularly troublesome in the present apparatus since calibrated conductances and gauges outside the discharge tube were used to carry out the measurements. Since none of the copper particles leaving the cathode aperture would be "seen" by the ionisation gauge in the main chamber, no indication of the pressure change due to evaporation was observed. Hence the Cu^{+} and Cu^{o} spectra actually refer to higher pressures than those indicated by the partial pressure of the carrier gas. The fact that the correct mode of operation of the discharge could only be obtained for a limited range of voltages during evaporation indicate that the pressure condition did change significantly. The limited life of the evaporant source made it impractical to measure the argon ion energy distributions during evaporation.

The energy distributions of the ionic and neutral species of evaporated copper leaving the discharge were carried out over the voltage range 0.6kV to 1.2kV. Typical spectra obtained for Cu^{+} and Cu^{o} at various voltages and a carrier gas partial pressure setting of 1.8×10^{-2} torr are shown in Figures 5.15(a) and (b). Similar trends were observed at all discharge conditions studied with a consistent shift of the spectra to lower energies as the pressure increased. The results of these measurements illustrating the observed peak shifts and broadening are summarised in Figures 5.16(a) and (b) where, as earlier, peak energies and full width half maxima (FWHM) are used to characterise the distributions.

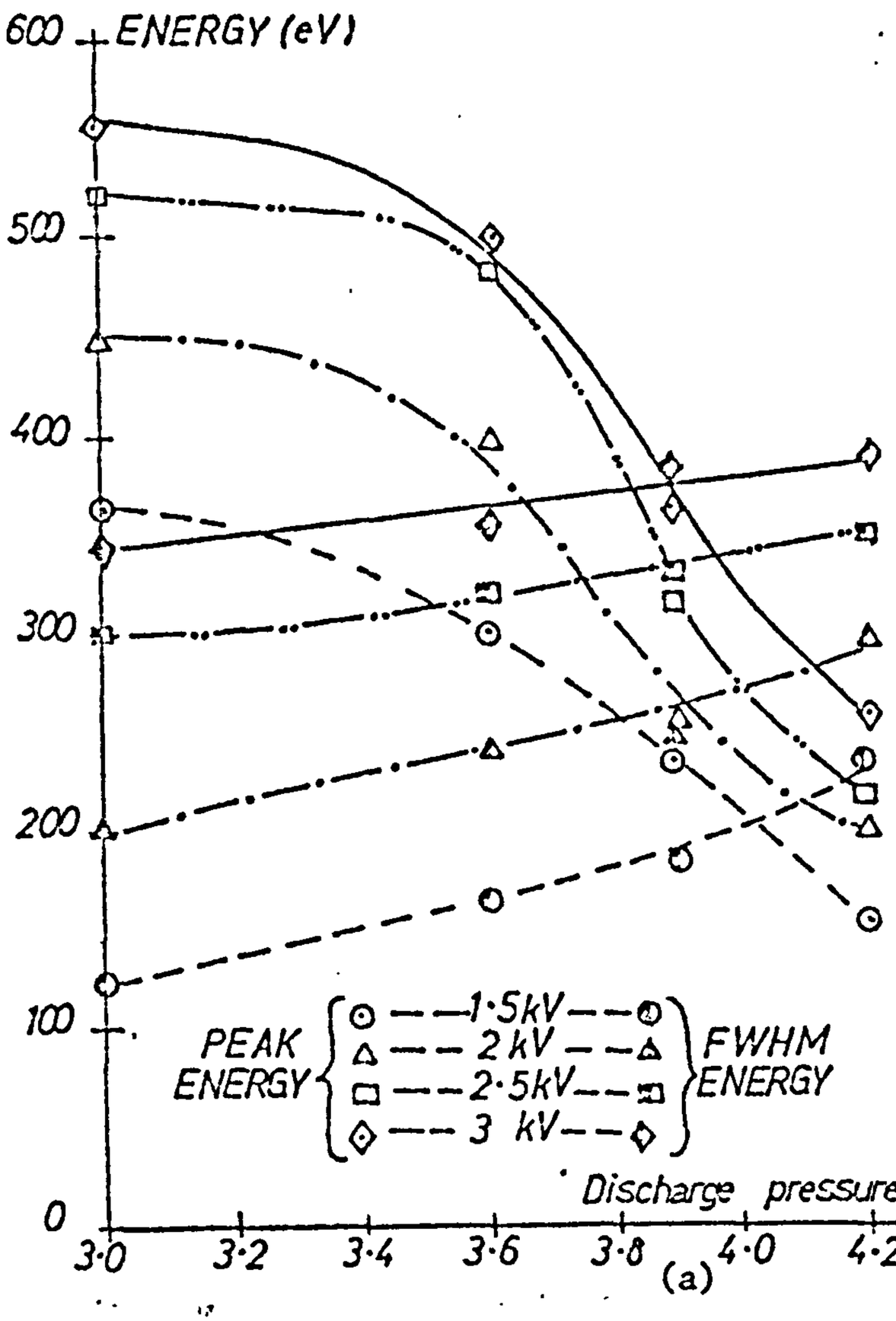

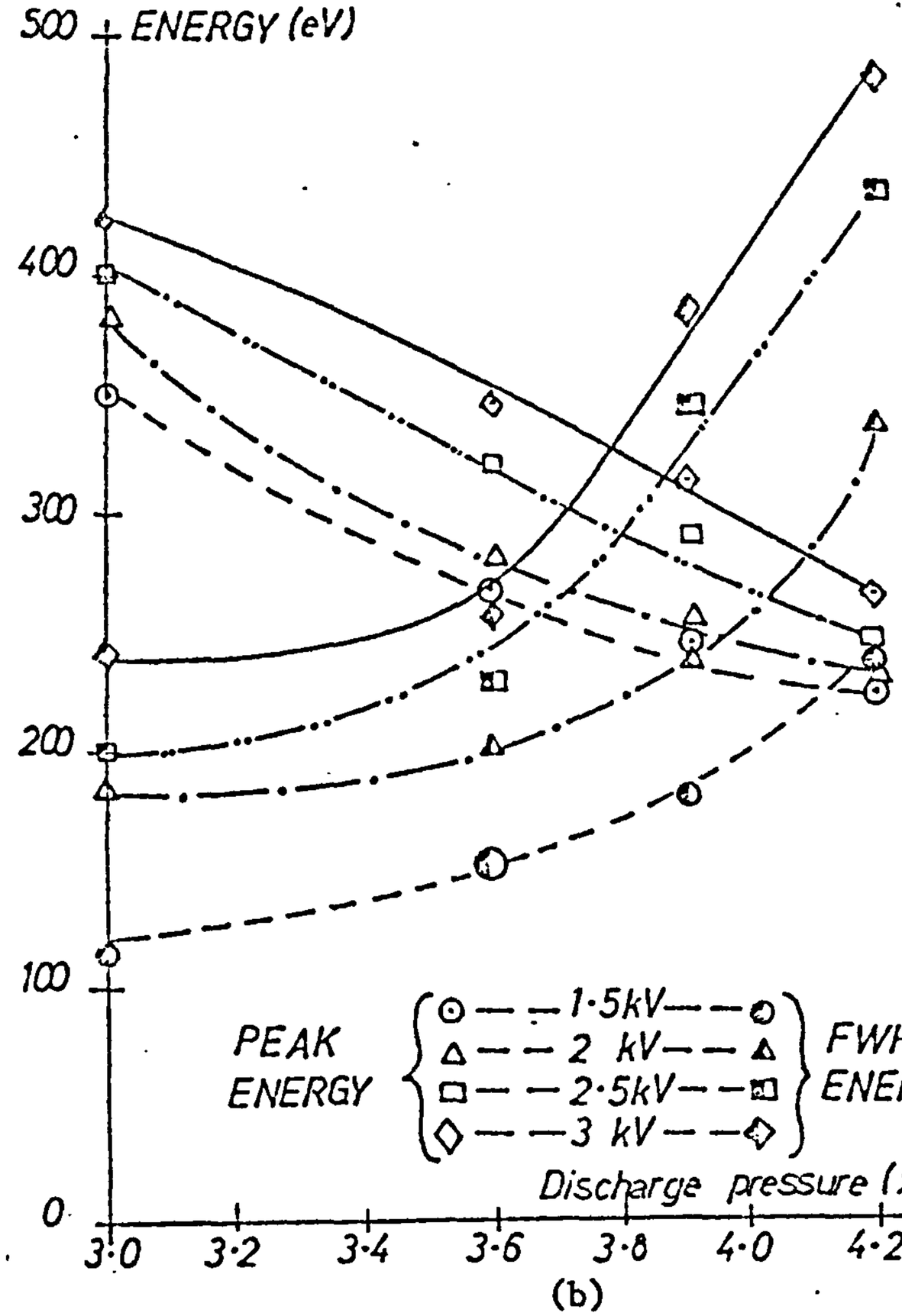

FIGURE 5.14 VARIATIONS OF THE PEAK ENERGY AND FULL HALF WIDTH MAXIMUM (FHWM), WITH PRESSURE, OF THE ENERGY SPECTRA OF THE NEUTRAL PARTICLES LFAVING PALTING DISCHARGE AT VARIOUS VOLTAGES·a - Ar^{o}, b - N^{o}

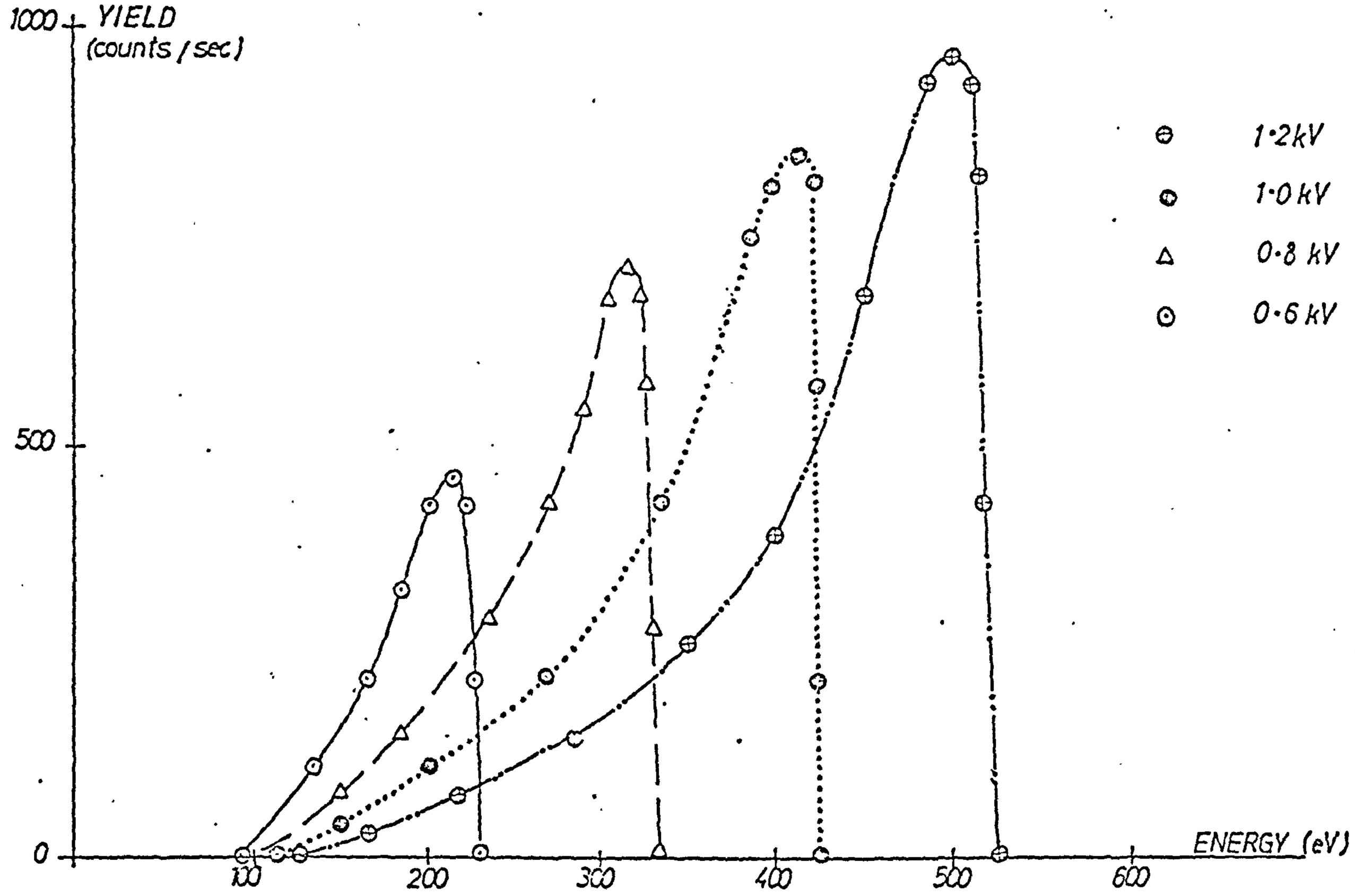

FIGURE 5.15(a) ENERGY DISTRIBUTION OF THE IONS OF THE FILM MATERIAL (CU^+) LEAVING PLATING DISCHARGES AT VARIOUS VOLTAGES AND CARRIER GAS PRESSURE READING OF 4.6×10^{-2} TORR.

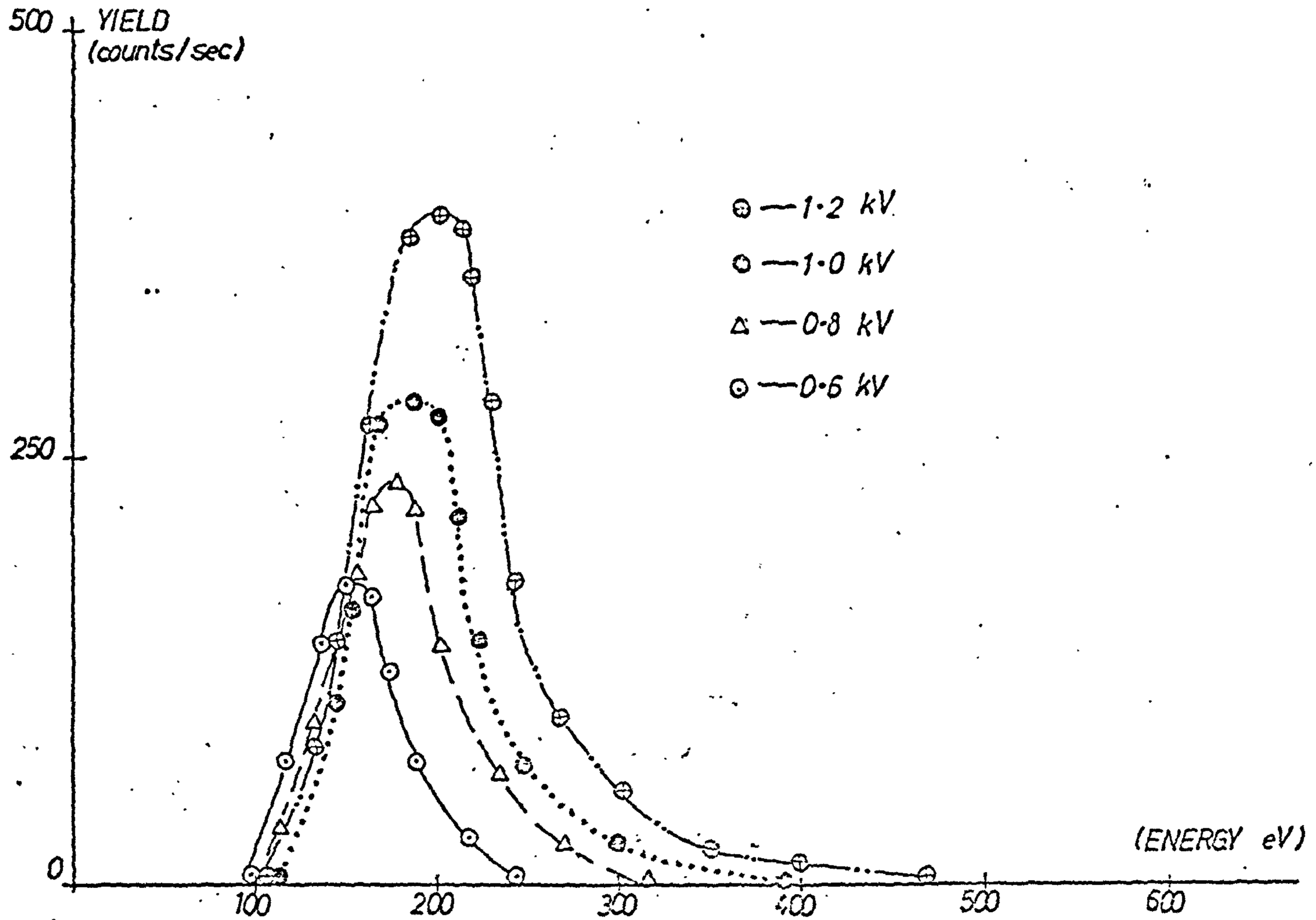

FIGURE 5.15(b) ENERGY DISTRIBUTIONS OF THE NEUTRAL PARTICLES OF THE FILM MATERIAL (CU^{o}) LEAVING PLATING DISCHARGE AT VARIOUS VOLTAGES. CARRIER GAS (ARGON) PRESSURE SETTING 4.6×10^{-2} TORR.

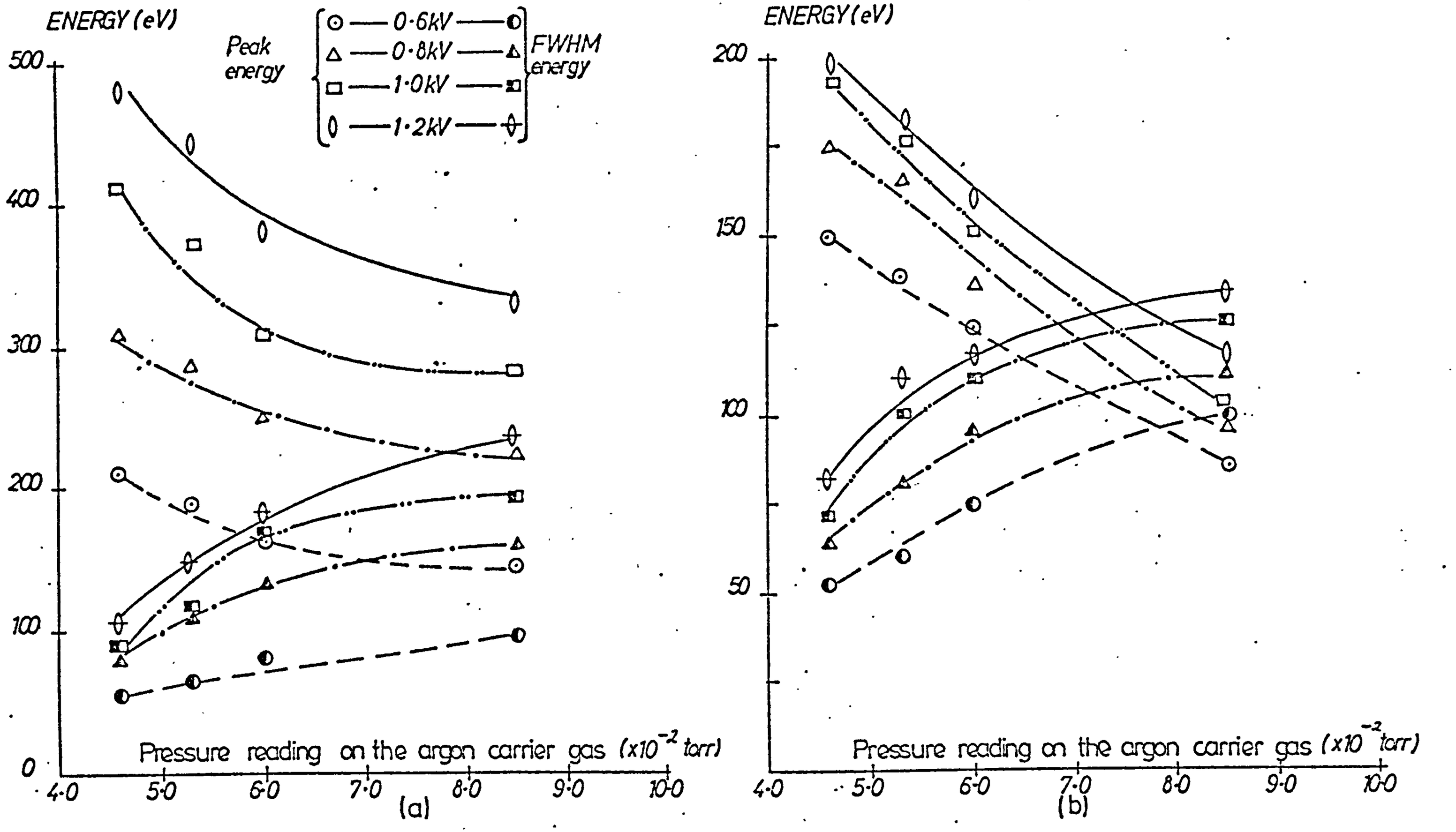

FIGURE 5.16 VARIATIONS OF THE PEAK ENERGY AND FULL HALF MAXIMUM (FWHM), WITH PRESSURE SETTING OF CARRIER GAS, OF THE ENERGY SPECTRA OF THE FILM MATERIAL IONS (CU^+) AND NEUTRAL ATOMS (CU^0) LEAVING PALTING DISCHARGES AT VARIOUS VOLTAGES.

It is immediately clear from inspection of the Cu^+ distribution that they are quite different from that obtained for Ar^+ or N^+ or any of the other species studied. The very steep high energy edge combined with the long low energy tail almost certainly reflect the higher discharge pressures under which the "evaporation discharge" were operating.

5.3.5 Comments

For all the energy distributions obtained, a consistent shift to lower energies is observed as the pressure is increased. The shift is accompanied, in all cases, by a broadening of the peak(s) of the energy distributions. As explained these phenomena can be explained in terms of the increased probability of undergoing charge exchange collosions at higher pressures.

The energy distributions of the neutral species peak at energies lower than those of their corresponding ionic species. In fact the maximum energies of all the neutral species studied were observed to be lower than the maximum energies of their corresponding ionic species. This is most probably due to the fact that the maximum ion energies correspond to those ions which traverse the entire cathode dark space without suffering a collisoin whereas charge exchange collisions which lead to the creation of the more energetic neutrals must take place after the ions leave the plasma and have been accelerated through part of the dark space potential. Hence the maximum neutral particle energies will always be less than the energies of ions.

The result of the measurements of the energy distributions show that particle energies involved in ion plating processes range from thermal energies to about 2.5keV for applied voltages up to 3kV. It is now possible to comment on some of the important physical processes which are believed to account for the formation and properties of films in ion plating.

5.3.5(a) Contribution of Energetic Particles to Film Formation

Probably the most fundamental requirement in the development of a proper understanding of ion plating, is the ability to estimate the relative contrib-

utions of energetic and thermal particles to the growth of film. The energetic particles reaching the cathode of an abnormal glow discharge emanate from the negative glow which is the plasma region formed by electron impact ionisation (and excitation) following acceleration of electrons across the cathode dark space. The characteristics of the heavy particles which impinge on the cathode will thus depend on the ion density in this region, the potential drop across the dark space, the width of the dark space, and the pressure. A rough estimate of the number of energetic ions leaving the negative glow can be obtained by considering a very simple model in which this region is considered to be a well defined cylinderical plasma (Figure 4.8 (a)). If it is further assumed that the axial flux density is determined by ambipolar diffusion then,

$$J = -D_a \frac{d\eta}{dz} \qquad 5.3.1$$

where D_a is the ambipolar diffusion coefficient. From this equation and a knowledge of the spatial distribution of the ion density in the plasma, an expression for the flux of ions entering the dark space can be deduced. For the sort of accuracy required here, the distribution can be assumed to be a fundamental mode diffusion distribution raised to the power of k,[2,3] i.e.

$$\eta(r,z) = N_o \left(J_o \left(2.405 \frac{r}{r_o}\right) \cdot \mathrm{Cos} \frac{\pi z}{\ell_o}\right)^k \qquad 5.3.2$$

where N_o is the central density. For k = o, this reduces to a uniform distribution which corresponds to the case where recombination is the dominant loss mechanism. In practice the distribution is extremely complex and is determined by a number of different generation and loss mechanisms and this feature is reflected in the use of values of k between 1 and 2 which are characteristic of situations in which both recombination and diffusion play a role. For the purpose of the present, order of magnitude calculation, the assumption that fundamental mode ambipolar diffusion is the dominant process, i.e. k = 1, yields the result,

$$J = N_o D_a \frac{\pi}{\ell_o} \quad \text{ions/sec/cm}^2 \qquad 5.3.3$$

N_o in the negative glow plasma is between 10^{12} and 10^{13} ions cm^{-3} and ℓ_o for a typical electrode spacing of 10cm is about 5cm. The value of D_a is more difficult to define because it depends on both the electron and ion diffusion coefficients and mobilities and hence on the electron and ion temperatures but a value of 5 cm^2/sec is probably reasonable. For these values, the flux density of ions leaving the negative glow is $3x10^{13}$ ions/sec/cm^2. This represents the maximum possible energetic ion flux because collision processes in the dark space reduce the number of particles of high energy arriving at the cathode. As a result of the discussion concerning the flux of neutral particles impinging on the cathode (see Chapter 3), the maximum energetic neutral flux must be highest by about an order of magnitude, than that of the ions and hence it must be about 10^{14} neutrals/sec/cm^2. Since, in a typical ion plating system, film growth rates corresponding to film material particle fluxes of between 10^{15} and 10^{16} atoms (or ions)/sec/cm^2 are used and the basic discharge current does not increase significantly during evaporation of the film material into the discharge, it becomes clear that the major contribution to film growth must come from more or less thermal energy particles which do not become ionised in the discharge. It can, therefore, be concluded that the energetic particle flux cannot, on its own, account for the growth of the film and hence the role of this flux is associated with the effects of the energy deposition.

5.3.5(b) Role of Energetic Particle Implantation

The fact that the energy distributions of the particles peak at about, or below 1.5keV, dictates that the energetic projected range of the bombarding particles will be of the order of tens of Angstroms.[4] The interface region of ion-plated films which, for some cases, has been reported to be in the range of hundreds of Angstroms to microns is clearly not always associated with direct implantation although this process, together with recoil and cascade mixing effects, may contribute to the formation of an interface which is several atomic layers thick.

5.3.5(c) Energy Deposition

In furthering the attempt to find an explanation for adhesion of ion plated films, a simple model, shown schematically in Figure 5.17 has been considered. The model comprises a film-substrate system bombarded with a flux of energetic particles. The charge state of these particles is not important for the energies under consideration since it is the repulsive part of the interaction potential which is important and, in practice, neutralisation is generally a very effective process near a surface[5]. As the particle approaches the atomic surface plane, its behaviour in terms of penetration beyond the surface layer, sticking on the surface or reflection will depend primarily on its energy. Hence if the initial energy of the atom is insufficient to enable it to pass through the surface plane (which will be easiest at the mid-positions between surface atoms where the total repulsive potential is lowest) it will be either reflected or will stick to the surface. While the more energetic non-penetrating particles (i.e. those with energies in the tens of eV) will tend to be reflected in quasi-binary collision (the surface atoms will appear to have an effective mass greater than their atomic mass), the lower energy component of this flux may be accommodated on the surface. This means essentially that during the repulsive phase of the interaction the surface atoms will recoil and dissipate lattice wave energy into the solid. Since the energy is not necessarily restored to the impinging atom, this will recoil with reduced energy. If this recoil energy is sufficiently low and the potential well outside the surface, sufficiently deep, there is a high probability of condensation or accommodation on the surface. Having been accommodated on the surface, the added atom may diffuse either on the surface itself or into the bulk. Its ability to overcome the diffusion barrier depends on the activation energy associated with the barrier and on the temperature. The latter parameter will also affect the sticking probability. Even if the adsorbed atoms cannot diffuse thermally in the bulk, it is possible that they can be activated to do so by the bombardment process. Having overcome the initial surface barrier, they may then be able to diffuse readily in the bulk.

In addition to the above process, the bombardment with energetic part-

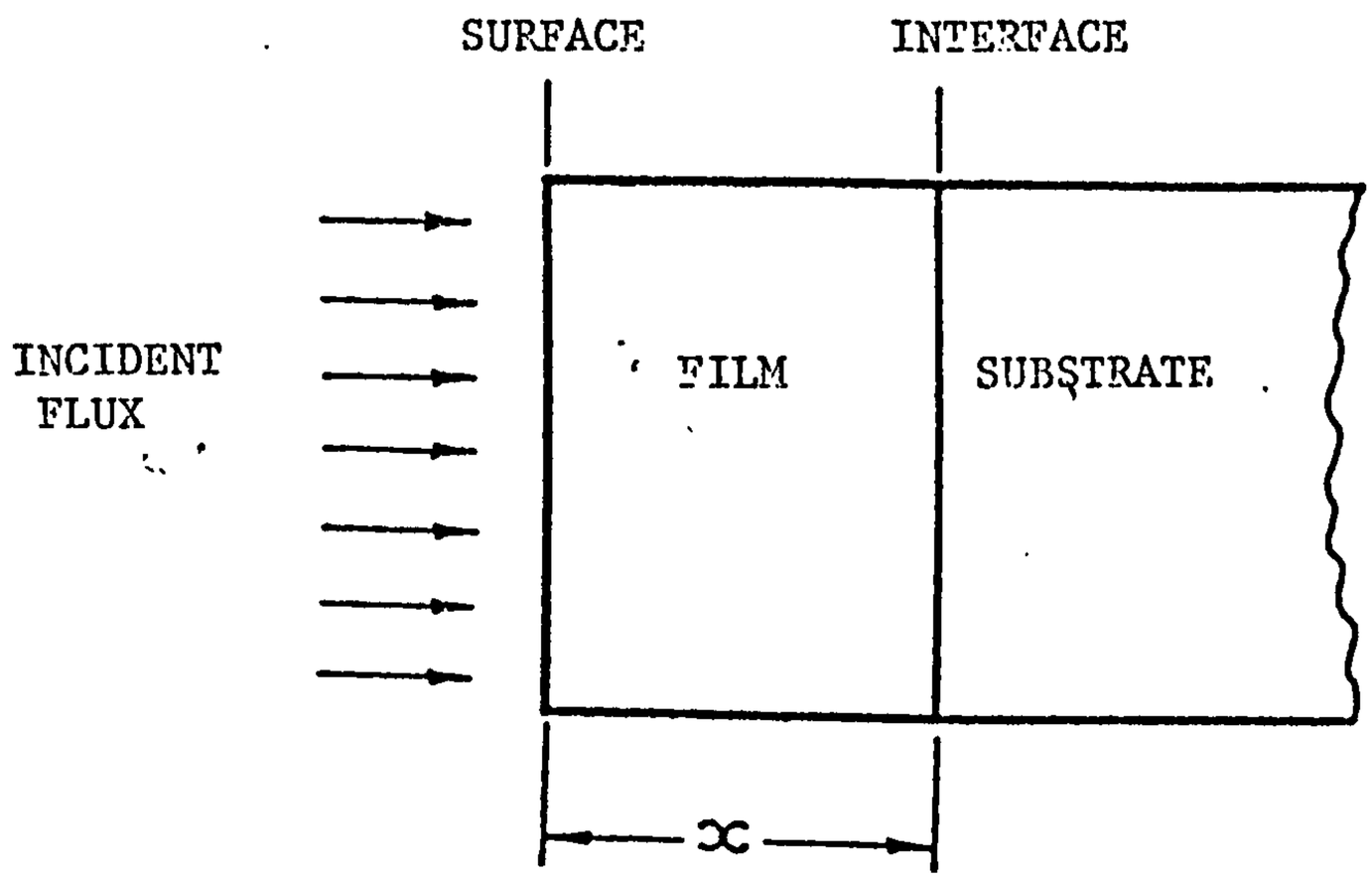

FIGURE 5.17

MODEL USED FOR THE CALCULATION OF INTERFACE BROADENING DURING ION PLATING

icles also leads to the deposition of energy at the film-substrate interface and hence to an effective diffusion process of substrate atoms into the film and film atoms into the substrate. In this way a graded interface may be built up. In fact the model shown in Figure 5.17 is based upon these two effects. Thus the plating process can be considered as being composed of:-

a) a low energy particle flux, J_T which is responsible for film growth, and,

b) an energetic particle flux J which is responsible for the mixing process.

In terms of this model, the rate of mass accumulation of film material is given by CmJ_T where m is the mass of the plating atom and C is the effective sticking probability. The growth rate of the film is given by (see Chapter 3)

$$\rho = \frac{dx}{dt} = \frac{\text{mass accumulation rate/unit area}}{\text{density of plating}} \qquad 5.3.4a$$

then

$$\rho = \frac{CmJ_T}{mN} = \frac{CJ_T}{N} \qquad 5.3.4b$$

According to the earlier discussion, the inward broadening of the film given by expression 3.4.16 is;

$$(\Delta x)^2 \Big| \simeq \frac{0.3J\ell^2\lambda\,\bar{\theta}(E,0)}{E_d \cdot CJ_T} \qquad 5.3.5$$

This broadening however, does not represent the entire effect and, for simplicity since only an order of magnitude estimate of the broadening is required, it is assumed that the outward broadening of the substrate into the film is the same as the inward broadening of the film into the substrate. Hence total broadening, Δx_T is

$$\Delta x_T \simeq 2 \sqrt{\frac{0.3J\ell^2\lambda\bar{\theta}(E,0)}{E_d\, CJ_T}} \qquad 5.3.6a$$

$$\Delta x_T \simeq \sqrt{\frac{J \ell^2 \lambda \bar{\theta}(E,0)}{E_d C J_T}} \qquad 5.3.6b$$

For a typical plating situation employing an argon discharge operating at a voltage of 2kV and a current density of 1ma/cm^2 of substrate surface area, a net film growth rate of 600 Å / minute i.e. 10 Å or approximately 2 x 10^{15} atoms/sec/cm^2 implies a value of $\frac{2J_T}{J}$. Since, for these conditions, the majority of the energetic particles have energies of about 500eV then one would expect the following values for the other parameters, $\ell \simeq$ 2 - 3 atomic spacing, $\lambda \cong$ 2 - 3 atomic spacing, and $\bar{\theta}$ 100 eV / atom layer, E_d in metals is approximately 25eV and hence, as given by expression 3.4.17,

$$\Delta x_T \simeq \sqrt{30b} = 6b \qquad 5.3.7$$

where b is the interatomic spacing ($\sim$3Å).

The cascade mixing model thus predicts that the film-substrate interface may be broadened by approximately 6 lattice spacings or about 20-30Å and interface regions of this order of magnitude have been measured [6] experimentally for some film-substrate combinations. The model also predicts that the broadening should be maximised by using high discharge voltages and low J_T/J ratios. At this stage it should be pointed out that in this analysis a perfect lattice is assumed (i.e. no thermal effects and smooth surface) which is the worst possible case.

5.3.5(d) Comparison With Davis and Vanderslice's Theory

Although, from a quantitative viewpoint, the nature of the part-

icles arriving at the cathode is difficult to specify, it is clear from the measurements that charge exchange collisions in the dark space have a significant influence on the energy distributions of the particles. Indeed,this effect is expected since the mean free path for charge exchange is known to be very much smaller than the dimensions of the dark space for the type discharge system under consideration. It is because of the dominance of the charge exchange contirbutions that Davis and Vanderslice[7] and more recently Teer,[8] ignored all other processes in their calculations of the expected form of the distributions, and their calculations which have been fully reviewed in Chapter 3 of this thesis, can be directly compared with the present experimental data.

To carry out this comparison, the experimental energy distributions have been plotted on the same axes as those prodicted on the basis of Davis and Vanderslice theory given by the expression.

$$\frac{dN}{N_o}\ \frac{V_c}{dV} = \frac{L}{\lambda}\ \exp\left(-\frac{L}{2\lambda}\cdot\frac{V}{V_c}\right) \qquad 5.3.9$$

where λ is the mean free path, L is the width of the dark space and V_c is the discharge. In a typical ion plating discharge $\lambda = 0.5cm$[3] and L = 10cm. For the energy analyser used the value of dV is taken to be about 1 e V. Since the expression 5.3.9 produces a family of curves for different values of N_o it is therefore necessary to produce a value of N_o for best fit with the experimental spectra. In the experimental spectra the yield obtained for the energy corresponding to the mid point on the high energy tail is taken to be b and the yield corresponding to the same energy in the theoretical calculation is taken to be a then $N_o = \frac{b}{a}$ provided the transformation coefficient for the best fit between the theoretical and experimental spectra. In the theoretical spectra a monotonic increase in the number of ions with decreasing energy was observed whereas in the experimental spectra the ion yield goes through a peak as the energy increases from zero to the voltage corresponding to the discharge voltage. The high energy tail of the experimental spectra displays more or less the same trends where as there is a clear discrepancy between the

theoretical and experimental spectra at lower energies. Typical comparison spectra are presented in Figure 5.18(a) to (e) for argon and nitrogen discharges where the low energy discrepancy is clarly observable. At the first sight this discrepancy may be attributed to one or both of the following:-

a) a fall in the transmission efficiency of the analytical system at low energy. However, as a result of the tests reported in Section 4.2.5 where the transmission characteristics of the analytical system were tested by applying potentials to the ioniser box, this effect can be disregarded.

b) the influence of particle scattering. This factor, which increases as the energy goes down, causes increased attenuation of the ion beam reaching the entrance aperture of the analyser.

It is therefore reasonable to assume that the latter factor makes the major contribution to the low energy discrepancy. On the basis of Davis and Vanderslice's theory the following effects can be discussed.

1- The effect of V_c (cathode voltage) changes at constant pressure. At constant discharge pressures, an increase in V_c reduces the length of the cathode dark space and hence reduces the number of charge transfer collisions. This implies that the ion energy spectra should shift to higher energies and peak at higher energies as V_c is increased. This effect was consistently observed in all the measured energy distributions.

2- The change in the mean free path (mfp). Since the mfp for resonant process e.g. Ar^+ in argon is smaller than that for non resonant process e.g. CO^+ in argon it is to be expected that the energy distribution of Ar^+ will peak at lower energies, with respect to the peaks in the energy distributions of CO^+, O_2^+, Ar^{++}, etc. This phenomenon was observed in both argon and nitrogen discharges and Figure 5.19(a) which shows typical energy spectra for a 3kV, 3×10^{-2} torr argon discharge clearly illustrates this effect.

The explanation of this effect is that in the resonant process the mean free path

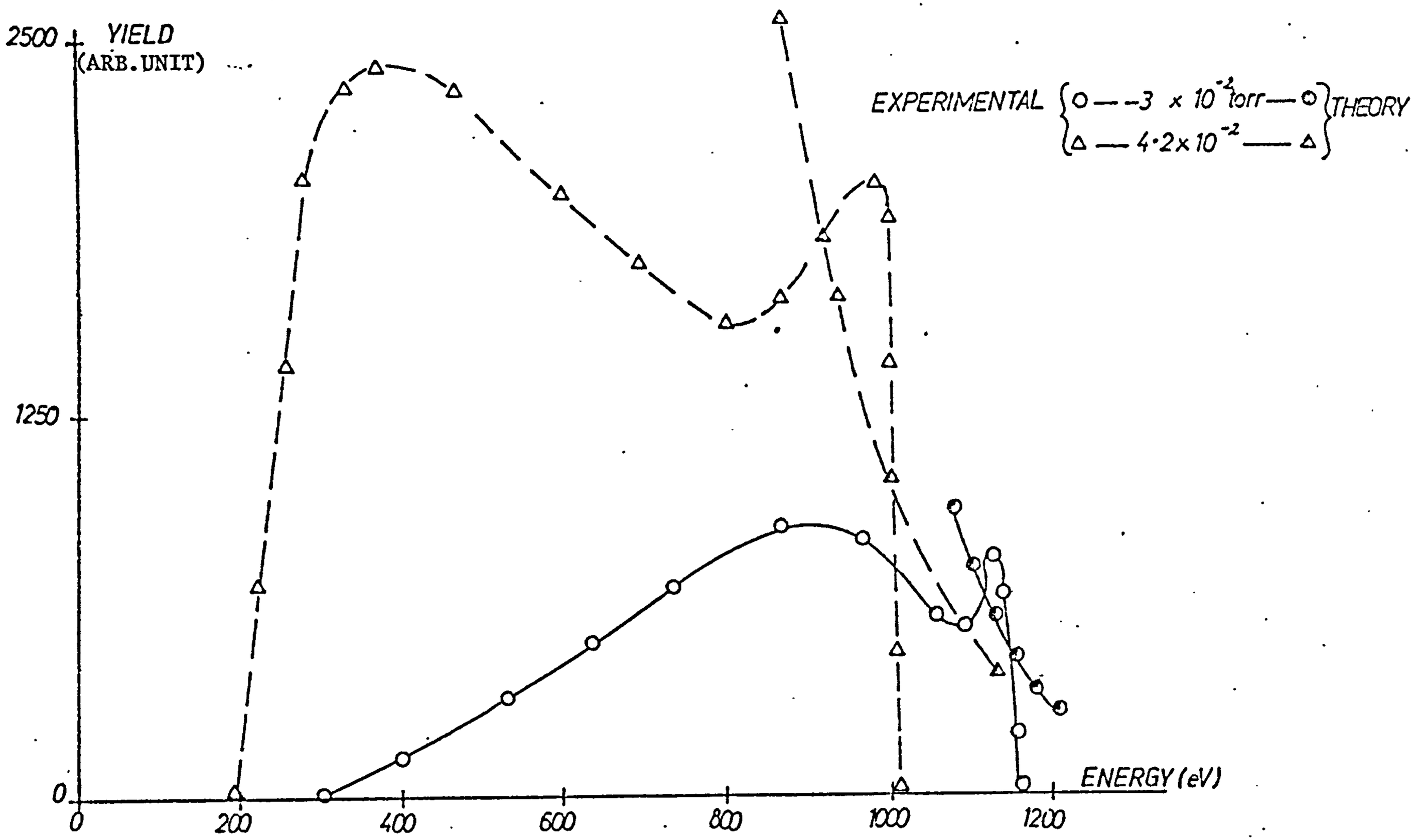

FIGURE 5.18(a) COMPARISON OF THE ENERGY DISTRIBUTIONS OF AR^+ OBTAINED FOR A 3kV DISCHARGE AT TWO DIFFERENT PRESSURES, RUN IN ARGON, WITH DAVIS AND VANDERSLICE'S THEORY.

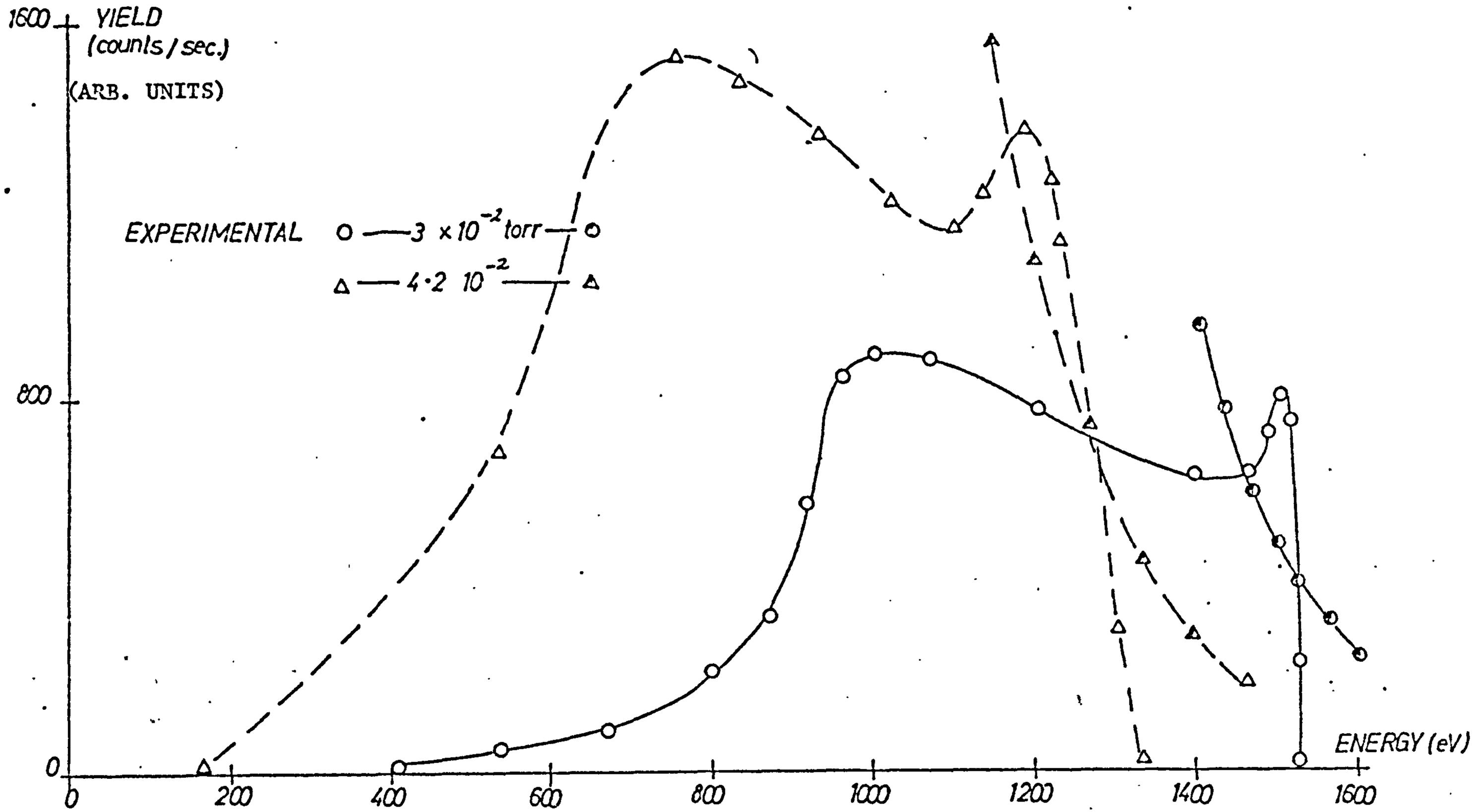

FIGURE 5.18(b) COMPARISON OF THE ENERGY DISTRIBUTIONS OF N^+ OBTAINED FOR A 3kV DISCHARGE AT TWO DIFFERENT PRESSURES, RUN IN NITROGEN, WITH DAVIS AND VANDERSLICE'S THEORY.

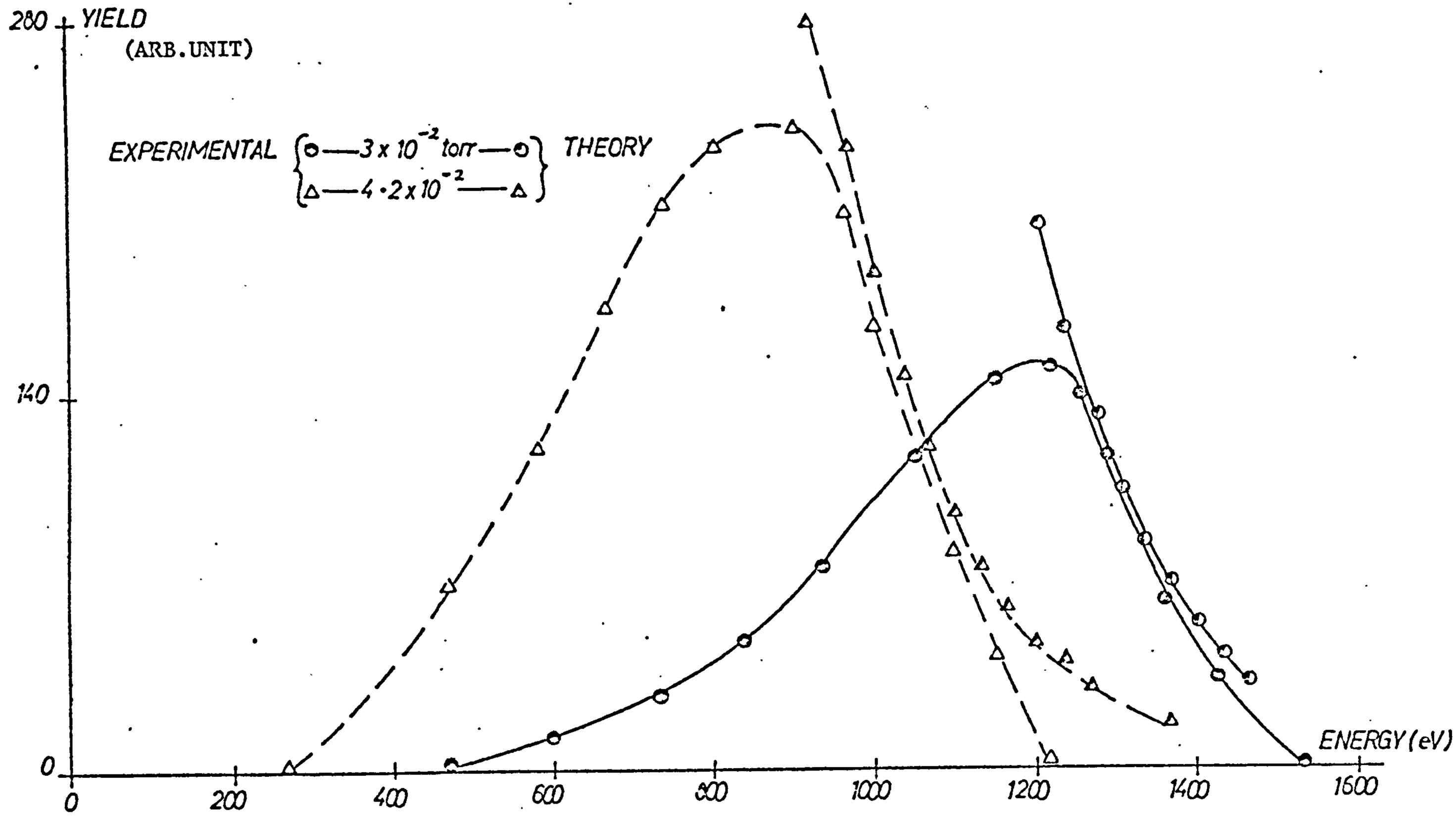

FIGURE 5.18(c) COMPARISON OF THE ENERGY DISTRIBUTIONS OF Ar^{++} OBTAINED FOR A 3kV DISCHARGE AT TWO DIFFERENT PRESSURES, RUN IN ARGON, WITH DAVIS AND VANDERSLICE'S THEORY.

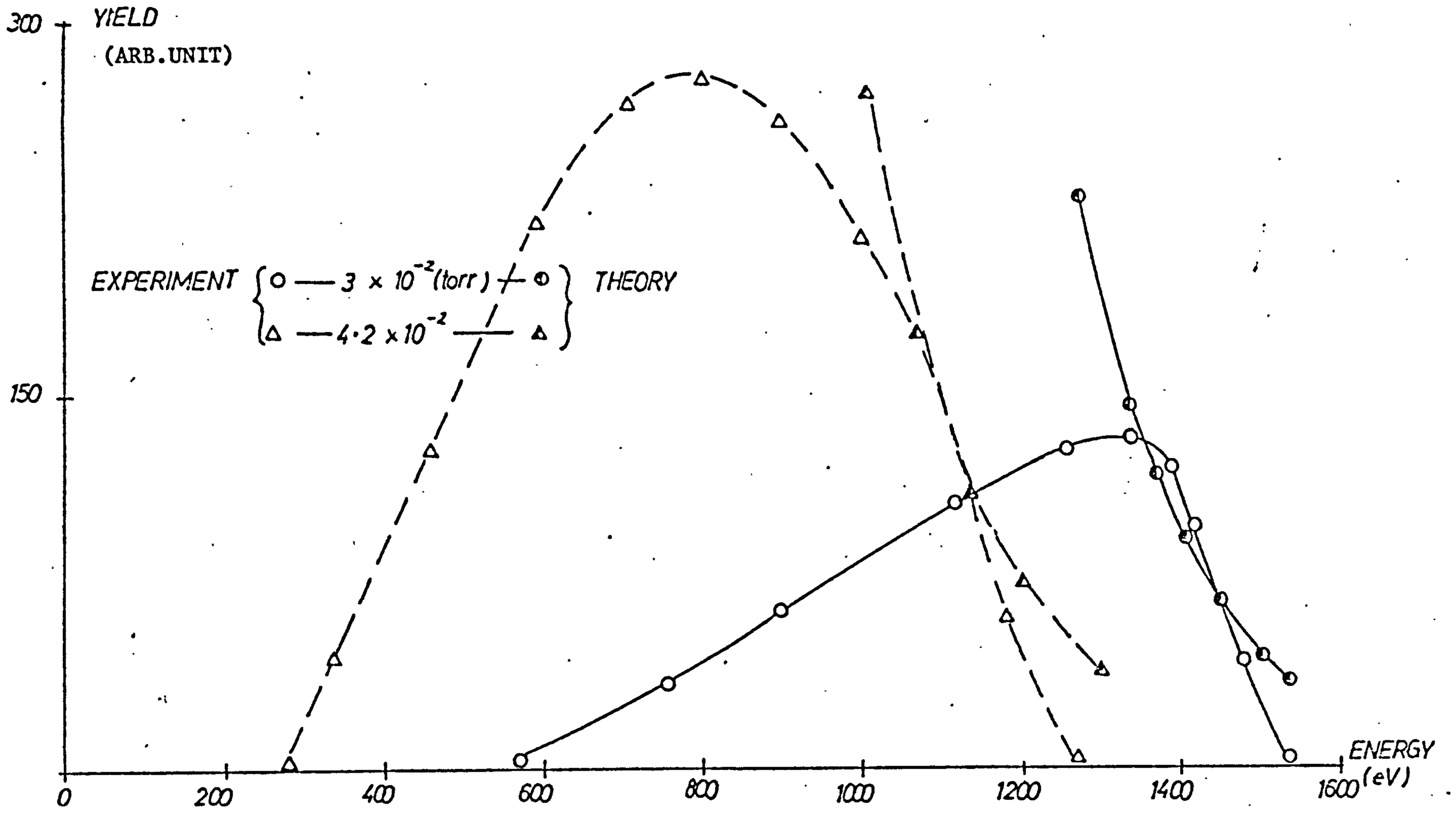

FIGURE 5.18(d) COMPARISON OF THE ENERGY DISTRIBUTIONS OF N^{++} OBTAINED FOR A 3kV DISCHARGE AT TWO DIFFERENT PRESSURES, RUN IN NITROGEN, WITH DAVIS AND VANDERSLICE'S THEORY.

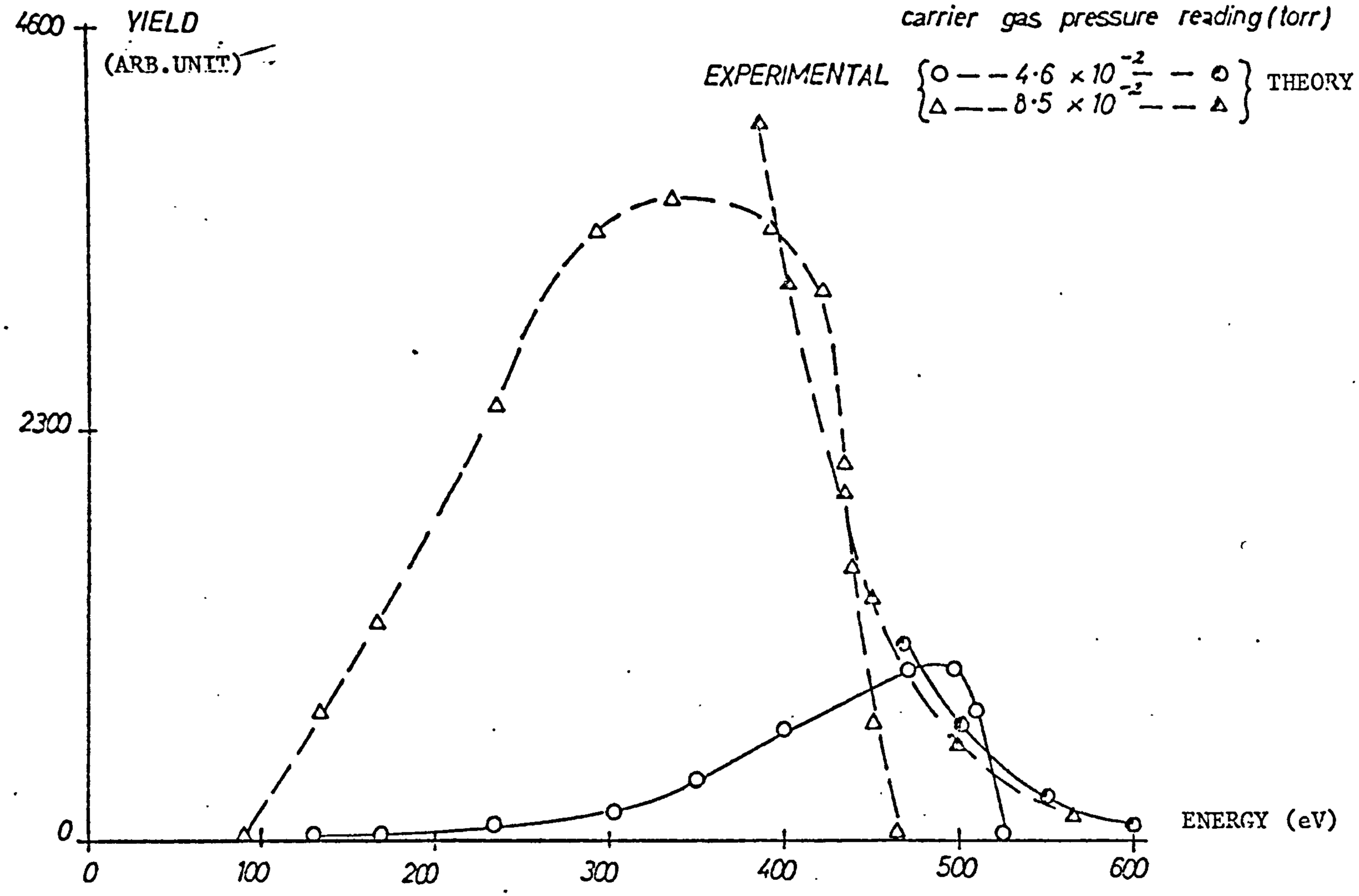

FIGURE 5.18(e) COMPARISON OF THE ENERGY DISTRIBUTIONS OF THE FILM MATERIAL IONS (CU^+) OBTAINED FOR A 1.2kV DISCHARGE, RUN AT TWO DIFFERENCT CARRIER GAS (ARGON) READINGS, WITH DAVIS AND VANDERSLICE'S THEORY.

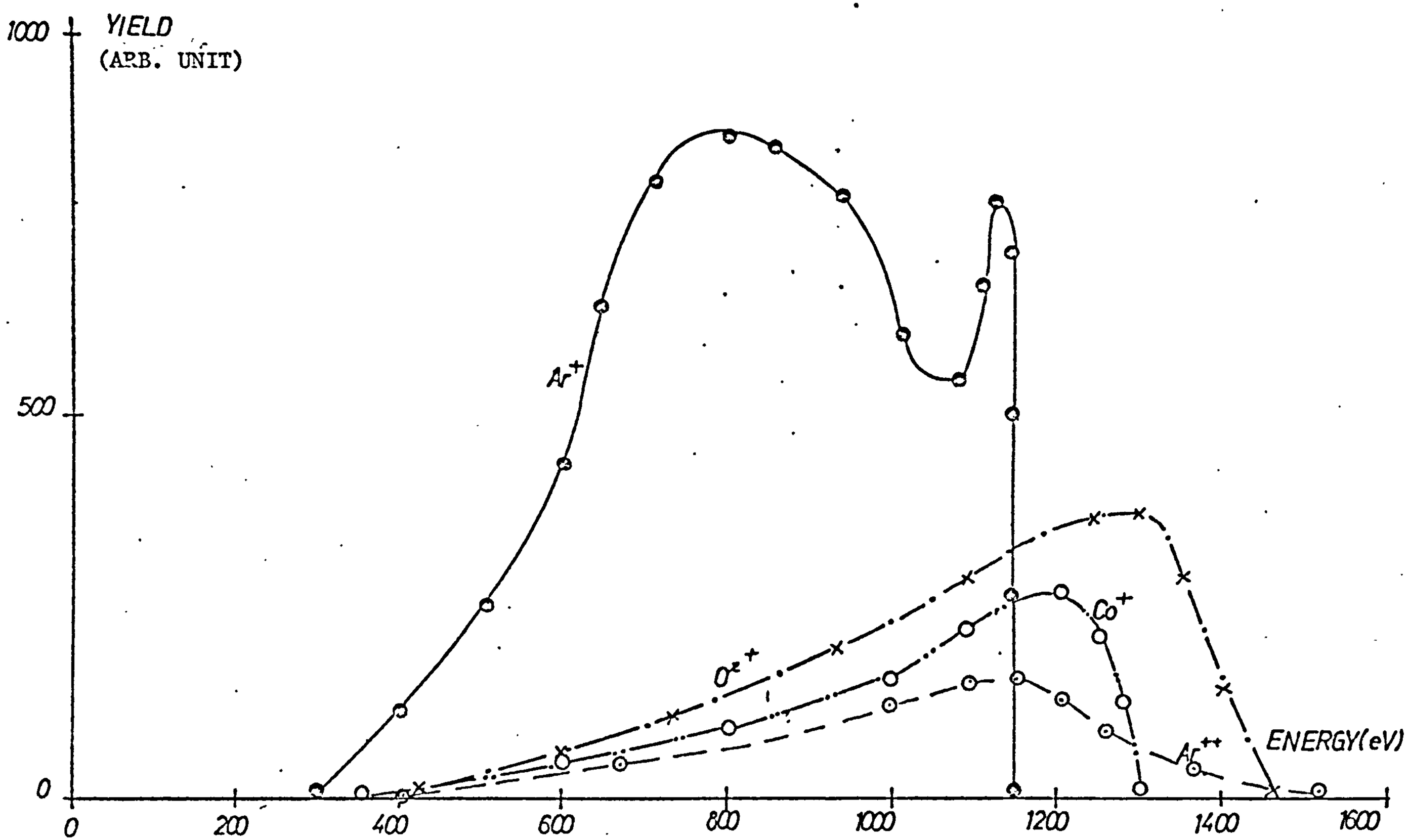

FIGURE 5.19(a) TYPICAL ENERGY DISTRIBUTIONS OF VARIOUS ION SPECIES IN AN ION PLATING DISCHARGE OF 3kV AT 3×10^{-2} TORR, RUN IN ARGON,

is smaller and hence more charge exchange collisions occur in the high field dark space region. This leads to an increase in the low energy content of the total ion flux. As a point of interest, simple addition of the spectra presented in Figure 5.19(a) results in the spectrum shown in Figure 5.19(b) which shows the distinctive two peak structure which was consistently observed in the measured total ion energy distributions i.e. non-mass analysed situation. Thus the two peak structure can be attributed to the different charge exchange efficiences for the various species.

It is still necessary, however, to explain the presence of two peaks in the energy distributions of Ar^+ and N^+ (Figure 5.8(a) and 5.9(a)). One possible explanation is that some of the carrier gas ions which leave the plasma in the doubly charged state are converted to the singly charged state after acceleration through a significant part of the dark space potential. These singly charged particles will have significantly higher energies than those which leave the plasma singly charged. The comparatively long mean free path for the $Ar^{++} \rightarrow Ar^+$ process will serve to emphasise this effect. Because they are not affected by processes other than straight-forward loss by charge exchange, the energy distributions of doubly charged carrier gas ions are found to match, the theoretical predictions of Davis and Vanderslice much more closely than is the case for singly charged particles. Typical comparison spectra such as those for 3kV discharges at different pressures which are presented in Figures 5.18(c) and (d) confirm this feature and also shows that the fitness improves as the pressure decreases.

Regarding the energy distributions of the neutral particles it is possible, on the basis of one of the assumptions made by Davis and Vanderslice (linear potential drop across the dark space), to establish straight-forward relationship between the ion and neutral spectra. Referring to Figure 5.20(a) when an ion undergoes a charge exchange collision at a point P with potential V_p it creates a fast neutral with energy $(V_c - V_p)$. The slow ion produced will accelerate through V_p and its energy will correspond to this value. Hence an ion at energy position of $e\,V_p$ will be associated with a neutral at $(V_c - V_p)$ and based on this transformation the form of the neutral spectrum can be deduced

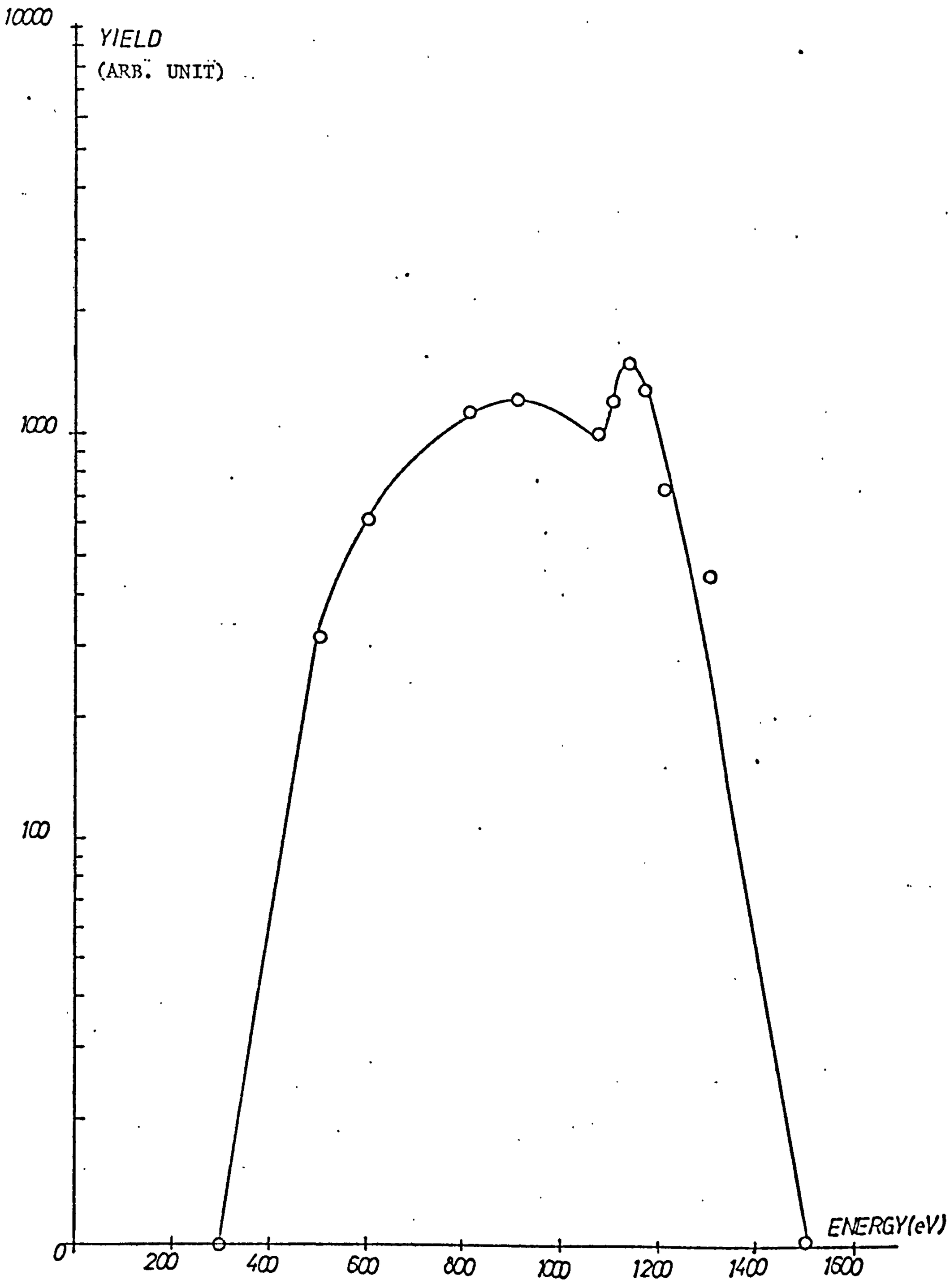

FIGURE 5.19(b) TOTAL ENERGY DISTRIBUTIONS OF AR^+; CO^+, O_2^+ AND AR^{++} IN A 3kV DISCHARGE AT 3×10^{-2} TORR.

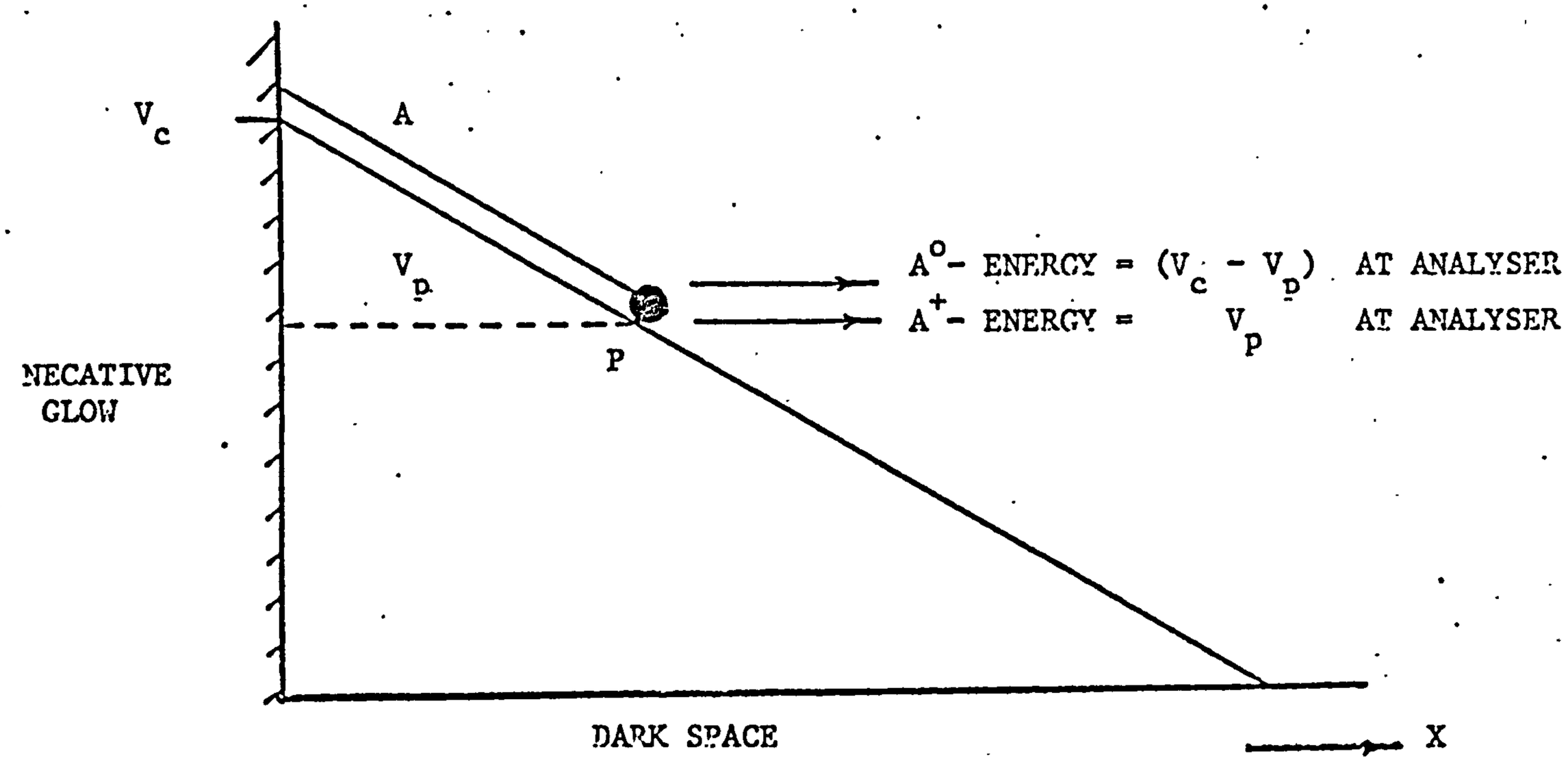

FIGURE 5.20 (a) A SIMPLE MODEL (WITH LINEAR FIELD VARIATION ACROSS DARK SPACE) FOR CALCULATION OF THE ENERGY OF THE NEUTRALS.

from the measured ion energy distribution. However, the spectrum obtained by the above transformation can not be directly compared with the measured neutral particle energy distribution since efficiency of ionisation system is inversely proportional to the velocity of the neutral particles (time spent in the electron beam). Hence a neutral particle with energy $e(V_c-V_p)$ has a velocity of v_p where

$$e(V_c-V_p) = \tfrac{1}{2}m\ v_p^2 \qquad 5.3.10$$

Thus v_p is proportional to the square root of the energy and to obtain the correct form of energy spectrum for the neutrals, the spectrum obtained by the above transformation, must be modified by multiplying each point by the square root of energy. Comparison of spectra obtained in this way with the measured spectra offers a means of assessing the validity of the assumptions concerning the potential distributions in the dark space and of checking the performance of the sampling system from the point of view of low energy neutral transmission. Transformed ion energy spectra have been determined for $Ar^+ \rightarrow Ar^o$, $N^+ \rightarrow N_o$ and $Cu^+ \rightarrow Cu^o$ and are compared with the equivalent measured neutral spectra in Figures 5.20(b), (c) and (d). It is immediately apparent that the measured spectra occur at very much lower energies than those predicted on the basis of simple transformation model and this rather extreme disagreement, if real, throws considerable doubt on the usefulness of some of the energy deposition calculations that have been based on the same assumptions as the present model. There are a number of possible explanations for the poor agreement:

1. The field in the dark space is not uniform and hence the whole basis of the transformation is invalid. It is possible, by assuming different potential distributions and charge transfer mean free paths to porduce transformation spectra with widely differing characteristics. In terms of Davis and Vanderslice's theory which predicts a preponderance of low energy ions and hence high energy neutrals it is, in fact, to be expected that the uniform field assumption will tend to move the

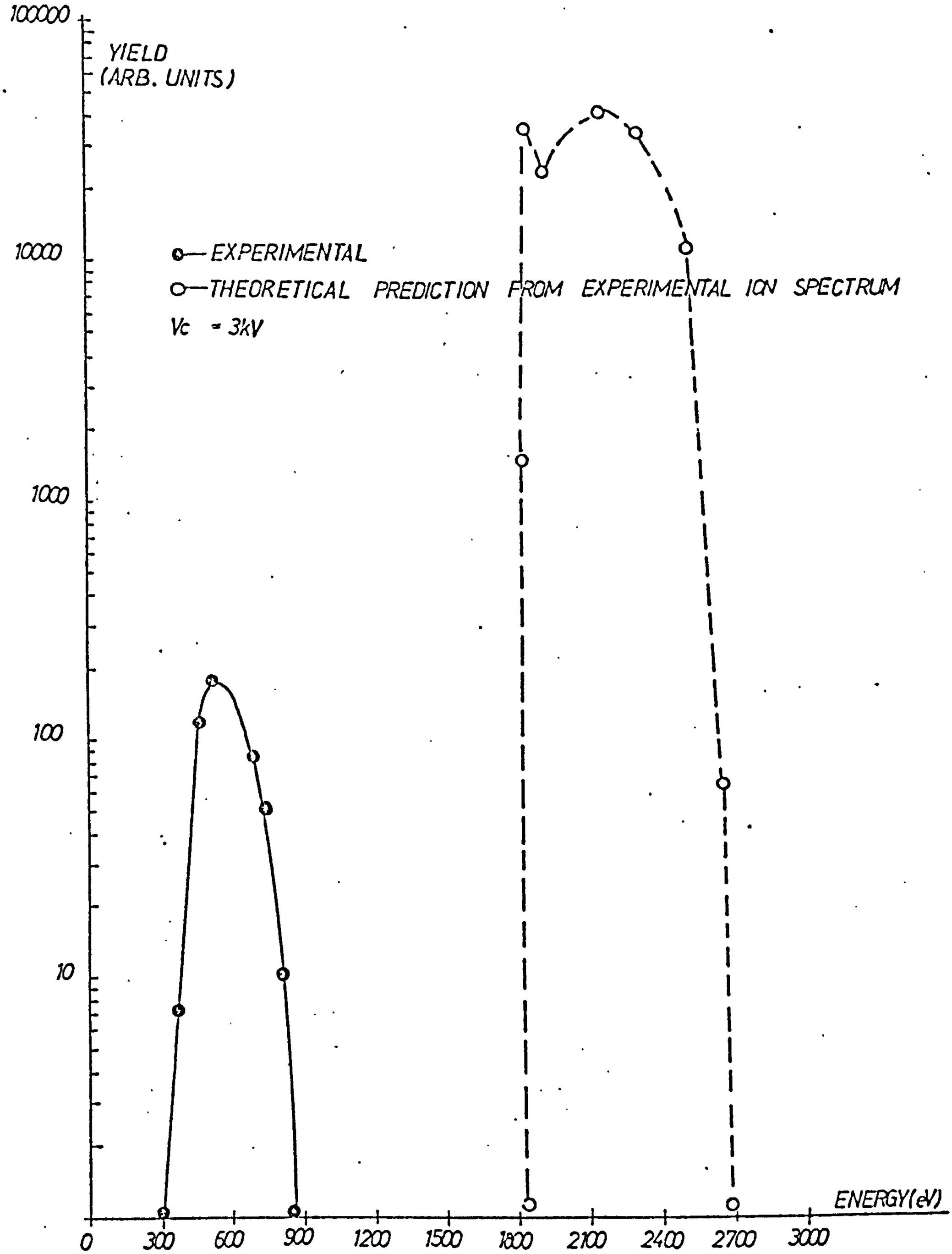

FIGURE 5.20(b) COMPARISON OF THE ENERGY DISTRIBUTIONS OF THE NEUTRAL PARTICLES OF CARRIER GAS (ARGON) OBTAINED BY EXPERIMENT, WITH THE THEORETICAL SPECTRUM OBTAINED ON THE BASIS OF DAVIS AND VANDERSLICE'S ASSUMPTIONS DISCHARGE PRESSURE: 3×10^{-2} TORR.

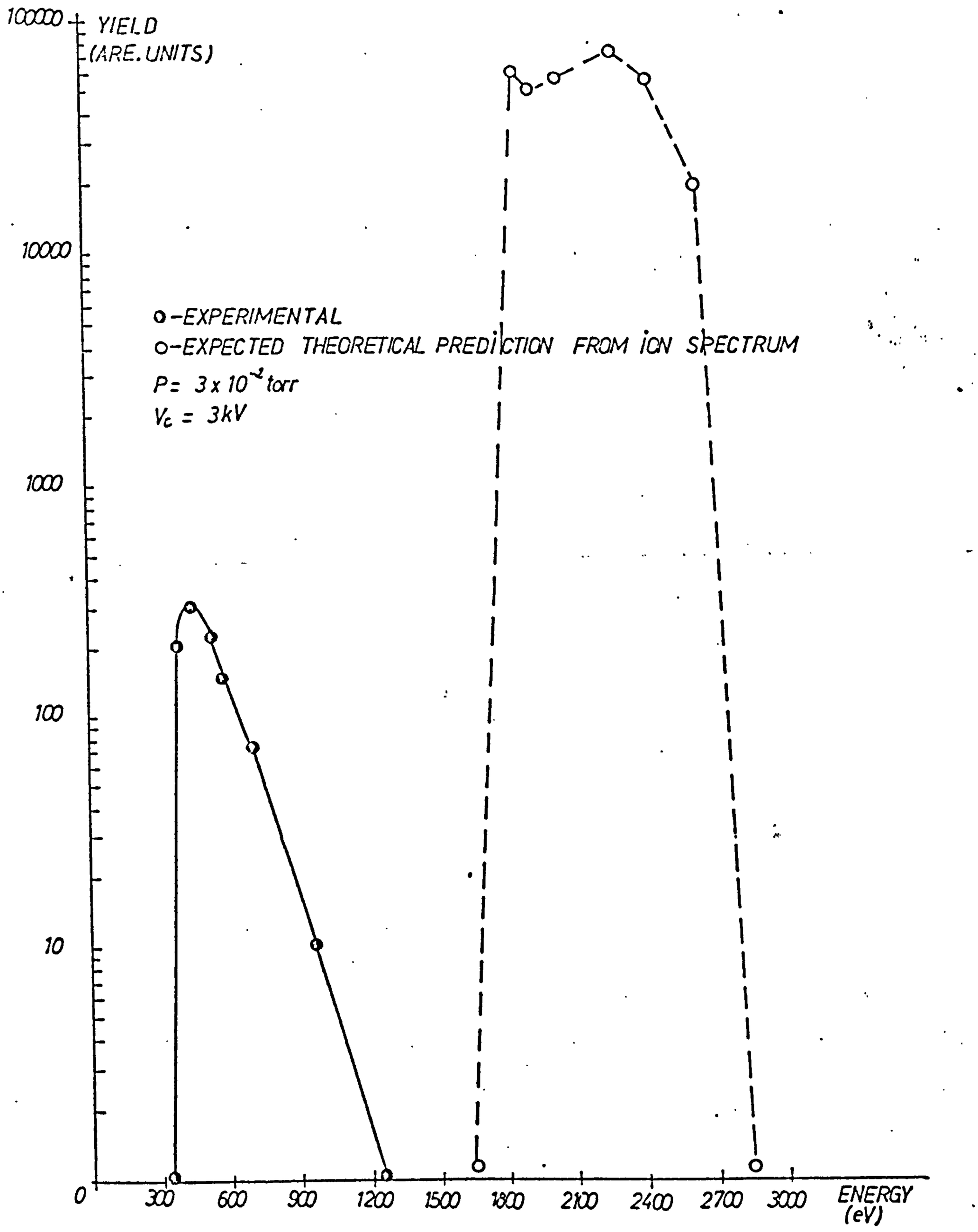

FIGURE 5.20(c) COMPARISON OF THE ENERGY DISTRIBUTIONS OF THE NEUTRAL PARTICLES OF THE CARRIER GAS (NITROGEN) OBTAINED BY EXPERIMENT WITH THE SPECTRUM OBTAINED ON THE BASIS OF DAVIS AND VANDERSLICE'S ASSUMPTIONS. DISCHARGE PRESSURE: 3×10^{-2} TORR CARRIER GAS: ARGON.

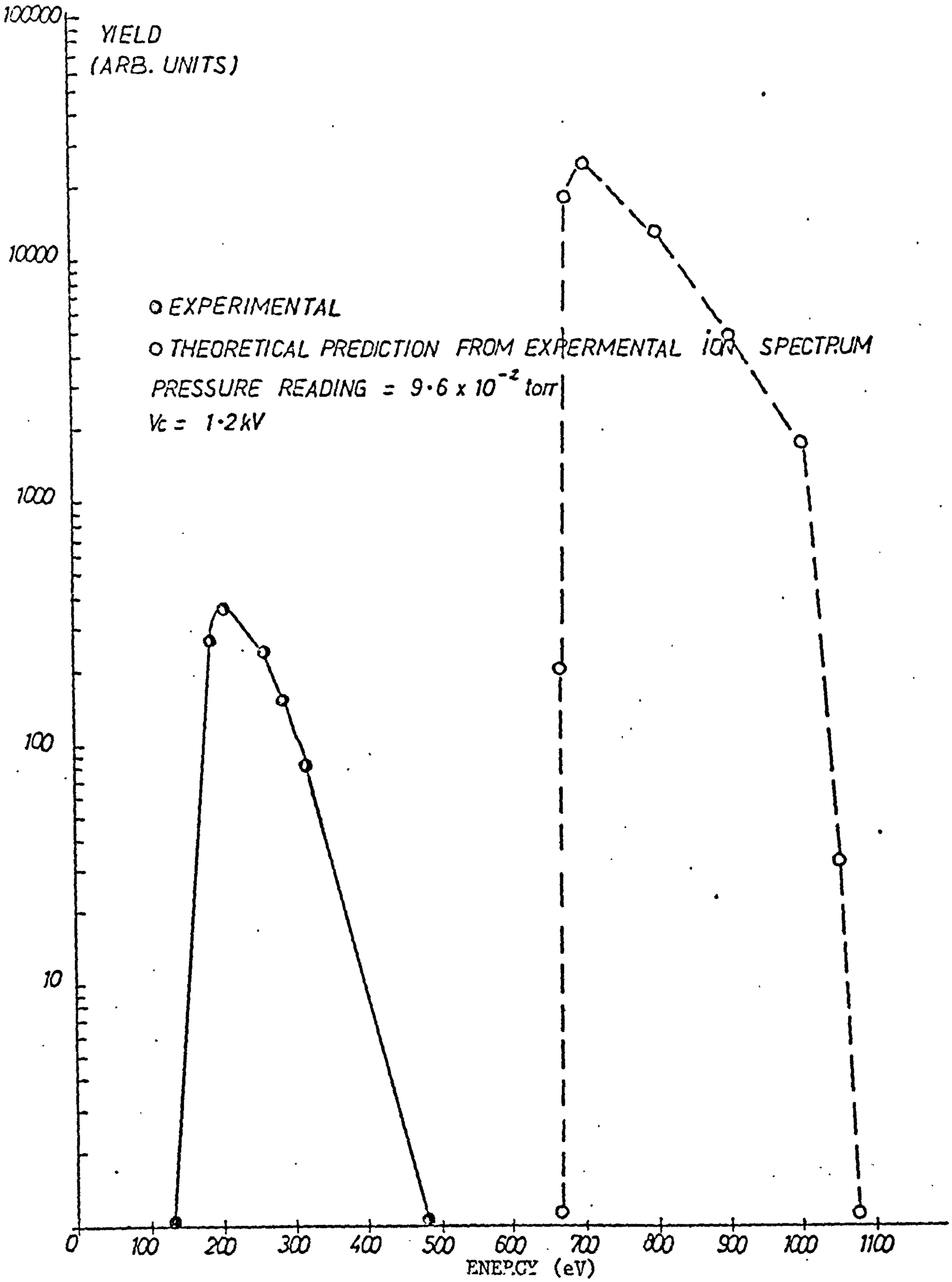

GURE 5.20(d) COMPARISON OF THE ENERGY DISTRIBUTIONS OF THE NEUTRAL PARTICLES OF THE FILM MATERIALS (CU^{o}), OBTAINED BY EXPERIMENT WITH THE THEORETICAL SPECTRUM OBTAINED ON THE BASIS OF DAVIS AND VANDERSLICE'S ASSUMPTIONS. CARRIER GAS(ARGON) PRESSURE SETTING 4.6×10^{-2} TORR.

neutral distributions to higher energies and the present comparisons, together with previously discussed discrepancies between the measured and theoretically predicted ion spectra suggests that for the type of discharge under study, the field may be non-uniform.

2- The anlysis system introduces systematic errors hence the transmission of the energy and mass analysis systems were checked over a very wide energy range and found to possess satisfactory characteristics, any source of "error" must be in the initial sampling region. The low energy neutrals are those formed in charge transfer collisions close to the plasma region since they involve ions which have only been accelerated through a small part of the total potential drop in the dark space. These neutrals are thus required to travel the maximum distance in the high pressure region prior to reaching the sampling aperture. In view of the high scattering cross-section considerable attenuation would be expected and consequently, if problems were encountered with the sampling, they would almost certainly be in the form of a reduced yield of low energy neutrals. This is not, of course, an error, since it is the nature of the particles which actually arrive at the cathode that is of interest but it does indicate that experimentally measured neutral energy distributions should actually lie above those predicted on the basis of a model which does not consider the effects of attenuation due to scattering. Hence the present discrepancy is not to be due to an instrumental or sampling factor.

5.4 Sputter-Redeposition

As briefly discussed in the description of the model shown in Figure 5.1, sputter-redeposition of target material is a process which can occur during ion plating. The flux of particles impinging on the substrate, in particular during the early stages of the plating process, is therefore comprised of a mixture of substrate and film material particles. As deposition proceeds the sub-

strate content in the mixture will inevitably be reduced as the surface concentration of substrate atoms decreases. In fact, it was the occurrence of this phenomenon which let some workers[9,10] to hypothesise that the formation of . graded interface is due to sputter-redeposition. In order to test this hypothesis, experiments were carried out in which the efficiency of the sputter-redeposition process could be measured using the R.B.S. technique.

5.4.1 Preparation of Film

The apparatus used in these experiments has been described in Section 4.5. In all cases low mass substrates, silicon and aluminium, were used in order to comply with the requirements of the R.B.S. technique, and the complete substrate - holder assembly was water cooled to reduce the possibility of surface diffusion. The choice of copper as the film material was based on its suitable mass from the point of view of the R.B.S. measurements and its good thermal conductivity which enabled the entire substrate assembly to be effectively water cooled. Sputter-redeposition experiments were carried out using discharge voltages of 0.5kV, 1kV, 1.5 kV, 2.0kV, 2.5kV and 3kV, in argon at a pressure of 2.5×10^{-2} torr. At the end of each discharge exposure the copper and argon contents of the substrate were measured using R.B.S. The choice of a suitable exposure period was determined empirically and the comparatively long time used was due to the low sputtering yield and hence slow redeposition rate.

5.4.2 Quantity of Redeposited Film

The quantities of sputter-redeposited copper on a polycrystalline aluminium and a single crystal silicon substrate were measured by Rotherford backscattering using 2MeV helium ions as the probe. A typical RBS spectrum , obtained for a 2kV discharge is shown in Figure 5.21. Similar spectra were observed for all the samples exposed to the sputter - redeposition discharges. The result of the RBS analysis showed that considerable quantities of copper were introduced into the sample during exposure to the discharge. Figure 5.22 shows the result of this

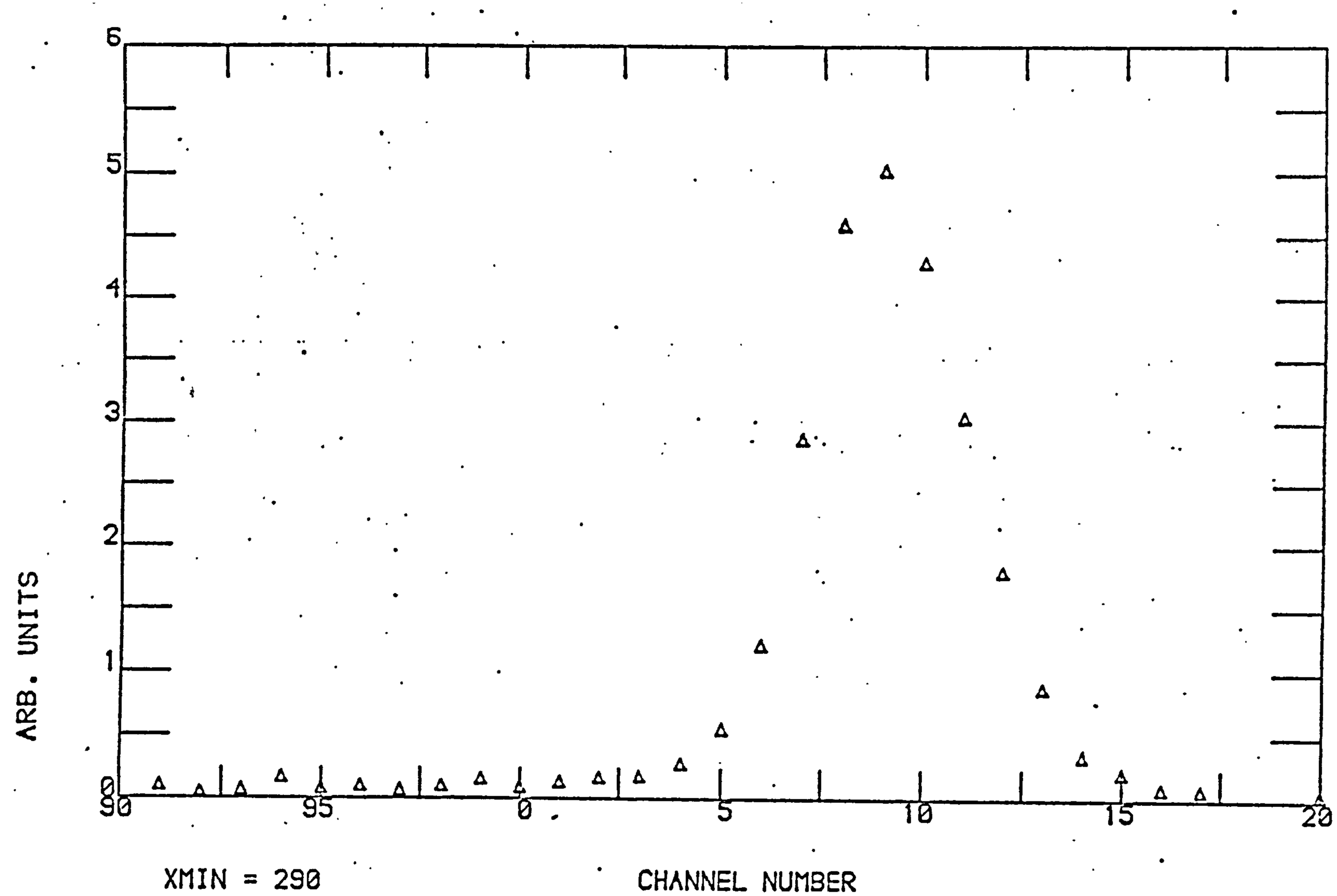

FIGURE 5.21 COPPER PEAK IN RBS SPECTRUM OF ALUMINIUM SPECIMEN

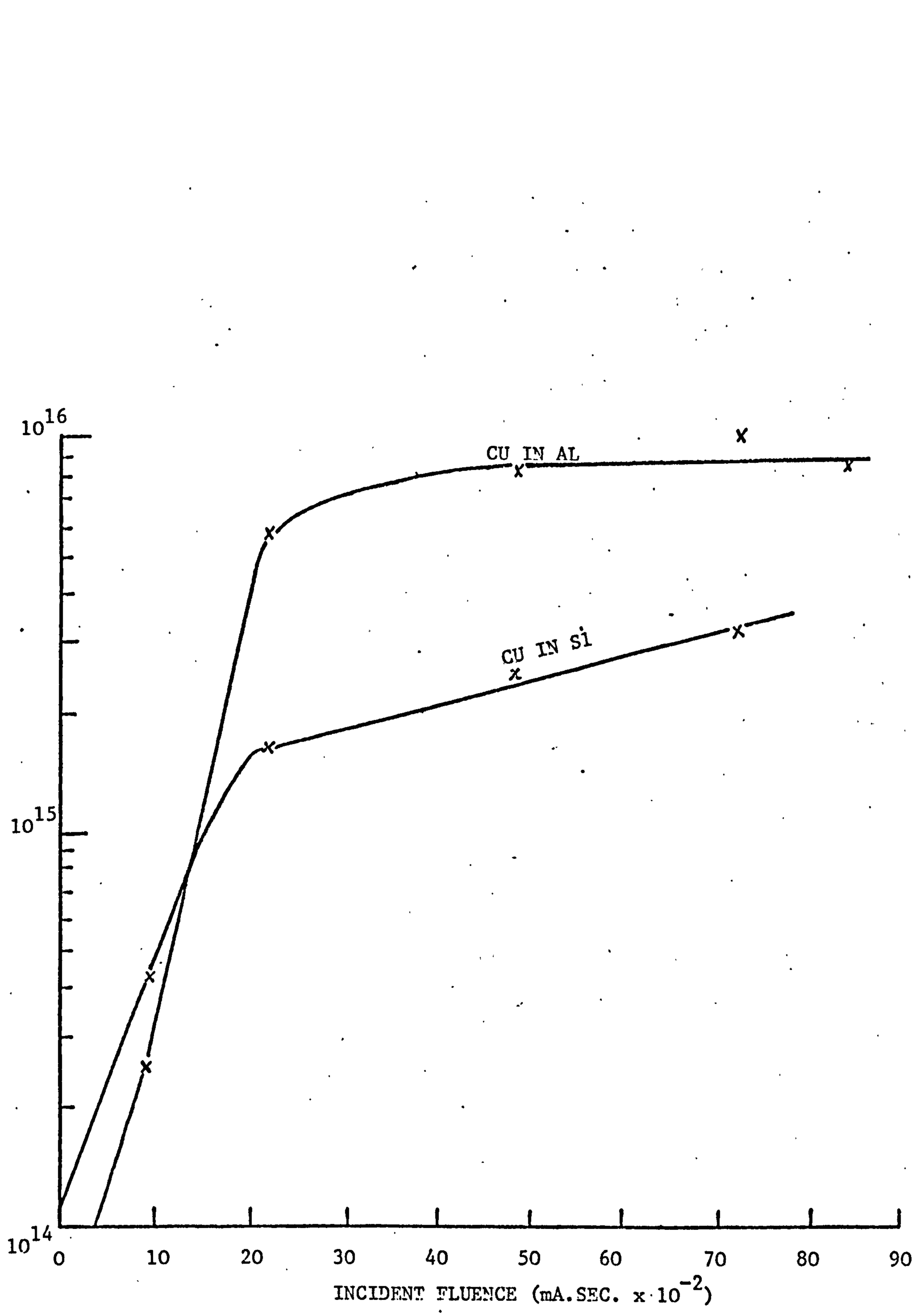

FIGURE 5.22 QUANTITIES OF COPPER TRAPPED IN ALUMINIUM AND SILICON SUBSTRATES AS A FUNCTION OF FLUENCE.

analysis and it can be seen that the copper content of the aluminium sample reached a saturation level of 10^{16} atoms/cm^2 after an argon fluence of 20×10^2 mA.sec. whereas for the silicon sample, there is continuous increase in copper concentration.

5.4.3 Comments

Although there are a number of interesting features associated with these measurements the most important information is that the sputter-redeposition process is very inefficient. Since the discharge employed was of the type employed in ion plating and deposition rates are typically of the order of hundreds to thousands of Angstroms per minute, then the formation of 10 monolayers of copper by sputter-redeposition in a period of about an hour means that this process can only play an insignificant role in interface formation unelss very low initial deposition rates are employed.

Since the entire substrate is exposed to the discharge then it would be expected that the quantity of copper would eventually saturate when the removal and deposition rates are equal. This effect is observed in case of aluminium substrate but for silicon a continuous increase in the amount of copper is observed. In view of the high diffusion coefficient for copper in silicon, it is quite probable that under the present experimental conditions, a continuous diffusion of copper into the bulk substrate was occurring.

The build up of argon in the substrate will be discussed in the following section, where the gas trapping and release processes are considered in more detail.

5.5 Carrier Gas Trapping

As a result of the discussion presented in Section 5.3.5(c) it can be concluded that the entrapment of carrier gas atoms in ion-plated films is inevitable and it is possible that some of the properties of ion-plated films are affected by the presence of the trapped gas atoms. In order to assess the

possible effects of these atoms it is necessary to assess the concentration level involved since thermal evolution measurements have indicated that the behaviour of the trapped gas depends strongly on this parameter.

As was the case for film growth, the build up of gas in the ion-plated film is associated with both trapping and removal processes and the equilibrium concentration reflects the relative efficiencies of penetration, trapping and sputtering. In a detailed investigation of the role of the trapped gas in ion plating, it is therefore essential to investigate the sputtering (of the entrapped gas atoms) as well as the trapping phenomena and in the present work the following experiments were carried out:

1. An investigation of the removal rate of previously implanted gas by exposure of the sample to an ion plating discharge.
2. The measurement of the concentration of trapped carrier gas in ion plating.

5.5.1 Experimental Procedure

To investigate the trapped gas sputtering capability of an ion plating discharge, xenon gas implanted into single crystal silicon samples prior to discharge exposure. The implantation was carried out in the Accelerator Laboratory of the University of Salford by bombarding the samples (at both normal and 10^{o} off-axis incidence) with 10 keV xenon ions to doses of 10^{14}, 10^{15}, and 10^{16} ions/cm^{2}. The samples were then exposed to an ion plating discharge of 3kV, $2.5x10^{-2}$ torr for 20 minutes using the apparatus described in Section 4.4.1. The effect of the discharge on the quantity of the pre-implanted gas retained was investigated using RBS after exposure to the discharge.

In the second part of the gas trapping study reported in this Section the quantity of carrier gas trapped in virgin samples exposed to ion plating discharge was measured. In fact the samples used in the sputter-redeposition studies, discussed in Section 5.4, were also used for this investigation and the measurements were carried out concurrently.

5.5.2 Analysis

RBS spectra of the samples, prior to exposure to the discharge, allowed intitial quantities of trapped xenon atoms to be assessed. The spectra for doses of 10^{14}, 10^{15} and 10^{16} ions/cm^2 are shown in Figure 5.23. Analysis of the samples, after 20 minutes of exposure to the argon discharge, showed that all the implanted xenon atoms were removed during the discharge. Spectra showing this and illustrated the build up of argon are shown in Figure 5.24. As is shown in these spectra trapped carrier gas was observed in all the samples exposed to the discharge.

The results of measurements of trapped carrier gas concentrations in both silicon and aluminium samples are shown in Figure 5.25. It can be seen that in the aluminium substrate the trapped argon reach saturation levels after a fluence of 20×10^{2} mA sec. This exposure corresponds to a quantity of 10^{15} ions (atoms)/cm^2.

5.5.3 Comments

For argon the saturation of about 1.5×10^{15} (atoms)/cm^2 is consistent with the levels expected from thermal evolution studies of trapping in other materials such as copper and nickel, and, again in common with the behaviour in these materials, it is highly probable that the saturation process is not simply dependent on the release of gas atoms by gas sputtering or sputtering of the substrate but that some form of trap saturation phenomenon leading to spontaneous release of implanted particles is occurring in all the samples exposed to the discharge.

The quantitative results of the measurements of trapped carrier gas concentration in both silicon and aluminium samples are shown in Figure5.25(b). It can be seen that in the aluminium substrate the trapped argon reach saturation levels after a flunece of 20×10^{2} mA. sec. This exposure corresponds to a quantity of approximately 10^{15} ion (atoms)/cm^2. For argon, the saturation of about 1.5×10^{15} atoms/cm^2 is consistent with the levels expected from thermal evolu-

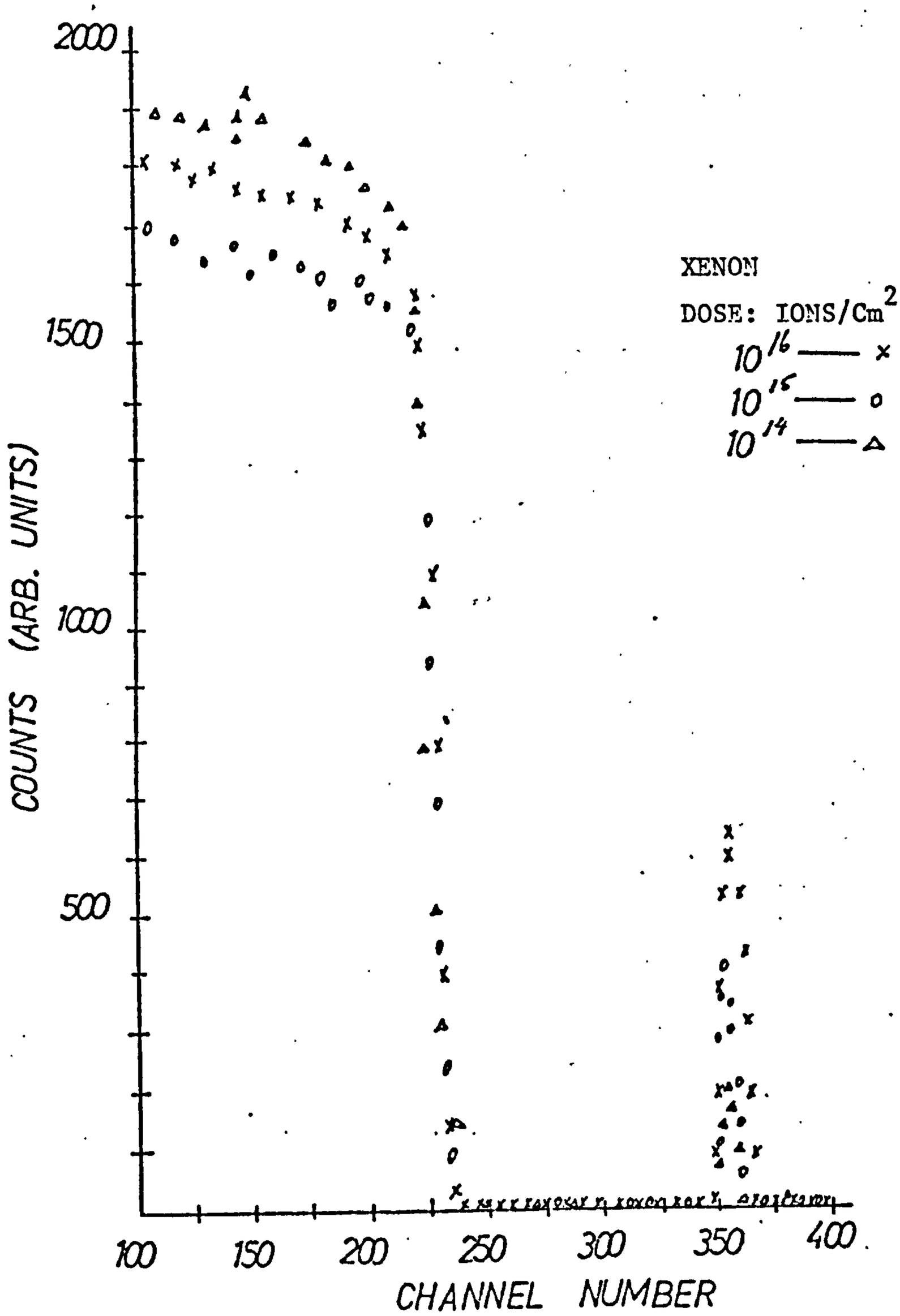

FIGURE 5.23 RBS SPECTRA SHOWING XENON PEAKS IN SILICON SUBSTRATES (PRIOR TO EXPOSURE TO DISCHARGE) PRE-IMPLANTED WITH VARIOUS DOSES OF XENON.

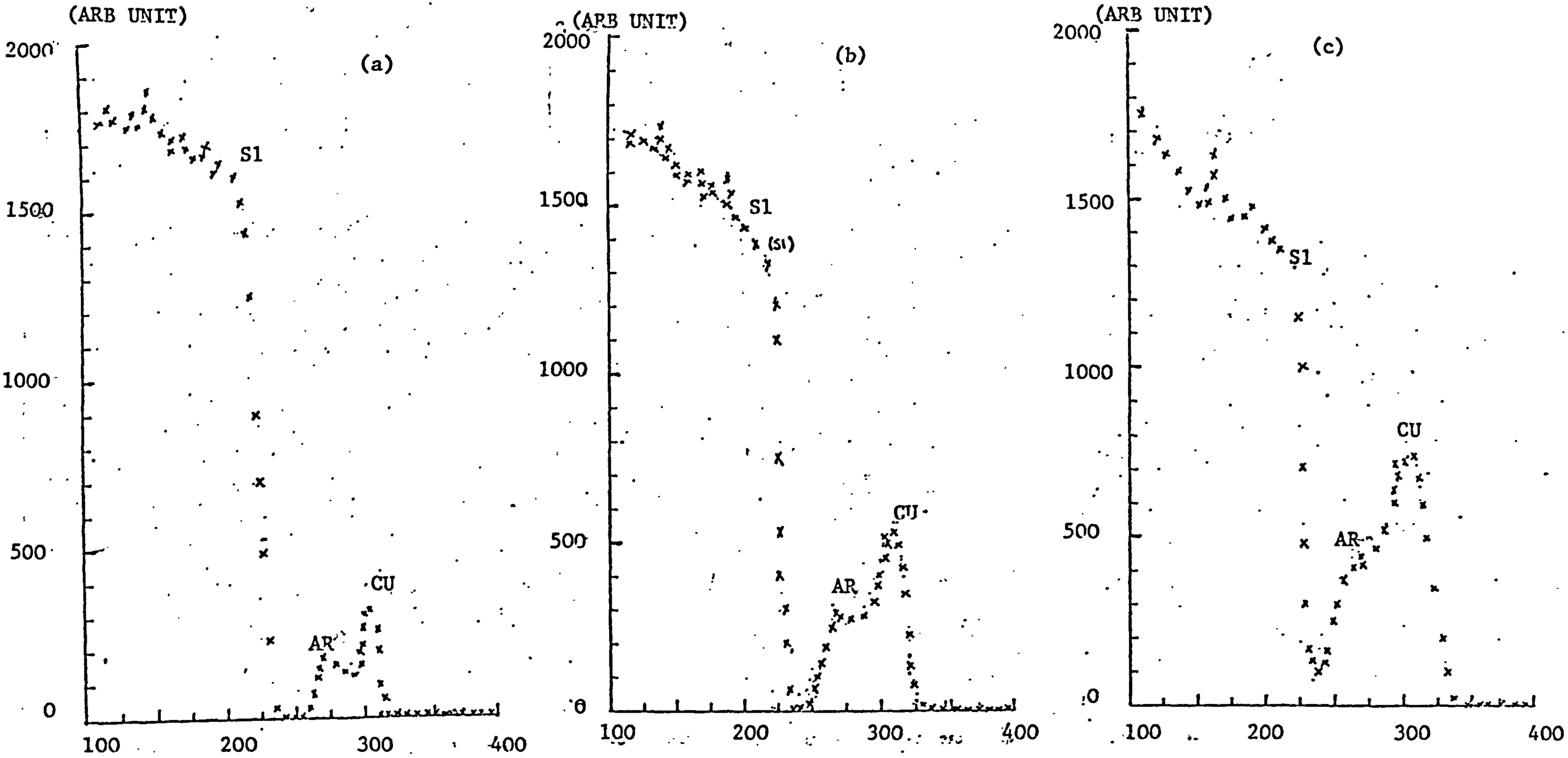

FIGURE 5.24 RBS SPECTRA OF SILICON SAMPLES, PRE-IMPLANTED WITH VARIOUS DOSES OF XENON, AFTER EXPOSURE TO SPUTTER -REDEPOSITION DISHCARGE. DOSES OF XENO PRE-IMPLANTATION a = 10^{14} ions/Cm^2, b = 10^{15} ions/Cm^2, c = 10^{16} ions/Cm^2.

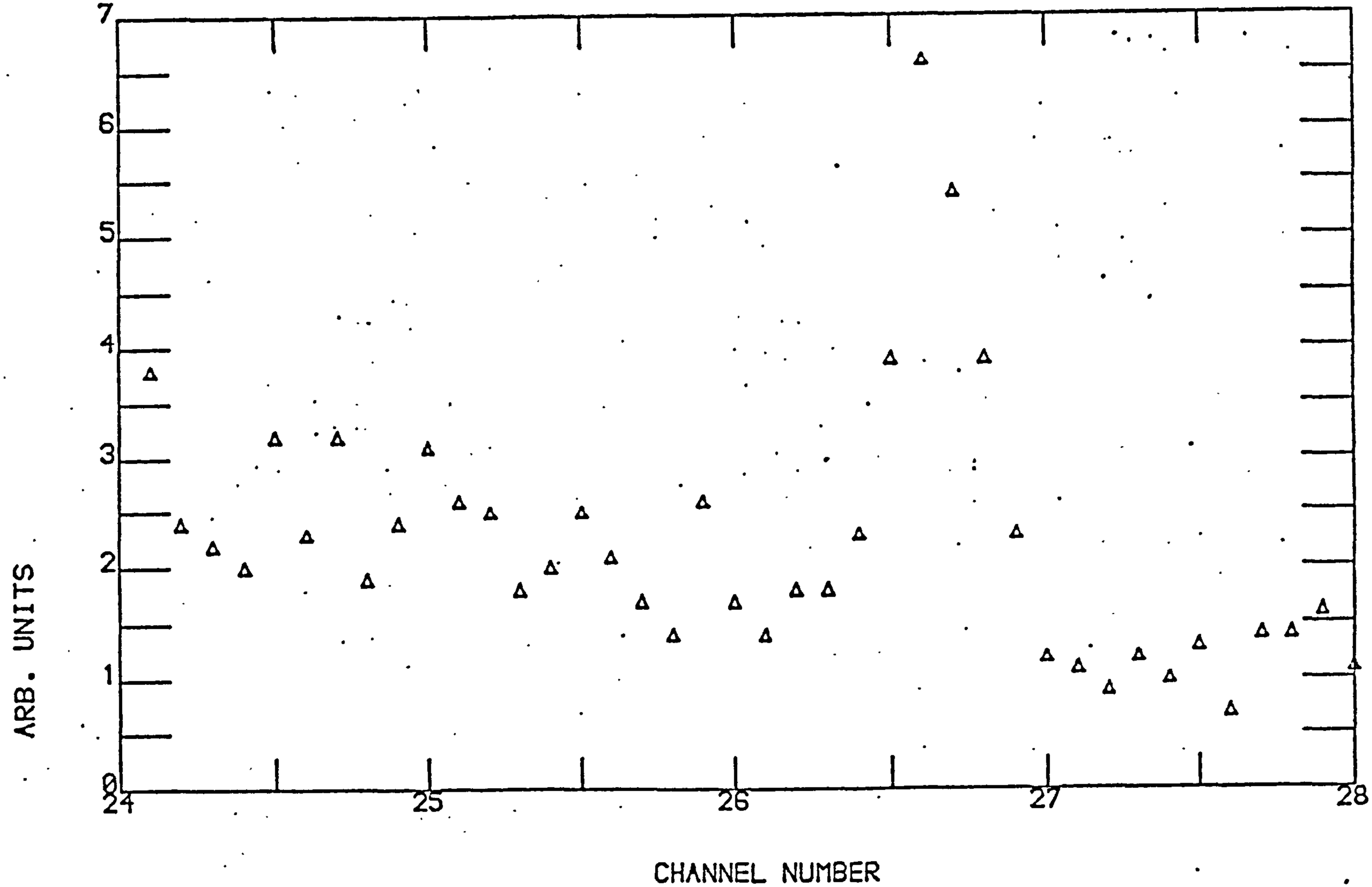

FIGURE 5.25(a) TYPICAL RBS SPECTRUM SHOWING ARGON PEAK IN ALUMINIUM SUBSTRATE.

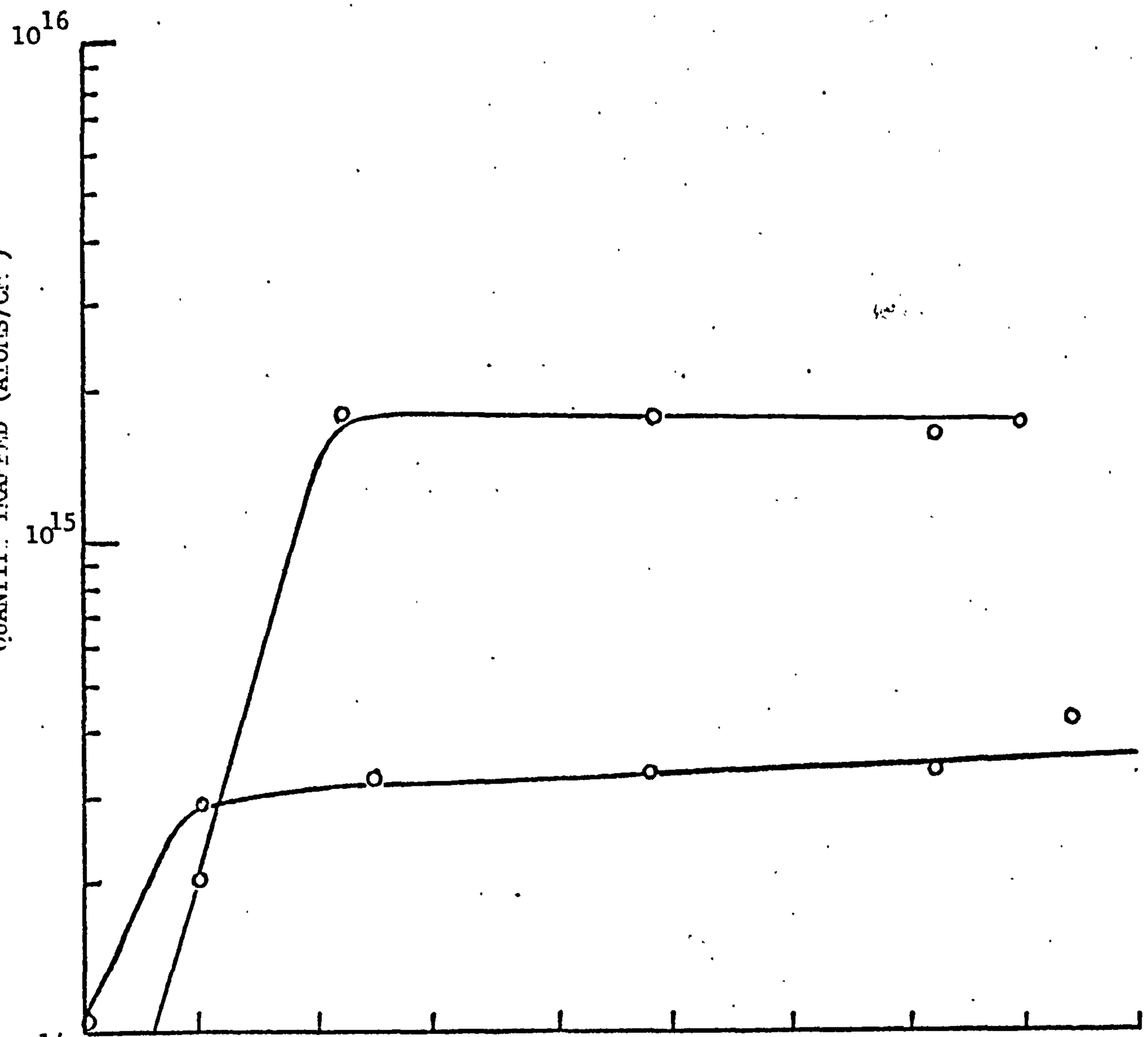

FIGURE 5.25(b) QUANTITIES OF CARRIER GAS (ARGON) TRAPPED IN ALUMINIUM AND SILICON SUBSTRATES AS A FUNCTION OF FLUENCE.

tion studies of trapping in other materials such as copper and nickel, and, again in common with the behaviour in these materials, it is highly probable that the saturation process is not simply dependent on the release of gas atoms by gas sputtering or sputtering of the substrate but that some form of trap saturation phenomenon leading to spontaneous release of implanted particles is occurring[11]. The concentration of argon trapped in silicon reached its saturation level after a fluence of 10×10^2 mA sec.

At the carrier gas concentration reached in these experiments, it is known that in normal, as opposed to film, materials gas-defect agglomeration processes lead to the formation of highly stable gas bubbles. If present in ion plating these bubbles, which are stable up to the melting point of the material,may lead to dislocation pinning and to the formation of smaller grains in the growing film and may thus affect the hardness of the film. However, the exposure time required to reach saturation are very long compared to the normal plating times and the condition probably does not occur in practical situations. The presence of gas atoms, trapped in simple defect sites may well affect the overall defect structure of the film and their role cannot be discounted when the film properties are considered.

5.6 Discussion and Summary

As a result of the experimental investigations presented in this Chapter a number of queries regarding the mechanisms responsible for the properties of ion-plated films have been answered. From the point of view of the actual mechanism(s) contributing to the superior film-substrate adhesion it has been shown that, although substrate surface cleanliness does make a contribution, optimum adhesion is only achieved when deposition takes place in the discharge. Hence, the formation of a "high adhesion" film-substrate interface must be attributed to one or more of the effects associated with bombardment of the substrate surface with energetic particles, and it was for this reason that the contributions of the three mechanisms:- sputter-redeposition, energetic

particle implantation, and energy deposition and recoil/cascade mixing were studied in the present investigation. The sputter - redeposition experiments which involved copper deposition onto aluminium and silicon substrates revealed that this process is too slow to have any significant effect on the formation of a graded interface during normal plating. Also the results of these experiments showed that although the concentration of copper in aluminium followed the expected saturation pattern a continuous increase in the amount of copper in silicon was observed. This effect is attributed to the rapid diffusion of copper into the bulk (silicon).

To understand and ultimately quantify the roles of energetic particle implantation, energy deposition and recoil and cascade mixing a knowledge of the energy distributions of the particles impinging on the substrate surface is clearly required and in the present experiments, measurements of the energy distributions of all the constituents of the energetic flux bombarding the substrate surface(s) were carried out. It was observed, as expected, that the bombarding flux is composed of energetic (energy $\gg$ thermal energy) ions and neutrals, and that even for the comparatively clean conditions used, impurity species such as H_2O, CO, O_2 etc could not be eliminated.

The measurements also confirmed that the earlier suggestion that doubly charged carrier gas ions are a constituent of the flux of ions impinging on the cathode. For typical ion plating discharges of 1.5 - 3kV the carrier gas energy spectra were found to peak at energies below about 30-40% of the total voltage while those relating to the impurity particles peaked at higher energies. This effect is explained by the fact that the mean free paths for non-resonant charge transfer collisions are greater than those for resonant cases and hence the impurity particles undergo fewer collisions in the dark space. The fact that this difference in peak energies exists was shown to be responsible for the double peak structure found in the energy spectra of the total(non-mass analysed) ion flux. The double peaks in the energy distributions of the carrier gas ions can be understood in terms of the conversion of doubly charged ions into singly charged ions after initial acceleration in the dark space. The high energy tails

observed in the experimental energy spectra can be explained quite well by the theoretical treatment proposed by Davis and Vanderslice, and hence the role of charge exchange is evident. However, the low energy tails are in clear disagreement with the simple theory and probably reflect the increasing role of large angle scattering at low energies.

On the basis of the energy measurements, the interface broadening cannot always be associated with direct implantation of the energetic impinging particles. This is because for the measured energy range (< 2.5keV) the ranges of the bombarding particles are not large enough to account for the reported widths of the interface (which for some cases be up to the range of microns). On the other hand the energy deposition/cascade mixing theory predict that for a perfect lattice and smooth surface with no thermal effects (which is the worst case) interface broadening of about 30 Å which is probably adequate to explain the improved adhesion in most cases. On the basis of these observations, it appears that the major contribution to film growth comes from the deposition of more or less thermal energy particles since the energetic flux cannot, on its own, account for the growth. It is also clear that the role of the energetic particles is intimately associated with the effects of energy deposition.

5.7 References - Chapter 5

1. Teer D.G., Proc. Int. Conf. on Iôn Plating and Allied Techniques, (IPAT), P.13, Edinburgh 1977.
2. Gillette Fellowhsip Report No. 2., Department of Electrical Engineering, University of Salford. 1979.
3. Armour D.G. Studies of Decaying Plasmas, Ph.D. Thesis, University of Liverpool, 1970.
4. Ahmad, N.A.G., Ion Plating, M.Sc. Dissertation. University of Salford, 1974.
5. Carter G., Colligon, J.S., Ion Bombardment of Surfaces, London: Heinemann) 1968.
6. Teer D.G. (private communication).
7. Davis W.D., Vanderslice T.A. Phys. Rev. 131, P.319, 1963.
8. Teer D.G. J. Adhesion 8, P. 289, 1977
9. Teer D.G. Delcea, B.L. Proc. Int. Conf. on Ion Plating and Allied Techniques (IPAT), Edinburgh, P.58, 1977.
10. Nelson, S.R. Ibid.
11. Togneitti, P. (private communication)

CHAPTER VI

CONCLUSIONS

CONCLUSIONS

Of all the available film deposition techniques, ion plating is unique in that it utilises technically simple apparatus and is capable of achieving high deposition rates and good throwing power while producing pore-free films of a wide range of materials on an equally wide range of substrates with excellent adhesion, improved density and uniformity together with improved grain structure. Despite the appreciation of all these properties, little effort has been expended in the study of the mechanisms of ion plating and the work presented in this thesis represents an attempt to rectify this situation. On the basis of the measurements the following conclusions can be made:-

1. The cleanliness of the substrate surface(s), which is an consequence of the continual ion impact desorption of adsorbed impurities, and which has been considered by some workers to play a major role in determining the strength of the film-substrate bond makes only a minor contribution for the cases studied. The main factor affecting the adhesion deposition in the discharge and the resulting bombardment of the growing film by energetic particles.

2. The energetic particles are comprised of both ions and neutral species and their energy distributions peak at energies below about 30-40% of the total discharge voltage. As a result of these measurements it became clear that the material growth of the film is not due to the energetic flux but due to particles with more or less thermal energies. The energetic particles appear to play a number of roles including the removal of impurities and poorly adhered film particles and the inducement of diffusion of the film particles into the substrate and vice versa - hence the formation of a graded interface. The diffusion and broadening of the interface is in general due to the deposition of energy by the energetic particles, since direct implantation cannot, on the basis of simple range consideration, be responsible for the interface broadening and sputter-redeposition is too slow to have any

significant effect under normal plating conditions.

3. The mass analysis of the particles leaving the discharge revealed that the total flux is comprised of singly charged ions and neutral particles of the carrier gas and impurities such as H_2O, CO and O_2 and doubly charged carrier gas ions. The energy distributions of both the singly charged carrier gas ions and the total ion flux have double peaks whereas the energy distributions of impurity ions contain only one peak at an energy higher than the peak energy of the corresponding singly charged carrier gas ion energy distributions. A point - by - point addition of the individual particle energy spectra yields a double peak spectrum and hence offers an explanation for the presence of the two peaks in the energy spectra of the total ion flux.

4. The low energy tails observed in all the measured energy distributions are clearly in disagreement with Davis and Vanderslice's theoretical predictions. This effect may be explained by the increased attenuation of the low energy particles, reaching the entrance aperture of the energy analyser, with decreasing energy due to increased large angle scattering.

The measurements have clearly indicated the complexity of the physical processes which are associated with ion plating and have emphasised the need for careful control of the experimental conditions. The increasing use of reactive systems in both plating and etching situations will undoubtedly lead to increased interest in the type of measurement described in this thesis and a programme of work in this area is already being planned.